MACROPHAGE SILICA NANOPARTICLE INTERACTIONS: CELLULAR UPTAKE AND FATE

by

Heather Leigh Herd

A dissertation submitted to the faculty of
The University of Utah
in partial fulfillment of the requirements for the degree of

Doctor of Philosophy

Department of Bioengineering

The University of Utah

December 2014

The University of Utah Graduate School

STATEMENT OF DISSERTATION APPROVAL

The dissertation of **Heather Leigh Herd**

has been approved by the following supervisory committee members:

Hamidreza Ghandehari	, Chair	**5/9/14** Date Approved
David Grainger	, Member	**5/7/14** Date Approved
Vladimir Hlady	, Member	**5/7/14** Date Approved
Alana Welm	, Member	**5/7/14** Date Approved
Ilya Zharov	, Member	**5/7/14** Date Approved

and by **Patrick Tresco** , Chair of the Department of **Bioengineering**

and by David Kieda, Dean of The Graduate School.

ABSTRACT

Phagocytes are important players in host exposure to nanomaterials, by processing nanomaterials and possibly contributing to host nanotoxicity. Macrophages in particular are believed to be among the "first responders" and primary cell types that uptake and process nanoparticles, mediating host biological responses by subsequent interactions with inflammatory signal pathways and immune cells. Thus, it is important to understand how nanomaterials are recognized, internalized, trafficked and distributed within this cell type and how this cell-based reaction furthers responses *in vivo*. This dissertation will focus on describing macrophage-based silica nanoparticle exposure, mechanisms of uptake, intracellular fate and potential initiation of downstream immunological processes, as a function of physicochemical properties such as size, surface properties and geometry. Alterations in physicochemical properties, specifically geometry of nanomaterials, can influence cellular uptake mechanisms. Specific macrophage phenotypes are shown to induce nanoparticle uptake *in vitro* and *in vivo*. Mechanistic evaluation has provided evidence of cellular machinery inducing autonomous antimicrobial defense and cytoplasmic clearance mechanisms such as autophagy in response to positively charged silica nanoparticle exposure. Understanding nanoparticle macrophage interactions may allow for the development of platforms to design biocompatible systems for specific intracellular uptake and fate.

For my mom, Marilyn, and sister, Sarah, without your love, support, and unwavering faith, I would be nothing.

CONTENTS

LIST OF FIGURES

Figure

LIST OF TABLES

Table

LIST OF ABBREVIATIONS

ADP	adenosine diphosphate
AFM	atomic force microscopy
APES	3-aminopropyltriethoxysilane
APTMS	Aminopropyltrimethoxylsilane
ATCC	American Type Culture Collection
ATP	adenosine triphosphate
AUC	area under the curve
BPE	bovine pituitary extract
BSA	bovine serum albumin
BSA-FAF	fatty acid free bovine serum albumin
BSS	balanced salt solution
C3	complement component 3
C3b	complement component 3 b fragment
CCLs	chemokine ligands
CD206	cluster of differentiation 206
CD47	cluster of differentiation 47
CD64	cluster of differentiation 64
CD68	cluster of differentiation 68

CD80	cluster of differentiation 80
CD86	cluster of differentiation 86
cDNA	complimentary DNA
CLSM	confocal laser scanning microscope
CR	complement receptor
CSFs	colony stimulating factors
CTAB	cetyltrimethylammonium bromide
DAMP	damage associated molecular pattern
DAPI	4',6-diamidino-2-phenylindole
DI	Deionized
DIC	disseminated intravascular coagulation
DLS	dynamic light scattering
DNA	deoxyribonucleic acid
DRAQ5	live cell imaging stain for DNA
FACS	fluorescence activated cell sorting
Fc	fragment crystallizable region
FDA	Food and Drug Administration
FITC	fluorescein isothiocyanate
FT-IR	Fourier transform infrared
GSH	glutathione
hEGF	human epidermal growth factor
HIV	human immunodeficiency virus
HSC	hematopoietic stem cell

IACUC	Institution animal care and use committee
IC50	50% inhibitory concentration
ICAM-1	intercellular adhesion molecule 1
ICP-MS	inductively coupled plasma mass spectrometry
IgE	Immunoglobulin E
IgG	immunoglobulin G
IgG2a	Immunoglobulin G2a
IL-10	interleukin 10
IL-12	interleukin 12
IL-13	interleukin 13
IL-1beta	interleukin 1 beta
IL-4	interleukin 4
IL-6	interleukin 6
IL-8	interleukin 8
INF-gamma	interferon gamma
iNOS	nitric oxide synthase
IR	Infrared
IV	Intravenous
JC-1	cationic carbocyanine dye
LAMP	lysosome-associated membrane protein
LC3-II	autophagic marker
LDH	lactate dehydrogenase
LDL	low density lipoprotein

LPS	Lipopolysaccharide
M1	classically activated macrophage
M2	alternatively activated macrophage
Mac-1	macrophage antigen 1
MAPK	mitogen activated protein kinase
MARCO	macrophage receptor with collagenous structure
MCP1	monocyte chemoattractive protein-1
MDA	Malondialdehyde
MIP	macrophage and inflammatory protein
MM-6	human monocytic cell line
MPS	mononuclear phagocytic system
MRI	magnetic resonance imaging
mRNA	messenger ribonucleic acid
MS	multiple sclerosis
MTT	3-(4,5-dimethylthiazol-2-yl)-2,5-diphenyltetrazolium bromide
MW	molecular weight
MWCNT	multi-walled carbon nanotubes
MyD88	myeloid differentiation primary response 88
NF-kappa beta	nuclear factor kappa-light-chain-enhancer of activated B cells
NLS	nuclear localization signals
NMR	nuclear magnetic resonance
NO	nitric oxide
PAMAM	poly(amido amine)

PAMP	pattern associated molecular patterns
PBMC	peripheral blood mononuclear cells
PBS	phosphate buffered saline
PCR	polymerase chain reaction
PECAM-1	platelet-endothelial cell adhesion molecule 1
PEG	poly(ethylene glycol)
PEGMA	poly(ethylene glycol) methyl ether methacrylate
PI	propidium iodide
PI3-kinase	phosphoinositide 3-kinase
PLGA	poly(lactic-co-glycolic acid)
PMA	phorbol myristate acetate
PRINT	particle replication in nonwetting templates
PRR	pattern recognition receptor
RA	rheumatoid arthritis
RES	reticulo-endothelial system
RGD	arginine-glycine-aspartic acid peptide
RIPA	radio-immunoprecipitation assay
RNS	reactive nitrogen species
ROS	reactive oxygen species
SCC	surface connected compartments
SEM	scanning electron microscopy
SIRP alpha	signal regulatory protein alpha
SNP	silica nanoparticle

SNT	silica nanotube
SPIO	superparamagnetic iron oxide
SR-A	scavenger receptor a
Streptococcal M6	Streptococcal M6 protein
TB	Tuberculosis
TBARS	thiobarbituric acid reactive substance
TEM	transmission electron microscopy
TEOS	tetraethyl orthosilicate
TGA	thermogravimetric analysis
TGF	transforming growth factor
Th1	T helper cell response 1
Th2	T helper cell response 2
TLR	toll-like receptor
TNF-alpha	tumor necrosis factor alpha
TPP	Triphenylphosphonium
TUNEL	terminal deoxynucleotidyl transferase dUTP nick end labeling
UV	Ultraviolet
VEGF	vascular endothelial growth factor
WST-8	2-(2-methoxy-4-nitrophenyl)-3-(4-nitrophenyl)-5-(2,4-disulfophenyl)-2H-tetrazolium

ACKNOWLEDGEMENTS

I am indebted to many without whom this dissertation would have been impossible:

First, I would like to thank my advisor Hamid Ghandehari for his continued faith and support while I performed the work presented within this dissertation. During the course of my PhD his work ethic, enthusiasm for science, drive for excellence were ever consistent. I would like to believe that he helped to instill this within me. His seemingly endless resources and contacts greatly enhanced the overall quality of my education and for that I will be forever grateful. I am also eternally indebted to him for allowing me to explore many research avenues even if they resulted in little to no outcome. As a mentor he allows the freedom and flexibility to learn and succeed. I have learned much over the course of my PhD, in great part due to him.

Claus Michael Lehr gave me an unprecedented opportunity to explore the German and global research environment. What I took from this experience has forever impacted the rest of my life. I am truly thankful for the opportunity and his overall impact on my research growth.

Alana Welm and David Grainger consistently helped me to identify important holes in my research. I am also indebted to their ability to instill the fear of god in me, despite their overall friendly demeanor, and as a result I have become a better scientist. I admire their work, love of science, drive to help students to succeed and support to make

the overall research community a better one. I strive to one day be in the same scientific league as these gentle giants.

I would like to thank Ilya Zharov for his and his lab's support in developing and characterizing silica nanoparticles. Without his guidance I truly would have been in a world of trouble.

Vladimir Hlady gave me an opportunity to go abroad during my PhD. The most fun and most important lessons I have learned in life were learned while I was there. He also instilled in me a respect for surface chemistry, protein adsorption, characterization and analysis. He is a true scientist.

Alexander Malugin, a gifted molecular biologist and mentor. Sasha gave me the gift of biology. He taught me well and instilled in me the importance of careful planning and meticulous experimental design. I will always be grateful for his guidance and support.

Nicole Daum, a friend, excellent scientist and mentor. Nicole was the first person I encountered as a student who truly understood the dynamic of the nanoparticle biological interface. She instilled this within me and for that I am grateful.

Arwyn Jones, his help was invaluable in the production and understanding of the work that I completed in endocytosis. His wit and scientific vigor have allowed me to become a better scientist.

Nancy Chandler, a gifted TEM giant and friend. She always provided me with the picture which spoke 1,000 words and did so with kindness and strength.

Cassandra Rice, a gifted molecular biologist, friend and *ad hoc* mentor. She was always willing to teach, share, and debate an idea, enhancing my overall educational

experience. I hope to someday give back to her as much as she has given to me.

My undergraduate student, Kristopher Bartlett, I am grateful for his help with the *in vivo* portion of this dissertation and being my extra hands.

Joshua Gustafson, my life ear and scientific sound board. His unconditional faith, support and love have kept me going when I wanted to fall. He drives me to be a better person and scientist, for this I will always have thanks.

Finally, to my family and friends you kept me sane and for that I am forever grateful.

INTRODUCTION

1.1 Introduction

Nanomaterials may be capable of directing specific internal cell trafficking and processing pathways. Specific trafficking and pathways can, in turn, lead to significant advances in overcoming roadblocks to drug delivery, which have prevented many types of treatments from becoming viable therapies. Nanoparticles can also be used as antigen presentation delivery vehicles, providing new routes of immunostimulation and potential vaccination. Despite the potential of engineered nanoparticles to traffic to specific intracellular destinations, little is known about the influence of their physicochemical properties on complex interactions with the surrounding milieu. To understand how nanomaterials are processed *in vivo* and their translational potential, we must first understand nanoparticle cellular uptake and intracellular fates. Cellular uptake and fate can be used to predict physiological destinies and engineer more effective multifunctional diagnostics and therapeutics.

Slight alterations in physicochemical properties of nanomaterials can significantly influence how they interact with the biological milieu (1-7). The impact of physicochemical properties on cellular uptake pathways and intracellular fates is important for drug delivery (8-13). Alterations in surface characteristics can produce unexpected adverse events, for example induced inflammatory cascades, mitochondrial dysfunction and autophagy (4, 6, 14-19).

A better understanding of how the interface between host and nanomaterial influences uptake, transport, distribution, and initiation of biological mechanistic responses will create increased therapeutic benefit and safety of nanomaterials as potential delivery agents. While evidence suggests that physicochemical characteristics profoundly influence these biological responses, not all characteristics are equally important and many responses are not understood. Ideally, one could assess, predict and correlate host biological response to various physicochemical characteristics of nanomaterials. Phagocytes are believed to initiate host biological responses and may help to solve global delivery issues.

Phagocytes are important players in host exposure to nanomaterials by processing and possibly contributing to host toxicity. Macrophages, in particular, are believed to be among the first responders and primary cell types that uptake and process nanoparticles. Macrophages may also mediate host biological responses by interacting with inflammatory signaling pathways and immune cells. Further, *in vitro* macrophage model systems have proven more susceptible to nanoparticle treatment and tend to predict *in vivo* outcomes better than other cellular *in vitro* systems (3).

Phagocytes recognize and process nanoparticles *in vivo*. Clinical data show a correlation of increased phagocytic activity with decreased therapeutic efficacy of carrier-mediated anticancer agents and with increased clearance rates in patients (20, 21). Increased residence time of nanomaterials in clearance organs is also generally attributed to increased phagocytic recognition *in vivo* (22-28). Inflammatory gene expression upregulation and increases in inflammatory phenotypes occur both *in vitro* and *in vivo* following nanoparticle exposure (10, 13, 29-38). How nanomaterials are recognized,

internalized, trafficked, and distributed within macrophages will help to eliminate this inflammatory response *in vitro* and *in vivo*.

The work in this dissertation will focus primarily on correlating macrophage responses to engineered silica nanoparticle exposure as a function of nanoparticle physicochemical characteristics, where results can be used to manipulate mechanisms of uptake and intracellular fate within macrophages. By deriving this basic understanding of initiation of biological responses, it will be possible to develop a platform with the ability to make either macrophage-targeted or macrophage-invisible systems with specific intracellular uptake and fates.

1.2 Hypothesis and Aims of this Dissertation

The central hypothesis is that engineered silica nanoparticle intracellular uptake and fate in macrophages can be manipulated by alterations in geometry and in surface characteristics, as discussed in the three aims below. A correlative understanding between how physicochemical properties induce macrophage uptake and fate could improve the therapeutic effect of drug delivery systems and avoid deleterious effects. This hypothesis was tested through three Specific Aims:

1. Assess the toxicity and intracellular fate of engineered positively charged silica nanoparticles as a function of geometry in macrophages.
2. Evaluate the intracellular uptake of positively charged silica nanoparticles as a function of geometry in macrophages.
3. Investigate the influence of variations in macrophage phenotype on cellular uptake and intracellular fate *in vitro* and *in vivo*.

1.2.1 Specific Aim 1: Assess the toxicity and intracellular fate of engineered positively charged silica nanoparticles as a function of geometry in macrophages

Successful clinical nanoparticle candidates deliver high payloads of therapeutics to intended intracellular compartments, increasing efficacy and minimizing potential side effects. The understanding of how physicochemical characteristics influence intracellular compartment delivery, however, is limited. Within this aim we evaluate the intracellular fate of highly positive-charged silica nanoparticles with geometric variations, to determine the effect of geometry on intracellular fate. Interestingly, changes in geometry did not alter intracellular fate within RAW 264.7 macrophages. In response to silica nanoparticle exposure macrophages induced autophagy, which, within this context, could follow autonomous antimicrobial defense mechanisms. Autophagic mechanisms appear to aid in cellular coping, reduce toxicity, provide potential clearance mechanisms and initiate nanoparticle stability *in vivo* (39). Other groups have shown similar fates for highly positive-charged gold nanoparticles, iron oxide, polyplexes and dendrimers (40-44). These results suggest that in some cases positively charged particles should not be used for targeted intracellular delivery. This is especially true in cases where the payload needs to be delivered to a specific intracellular compartment since positively charged systems are most likely trafficked to intracellular compartments that do not allow for therapeutic escape.

1.2.2 Specific Aim 2: Evaluate the intracellular uptake of positively charged silica nanoparticles as a function of geometry in macrophages

Chapter 4 evaluates the ability of nanoparticle geometry to induce uptake mechanisms. The results show that nanoparticle physicochemical characteristics, specifically geometry and surface contact area, can be manipulated to induce endocytosis and phagocytosis. By inducing pinocytosis/phagocytosis, intracellular fate gene expression was altered, which suggests that manipulation of uptake mechanisms of nanoparticles could lead to specific intracellular fates (45). For example, endosomal compartments have known internal intracellular trafficking receptors, which can be drug targets (46). In this case, therapeutic efficacy would benefit from specific uptake and endosomal trafficking mechanisms. Such design manipulation would likely enhance targeted intracellular delivery. This chapter suggests that altering the geometry or cellular surface contact area of the delivery system will enhance design. Therefore, Chapter 4 suggests directing intracellular uptake mechanisms would be advantageous when developing delivery systems in order to influence fate or avoid deleterious effects.

In addition Chapters 3 and 4 contain supplemental information on the impact of physicochemical characteristics on intracellular uptake and fate in A549 cells. A549 cells are a human lung cancer model system, which behaves similarly to RAW 264.7 cells. In Chapter 4, A549 cells were compared to primary human lung epithelial cells. Results showed that A549 cells did not uptake particles like normal human lung tissue. In Chapter 4, RAW 264.7 macrophages, however, did follow similar particle uptake and trafficking patterns when compared to normal primary human macrophages. Due to the

lack of comparison between normal tissue and A549 cells, I present the data but have opted to leave a discussion of that data out of this dissertation.

1.2.3 Specific Aim 3: Investigate the influence of variations in macrophage phenotype on cellular uptake and intracellular fate *in vitro* and *in vivo*

Macrophages have been shown to alter phenotype and differentiation states as a function of their environmental cues *in vitro* and *in vivo* (47). The various macrophage phenotypes perform different physiological functions *in vivo*. Therefore it is possible to infer that different macrophage phenotypes are likely to exhibit different intracellular uptake and fate pathways when interacting with nanoparticles. Chapter 5 explores the uptake, toxicity and intracellular fate of nanoparticles within two *in vitro* macrophage polarization models: M1 induced with INF-gamma and LPS, and M2 induced with IL-4. Afterwards, the macrophage polarization results are correlated to *in vivo* systems.

This exploration found nanoparticle uptake, morphology and cytokine/chemokine release are altered by changes in macrophage phenotype. Results suggest that M1 macrophages are the primary mediators for nanoparticle uptake, while M2 macrophages appear to play little to no role. Macrophage residence within splenic and liver tissues increases over time. Liver and splenic tissues were also shown to be the primary sites of nanoparticle accumulation via quantitative ICP-MS. *In vivo*, M1 macrophages were primarily upregulated and nanoparticles appeared to be accumulating within the vacuoles of these cells. This work shows that M1 macrophage-mediated uptake could influence *in vivo* and *in vitro* silica nanoparticle processing.

This final aim demonstrates the importance of selecting for phenotype in *in vitro* studies investigating nanoparticle design. Specifically, Chapter 5 shows a higher correlation to *in vivo* results when utilizing M1 model systems. This system may provide an *in vitro* mechanism to study macrophage avoidance *in vivo*, helping to improve *in vivo* payload delivery and therapeutic effect.

This dissertation discusses nanoparticle physicochemical characteristic influence on biological interactions. A review of literature relevant to this work is discussed in Chapter 2 (48). Chapter 3 discusses the impact of physicochemical characteristics on intracellular fate. Chapter 4 discusses the impact of physicochemical characteristics on intracellular uptake. Chapter 5 discusses the impact of macrophage phenotype on uptake and fate and correlates this to *in vivo* mechanisms. (39, 45, 49). Across these chapters I will explore the possibility of manipulating physicochemical characteristics to influence nanoparticle macrophage mediated uptake and intracellular fate. Finally, Chapter 6 will discuss conclusions and future directions.

1.3 References

1. Aggarwal P, Hall JB, McLeland CB, Dobrovolskaia MA, McNeil SE. Nanoparticle interaction with plasma proteins as it relates to particle biodistribution, biocompatibility and therapeutic efficacy. Adv Drug Deliv Rev. 2009;61(6):428-37.

2. Albanese A, Tang PS, Chan WC. The effect of nanoparticle size, shape, and surface chemistry on biological systems. Annu Rev Biomed Eng. 2012;14:1-16.

3. Dobrovolskaia MA, McNeil SE. Understanding the correlation between in vitro and in vivo immunotoxicity tests for nanomedicines. J Control Release. 2013;172(2):456-66.

4. Etheridge ML, Campbell SA, Erdman AG, Haynes CL, Wolf SM, McCullough J. The big picture on nanomedicine: the state of investigational and approved nanomedicine products. Nanomedicine: Nanotechnology, Biology, and Medicine. 2013;9(1):1-14.

5. Greish K, Thiagarajan G, Ghandehari H. In vivo methods of nanotoxicology. Methods Mol Biol. 2012;926:235-53.

6. Karmali PP, Simberg D. Interactions of nanoparticles with plasma proteins: implication on clearance and toxicity of drug delivery systems. Expert Opin Drug Deliv. 2011;8(3):343-57.

7. Walkey CD, Chan WC. Understanding and controlling the interaction of nanomaterials with proteins in a physiological environment. Chem Soc Rev. 2012;41(7):2780-99.

8. Chao Y, Karmali PP, Mukthavaram R, Kesari S, Kouznetsova VL, Tsigelny IF, et al. Direct recognition of superparamagnetic nanocrystals by macrophage scavenger receptor SR-AI. ACS Nano. 2013;7(5):4289-98.

9. Lunov O, Zablotskii V, Syrovets T, Rocker C, Tron K, Nienhaus GU, et al. Modeling receptor-mediated endocytosis of polymer-functionalized iron oxide nanoparticles by human macrophages. Biomaterials. 2011;32(2):547-55.

10. Orr GA, Chrisler WB, Cassens KJ, Tan R, Tarasevich BJ, Markillie LM, et al. Cellular recognition and trafficking of amorphous silica nanoparticles by macrophage scavenger receptor A. Nanotoxicology. 2011;5(3):296-311.

11. Gratton SE, Ropp PA, Pohlhaus PD, Luft JC, Madden VJ, Napier ME, et al. The effect of particle design on cellular internalization pathways. Proc Natl Acad Sci U S A. 2008;105(33):11613-8.

12. Champion JA, Mitragotri S. Role of target geometry in phagocytosis. Proc Natl Acad Sci U S A. 2006;103(13):4930-4.

13. Sharma G, Valenta DT, Altman Y, Harvey S, Xie H, Mitragotri S, et al. Polymer particle shape independently influences binding and internalization by macrophages. J Control Release. 2010;147(3):408-12.

14. Dobrovolskaia MA, Aggarwal P, Hall JB, McNeil SE. Preclinical studies to understand nanoparticle interaction with the immune system and its potential effects on nanoparticle biodistribution. Mol Pharm. 2008;5(4):487-95.

15. Fubini B, Hubbard A. Reactive oxygen species (ROS) and reactive nitrogen species (RNS) generation by silica in inflammation and fibrosis. Free Radic Biol Med. 2003;34(12):1507-16.

16. Zhu M, Nie G, Meng H, Xia T, Nel A, Zhao Y. Physicochemical properties determine nanomaterial cellular uptake, transport, and fate. Acc Chem Res. 2013;46(3):622-31.

17. Khan MI, Mohammad A, Patil G, Naqvi SA, Chauhan LK, Ahmad I. Induction of ROS, mitochondrial damage and autophagy in lung epithelial cancer cells by iron oxide nanoparticles. Biomaterials. 2012;33(5):1477-88.

18. Wang F, Gao F, Lan M, Yuan H, Huang Y, Liu J. Oxidative stress contributes to silica nanoparticle-induced cytotoxicity in human embryonic kidney cells. Toxicol In Vitro. 2009;23(5):808-15.

19. Xia T, Kovochich M, Brant J, Hotze M, Sempf J, Oberley T, et al. Comparison of the abilities of ambient and manufactured nanoparticles to induce cellular toxicity according to an oxidative stress paradigm. Nano Lett. 2006;6(8):1794-807.

20. Caron WP, Song G, Kumar P, Rawal S, Zamboni WC. Interpatient pharmacokinetic and pharmacodynamic variability of carrier-mediated anticancer agents. Clinical Pharmacology and Therapeutics. 2012;91(5):802-12.

21. Caron WP, Lay JC, Fong AM, La-Beck NM, Kumar P, Newman SE, et al. Translational studies of phenotypic probes for the mononuclear phagocyte system and liposomal pharmacology. J Pharmacol Exp Ther. 2013;347(3):599-606.

22. He X, Nie H, Wang K, Tan W, Wu X, Zhang P. In vivo study of biodistribution and urinary excretion of surface-modified silica nanoparticles. Anal Chem. 2008;80(24):9597-603.

23. Huang X, Li L, Liu T, Hao N, Liu H, Chen D, et al. The shape effect of mesoporous silica nanoparticles on biodistribution, clearance, and biocompatibility in vivo. ACS Nano. 2011;5(7):5390-9.

24. Kumar R, Roy I, Ohulchanskky TY, Vathy LA, Bergey EJ, Sajjad M, et al. In

vivo biodistribution and clearance studies using multimodal organically modified silica nanoparticles. ACS Nano. 2010;4(2):699-708.

25. Liu T, Li L, Teng X, Huang X, Liu H, Chen D, et al. Single and repeated dose toxicity of mesoporous hollow silica nanoparticles in intravenously exposed mice. Biomaterials. 2011;32(6):1657-68.

26. Liu Y, Hu Y, Huang L. Influence of polyethylene glycol density and surface lipid on pharmacokinetics and biodistribution of lipid-calcium-phosphate nanoparticles. Biomaterials. 2014;35(9):3027-34.

27. Ohno K, Akashi T, Tsujii Y, Yamamoto M, Tabata Y. Blood clearance and biodistribution of polymer brush-afforded silica particles prepared by surface-initiated living radical polymerization. Biomacromolecules. 2012;13(3):927-36.

28. Owens DE, 3rd, Peppas NA. Opsonization, biodistribution, and pharmacokinetics of polymeric nanoparticles. Int J Pharm. 2006;307(1):93-102.

29. Albanese A, Sykes EA, Chan WC. Rough around the edges: the inflammatory response of microglial cells to spiky nanoparticles. ACS Nano. 2010;4(5):2490-3.

30. Bonilla DL, Bhattacharya A, Sha Y, Xu Y, Xiang Q, Kan A, et al. Autophagy regulates phagocytosis by modulating the expression of scavenger receptors. Immunity. 2013;39(3):537-47.

31. Carter JM, Driscoll KE. The role of inflammation, oxidative stress, and proliferation in silica-induced lung disease: a species comparison. J Environ Pathol Toxicol Oncol. 2001;20 Suppl 1:33-43.

32. Cho WS, Choi M, Han BS, Cho M, Oh J, Park K, et al. Inflammatory mediators induced by intratracheal instillation of ultrafine amorphous silica particles. Toxicol Lett. 2007;175(1-3):24-33.

33. Driscoll KE. TNFalpha and MIP-2: role in particle-induced inflammation and regulation by oxidative stress. Toxicol Lett. 2000;112-113:177-83.

34. Gazi U, Martinez-Pomares L. Influence of the mannose receptor in host immune responses. Immunobiology. 2009;214(7):554-61.

35. Nishanth RP, Jyotsna RG, Schlager JJ, Hussain SM, Reddanna P. Inflammatory responses of RAW 264.7 macrophages upon exposure to nanoparticles: role of ROS-NFκB signaling pathway. Nanotoxicology. 2011;5(4):502-16.

36. Pajarinen J, Kouri VP, Jamsen E, Li TF, Mandelin J, Konttinen YT. The response of macrophages to titanium particles is determined by macrophage polarization. Acta Biomater. 2013;9(11):9229-40.

37. Park EJ, Park K. Oxidative stress and pro-inflammatory responses induced by silica nanoparticles in vivo and in vitro. Toxicol Lett. 2009;184(1):18-25.

38. Velard F, Braux J, Amedee J, Laquerriere P. Inflammatory cell response to calcium phosphate biomaterial particles: an overview. Acta Biomater. 2013;9(2):4956-63.

39. Herd HL, Malugin A, Ghandehari H. Silica nanoconstruct cellular toleration threshold in vitro. J Control Release. 2011;153(1):40-8.

40. Chen GY, Yang HJ, Lu CH, Chao YC, Hwang SM, Chen CL, et al. Simultaneous induction of autophagy and toll-like receptor signaling pathways by graphene oxide. Biomaterials. 2012;33(27):6559-69.

41. Li JJ, Hartono D, Ong CN, Bay BH, Yung LY. Autophagy and oxidative stress associated with gold nanoparticles. Biomaterials. 2010;31(23):5996-6003.

42. Perez-Carrion MD, Perez-Martinez FC, Merino S, Sanchez-Verdu P, Martinez-Hernandez J, Lujan R, et al. Dendrimer-mediated siRNA delivery knocks down Beclin 1 and potentiates NMDA-mediated toxicity in rat cortical neurons. J Neurochem. 2012;120(2):259-68.

43. Wu L, Zhang Y, Zhang C, Cui X, Zhai S, Liu Y, et al. Tuning cell autophagy by diversifying carbon nanotube's surface chemistry. ACS Nano. 2014;8(3):2087-99.

44. Vercauteren D, Deschout H, Remaut K, Engbersen JF, Jones AT, Demeester J, et al. Dynamic colocalization microscopy to characterize intracellular trafficking of nanomedicines. ACS Nano. 2011;5(10):7874-84.

45. Herd H, Daum N, Jones AT, Huwer H, Ghandehari H, Lehr CM. Nanoparticle geometry and surface orientation influence mode of cellular uptake. ACS Nano. 2013;7(3):1961-73.

46. Hymel D, Peterson BR. Synthetic cell surface receptors for delivery of therapeutics and probes. Advanced Drug Delivery Reviews. 2012;64(9):797-810.

47. Wynn TA, Chawla A, Pollard JW. Macrophage biology in development, homeostasis and disease. Nature. 2013;496(7446):445-55.

48. Herd H, Ghandehari H. Synthetic and toxicological characteristics of silica nanomaterials for imaging and drug delivery applications. Sitharaman B, editor. Boca Raton, FL: CRC Press; 2011.

49. Herd H, Ghandehari H. Phagocytic silica nanoparticle response is phenotypically dependent. Submitted to Biomaterials.

CHAPTER 2

LITERATURE BACKGROUND

2.1 Introduction

Nanoparticles have substantial clinical potential; they may be capable of directing specific internal cell trafficking and processing pathways that could lead to significant advances in overcoming roadblocks to drug delivery that have prevented many types of treatments from becoming viable therapies. For example, hydrophobic drugs, nucleic acids and proteins have been encapsulated within nanoparticles to reduce intracellular degradation, increase circulation and improve efficacy. As a result, nanoparticles as antigen presentation delivery vehicles have become more popular, providing new routes of immunostimulation and potential vaccination. In 2013, 241 companies and institutions had, combined, 789 ongoing clinical trials and 103 unique investigational products in nanomedicine (1).

However, despite the great potential and sharp rise in clinical trials and investigational products, only 38 products have received FDA-approval across the 60 years of investigational research (1). The field of nanomedicine faces significant challenges related to clinical development when compared to the 32 traditional small molecular weight therapeutics the FDA approved in 2012 alone. Nanomaterials face a different set of challenges from small molecular weight therapeutics given that

nanomaterials are on the same size scale as biologicals, facilitating increased interactions. The size scale may also help to explain limitations in clinical translation, probably connected to nanoparticle clearance potential. This chapter will discuss nanoparticle clearance, the cells responsible, and strategies to attain better retention to improve translatability.

Slight alterations in properties of nanomaterials can significantly influence how these materials interact with the biological milieu (1-7). Surface characteristics may also produce unexpected adverse biological events, for example, induced inflammatory cascades, mitochondrial dysfunction and autophagy (1, 6, 8-14). The impact of drug delivery properties is particularly important on cellular uptake pathways and intracellular fate destinations (15-21). A better understanding of how the interface between host and nanomaterial influences uptake, transport, distribution and initiation of biological mechanistic responses is required to assess therapeutic benefit and safety. Ideally, one could assess, predict and correlate host biological response to various physicochemical characteristics of nanomaterials. Physicochemical characteristics, such as surface chemistry, charge, shape and topography profoundly influence uptake, transport, distribution and initiation of biological mechanistic responses. However, not all characteristics are equally important and few mechanisms are clear. Yet, phagocytes appear to play a clear role in modulation of these responses.

Phagocytes are important players in host mechanistic responses to nanomaterials, processing these materials and contributing to host toxicity. Macrophages, in particular, are among the “first responders” and primary cell types that uptake and process nanoparticles, mediating host biological responses by subsequent interactions with host

inflammatory signaling pathways and immune cells. The following examples will help to illustrate the need to understand how nanomaterials are recognized, internalized, trafficked and distributed within macrophages and how macrophage response influences outcomes *in vivo*. *In vitro* macrophage model systems have proven more susceptible to nanoparticle treatment and tend to predict *in vivo* outcomes better than their *in vitro* counterparts (4). Clinical data have correlated increased phagocytic activity to decreased therapeutic efficacy of nanoconstructs and increased clearance rates in patients (22, 23), while increased residence time of nanomaterials in clearance organs is also generally attributed to increased phagocytic recognition *in vivo* (24-30). Following nanoparticle exposure, inflammatory gene expression and phenotypes increase both *in vitro* and *in vivo* (18, 21, 31-40). Macrophages clearly play an essential role in nanoparticle processing and neglecting their role could be detrimental to nanoparticle translation.

In this chapter, I will argue that a majority of the nanoparticle drug delivery and imaging literature has neglected the role of macrophages in *in vivo* nanoparticle processing, which has caused deficiencies in nanoparticle design resulting in limited clinical translation. Design and translation could be improved by understanding macrophage-nanoparticle interactions. This chapter will address failures and success of nanomaterials as a function of macrophage nanomaterial interactions with the goal of improving translational capacity.

2.1.1 The role of the mononuclear phagocytic system in nanoparticle processing

The low FDA approval rates, mentioned earlier, of nanoparticle therapeutics and diagnostics illustrate the limitation of nanoparticle clinical translation in human patient populations. Failure can be attributed to rapid excretion of therapeutics and diagnostics or induction of inflammatory responses due to nonspecific recognition and uptake of nanoconstructs by macrophages. Rapid excretion limits accumulation at target delivery sites and inflammatory responses induce toxicity.

Clinical trials of IV-administered systems, which represent 120 of these 789 ongoing clinical trials, illustrate the important role of excretion rates and the important clinical role of the mononuclear phagocytic system (MPS) in nanoparticle delivery. Successful nanoparticle clinical candidates should deliver high payloads to target sites; however, only ~.01% of the total injected dose of drug is delivered to its target site (outside of the liver and spleen). The other 99.99% of dose ends up being cleared or residing in nonspecific clearance organs (41).

Current literature attributes this to the rapid association of these nanomedicines with elements of the MPS (42). To some extent association of nanoparticles with the mononuclear phagocytic system is a function of the opsonization that the particle undergoes when exposed to the blood and the recognition of these opsins via the MPS (43), particularly Kupffer cells and splenic macrophages. If macrophages are indeed responsible for high clearance rates, the disappointing efficacy due to poor delivery of active drug payloads to specific targets is likely a result of macrophage-nanoparticle recognition and subsequent processing. If delivery vehicles were designed such that they

either avoided or harnessed this recognition system, payload delivery and subsequent efficacy could be enhanced significantly. However, in order to design appropriate systems an understanding is needed of nanoparticle-macrophage interactions both at a cellular and a system-wide level. Macrophages recognize opsonized proteins, specific surface chemistries, and other surface and biological characteristics marking these nanoparticles for clearance and/or toxicological fates. Physicochemical characteristics can influence these interactions and may also potentiate toxicological mechanisms. What is not understood is how nanoparticle surfaces interact with the biological environment and how this interaction influences phagocytic clearance and toxicological fates. Developing a correlation between nanoparticle physicochemical characteristics and nanoparticle uptake, processing and clearance mechanisms in macrophages would aid the design of new, more efficacious and safer nanomaterial platforms.

While increased clearance capacity and improved circulation rates would be beneficial to increasing translation, the future of nanomaterial design needs to focus on reducing nanoparticle inflammatory related toxicity. Safer nanoparticle platforms are key to ensuring clinical translation and an understanding of MPS-nanoparticle interactions could help to design new nanoparticle systems to avoid inflammatory adverse events. Orthopedic implant-centered inflammation represents one of the best clinical examples of induced MPS-nanoparticle inflammation. Implanted metallic biomaterials, such as those utilized in total knee or hip replacements, release nanoparticulates as a result of environmental stress placed on the given medical device. Released nanoparticles are believed to cause the development of aseptic osteolysis, which is the result of local macrophage recruitment, i.e., phagocytosis of the particles shed from the device, and a

resulting local inflammatory response (44). Patient hip tissue samples from cases of implant-centered inflammation have been examined histopathologically and large numbers of CD68-positive foamy macrophage cells were observed in the surrounding tissue (44). The increased macrophage populations indicate large local macrophage recruitment as a result of implant inflammation. Subsequent gene expression analysis illustrated that foamy macrophages are strongly associated with expression of osteolytic proteins (44). These findings have been correlated *in vitro* with macrophage inflammatory genomic profiling as a result of particle wear exposure (45). This suggests the role of macrophages in the induction of aseptic osteolysis, a chronic local inflammatory disorder. This local inflammatory reaction could be indicative of what could result in tissue; with a large accumulation of nanoparticles this could facilitate similar inflammatory mechanisms. These mechanisms could cause negative inflammatory effects in certain tissue accumulation sites, especially clearance organs, potentially impacting future nondegradable nanoparticle design for imaging or drug delivery systems.

2.1.2 What is a phagocyte/macrophage?

Understanding the role of macrophages in nanoparticle processing requires a basic understanding of macrophage cellular characteristics. What is not well known is how these cellular characteristics influence cellular-nanoparticle interactions, required for effective design of nanomaterials. Ideally, a correlation would be drawn between nanoparticle-macrophage interactions and *in vivo* delivery fates and toxicity, improving circulation, safety and clearance potential of nanomaterials.

Macrophages are key *in vivo* components of normal inflammatory and immunological processes. Certain forms of this cell type are essential in the destruction and removal of deleterious materials, pathogens, and damaged or abnormal tissue from the body; these native roles may be used in nanoparticle processing. These cell types also play an essential role in wound healing, introducing local angiogenesis and tissue remodeling. Macrophages also play a primary role in the macroscale foreign body response to engineered biomaterial implants, initiating local fibrosis and unresolved inflammation. These pathologies may also be implicated in the *in vivo* fate of nanomaterials. Alterations in the role of macrophages arise from changes in phenotypic characteristics, which may also induce variations in nanoparticle interactions.

Macrophage is a broad classification for a cell type whose phenotype is influenced by environmental cues that alter morphology, surface receptor expression and function. Phenotypic changes induce variations in interactions with nanoparticles, as changing surface receptors and overall function can alter recognition and uptake patterns. Understanding macrophage phenotype and lineage may help to identify how to harness uptake and recognition patterns. Macrophages had been thought to derive solely from the hematopoietic stem cell (HSC) lineage; however, more recent literature in the field of developmental biology observed some of these cells in the embryo prior to the development of HSC lineage. This suggests that at least a portion of what we currently classify as macrophages may be genetically distinct from the hematopoietic progeny, suggesting that in order to understand macrophage-nanoparticle interactions one must look at multiple phagocytic model systems (46). Experts studying dendritic cells and macrophages, both subsets of traditional end point HSC cell types, recently suggested

that these subsets are more similar than originally thought (47). These two cell types might be phenotypes of the same cell.

As stated previously, the large variations in morphological features and functional roles of this cell type may be due simply to environmental factors. Evidence suggests that local microenvironmental factors and cues drastically alter the phenotype and differentiation states of macrophages (48). Environmental factors directly impact how these cells interact, positively or negatively, with the surrounding tissue and homeostatic environment, and also may impact how they process nanomaterials *in vivo*.

2.1.2.1 Macrophage interaction with extracellular environment

The response of macrophages to their local external environment has the potential to substantially impact how nanomaterials are handled *in vivo,* understanding this impact could improve delivery. The following two studies illustrate the need to understand the overall state of macrophages *in vivo* and how macrophage responses to unrelated factors may potentially drastically alter the quiescence and uptake of nanoparticulate drug delivery systems, such as systemic inflammation or specific disease states. In the first study, local activation of normally quiescent tissue macrophages may rearrange surface receptors, which make them more susceptible to nanoparticle recognition, and leads to abnormally increased internalization rates in phagosomes (49). Increased clearance rates were observed in animals treated with zymosan to activate local macrophages. This appears to be opsonization-independent and is enhanced compared to control (50). A similar study evaluated the priming effect of INF-gamma on the increased uptake of chitin particles in an alveolar macrophage model (49). This priming enhanced uptake

within the macrophage system and probably polarized them to a more phagocytic phenotype. This heightened phagocytic phenotype would account for the observed increase in uptake.

2.1.2.2 Macrophage phenotype and environmental factors

Macrophage polarization states drastically alter nanoparticle uptake and biological response, so understanding this impact could improve delivery. According to the Th1/Th2 paradigm, in some cases macrophages can reside within a classically activated state (M1) or alternatively activated state (M2). M1s are induced via INF-gamma and are what we would normally consider immune-activating phagocytic janitorial cells. M2s are induced via IL-4/IL-13 and activate angiogenesis, immune suppression and tissue breakdown/remodeling (Figure 2.1). However, the Th1/Th2 model system has proven to be overly simplified, as many macrophages lie in a state in-between the M1 and M2, or even in an M1/M2 unrelated cellular state. However, the Th1/Th2 system does permit the study of how environmental factors can influence nanoparticle processing. For example, M1 macrophages provide the most robust and drastic response to titanium particulate exposure, when compared to M2s. M1s increased inflammatory cytokine and chemokine production, while M2 cells, despite uptaking particles, showed a broad suppressed inflammatory response. This difference suggests that microenvironmental factors capable of inducing phenotypic changes can influence how cells, particularly macrophages, might respond to particulate exposure (38). Suggesting one should use multiple phenotypes in *in vitro* culture model systems to ensure that relevant correlative *in vivo* information is derived. Variations in surface characteristics or adsorbed proteins may alter how

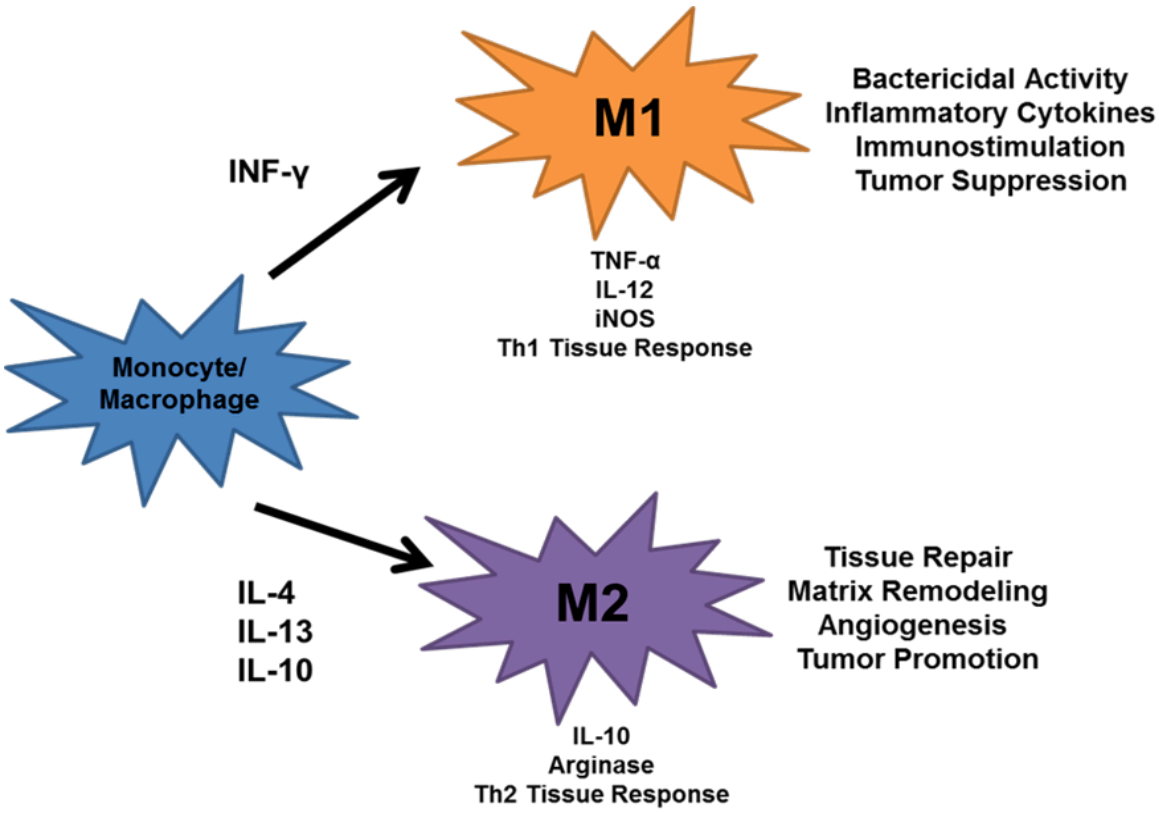

Figure 2.1: Environmental impact on macrophage phenotype and function. Environmental cytokines known to induce specific macrophage phenotypes are outlined below the arrows. The cytokines/chemokines that are known to be released from the specific macrophage phenotypes are outlined below the macrophages. The functions of the phenotype *in vivo* are outlined to the right of the macrophages.

nanoparticles interact with macrophage phenotypes.

2.1.3 Presentation of nanomaterials to phagocytes

A host system never sees a bare nanomaterial, due to immediate host protein adsorption upon blood or tissue contact (e.g., serum proteins such as IgG, fibrinogen, or albumin). As the field of nanomaterials progresses, it becomes essential to understand the adsorption process of proteins and what characteristics of nanoparticles initiate desired and adverse effects, as well as how presence and conformation of adsorbed proteins influences the presentation of nanoparticles to phagocytes. Understanding this recognition will help to ensure that nanoparticles are not cleared too rapidly or induce adverse toxicological effects. The composition and conformation of proteins adsorbed to the surface of nanoparticles influences how nanoparticles interact with macrophage surface receptors and mediates phagocytic recognition. Depending on the nature of protein adsorption to a surface, conformational changes could occur which can facilitate adverse opsonization, initiating phagocytosis and potentially inflammatory reactions. Physicochemical characteristics are important mediators of such adsorptive properties. Conformational changes in these proteins can result from surface curvature, topography and hydrophobicity. These adsorption characteristics allow for the presentation of nanoparticles to phagocytes to vary widely, initiating both advantageous and adverse events, which could range from bioinvisibility to complement activation resulting in increased toxicity.

2.1.3.1 Surface curvature

The physicochemical characteristics of the surface of nanoparticles can influence protein conformational adsorption to nanomaterials, which can increase or decrease phagocytic recognition. If the protein maintains its original conformation, detrimental cellular uptake or induced toxicity is unlikely to occur. However if native protein confirmation is not maintained, certain epitopes can be exposed and this may initiate phagocytic uptake, complement activation, or thrombosis formation. Surface curvature of nanoparticles has been proven to stabilize protein conformation (51); however, the degree of curvature can drastically affect this stabilization and cause stable and irreversible protein denaturation. For example, Vertegel et al. (52) found that lysozyme adsorbs to the surface of silica nanomaterials with diameters as small as 4 nm and as large as 100 nm. They further observed that smaller nanoparticles with higher surface curvatures retained native conformational shapes of lysozyme to a greater degree than larger nanoparticles with less surface curvature. Albumin was also observed to retain its native conformation on particles with a higher surface curvature while fibrinogen exhibited the opposite effect (53). These studies suggest that all protein adsorption onto nanoparticle surfaces could potentially be manipulated through controlling surface curvature. While albumin adsorption onto large silica nanoparticles does not appear to significantly perturb its conformation, macrophage uptake of albumin-coated silica occurs via scavenger surface receptors and fibrinogen adsorption of Mac-1 surface recognition (43, 54). Recognition of conformationally modified proteins via surface receptors may potentiate faster clearance and/or local inflammatory and fibrotic events, which would be adverse to nanoparticle design.

2.1.3.2 Topography

Similar to surface curvature, surface topography of nanoparticles could cause protein adsorption or alterations in protein folding, influencing phagocytic cellular uptake (55). Bovine serum albumin (BSA), for example, adsorbs more heavily to rough platinum surfaces compared to smooth platinum surfaces (56). Increased BSA adsorption likely explains why rough gold nanomaterials have shown reduced uptake when compared to smooth gold nanorods and spheres in neuronal microglial cells (31), suggesting that uptake might be a function of variations in protein coronas. These spikey gold nanoparticles also interact with proteins on neuronal cell surfaces, which seemed to facilitate reduced expression of certain proteins, such as granulocyte macrophage colony stimulating factor (31). The result of this protein adsorption was a dissipation of phagocytic activity of these systems. Further studies could elucidate how to enhance such topography to help create "bioinvisible" systems by encouraging adsorption of specific proteins in specific conformations.

2.1.3.3 Surface hydrophilicity and hydrophobicity

Altering surface hydrophilicity can influence protein adsorption, potentially decreasing phagocytic recognition of nanomaterials increasing circulation times. The degree of surface hydrophobicity in gold nanoparticles (57) affects the amount of albumin adsorbed to nanoparticle surfaces. More hydrophobic nanoparticles exhibit increased albumin adsorption, which drastically decreases their cellular uptake when compared to hydrophilic systems with less albumin adsorption. Poly(ethylene glycol) (PEG) is another common surface modification, used to increase hydrophilicity and

reduce nanomaterial recognition. PEG increases the blood half-life of many injected materials, leading to decreased macrophage uptake and protein adsorption in a grafting density-dependent manner (58). This study illustrates the importance of surface hydrophilicity on phagocytic uptake, illustrating that increasing density and hydrophilicity helps to reduce uptake and increase circulation to improve translation.

The curvature, topography and hydrophobicity of a nanoparticle illustrate only a few of the physicochemical characteristics that can be changed to show that physicochemical characteristics play an essential role in the adsorption process of proteins on the surface of nanomaterials. Other characteristics could potentially alter these profiles as well. For a more extensive review on nanoparticle protein adsorption, readers are directed to recent reviews on the topic(6, 7).

2.1.4 Phagocytic uptake and intracellular fate

The mechanisms by which the body handles foreign materials and invading pathogens are likely harnessed in nanomaterial processing as well. Understanding how the body's mechanistic processes work may help to identify both how phagocytes recognize and process nanomaterials and the reasons for global nanomaterial failure. Specifically, reviewing the literature of this native pathogenic processing will likely provide insights into how nanomaterials are handled by phagocytes. Understanding of phagocytic recognition of nanomaterials will provide the capability to manipulate physicochemical characteristics to minimize phagocytic uptake and inflammatory mediated events increasing the benefits of nanomaterials to the patient population.

2.1.4.1 Recognition of nanoparticles via surface activation

Many nanomaterial uptake and cellular processing mechanisms parallel normal pathogenic processing, suggesting conservation in cellular recognition and pathway regulation. A variety of native surface receptors, called pattern-associated recognition receptors (PRRs), are able to recognize patterns, for example, on the surfaces of pathogens or within damaged tissues (59). Patterns occurring on the surface of pathogens are conserved across a variety of microorganisms, termed pathogen-associated molecular patterns (PAMPs). PAMPs identify injury or cell death patterns, termed damage-associated molecular patterns (DAMPs)(60). DAMPs usually correspond to tissues undergoing necrosis and are danger signals that initiate local recruitment of immunological cells. Because foreign material, pathogens and deleterious native tissues present with patterns recognized by surface receptors on phagocytic cells, nanoparticles could also potentially present molecular patterns due to protein adsorption, or due to the native material itself from specific physicochemical properties. Further, these patterns could potentially initiate inflammatory events mediated by phagocytic cells. Four specific macrophage surface receptors, which are phagocytic receptors responsible for nanoparticle-mediated cellular uptake, will be highlighted in the following four sections: (1) toll-like receptors, (2) mannose receptors, (3) scavenger receptors and (4) Fc receptors (Figure 2.2).

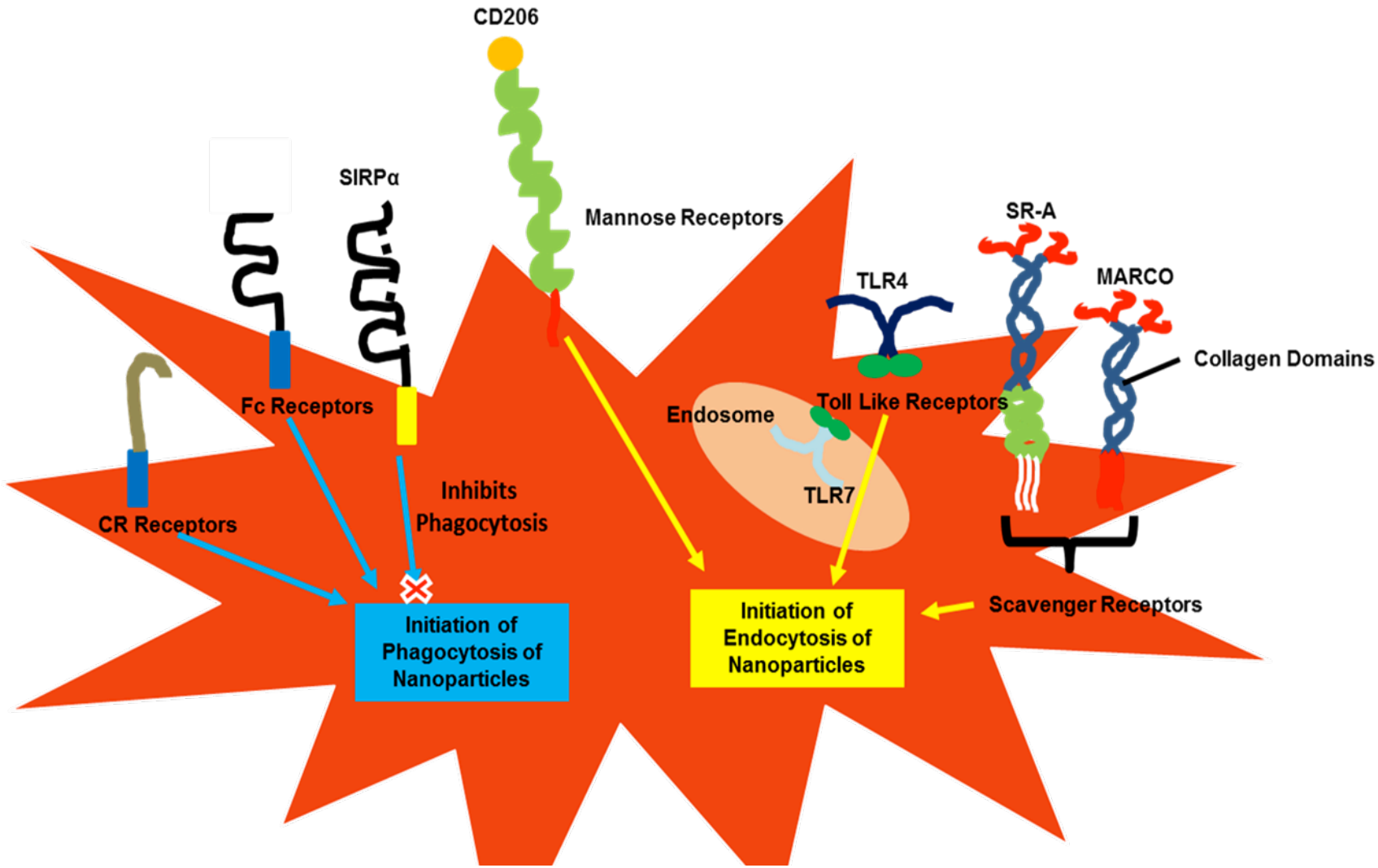

Figure 2.2: Depiction of macrophage surface receptors. These receptors are responsible for nanoparticle and foreign material recognition.

2.1.4.1.1 Toll-like receptors and targeting specific intracellular destinations

Toll-like receptors (TLRs) represent a broad first line of defense against pathogens and potentially nanomaterials, directing intracellular destinations and potentially initiating inflammatory events mediated by phagocytes. Ten TLRs have been identified in humans, residing both on the surface of phagocytes (TLRs 1, 2, 4, 5 and 6) as well as within intracellular compartments (TLRs 3, 7, 8 and 9) (61). Methods utilizing nanoparticulate TLR receptor-targeting have provided efficacy clinically. For example, poly(lactic-co-glycolic acid) (PLGA) -encapsulated monophosphoryl lipid A upregulates inflammasomes to help rid hosts of pathological infections (62). The inflammasome and its subsequent release of IL-1beta are an observed activation state of TLRs. This activation state induces inflammatory reactions, which frequently involve the myeloid differentiation factor 88 (MyD88) and induction of NF-kappa beta activation, both hallmarks of inflammatory induction. However, TLRs have also been linked to autophagic processing (TLR4, 2, 3 and 7) (63, 64), a cell survival and inflammatory reduction mechanism. These contrasting mechanisms, inflammasome modulation and autophagy, suggest that variations in physicochemical characteristics could potentially regulate the ultimate fate of nanoparticle systems. For example, carbon nanotubes with variations in surface characteristics in the presence of TLR ligands induced inflammasome activation and IL-1beta release as a function of dose. However, benzoic acid modifications had significantly less activation and release when compared to the raw carbon nanoparticles, suggesting surface modification can mitigate the inflammatory response, at least to some degree (65).

Variations in nanoparticle surface modifications can lead to recognition by different TLRs and, via this recognition, alter the intracellular fate of the nanoparticle system. For example, modification of PLGA with LPS significantly increases the antigen-presenting capacity of these delivery vehicles. LPS is a common contaminant arising from bacterial adsorption on nanoparticles and is recognized by TLR4 surface receptors and activates inflammasome production (66, 67). The enhanced efficacy of these systems results from the TLR4-targeting capabilities of the phagocytes, which activate inflammasome and IL-1beta production(68). Similar results have been shown with LPS-coated polystyrene particles, helping to support surface recognition (12). TLR4 has also been involved in the processing of graphene oxide in macrophages(69). Graphene oxide, however, has also been implicated in activation of TLR9 and autophagic signaling and compartmentalization, yet the surfaces of TLR4 and TLR9 recognized systems varied(70). This variation in TLR recognition suggests that, in some cases, one could alter the surface of a nanoparticle to direct cellular fate, increasing or decreasing payload delivery.

2.1.4.1.2 Mannose/lectin receptors and multivalency effects

Engineering nanoparticles to engage a number of surface receptors can enhance specificity and increase uptake of nanoparticles, enhancing phagocytic recognition and potentially phenotypic recognition. Multivalency increases the endocytic effect in phagocytes. For example, sugar lectin-mannose macrophage interactions can be harnessed with nanoparticulates decorated with large numbers of sugar-like motifs (71, 72). Mannose-lectin receptors are abundantly expressed on the surface of macrophages.

The main function of these receptors is to recognize complex carbohydrates, detecting mannose, glucose or sugar structures on pathogenic material and glycoproteins (73). The engagement of C-type lectin receptors on macrophages has been used by decorating the surface of nanoparticles with large numbers of di-mannose and galactose (74). Multiple sugar residues drastically enhanced the inflammatory activation phenotype of the cells following nanoparticle uptake, enhancing antigen presentation of the encapsulated payload, increasing overall efficacy (74). Similar results have been shown with mannan (36) and glycan (75). These examples suggest that by engineering nanoparticles to engage a number of specific surface receptors, one can drastically enhance the utility of such nanoparticles for delivery of therapeutics. Mathematical modeling of the multivalency phenomenon illustrates if ligand density on the surface of the nanoparticles is sufficient, membrane wrapping around the nanoparticles would be optimal when their diameter ranges between 20-35 nm and ligand density is approximately 80% with a minimum coverage of 20% (76). This model suggests that uptake can be altered significantly with optimization of surface coverage, because this can facilitate energetically favorable membrane wrapping. This phenomenon can be applicable to most surface receptor interactions and is not specific to sugars.

Mannose receptors are unique, however, in that they provide specificity to phagocytes and might increase uptake and overall efficacy of nanomaterials. The following few examples illustrate the utility of using mannose as a phagocytic target receptor to enhance overall payload delivery. Mannan has been used to coat gelatin nanoparticles to increase specificity of delivery of didanosine to macrophages for the treatment of HIV (77). These nanoparticles substantially increased the amount of drug

delivered to the brain, lymphatics and splenic tissue regions, increasing specificity of delivery and decreasing systemic side effects (78). Other mannose targeting strategies have been employed to gain similar effects, such as mannose (CD206) surface receptors to target Th2 polarized macrophages for certain chronic inflammatory disease states (79, 80). For example, carbohydrate surface modification was utilized to help direct tumor targeting of mesoporous silica nanomaterials for thermoablative therapy, which reduced tumor size significantly compared to control in treated animals (81). Specificity towards macrophage phenotypic receptors could enhance the delivery of nanoparticles to specific disease states.

2.1.4.1.3 Scavenger receptors and initiation of specific subcellular events

Scavenger receptors have been implicated in nonspecific macrophage-nanoparticle uptake and are in part responsible for *in vivo* failure due to their capacity for increasing phagocytic recognition and decreased circulation potential. These receptors are responsible for the recognition and internalization of foreign pathogens, oxidized or acetylated native proteins (i.e., low density lipoproteins (LDLs) and maleylated albumin) and apopotic cellular debris (82). They also play a primary role in the recognition and identification of LPS on gram-negative bacteria and lipoteichoic acid on the surface of gram-positive bacteria, which are both common contaminants on the surface of nanoparticles (83). Contamination could explain the ubiquitous nature of the recognition of nanoparticle uptake in macrophages. When developing nanoparticles for biological applications, extensive chromogenic endotoxin testing should be done to ensure that the

surfaces are free of LPS in order to reduce macrophage recognition. Macrophages may still, however, recognize the native nanoparticle surface. For example, ligands developed for targeting scavenger receptors are polyanionic in nature (84), suggesting that negatively charged nanomaterials could be taken up via this scavenger receptor recognition mechanism. Superparamagnetic iron oxide nanoparticles coated with nonaggregated dextran, a polyanionic sugar (Dextran-SPIO) have initiated uptake via SR-AI/II scavenger receptors (15). This was attributed to the increased polyanionic charge on their surface due to iron oxidation, which associates with the positively charged collagen-rich domain of the scavenger receptor. However, when the particles were coated with a proprietary polymer brush, uptake via these receptors was significantly diminished or eliminated (15, 17). The elimination of uptake illustrates that surface modifying particles can significantly reduce phagocytic recognition and help to improve overall efficacy and delivery.

Scavenger receptors' recognition and uptake of nanoparticles in macrophages has been linked to increased inflammatory events, which initiate nanoparticle-induced toxicity. This may be a result of the intended purpose of scavenger receptors, pathogenic material recognition which induces an inflammatory reaction as a preservation mechanism. For example, silica nanoparticle uptake and subsequent proinflammatory cytokine release was drastically reduced following SR-A receptor expression silencing (18). This result suggests that nanoparticles could reduce their inflammatory potential if the silica nanoparticle surface is modified to decrease SR-A uptake. Scavenger receptors also play an essential role in the clearance of cellular apoptotic bodies, and can initiate inflammatory pathways as a result of apoptotic uptake. This removal could also help

explain how nanoparticles initially taken up via another cell type could ultimately reside within macrophages, which could help to link the role of macrophages to systems that are not originally uptaken by macrophages. For example, cells that had ingested nanomaterials and undergone apoptosis as a result had surface apoptotic markers, which could facilitate scavenger receptor-mediated uptake by macrophages. This uptake could lead, potentially, to indirectly induced inflammation. Macrophage receptor with collagenous structure (MARCO) and scavenger receptor A (SRA) are only a few of the surface receptors that both recognize these apoptotic bodies and have the capability of recognizing a multitude of PARPs, which could help to induce nanoparticle uptake. Studies involving a direct link to macrophage-nanoparticle uptake as a result of nanoparticle apoptotic cell death have yet to be performed; however, MARCO has been linked to the uptake of polystyrene nanoparticles(85) within alveolar macrophages as well as aggregates of iron oxide(86). This MARCO link to polystyrene and iron oxide suggests that scavenger receptors are promiscuous. If promiscuity exists, identification of which portions of the receptor and what physicochemical characteristics induce recognition are required when designing new nanoparticle systems to ensure inflammation is reduced.

2.1.4.1.4 Fc Receptors and phenotypic role of uptake

Fc receptors recognize the Fc region of IgG, one of the most abundant proteins in the human body and a vital part of the innate and humoral immune systems. IgG adsorption to the surface of nanoparticles is well characterized and in some cases represents a large capacity of local protein opsonization on the surface of the

nanomaterial (87-89), suggesting Fc-mediated recognition and increased phagocytic response. For example, activation of THP-1 cells (human monocytic cell line) via PMA leads to a fourfold increase in uptake of IgG-coated nanoparticles as compared to undifferentiated cells. This increase can be explained in part by the fact that adherent cellular systems tend to uptake nanoparticles to a much higher extent (90). Surprisingly, the nonadherent monocyte-like cells internalized the amine-modified systems more rapidly than the adherent macrophage-like cells. The opsonization observed on these monocytes appears to be the result of an interaction on the macrophage with an Fc receptor, the CD64 receptor (also known as Fc-gamma receptor 1), which induces phagocytosis. However, the monocytic cell lines uptake the nanoparticles via a dynamin-mediated endocytic process (16). An *in vivo* comparison of the uptake kinetics of nanoparticles by monocytes and macrophages would be an important future direction for the field. This difference in phagocytic uptake shows the significant differences observed in macrophage differentiation and activation states. Understanding which phagocytic phenotype outplays others *in vivo* will play an important role in the design of nanomaterials and help to identify toxicity and uptake.

2.1.4.1.5 Comparative importance of macrophage surface receptors

While all of these receptors influence the uptake of nanoparticles within macrophages, Fc and mannose receptors might play a more important role than others. Comparative phagocytosis studies have focused on studying rates of uptake between scavenger, mannose and Fc receptors. The nanoparticles targeted to the mannose and Fc receptors appear to be internalized rapidly, while the scavenger receptors take a

significantly longer time (91). This suggests that Fc and mannose receptors are better poised to internalize nanoparticles. Fc and mannose receptors may or may not be expressed on macrophages, and the levels of expression for each receptor type vary widely between polarization and activation states of these cells (91). Additionally, many of these macrophage surface receptors have evolved to detect opsonized materials to increase nanoparticle uptake and many of the receptors may work in parallel. Thus, targeting via directed protein adsorption may be accomplished by understanding protein adsorption properties and engineering surfaces such that certain proteins adsorb in conformationally appropriate states for receptor recognition. For example, IgG and C3b induce phagocytosis through the Fc and complement receptors (91), a strategy which could be used to target macrophages directly. However, macrophages still uptake nanoparticles in the absence of serum, which suggests these four receptors may natively recognize nanomaterials (92). In some cases, proteins can also mask the materials from surface receptor recognition (93). An understanding of which proteins and what adsorption conformation provide this masking will be important if the goal is bioinvisability of the particle.

2.1.4.2 Phagocytic internalization mechanisms

Payload delivery to specific cellular compartments could enhance efficacy in drug delivery. Some drugs act on specific cellular organelles and need to be trafficked efficiently while avoiding uptake by detrimental compartments. For example, nucleic acids act primarily through nuclear localization. Therefore they will be unsuccessful if they are trafficked to autophagosomes or lysosomes instead. The following section

outlines the specifics of uptake processes, which will aid in efficient design of nanomaterials and increase payload delivery.

After cellular recognition via pattern recognition receptors, foreign materials must be internalized within phagocytes, primarily utilizing cellular cytoskeletal rearrangements and vesicle development. These internalization mechanisms can be broadly classified as phagocytosis or pinocytosis (Figure 2.3).

Phagocytosis is a broad definition to describe the actin rearrangement and pseudopodial envelopment of large bodies into cells and is a primary mechanism for nanoparticle uptake (94). Phagocytosis is usually associated with Fc- and CR-mediated receptors, enveloping material in a zipper-like fashion. Only certain classes of cells, usually termed "professional phagocytes," have this type of cytoskeletal rearrangement capability. These professional phagocytes include macrophages, neutrophils, dendritic cells, monocytes, and in special cases, endothelial and secretory epithelial cells. These pseudopodial vesiculations are concurrent with granule movements and subsequent granule fusion within the cell. Usually following phagocytosis, the vesicle fuses with lysosomal compartments and they undergo a large pH reduction; however, in some pathogenic scenarios this fusion is avoided. For example, when M. Tuberculosis or Chlamydia are ingested, the phagosomes do not acidify, due to the lack of ATPase and LAMP markers, respectively (95). Nanomaterials could utilize similar mechanisms to reduce fusion.

Pinocytosis, in contrast, is present in all mammalian cells and can be in some situations responsible for nanoparticle uptake. This mechanism can be classified into large volume extracellular internalization (e.g., macropinocytosis and circular dorsal

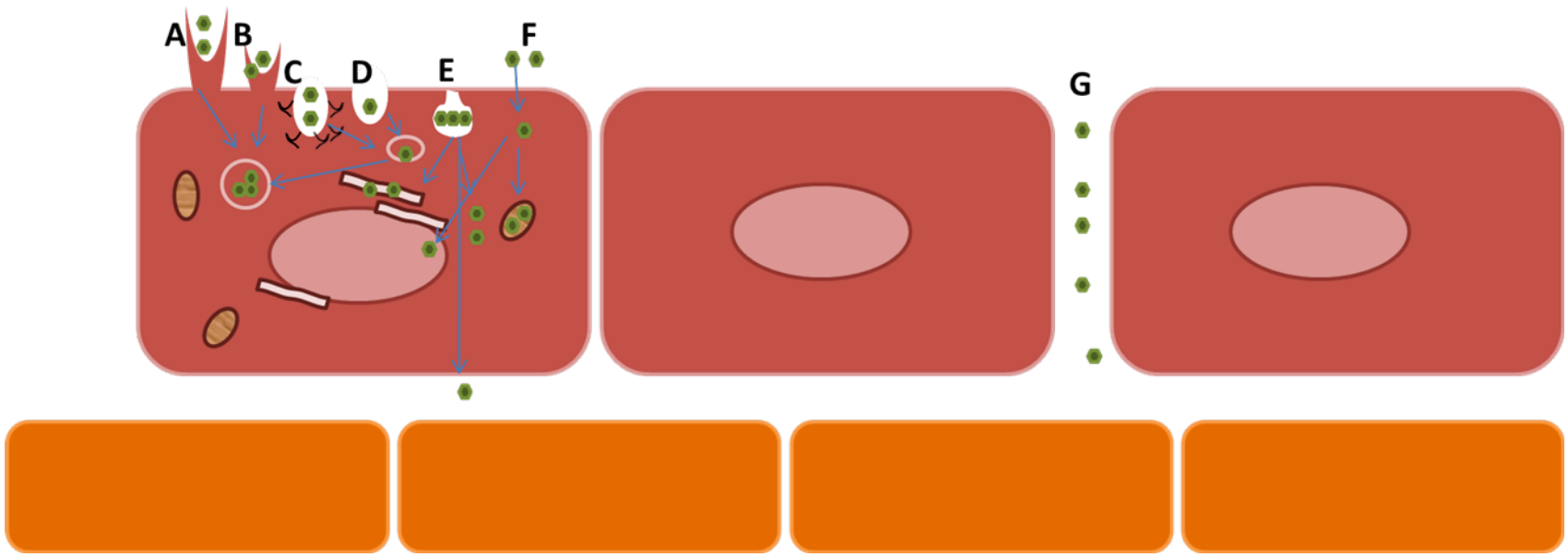

Figure 2.3: Mechanisms of nanoparticle uptake: (A) phagocytosis, (B) macropinocytosis, (C) clathrin mediated endocytosis, (D) clathrin and caveolae independent endocytosis, (E) caveolae-mediated endocytosis, (F) trans-membrane transport, (G) paracellular transport. Adapted from Muhlfeld, 2008 (300).

ruffles responsible for .5-5 um internalization) and smaller volume internalization (e.g., clathrin and clathrin independent mechanisms 20-500 nm). However, larger volume internalization mechanisms rarely occur without clathrin-mediated internalization. Macropinocytosis and circular dorsal ruffles are characterized via their large protrusions from the membrane and actin-dependent polymerization mechanisms, similar to phagocytosis. However, zipper-like phagocytic uptake is absent in these processes. Rather cells simply envelop the entire substance into the cytoplasm. This process is implicated in the uptake of viruses and macromolecules and potentially nanomaterials. Clathrin-mediated endocytosis is probably the most well-known and studied of the internalization mechanisms. Scavenger, mannose and TLRs are known induction mechanisms for this internalization process. This process involves the formation of clathrin pits, which wrap and pinch their cargo into the cell. Once enveloping the cargo, these pits are cut via dynamin scission to form internalized vesicles. These vesicles are trafficked to early endosomes, followed by acidification and transformation to late endosomal vesicles where they are then trafficked to other intracellular destinations including lysosomal compartments, a mechanism that nanoparticles could harness.

Unlike clathrin-mediated endocytosis, which is responsible for internalization of size ranges from approximately 100-350 nm, caveolin-mediated endocytosis is responsible for 20-100 nm endocytosis, size ranges in which nanomaterials fall. Replacing the clathrin bowls are caveolae, which generally reside within lipid raft domains. As such, they differ in their internalization mechanism. Rather than membrane wrapping this invagination typically appears after completion of a bowl just below the surface, ingesting the cargo via membrane dropping. These vesicles are typically

transported to the golgi or are excreted from the cell, a mechanism which could be harnessed in particular nanoparticle delivery scenarios. Cholera toxin utilizes this mechanism advantageously by avoiding lysosomal internalization, a method that could be utilized in nanomaterial drug delivery. Other mechanisms exist for these uptake types.

As outlined above, surface recognition patterns induce uptake via interactions with phagocytic receptors, but alterations in physicochemical characteristics such as geometry and surface chemistry also can alter uptake patterns and may help to induce specific intracellular fate patterns, improving delivery. Geometry and surface chemistry will be discussed as a way of highlighting how physicochemical characteristics can impact phagocytic recognition and uptake.

2.1.4.2.1 Implications of geometry on cellular uptake

Geometry can influence nanoparticle internalization mechanisms and may alter uptake patterns (19, 96). Utilizing particle replication in nonwetting templates (PRINT) technology, which enables the production of nanoparticles with defined size and geometry, nanoparticle entry has shown a size-dependent phenomenon impacting phagocytic uptake. This geometric uptake phenomenon has been corroborated in other types of systems as well (97, 98). Smaller nanoparticles with the capability of interacting with lipid rafts tend to be taken up via caveolin-mediated mechanisms (under ~60 nm), while nanoparticles within a 60-300 nm size range are taken up via clathrin-mediated mechanisms and pinocytosis/phagocytosis generally take over when nanoparticles are above 300 nm (19). When particles are above 300 nm and are internalized via phagocytosis, geometry has a significant effect on the rate and extent of uptake.

Interestingly, the results of these studies revealed an angle dependent uptake pattern: if a particle contained an edge with an angle larger than 45 degrees, the nanoparticle was unable to be completely phagocytosed, indicating that particles above this size may not be internalized. Below this value, the nanoparticle was completely enveloped and internalized into cellular compartments (20, 99). Predictions based on computational models have suggested that membrane-wrapping in phagocytic processes is dependent on the ability to overcome high-energy conformations to obtain an energy-minimized state. If an edge angle is too large, for example on a cylindrical particle, the nanoparticle can associate with the cellular membrane but membrane wrapping cannot occur due to the energetically unfavorable conformation required to temporarily wrap over the sharp edge (100). Oblated ellipsoidal particles have more efficient phagocytic internalization capability than prolated ellipsoidal particles due to a similar phenomenon (21). Shape has a profound effect on the phagocytic uptake processing of particles and suggests that computational model-assisted design and geometric alterations could help in the ultimate evasion or reduction in phagocytic uptake and processing. Further the toxicological implications of this inability to complete membrane wrapping are unknown, and could potentially influence macrophage content release. The result might follow similar patterns to what is seen in the foreign body response in biomaterial implants and facilitate the creation of multinucleated cells and an inflammatory response, or might elicit a different mechanism altogether.

Nonphagocytic processes, such as clathrin-mediated endocytosis, also show similar sensitivity to particle geometry and may influence the degree of phagocytic uptake, an effect which has been shown both computationally and experimentally (101).

Rod-like nanoparticles with rounded ends are uptaken more rapidly than their true cylindrical counterparts, which possess 90 degree edges at their ends (19). In another model system, spherical particles were taken up more rapidly than rods (102). Additionally, the size of spherical particles drastically alters the mechanism by which they are internalized, which has been attributed to membrane wrapping of the particle (103). For example, clathrin-mediated invaginations were due to elastic membrane deformations, and only particles around 50-200 nm in radius were internalized by this mechanism (101, 104). This study suggests that when the nanoparticle radius is greater than 200 nm, the cell membrane is unable to form a large enough pit for the particle, reducing clathrin-mediated uptake. If clathrin-mediated mechanisms are not involved in the uptake of spheres larger than 200 nm, other pinocytic mechanisms such as macropinocytosis must take over and enable uptake of the particles. This could be an important consideration in understanding uptake capacity. By altering the size and geometry of the nanoparticles, one may potentially be able to dictate specific uptake mechanisms, consequentially improving delivery.

2.1.4.2.2 The influence of surface functionality on nanoparticle uptake

Surface functionality of nanoparticles may play an important role in the mediation of uptake of nanoparticle systems. Specifically, surface charge greatly affects levels of cellular uptake, with positively charged materials generally taken up to a greater degree than their neutral or negative counterparts (104, 105). This effect has been shown with phagocytosis in a macrophage model system (106). This might occur because sialic acid

is prominently displayed on the surface of macrophages, resulting in a negative surface charge thought to attract positively charged materials, increasing their rates of internalization. This was investigated in a study in which alveolar macrophages were analyzed for their ability to uptake 50 nm gold nanoparticles following preincubation with known sialic acid binding proteins, wheat germ agglutinin and limulus protein (107). Under preincubation conditions, negatively charged nanoparticles were taken up at the same rate as controls while uptake of the positively charged systems was blocked by the pretreatment. Uptake has also been observed in the presence and absence of serum in macrophage models. This suggests that surface receptors can and do recognize specific surface functionality, and uptake those nanoparticles in a similar fashion to traditional foreign pathogenic materials. An understanding of how simple surface chemistries affect uptake patterns could be used as a design factor to modify uptake.

Modification of the surfaces of nanoparticles with ligands that are specific to well-known internalization mechanisms can also be utilized to harness specific uptake pathways. Clathrin-mediated uptake mechanisms utilizing transferrin or folate are commonly used in targeting clinical nanoparticle systems to treat or diagnose cancer, as these receptor-ligand interactions are commonly upregulated in cancerous tissue. Transferrin-mediated mechanisms have been translated clinically into two liposomal formulations, CALAA-01 (108) and MBP-426 (109). Vynfinit is an example of a folate-targeted chemotherapeutic nanoparticle that is clinically approved for ovarian cancer use in Europe (110). While transferrin and folate targeting provide benefit for targeting cancer cells specifically, macrophage targeting would benefit from utilization of one of the 4 receptors discussed previously. Scavenger receptors, for example, induce clathrin-

mediated endocytosis, and Fc receptors induce phagocytosis. Specific targeting ligands could be engineered to induce the particle's intracellular uptake. The engineered uptake patterns could further induce specific intracellular fates. Phagocytic uptake commonly results in localization in phagocytic vesicles with little to no further intracellular trafficking; however, pinocytic mechanisms have the potential for delivery to specific intracellular compartments. For example, endosomal compartments have known internal intracellular trafficking receptors (111), which can be targeted by drugs or endosomal escape strategies. Such design manipulation could enhance targeted intracellular therapeutic delivery.

Targeting the phagosomal route may still be advantageous, even if the specificity can be inferior to pinocytic uptake mechanisms. Many systems have harnessed this uptake mechanism to increase efficacy and improve delivery. For example, the propensity of the MPS to phagocytose or engulf foreign material has also aided in the development of delivery systems to parasitophorous vacuoles within macrophages. Ambisome®, a liposomal form of amphotericine B, an antifungal agent, utilizes toll-like receptor targeting to harness parasitophorous targeting mechanisms, thus increasing efficacy compared to the free drug alone and reducing local systemic toxicity (112). This formulation has been on the market for over 15 years and shows the capacity of harnessing phagocytic systems to improve overall delivery.

The critical takeaway on nanoparticle design is the understanding that a link can be drawn between internalization mechanisms and ultimate intracellular fate. A more complex view of intracellular uptake can also help to drive understanding of intracellular pathways leading to specific and desirable downstream events.

2.1.4.3 Phagocytic nanomaterial processing

Understanding traditional nanoparticle fates in macrophages, as a result of physicochemical properties will allow for direct intracellular delivery improving payload efficacy. In turn, the ability to manipulate physicochemical properties can help develop engineering mechanisms that home to specific cell compartments.

2.1.4.3.1 Autophagy as a nanoparticle processing mechanism

Three likely processing events exist for nanomaterials in phagocytes: (1) cell-autonomous antimicrobial defense mechanisms, (2) native pathogenic or foreign material cellular process mechanisms, and (3) opsonization recognition events due to specific structural surface similarities with pathogen and foreign materials. Autophagy is an example of an innate defense mechanism, with activity against intracellular microbes, dysfunctional cellular organelles, and misfolded proteins. Autophagy is induced in nanoparticle uptake via pattern recognition receptors (113). Autophagy can lead to increases in phagocytic activity, leukocyte migration, and inflammatory responses such as specified polarization of immune cells and release of proinflammatory cytokines (113-119). In some cases, however, autophagy can be beneficial as it provides a cellular coping mechanism and reduces the likelihood of toxicity emerging from exposure to nanoparticle systems.

Autophagy is a primary mechanism by which highly positively charged nanoparticles are trafficked intracellularly. Postively charged dendrimers, polyplexes, gold nanoparticles, iron oxide and silica nanoparticles harness this mechanism (11, 117, 119-121). However, little to no evidence currently exists linking other surface

functionalities to autophagic mechanisms. Other surface chemistries could induce or mediate autophagy.

While autophagy may be beneficial for the reduction of toxicity, it may be detrimental to the delivery of cargo, as trafficking of these positively charged systems to autophagosomes eliminates the capacity for delivery to other organelles. For example, polyplexes are commonly utilized as nucleic acid delivery systems, which by and large need to be delivered directly to the nucleus to work effectively. However, if nucleic acid delivery systems ultimately reside in autophagic compartments, very little to none of the cargo is delivered to the target site, severely limiting efficacy. Fortunately, approaches for controlling autophagy with surface modifications of nanoparticles have been identified. For example, modifying the surface of MWCNTs with organic compounds can help to avoid an autophagic response. A series of LC3-II screening assays illustrated that autophagy is highly dependent on surface characteristics in astrocyte and human embryonic kidney cell models. They were able to identify certain organic compounds that more strongly upregulate autophagy and other organic compounds that appear to have little to no effect on mechanistic regulation (122). This suggests that surface chemistry in other systems can be manipulated to potentially evade this process. Development of such nanoparticles may possibly aid in the design of new materials to modulate downstream inflammatory events. In some cases the utilization of autophagy may allow for pathogenic removal and, as a result, would represent a promising treatment mechanism. Mycobacterium tuberculosis (M.tb.), a pathogen well-known for its survival and proliferation within phagosomes, inhibits the development of autophagy within macrophages. In alveolar macrophages, PLGA nanoparticles are phagocytized and use

rapamycin to induce autophagy, which leads to M.tb. elimination (123). This therapy illustrates the importance of understanding the target site of the construct in designing new delivery systems. Autophagy in this case enhances efficacy, while as mentioned previously in nucleic acid delivery is detrimental to efficacy.

Autophagosome-like compartments that connect to the cell surface, termed surface-connected compartments (SCC), can also process pathogens and foreign materials, so may be useful in nanotherapy. SCCs are a series of connected intracellular compartments formed when macrophages are subjected to large numbers of highly hydrophobic nanoparticles. These SCC compartments serve as a cellular tool to digest foreign material and quickly release contents back out to the extracellular space, potentially facilitating the degradation of nanomaterials. SCC is observed in uptake of LDL, hydrophobic gold and hydroxyapatite particles (124-126). These SCC compartments form only when particles are below 500 nm and phagocytosis occurs with particles above this size range (124). These compartments are mainly formed through actin rearrangement and remain open to the extracellular space while appearing to be connected to the plasma membrane. If autophagic compartmentalization and SCC formation are linked, this could be a universal phenomenon for macrophage-nanoparticle processing and raises the possibility for evolutionarily developed nanoparticle processing mechanisms.

2.1.4.3.2 Directed intracellular delivery

Effective cargo delivery should target specific intracellular organelles and would enable site-specific action. After foreign materials are taken up into endosomes or

phagosomes, they fuse with lysosomal compartments, which are used by cells to combat the foreign material with heavy enzymatic digestion and reduced pH. This fusion allows the cells to degrade or remove the pathogen from the environment. However, these vesicles also encompass recognition motifs that can traffic ingested material to specific cellular compartments (127). These motifs, in turn, can be utilized for site-directed delivery. Additionally, systems can be engineered to escape these compartments through either peptide motifs or basic surface compositional alteration, such as increasing the positive charge on the surface of the nanoparticle to induce lysosomal burst through the so-called proton sponge effect (128). After release from the lysosomal compartment, delivery vehicles can then be trafficked to a specific intracellular compartment and could potentially be advantageous for delivery of bioactive agents.

Specific strategies would allow for targeted drug delivery systems to the mitochondria to induce apoptosis in cancer, alter potassium dysregulation in heart abnormalities, and reduce the effects of aging (129). One strategy in mitochondrial delivery is to utilize the difference in the local compartmental membrane potential, which is significantly lower than the rest of the cellular compartments. By attaching mitochondriotropic cationic molecules to the surface of a nanoparticle, for instance triphenylphosphonium (TPP), one can harness this membrane potential difference and achieve high mitochondrial localization (130, 131). Understanding intracellular fate can reduce overall phagocytic toxicity, improving efficacy and reducing translatable failure.

Peptides have been used to target other specific intracellular compartments such as the nucleus and endoplasmic reticulum and could also be advantageous for drug delivery (132). The nucleus is a key organelle for delivery of many bioactive agents

including nucleic acids. Attachment of nuclear localization signals (NLS), which can be recognized via importin protein family members, can mediate nuclear transport mechanisms. Doxorubicin-loaded nanoparticles with NLS increase antiproliferative effects and the capability for intracellular localization to enhance delivery. These specific targeting strategies to subcellular compartments are reviewed elsewhere (133, 134). Directing intracellular fate pathways will be important when utilizing engineering platforms in order to ensure they do not interfere with uptake mechanisms or alter ultimate *in vivo* circulation and biodistribution.

Due to the complexity in utilizing these intracellular fate ligands and surface characteristics, many researchers choose not to incorporate these properties into their nanomaterials. However, materials without directed cellular targets may potentially have indirect targeting as a function of physicochemical properties and may elicit toxicity.

2.1.4.3.3 Indirect intracellular targeting and resulting potential toxicity

Knowledge of cellular localization of delivery systems could provide information regarding both the intracellular targeting of appended therapeutics, as well as a starting point for evaluation of possible mechanisms of toxicity. For example, clues about specific cytokine and chemokine release and possible mechanistic dissection of downstream effects can be used to predict toxicity if the ultimate intracellular destination of nanomaterials is known. If the nanomaterial is left without a specific targeting mechanism to a known intracellular location, understanding of toxicological consequences becomes difficult as they can differ both from cell type to cell type and in

the context of specific environmental factors.

If a nanoparticle targets the mitochondria nonspecifically it can induce mitochondrial dysfunction and nanoparticle toxicity. As mentioned earlier, there is a mitochondrial membrane potential, an electron transport chain which provides a proton gradient through which ADP is phosphorylated to yield ATP. If mitochondrial membrane potential is altered, cytochrome C is produced and apoptosis can be initiated. Nonspecifically targeted iron oxide particles and carbon nanotubes home to mitochondria, affecting the cellular mechanistic energy machinery and ultimately leading to cell death (135, 136). Mitochondrial dysfunction has been observed after treatment with silica nanoparticles. In these studies, JC-1 mitochondrial potential assays provide evidence that nanoparticle size and surface modification have an effect on the membrane potential change. Smaller and more positively charged nanoparticles have increased induction of these potential changes (137). Crystalline silica nanoparticles initiate both necrotic and apoptotic cell death mechanisms, a result of mitochondrial damage. Early stages of toxicity with these particles show phago-lysosmal escape and cellular damage, resulting in drastic changes in mitochondrial potential (138). These temporal changes resulted in hyperpolarization or depolarization causing apoptotic or necrotic cell death, respectively. Such processes are detrimental and facilitate drastic nanoparticle toxicity and should be avoided in nanotechnological design and development. The mechanism and biological motivation for these processes remain unknown.

Nanoparticle composition can generate reactive oxygen species (ROS) and cause mitochondrial damage in macrophages (14), which in some studies led to gene up-regulation to induce inflammation. Surface hydroxyl groups can initiate interactions with

iron in biological environments to initiate the Fenton reaction, which leads to free radical production (139, 140). Increased ROS formation leads to the initiation of an inflammatory response. Increased levels of oxidative stress, mitochondrial dysfunction, and inflammatory gene expression after nanoparticle treatment have been observed during these responses (13, 39, 137, 141, 142). For example, porous silica nanoparticles were observed to increase ROS generation and adversely affect ATP and TNF-alpha content in macrophages and other hematopoetic cells. These results were more pronounced with charged surfaces, particularly positively charged modifications, while hydrophilicity played little to no role (143). This surface charge phenomenon suggests that in nanoparticle design, highly positively charged systems should be avoided.

In addition to charge, other surface modifications might warrant nanoparticle macrophage avoidance, such as topography. Further environmental nanotoxicity studies showed that the crystal size of the nanoparticle significantly affected the induction of ROS (141). This is due to the differences in uptake mechanisms, as a result of the size of the nanoparticles. Smaller nanoparticles induced increased toxicity compared to larger nanoparticles, which could be a function of the increased surface area of the nanoparticle systems. This suggests that an optimal size range exists in nanoparticle development, in which translational potential is greatest. Porosity also appears to influence inflammatory activation. Investigation of nonporous and porous silica nanomaterials demonstrated a drastic increase in MAPK, TNF-alpha, Il-1beta and NF-kappa beta production when macrophages were subjected to nonporous material, while porous silica yielded no such effect (144). Porous materials may have increased biocompatibility. However, epigenetic modifications in DNA methylation, a sign of chronic inflammatory activation, have also

proven to be present in environmental macrophage exposure to nanoparticulates (145). Future studies should help to elucidate exactly which modifications and surface characteristics elicit toxicity and will help to direct new nanoparticle design.

2.1.5 *In vitro* macrophage model systems and their correlation *in vivo*

Little is known about the mechanisms through which the physicochemical characteristics of nanoparticles induce up-regulation of inflammatory genes or in which stage of nanoparticle-macrophage interaction inflammatory gene upregualtion happens: presentation to biological milieu, cellular contact, or after internalization. An understanding of these mechanisms, stages and characteristics would be beneficial when designing nanoparticle systems. More importantly, inflammatory gene upregulation upon nanoparticle insult needs to be studied *in vivo*. Macrophage models may help to decode these understandings, as many macrophage model systems help to predict inflammatory mediated events.

In vitro macrophage models do appear to correlate well with nanoparticle *in vivo* study results. Studies with isolated primary Kupffer cells assessing toxicity of the uptake of quantum dots (146), for example, have shown upregulations of TNF-alpha, Il-1beta and IL-6. These studies predicted an acute inflammatory response *in vivo*, which is corroborated by results of *in vivo* quantum dot experiments (146). Similar results have been observed with a multitude of other nanoparticles (146).

Macrophage model systems appear to be capable of predicting correlations between nanoparticle characteristics and inflammatory induction. For example, some

nanoparticles induce toxicity in hemopoietic lineages (147). In one study, nanoparticle treated primary isolated hemopoeitic cells were compared to traditional monocytic immortalized cell lines. The traditional monocytic cell lines (147) show little to no toxicity towards antimony oxide nanoparticles; however, the nanoparticles did induce significant toxicity within the primary monocytic cell lines. A recently published review suggests that macrophage *in vitro* assays correlate well with *in vivo* results (4). Macrophage phagocytosis assays correlate with *in vivo* retention in the MPS system. Release *in vitro* of TNF-alpha, IL-1beta and IL-8 from macrophage model systems can, for example, accurately predict disseminated intravascular coagulation (DIC) and cytokine storm disorders *in vivo*. Leukocyte proliferation *in vitro* correlates with immunostimulation or immunosuppressive effects. Myelosuppressive potential *in vivo* can be correlated with colony forming unit-granulocyte macrophage assays (4). The ability of *in vitro* assays to predict *in vivo* results suggests that macrophages are an important model system for translation, allowing screening with a lower cost, less time-intensive model system compared to *in vivo* models.

However, *in vitro* model systems do not always correlate with *in vivo* results. In general, cellular model systems are usually more sensitive than *in vivo* model systems, due to their less complex nature and inability to compensate via homeostatic balances. For example, quantum dots are traditionally thought of as highly toxic systems *in vitro,* but *in vivo* they tend to be tolerated with little to no observable toxicity (148). Similar disparities may exist with silica, gold, and iron oxide, emphasizing the importance of accurate translation of *in vitro* results to an *in vivo* context.

2.1.6 Phagocyte-nanoparticle interactions in an *in vivo* context

Macrophage processing *in vivo* is significantly more complex than the *in vitro* environment and can alter tissue residence patterns, disrupt payload target delivery, increase clearance or facilitate the induction of toxicity. Understanding how macrophages facilitate organ-specific uptake, toxicity and clearance within an *in vivo* context will help to improve clinical translational potential of nanoparticle systems by increasing circulation and reducing toxicity.

Not all macrophages are identical and heterogeneity arises as a function of environmental conditioning, and could affect nanoparticle processing. For example, Kupffer cells vary phenotypically with regard to tissue location (149, 150). Those cells that reside within the portal region have increased levels of scavenger receptors, phagocytosis and lysosomal enzyme activity when compared to centrally located cells, which have increased cytokine activity (151). In contrast to portal region cells, splenic macrophages that reside within the red pulp, white lymphatic pulp and marginal regions vary significantly in levels of endocytosis, with marginal zone macrophages having a significant increase in MARCO receptors (152). If one could discern between these macrophage phenotypes and target recognition mechanisms of specific subpopulations, nanosystems could be designed to increase circulation times and deliver to specific tissue sites. The potential to control the environment and prime these macrophage sites to specific activation states that either present antigens or polarize to specific Th1 or Th2 states, could be used to increase local wound healing and bactericidal activity.

Certain physicochemical characteristics such as size, shape and surface modification appear to play an important role in nanoparticle tissue accumulation. For

example, size appears to play a significant role in nanoparticle residence in clearance organs, specifically the liver and spleen. Splenic meshwork size ranges are between 200-500 nm. Thus, as blood containing nanoparticles filters through it, nanoparticles that are below 200 nm should be able to move freely, increasing circulation times of therapeutics. In contrast, nanoparticles above 200 nm may provide spleen-directed targeting. Depletion of local macrophages via clondronate in the spleen does not drastically reduce the uptake of nanoparticles within this environment, which suggests that physical mesh may play a more important role than cellular recognition in local uptake (153). In the case of the liver, however, liposomal formulations below 100 nm increase in local uptake in hepatocytes and Kupffer cells. This could be due to the small size of liver fenestrations (~100-150 nm). These lower nanoparticle sizes appear to have a diffusive penetration potential in the liver tissue. The penetration could be enhancing local cellular recognition and may lead to increased clearance rates. If longer circulation is preferred in new nanoparticle system, an ideal size range should be within 130-200 nm, based on these physical tissue parameters (152).

2.1.6.1 Clearance mechanisms and tissue residence

Ideally after payloads have been delivered to their intended site, nanomaterials would be cleared from circulation and would not induce an inflammatory response. Many therapeutic nanoparticles that have degradation capabilities or are within a small enough size do show clearance through biliary or renal excretion mechanisms helping to facilitate this ideal situation. However, studies suggest that even after 2 weeks only limited nondegradable nanomaterial clearance occurs, with a majority of dosed nanoparticles

(~95%) accumulating in clearance organs (26, 154, 155). The possibility of chronic toxicity as a result of nanoparticle accumulation, as is the case with traditional biomaterial implants, remains to be seen.

2.1.6.1.1 Size effect on clearance

Size appears to play a significant role in nanoparticle residence in clearance organs. Traditionally particles below 15 nm are thought to be trafficked to the kidney and excreted through renal mechanisms. Larger nanoparticles however tend to reside in the liver and spleen. For example 25 nm silica nanoparticles are excreted through biliary clearance mechanisms at 2 weeks post treatment, at which point little to no toxicity or tissue abnormalities were observed (26). Similar results have been shown for 17 nm gold nanoparticles (26, 156). However larger nanoparticles do reside within clearance organs even past 2 weeks. Forty nanometer gold particles persisted in Kupffer cells of mouse and beagle dogs for at least 6 months, and would probably persist for the duration of the life of the animal (157, 158). This suggests that to ensure clearance, the nanoparticle should be below 25 nm. Larger size ranges and degradation mechanisms need further investigation.

2.1.6.1.2 Shape effect on clearance

Shape appears to mediate tissue macrophage-nanomaterial interactions and to influence clearance. For example, short rod-like nanoparticles with an aspect ratio of 1.5 primarily accumulated in the liver, while rod particles with an aspect ratio of 5 resided within the spleen (25). These rod-like nanoparticles were mesoporous systems, which in

some cases have the capability of breaking apart into smaller particulate forms. This break apart could explain the clearance of these nanoparticles primarily through biliary mechanisms; however, modifications to the surface with PEG resulted in slower clearance, with longer half-lives and altered distribution states (159). This contradicts other studies that suggest PEG modification reduces clearance rates and extends half-lives (160). Yet, increased clearance may mean reduced recognition by macrophages and thus less exposure of delivery systems to degradation mechanisms resulting in increased therapeutic efficacy.

2.1.6.1.3 Surface modification effect on clearance

Surface modification can enhance nanoparticle accumulation and apparent clearance mechanisms. Increasing PEG density on the surface of nanoparticles increased uptake by Kupffer cells, while decreasing the density showed increased uptake via macrophage-like kidney mesangial phagocytes (28). This suggests that altering surface modifications of delivery systems could direct specific tissue residence. In addition to PEG, other surface modifications have been tested. For example, gold nanoparticles surface coated with BSA or GSH and an average of 8.2 nm were evaluated *in vivo* (161). The BSA nanoparticles formed large aggregates and accumulated in the liver and spleen, inducing toxicity within these organ systems. However, the GSH-coated nanoparticles were quickly recognized via macrophages in the kidney and showed renal excretion, which suggests BSA is detrimental to delivery.

Polymer chain length alterations on the surface of nanomaterials appear to help circulation potential suggesting macrophages avoid recognition (29). Polymer brushes of

poly(ethylene glycol) methyl ether methacrylate (PEGMA) ranging in molecular weight (MW) from ~50,000-750,000 Da were grafted onto the surface of nanoparticles ranging in size between 130 nm-1550 nm. Above 500,000 Da MW limit they observed rapid clearance of the nanoparticles. Interestingly, 290 nm silica nanoparticle constructs with grafted ~130,000 Da MW polymers had a similar hydrodynamic size to 130 nm nanoparticles with ~290,000 Da MW polymers. The larger constructs had higher clearance rates when compared to the smaller nanoparticles. This suggests that polymer chain length may help to avoid opsonization and recognition via phagocytes.

Charge also appears to play an important role in the uptake and tissue residence of nanoparticle systems. For example, neutral and zwitterionic-gold particles have long circulation times, while their positively and negatively charged counterparts exhibited reduced circulation rates, probably due to macrophage recognition and association within clearance organs (162). Similar results were shown with silica nanoparticles: charged systems increased opsonization and clearance rates via biliary mechanisms (163).

Currently, opsonization directs nanomaterials' biodistribution and clearance mechanisms. An *in vitro* / *in vivo* correlation between the amount of protein binding and the subsequent degree of phagocytosis by RAW 264.7 mouse macrophage cell lines and their retention within organs has been studied (4). Nanoparticles made of poly(vinyl-pyrrolidone)-block-poly(D,L-lactide) copolymers have increased phagocytosis and protein binding. This correlated with the splenic and hepatic residence of these nanoparticle systems (164). This residence may suggest that macrophages help to play a role in the tissue residence and increased accumulation in clearance organs. A similar phenomenon has also been observed with gold nanoparticles (98), helping to support a

global nanoparticle macrophage recognition phenomenon that correlates to clearance organ residence.

2.1.6.1.4 Hydrophobicity effect on clearance

Altering the surface hydrophobicity in silica nanoparticles significantly alters protein adsorption and subsequent organ distribution (165). Hydrocarbon coatings on nanoparticles increase splenic residence; however, when surfaces were coated with hydrophobin (a natural fungal hydrophilic coating) nanoparticle residency increased in the liver. When protein adsorption on the surface was examined after incubation with serum, the hydrophobic coating adsorbed more abundant proteins, such as albumin, IgG and fibrinogen. This suggests that protein adsorption plays an essential role in organ uptake and recognition. In the development of nanoparticles for biomedical applications, an understanding of the kinetics of protein adsorption to the surface of nanoparticles as well as the identities of adsorbed proteins will be important, as well as the effects of protein adsorption on distribution and ultimate nanoparticle clearance (166). For further information on how the protein corona affects biological mechanisms and how to study such adsorptive properties readers are directed to the following review (167).

2.1.6.1.5 Effect of long-term tissue residence of nondegradable nanoparticle systems

Recent evidence suggests that long-term nanoparticle residence within clearance organs such as the liver and spleen, initiate lesions via infiltration and microgranulation of hepatocytes and long-term inflammatory response (27, 168). Inhalation of

nanoparticles has also initiated lesions within the lung tissue (169, 170). This suggests that rather than clearing nanoparticles, the body has developed a local response to isolate these foreign materials from host biological environments. The unanswered question is if this local response is initiating adverse chronic inflammatory or immunological responses. Even more concerning are local responses that can lead to diseases such as cancer and immunological disorders. However, lesion formation has been mitigated, at least to some extent, by surface modifications in hydrophobicity and charge. For example, lung fibrosis occurs for cationic silica nanoparticles, while those with polar or anionic surfaces tended to migrate to the mediastinal lymph nodes (171). This might suggest that some drug delivery design principles could avoid such response, decreasing toxicity.

The ultimate fate of nanoparticle systems appears to be primarily within clearance organs such as the spleen, liver and kidney. Most evidence linking cellular uptake *in vivo* shows correlations between macrophage uptake and residence within those tissues. Important future studies include investigations of (1) which macrophages in those tissues are responsible for uptake; (2) how macrophage type affects the surrounding environment; and (3), how and if nanoparticle clearance occurs. Macrophages may traffic to biliary tracks and dump their contents or themselves, or the harsh intracellular conditions within the macrophages may manipulate and degrade these ‘nondegradable’ systems.

2.1.6.2 Adverse toxicological effects *in vivo*

Macrophage-nanoparticle interactions *in vivo* appear to initiate global toxicity, and may be a result of indirect activities such as complement and thrombolytic events. The interactions which elicit these responses remain unknown, and will be important to understand and consider when designing new materials. Complement activation and thrombolytic events initiate the release of cytokines and chemokines and promote immune and macrophage cellular recruitment, differentiation, and response. Complement and thrombolytic responses can be mitigated with variations in surface properties (172, 173).

2.1.6.2.1 Complement activation upon nanoparticle-blood contact

Complement activation is a destructive issue for nanoparticles, initiating phagocytic uptake and inflammation. For example, liposomal formulations of doxorubicin have in some cases caused severe hypersensitivity due to initiation of an inflammatory cascade (174). Hydroxyl modifications initiate complement activation, due to the interaction with C-reactive protein inducing inflammation. Additionally, iron oxide nanoparticles surface-activate C3 and initiate inflammatory mechanisms (175). Activation of iC3b by nanoparticles might lead to erythrocyte binding and splenic clearance (176, 177). These examples illustrate the need to understand surface modifications and how they relate to complement activation that induces inflammation.

Surface modifications can cause significant differences in the degree of complement activation (175). Dextrans have been used as excipients for decades to reduce protein adsorption and complement/phagocytic activity, resulting in increased

half-life of nanoparticles. Similar methods have been utilized with poly(ethylene glycol) (PEG) (8) and other water soluble polymers, under the assumption that these hydrophilic brushes decrease the surface reactivity and thermodynamic favorability for adverse protein adsorption. While this has been met with some success, protein adsorption within these systems is inevitable and only a matter of time for proteins to find an energetically favorable conformation to adsorb. Systems similar to these might also potentiate dysopsonin binding *in vivo*, reducing the recognition by the immune system. That said, a phagocytic recognition still occurs over time, suggesting that inflammation can result in a chronic inflammatory cascade.

2.1.6.2.2 Thrombolytic nanoparticle activation

Thrombolytic activation is another potential consequence of nanoparticles contacting blood. Modulation of surface charge and density can initiate variations in clotting mechanisms (178). Specifically, negatively charged nonporous silica nanoparticles induce platelet aggregation, but when the same particles were surface-modified with amines this response was reduced (178) and similar results have been shown with carbon nanoparticles (179). Interestingly, increased platelet aggregation has been correlated with an increase in particle phagocytosis, suggesting that macrophages could ingest the nanoparticle-centered clots and initiate downstream responses (180).

Aggregation and thrombotic initiation has also been observed with cationic dendrimers in blood (181, 182), but not with hydroxyl- or carboxyl-terminated systems. This suggests that surface modifications can mitigate thrombolytic events to some degree. Extensive review of nanoparticle systems and their blood compatibility are summarized

elsewhere (183). Delineation of mechanistic details by which surface properties initiate thrombogenesis and complement activation, and whether procoagulant properties observed with cationic dendrimers extend to other nanoparticle structures such as larger nanoparticles, remain to be investigated. The key question is how surface properties influence these phenomena and how one can potentially harness such powers in order to influence engineering of more effective and safe materials.

2.1.6.3 Toxicological implications of nanoparticle-mediated inflammation *in vivo*

Global inflammatory effects of nanoparticles may potentially be directly related to thrombogenesis and complement initiation; however, the particles may still induce inflammation without any contribution from these systems. The current lack of understanding of the chronic toxicity of nanoparticles could have serious consequences and impede advancement to the clinic when intended exposure is desired. The mechanistic details which initiate potentially toxic outcomes remain unknown. For example, two iron oxide particles with similar cores but different surface chemistries initiated very different responses to cytokine levels of IL-1beta, IL-8 and TNFalpha *in vivo*. One formulation displayed little to no increase, while the other showed significant increases. The increased expression levels of these cytokines correlated with an induced *in vivo* cytokine storm, resulting in splenic congestion. Several experimental studies showed when nanoparticles are incubated *in vitro* with PBMCs and MM-6 (monocytic and macrophage lines), the increase in cytokine activation directly correlates with toxicity *in vivo*, such as DIC and cytokine storms (4). IL-8 is also upregulated by 4 nm gold

nanoparticles (184). However, many reports suggest little to no induction of inflammatory cytokines (i.e., gold (185) and iron oxide (186)). A study comparing gold and silver nanoparticles found that short-term silver nanoparticle exposure resulted in induction of ROS and NF-kappa B signaling, which led to direct increases in TNF-alpha and IL-6; however, gold nanoparticles did not exhibit similar profiles over the same time period. When exposure time of gold was increased, they did observe a significant inflammatory response (37). Additionally, osteolysis might be initiated by NF-kappa B induction in response to nanoparticle exposure, because the subsequent induction of IL-8 helps to induce TNFalpha and IL-6 (40). These examples may suggest that inflammatory responses are global nanoparticle phenomena and result after prolonged exposure independent of the nanoparticle.

Numerous studies have investigated how particle size is related to cytokine inflammation. For example, 5 nm silver nanoparticles exhibited higher toxicity than 100 nm silver nanoparticles in macrophages (187). Nanoparticle toxicity might actually be a function of surface area exposed to macrophages rather than size (188). This may suggest surface interactions are mediating inflammatory events.

Inflammatory events could be mediated by specific physicochemical properties or may be a result of nanoparticles themselves. These inflammatory events could be biologically detrimental such as in the case of chronic inflammatory events or could be resolved via normal hemostatic balances. Development of a fundamental understanding of what long-term exposure to nanoparticle systems does to the host environment is imperative, whether the effect is inert or destructive in nature. This information can provide an understanding of the safety and design considerations for these materials, yet

based on this incomplete picture nanoparticles are being advanced into clinical development.

Acute inflammatory reactions to nanoparticles can have profound effects. For example chronic silica exposure is associated with autoimmune diseases and chronic inflammatory states (188). Toxicological studies provide evidence that the crystalline form of silica induces upregulation of inflammatory and oxidative stress agents, such as cytokines, chemokines, reactive oxygen species (ROS), reactive nitrogen species (RNS) and nitric oxide (9, 170, 189-191). Most findings were associated with silicosis and lung cancer in mine workers (33, 170, 192-194), which are inflammatory events that have occurred after chronic exposure to crystalline silica exclusively via the inhaled route. However, little information exists on the long-term biological effects of amorphous silica. The rate of dissolution, degradation and elimination of amorphous silica are not well studied. Degradable forms of silica can potentially reduce these inflammatory events, paving the way for their utility in biomedical applications. Molecular silicates are not detrimental to the human environment at current levels of exposure, suggesting that degradation products could be well-tolerated (195). A prerequisite, however, for successful development of degradable constructs is to understand the biological fate of the degradation products.

2.1.6.4 Designing systems to reduce phagocytic recognition

It might be beneficial to facilitate bioinvisibility of nanomaterials to increase biocompatibility and reduce macrophage recognition *in vivo*. PEG and other hydrophilic polymers are commonly used in drug delivery to facilitate bioinvisibility. However, these

systems are still recognized by the innate immune system, taken up by phagocytes and rapidly removed from circulation. Researchers attribute this effect to the formation of antibodies against these polymers and other pharmaceutical excipients that are in heavy use. The formation of these antibodies can be attributed to the increased use of these systems in food additives and many dosage forms (196). Development of these antibodies directed towards hydrophilic systems creates immune reactions and increased clearance rates, highlighting the learning potential of our own adaptive immune system. This could be utilized to our advantage to potentially mask the surface of these systems with self-identifying proteins. By utilizing pathogenic or eukaryotic mimicry, reduction of complement activation and thus local recognition and uptake may be possible. For example, factor H is a cofactor for Factor I that mediates C3b cleavage and dissociation of the Bb complex inactivating the complement pathway (197). Pathogens that utilize Factor H binding in their immune defense mechanisms include HIV-1 and streptococcal M6. Researchers have utilized sialic acid, the main component on the surfaces of these pathogens, to bind Factor H in helping to evade complement activation and thus immune recognition. This component is also over expressed in erythrocytes such that as the erythrocytes age they undergo desialyation and initiate complement activation and phagocytic destruction (198).

Another potential surface ligand to aid in long circulation of nanomaterials is CD47. CD47 is a marker of self, overexpressed on erythrocytes, that helps them to evade the immune system during their long circulation period by binding to the SIRP-alpha receptor (199). Pathogens have already identified the utility of this system and overexpressed the system on some viruses, such as smallpox (200). The active binding

sequence of this protein has been recently identified and attached to the surface of nanoparticles with a resulting reduction in uptake via the MPS and drastically increased circulation times (201). More information on how nanoparticles interact with the complement system can be reviewed elsewhere (197). In general, these results suggest that utilization of markers of self can significantly reduce complement activation and phagocytic recognition, helping to promote drug delivery safety and efficacy.

2.1.6.5 Clinical nanoparticle-macrophage interactions

Therapeutic capacity and clearance mechanisms have been linked with macrophage activity in clinically relevant nanomaterial therapies. For example, liposomal chemotherapeutic formulations have been prescribed clinically on- and off-label for decades (e.g., doxil). These formulations exhibit increased plasma half-life as patients' age increases or monocytic activity decreases (Figure 2.4) (22, 23). Decreased levels of clearance appear to be a direct result of the decrease in phagocytic response, while increased phagocytic activity appears to increase clearance rates (22, 23). This propensity for clearance should provide clinical evidence for understanding nanoparticle MPS interactions.

Environmental nanoparticle MPS interactions induce well-known inflammatory morbidities (169, 202, 203). These mechanistically well understood and clinically relevant disease states, including silicosis, mesothelioma and pneumoconiosis, present after years of initial exposure. While the characteristics of the environmental particles responsible for these diseases differ from what is engineered today, the initial phases of these diseases follow similar patterns to what is observed in the acute toxicity studies of

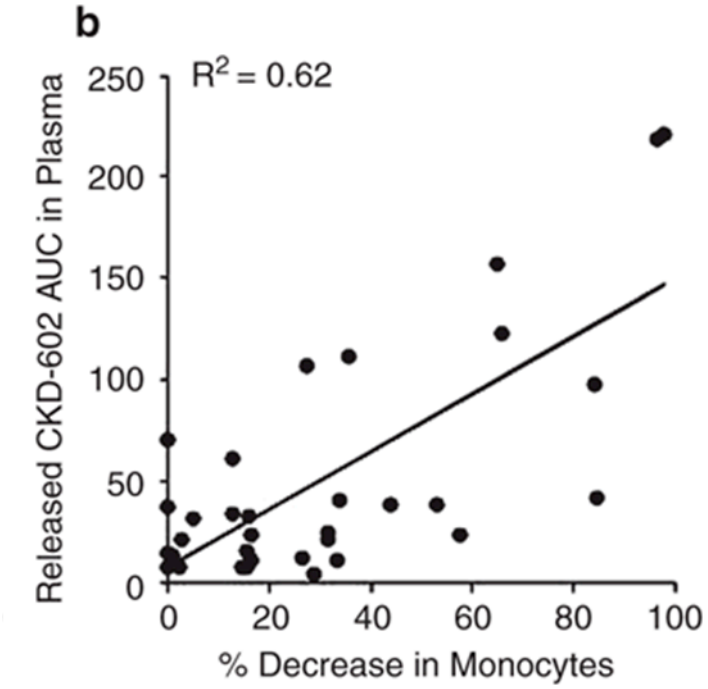

Figure 2.4: Increased monocytic activity in patients decreases AUC. This suggests the involvement of macrophages in clearance of nanoparticle formulations. Reprinted with permission from Caron 2012 (22).

engineered nanoparticles. These observations include local fibrotic lesions with increased recruitment of polymorphonuclear- and antigen-presenting cells, macrophages and dendritic cells (203). Some research argues engineered nanomaterials are “inert” and attempt to disprove parallels drawn between engineered nanomaterials and traditional environmental nanomaterial exposure disease states. This research suggests that large aggregates or microparticulates are responsible for these disease states, and that smaller nanoscale materials are completely cleared.

Generally, fibrotic mechanisms proceed over larger scales; we have no evidence to assume that under certain circumstances smaller nonclearable agents would not elicit similar responses (204). For example, tuberculosis (TB) is a chronic inflammatory fibrotic disease state, with hallmark macrophage involvement. TB is within the typically clearable size range; however, the pathogen is not cleared. To compensate, the body initiates fibrotic lesions as the control mechanism (205). The body may utilize similar mechanisms for potentially clearable nanomaterials.

Similar mechanisms could be initiated in other pathogenic or particulate exposures in multiple organ systems. For example, silica nanoparticles induce the release of inflammatory mediators such as interleukins, tumor necrosis factor alpha, transforming growth factor, monocyte chemoattractant proteins, and other inflammatory mediators (35, 39, 189). After silica nanoparticle treatment direct correlations are observed between the release of these factors and migration, proliferation, and differentiation of inflammatory and immunological cells (39, 154). These acute inflammatory events reflect potential for local recruitment and involvement of phagocytes and eventual development of chronic inflammation. How nanoparticles initiate these events and the specific role of surface

properties on altering inflammatory mediators and leukocyte infiltration remains unknown. Understanding initiation will be particularly important knowledge when designing systems that are intended to exhibit long-term residence within organs or circulation due to the potential of long term inflammatory affects, which could elicit toxicity.

2.1.7 Nanoparticle MPS interactions: Conclusions

Nanoparticle based drug delivery and imaging systems have the potential to be the next breakthrough for medical science. However, enormous complexity complicates understanding how these nanoparticles interact with the biological environment, and in the context of this review interaction with macrophages. The ability to engineer nanoparticle systems to overcome and avoid the deleterious effects or potentially utilize them to our advantage requires more knowledge of how current nanoparticles and macrophages interact. As we move forward, consideration of biological pathogenic interaction studies, known clinical effects from environmental nanoparticle exposure, and the rising studies in the engineered nanoparticle community will be of increased importance. Combining this knowledge will help to develop a platform that will provide us with the ability to make biocompatible systems with direct target affect including high affinity and specificity.

2.2 Synthetic and toxicological characteristics of silica nanomaterials for imaging and drug delivery applications

The chemical properties, structural properties, and abundance of silica provide unique, and inexpensive synthetic alternatives for product development. In recent years, the industrial world has seen a drastic increase in the production of products and processes that utilize several forms of silica (206, 207). Silica can now be found in many cosmetics, foods, and electronics. Due to its attractive synthetic properties it has become an ideal candidate for biomedical applications including but not limited to sensors (208), drug and gene delivery systems (209) and contrast agents (210).

Silica itself is the second most prevalent element in earth and as such is found in many living systems. This element can be found naturally or synthetically and is classified either as crystalline or amorphous. Crystalline materials are by far the most common, as much of the natural element is comprised in quartz, the main component in several rock types and sand. While silica is still considered to be nonessential to sustain life, it does appear to play an important role in maintaining homeostasis and the health of many living organisms (211, 212). As such, it is incorporated into various supplemental plant fertilizers to help maintain growth, mineral nutrition, and ward off fungal diseases (212, 213). Interestingly, several plant and marine life forms also include cellular pathways that are able to take natural elemental forms of silica and process it into an alternative organic form (214, 215). The organic form has proven to play a principal role in plant and animal life, assisting in structural and developmental characteristics in a variety of fashions, such as strengthening of cell walls, bone and cartilage (211, 213).

Individuals and animals which lack organic silica as a dietary supplement have shown increased risk for cardiovascular disease, osteoporosis, and Alzheimer's (216, 217). Much of this is linked to the ability of silica to interact chemically with native metallic ions such as aluminum and iron (216, 218, 219). However it remains unclear at what pivotal concentration level and chemical composition silica switches from a beneficial to detrimental state.

Silica exposure has been associated with autoimmune disease and crystalline silica has been classified by the International Agency for Research on Cancer as a class one carcinogen(188). Numerous toxicological studies provide evidence that the crystalline form induces upregulation of inflammatory and oxidative stress agents, such as cytokines, chemokines, ROS, RNS, and nitric oxide (9, 170, 189-191). Most of these studies are associated with silicosis and lung cancer in mine workers (33, 170, 192-194). While amorphous silica does not seem to present the same oral or inhalation risks as crystalline silica, the implication of introducing such a material via alternate routes of administration remains unknown. Thus extensive toxicological studies are needed to understand the environmental and health impacts of silica nanoparticles.

This portion of the chapter will address current amorphous silica nanoparticle synthesis, preparation, characterization, and subsequent toxicological evaluation. Emphasis will be placed on the use of these nanomaterials for drug delivery and imaging applications.

2.2.1 Amorphous silica nanoparticle synthesis

The unique inorganic chemical properties of silica provide an exceptional platform from which to build drug delivery and imaging systems. Synthetic sol-gel and polymerization methods provide a simple way to produce these nanomaterials in a large scale. The advantages of silica nanoparticles include:

1. *Relative chemical and thermal stability*
2. *Synthetic control over size and size distribution*
3. *Potential to induce alterations in geometry*
4. *Ease of surface modification*
5. *Ability to control encapsulation of molecules of interest*
6. *Economic affordability and ease of scale up*

These advantages will be individually discussed with a focus on implications in toxicity and their subsequent potential for drug delivery and imaging applications.

2.2.1.1 Relative chemical and thermal stability

Silica nanoparticles are generally synthesized via aqueous polymerization of silicic acids or through the Stober method which is the utilization of silicon alkoxides and their subsequent hydrolysis and condensation (220, 221). The two produce two very different core materials, with variations in density. Polymerization tends to permit for classically uniform particles, by allowing for full hydrolysis of monomer repeat units (222). Stober synthesis or silicon alkoxide nanoparticle formation however is generated through cluster aggregation, preventing full hydrolysis and thus a reduction in uniformity (Figure 2.5) (195, 221). However with the development of modified Stober methods or

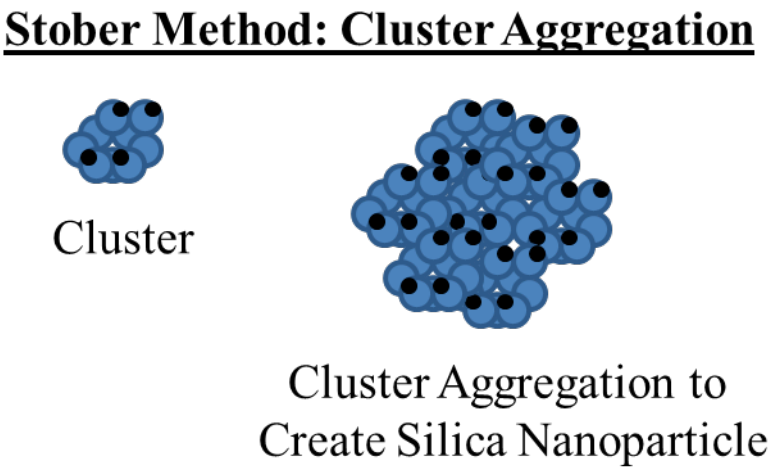

Figure 2.5: Stober method of silica nanoparticle synthesis. In the Stober method, silica undergoes spontaneous cluster formation which then can be used to produce particles. Adapted from Iler 1979 (201).

sol-gel chemistries, one is able to more carefully control synthetic procedures (223). Once formed, both of these processes lead to a very stable, relatively inert colloidal solution, which cannot be disrupted or degraded without further synthetic modification (222). This property is highly sought after in both drug delivery and imaging applications, as it provides a protective environment for the encapsulated material and assists in the reduction of systemic side effects in the human body. Current alternative nanoparticle carriers such as liposomes and micelles have the potential to dissociate *in vivo* and release potentially toxic materials into circulation (224, 225). Additionally, the native surface functionality of these particles is a terminal hydroxyl group, which provides a relatively hydrophilic surface, a property that is known to reduce systemic opsonization and increasing circulation times (226). It remains largely unknown if mechanism of toxicity of bare silica nanoparticles is due to hydroxyl functional interactions with the physiological environment or other physiochemical interactions. As will be shown later the masking of these hydroxyl groups does appear to reduce toxicity and hydroxyl groups facilitate functionalization.

2.2.1.2 Synthetic control over size and size distribution

Both polymerization and the Stober method allow for excellent control over polydispersity and size of spherical nanoparticles. By simply controlling the reagent concentrations and reaction conditions one can create a wide range of differing spherical nanoparticle sizes with a polydispersity index within 5% of the total synthesized particle (Figure 2.6) (222, 227). This provides an advantage over traditional drug delivery and imaging contrast agent systems such as random copolymers, liposomal and micellar

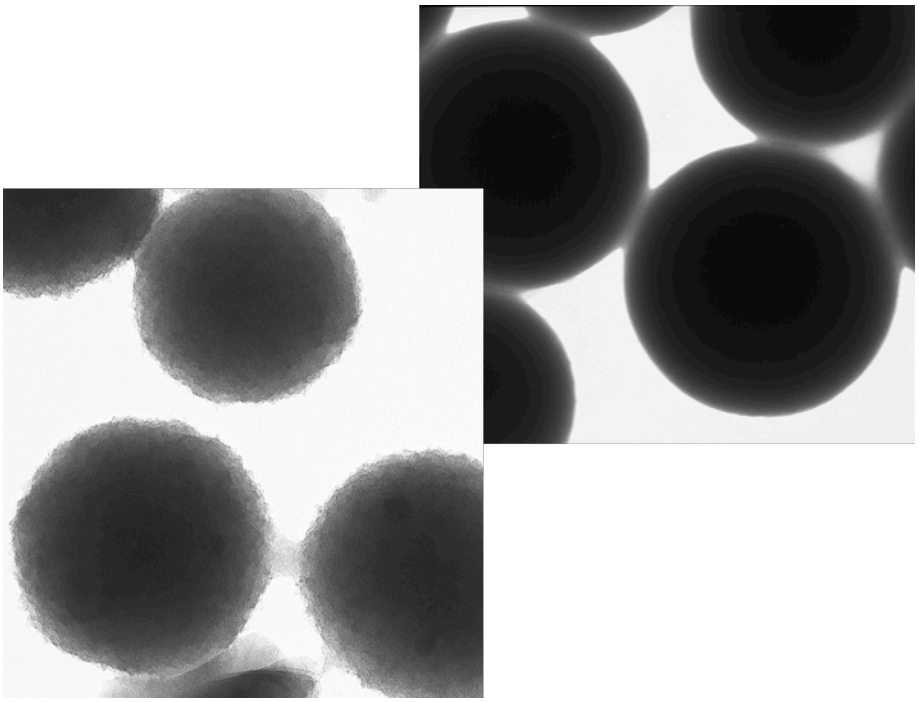

Figure 2.6: Transmission Electron Microscopy (TEM) images of porous and nonporous silica nanoparticles. Images illustrate uniformly synthesized porous (A, scale bar 100nm) and nonporous silica nanoparticles (B, scale bar 100nm) produced via the Stober and modified Stober methods. Unpublished data.

constructs, with potentially higher polydispersities (224, 225). This leads to increased error in loading and dosing, as variability in size ranges can increase or decrease encapsulation. Variation in size distribution can also influence cellular uptake, toxicity and biodistribution. This is extremely important as the literature outlines nanoparticle size dependent effects on toxicity, biodistrubution and uptake (142, 154, 228). Smaller nanoparticles generally have increased uptake and toxicity, mostly contributed to their increased surface area or exposure to cell surfaces (Figure 2.7) (142, 229). The ability to synthesize silica nanoparticles with defined size and size distribution allows systematic correlation of these parameters with cellular uptake, toxicity and biodistribution, which in turn enables development of constructs for safe and effective biomedical applications. Biodistribution and clearance routes have threshold size ranges which prevent or allow for particle accumulation. Thus, this characteristic will be important in engineering or designing drug delivery and imaging systems, as changes in size distribution could significantly alter targeting strategies and dosing mechanisms.

Systematic evaluation is not limited to controlled size and monodisperse systems. Investigators have also explored other synthetic routes to create other nanoparticles. Beck et al. (230) created one of the first most commonly used mesoporous silica nanoparticles, with the addition of a surfactant, cetyltrimethylammonium bromide (CTAB), using the Stober method. This surfactant facilitates the creation of micelles which are coated by initial silica crystals and assists in creating larger gaps during synthetic aggregation hydrolysis by inducing hydrophobic interactions. Similar processes have shown to create mesoporous nanoparticles via polymerization and acid catalysts (222, 231, 232). Alterations in surfactant and polymerization chemistry have allowed for the development

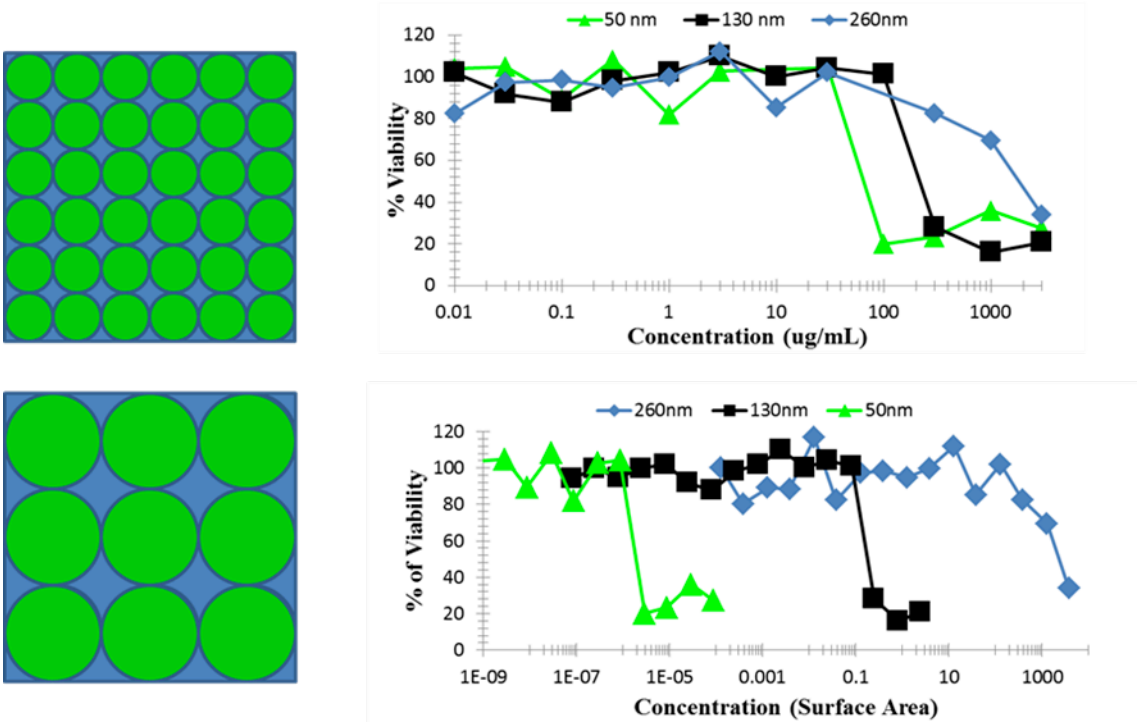

Figure 2.7: Plain silica nanoparticle toxicity is dependent on particle-cell surface contact area. The figure illustrates that at equal surface area, smaller particle size yield greater particle number (i.e., for every one 200 nm particle there exist sixteen 50 nm particles and for every one 100 nm particle there exist four 50 nm particles) and higher toxicity on RAW 264.7 macrophages. Fifty nanometer particles induced the highest toxicity, followed by 100 nm and finally 200 nm. Note that if particles are graphed via particle number, larger particles remain more toxic due to larger cell surface contact area. A. Demonstrates the toxicity profile when plotted against particle number; a larger particle facilitates higher toxicity due to larger contact area B. Demonstrates toxicity profile when plotted against mass. C. Demonstrates the toxicity profile when plotted against the surface area; all particles maintain similar toxicity profiles. Modified data from Malugin, 2010 (296).

of structurally different pores, significantly altering small molecule diffusion patterns (233, 234). The control over these diffusion patterns is key to being able to manipulate drug or contrast agent release. By following this process with acid extraction or calcination, the surfactant is effectively removed, leaving the amorphous material with large pores or holes (235, 236). It is interesting to note that toxicity profiles of some porous silica nanomaterials have not shown a significant difference when compared with their bare silica counter parts (others have shown opposite effects (237), and some *in vitro* studies have even proven to have a reduction in hemolytic capacity of porous materials (219, 238). This reduction could potentially be due to a decreased number of hydroxyl groups exposed to erythrocytes in circulation. Such a modification provides additional versatility in silica nanoparticles for delivery applications, as it allows for variations in functionalization and molecular encapsulation within the pores, which have been used potentially for subsequent drug release studies (209, 239).

2.2.1.3 Potential to induce alterations in geometry

Mesoporous silica synthetic characteristics helped to introduce the production of more diverse geometries. Modifications in surfactants, solvents, catalysts, salts, etc. can significantly alter the structural characteristics of the nanoparticles (235). Sol-gel solution phase chemistries can be altered and generate variations in geometries with a change, as little as, an adjustment of the surfactant properties (240). The surfactants introduce a unique alteration in the interfacial chemistry, causing significant modifications in formation of the solid crystal structure. These changes in the crystal structure facilitate changes in the morphological characteristics. For example helical mesoporous silica

nanorods have been produced utilizing CTAB and co-surfacant hexanol (241). A variety of different morphologies have also emerged utilizing CTAB and the addition of different functional silanes, which provide additional functional alterations in the interfacial chemistry (235). These examples illustrate exciting synthetic results because one can easily manipulate sol-gel principles to introduce dramatically different geometries. These geometries have proven to drastically alter toxicity and uptake (240).

Once the discovery had been made that surfactants could alter crystal and chemical bulk structural formations, investigators started experimenting with differences in nucleation of the same sol-gel chemistry. Instead of utilizing the base alkoxide or acid other inorganic or surface materials were used. Nuraje et al. (242) produced such an example of creating variations in geometry utilizing interfacial chemistries. At the interface of an organic and aqueous phase, where the aqueous phase contains catalyzing ions, one can introduce a silicon alkoxide and subsequently nucleate from that interface (Figure 2.8) (242). This effectively creates a face for the geometric nanoparticle, and one can alter the shapes obtained by altering the catalyzing ions and organic phase. An aqueous sodium hydroxide (NaOH) phase with an organic butanol phase for example will generate squares, while an aqueous hydrochloric acid (HCl) phase with an organic chloroform phase will generate triangles (Figure 2.9) (242).

Similarly with utilization of sol-gel chemistries and a template nucleation surface, synthetic silica schemes have been developed that provide unique tubular geometries. A template synthesis normally involves the introduction and subsequent nucleation of silica on the surface of a porous alumina membrane. After the silica has coated the inner layer of the membrane, the aluminum is generally dissolved away with phosphoric acid,

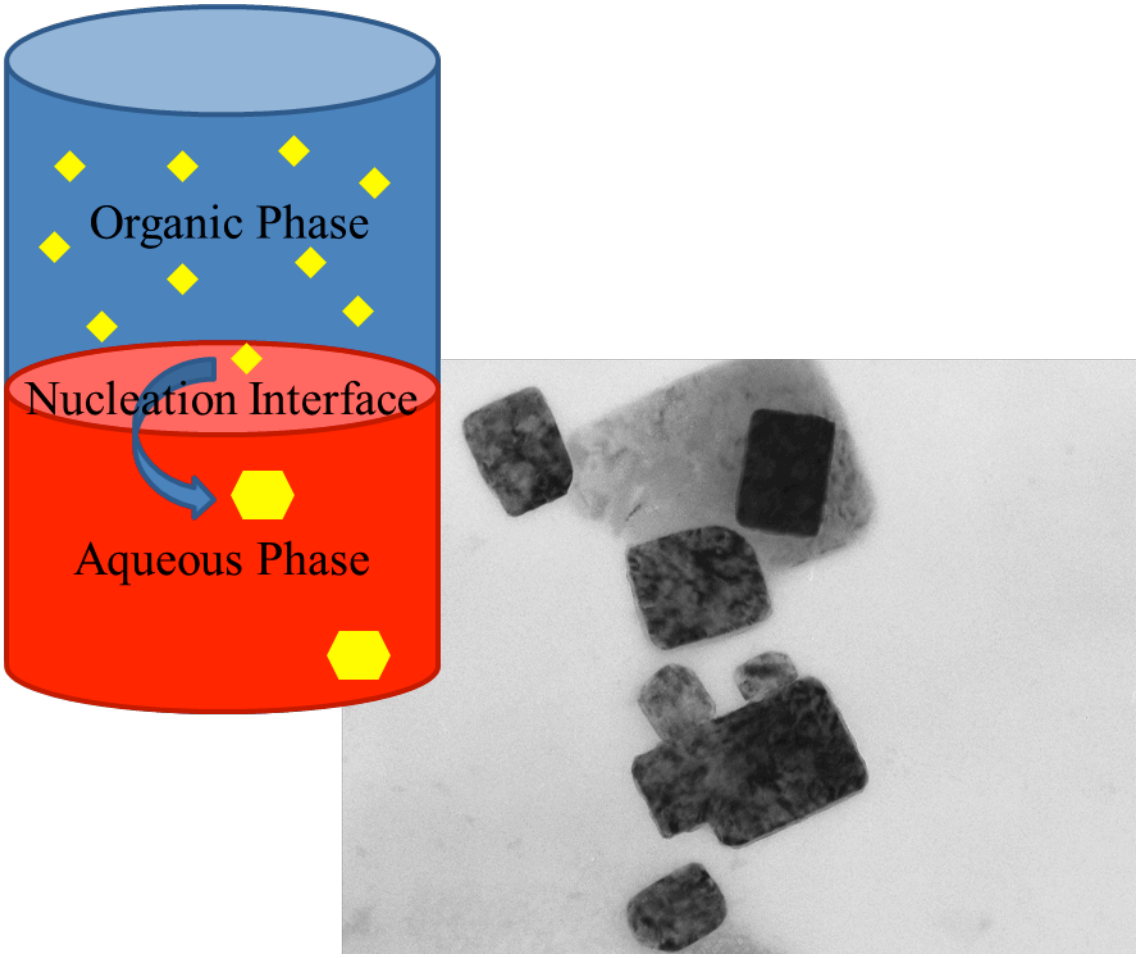

Figure 2.8: Silica nanoparticle interfacial chemistry. The separation between the organic and aqueous phases produces a nucleation interface, where a silica nanoparticle can form and precipitate into the aqueous phase. Diagram modified from Nuraje 2007 (238).

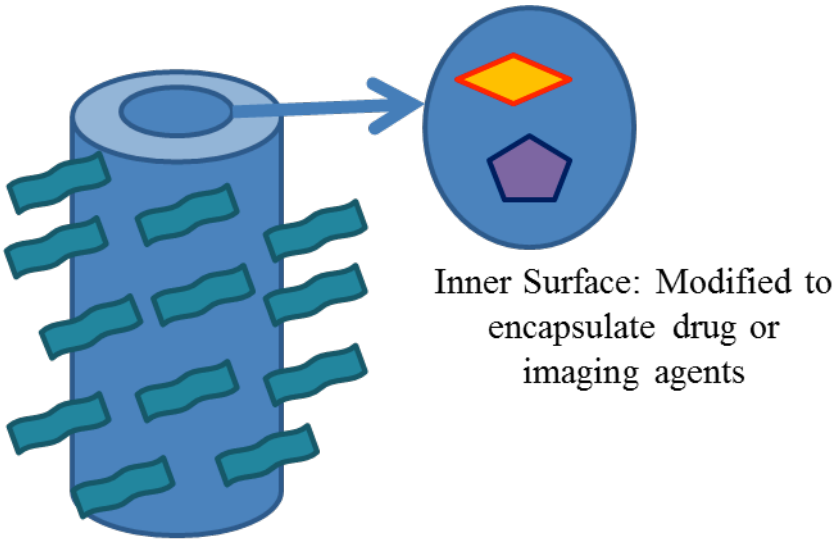

Figure 2.9: Inner and outer surfaces of silica nanoparticles can be differentially activated to increase biocompatibility and include drugs or imaging agents. Modified from Nan, 2008 (240).

leaving behind tubular or rod-like structures. One can alter the thickness of the tube wall by controlling the addition of silica to the reaction (243, 244).

The addition of another nanoparticle made out of differing materials, such as gold, polystyrene or other polymers, can also create a nucleation surface (245-247). The silica nanoparticle can grow off of this surface and one can subsequently remove the nanoparticle via high temperature burning or desolvation principles. Investigators have utilized these hollow silica spheres and rods to encapsulate a variety of different materials (239, 248).

As stated earlier, the development of materials with alterations in geometry could potentially influence toxicity, cellular uptake and biodistribution profiles. Recent studies with silica nanotubes in MDA-MB231cells (human breast cancer epithelial cells) suggest that alterations in nanoparticle surface properties, aspect ratio or size can influence cellular uptake (240, 244, 249, 250). Sol-gel mesoporous materials also show significant changes in cellular uptake, as mesoporous tubular like structures were not taken up as significantly as mesoporous spherical structures (251).

The use of various geometries of silica in biomedical applications proves to be an exciting prospect. First they introduce the ability to potentially change cellular uptake, biodistrubution and toxicity profiles. Second they provide unique functionalization capabilities where the inner and outer surface can facilitate differential functionalization. As one changes the geometry of the nanoparticle, it provides the potential to present several surfaces, each with the possibility of a different surface characteristic. For example a silica nanotube (SNT) presents an inner and outer surface (Figure 2.9). One is able to functionalize the inner surface of SNTs so that it incorporates hydrophobic agents,

while the outer surface is modified with hydrophilic biomolecular agents (243, 244). This characteristic will be helpful in drug delivery and imaging systems, as many prospective deliverable payloads are hydrophobic and in order to increase circulation, statistical site accumulation and biocompatibility of the construct that is delivered, it may be helpful to induce hydrophilic surface properties.

2.2.1.4 Ease in surface modification

Silica nanoparticles have a simple unique surface covered by hydroxyl functional groups. This surface can be easily modified via traditional silane chemistry. Silane chemistry has become an industry standard and is available commercially. The wide array provides the ability to functionalize the surface of these nanoconstructs with a broad variety of materials. This initiates surfaces that have much different characteristics than their respective silica core. These characteristics can be exploited and increase silica nanoconstruct potential for engineering drug delivery and imaging systems.

Functionalization can be as simple as small molecular weight functional groups attached via a silane, such as an amine or a carboxyl, which alters the charge density of particles. Charge density has proven to be extremely important to toxicity, distribution and uptake in silica nanoparticle constructs (24, 229). Positively charged silica nanoparticles were taken up by mesenchymal stem cells via endocytosis to a greater extent than plain silica nanoparticles while maintaining low toxicity (252). While these functional groups can alter toxicity and biodistribution profiles they also provide the option for introduction of more complex surface chemical synthesis.

Blaaderen et al. (253) have developed a novel fluorescent silica tagging method.

By utilizing the spontaneous addition reaction of the amine group of a 3 (aminopropyl)triethoxysilane (APES) and the thioisocyanate group of a fluorescein isothiocyanate (FITC) they were able to create a fluorescent silane group that could be easily coupled to the surface of a silica nanomaterial. This group then proceeded to coat the silica nanoparticle surface with a tetraethoxysilane (TEOS) which provided the FITC with a protective coat that significantly reduced photobleaching (Figure 2.10) (253). Subsequently research groups have attached other fluorescent molecules to the surface of the nanoparticles and proceeded to assess and compare the potential toxicity of these constructs to their bare silica counter-parts (254, 255). It is important to note that these groups have found that fluorescent particles have similar toxicity profiles to their bare counterparts. The development of this construct was important to translation of these nanoparticles to drug delivery and imaging systems. As it is essential that detection methods that aid in devolving uptake, toxicity and transport mechanisms should not affect the properties of the construct.

These functional surface modifications have also provided the ability to increase circulation times by reducing protein absorption and opsonization with the addition of hydrophilic surface groups, such as poly(ethylene glycol) (PEG) and other polymers (235, 256-259). Stayton et al. (260) conducted an extensive study investigating the effects of specific protein adsorption, on 13.3 nm silica nanoparticles in A549 cells (human lung carcinoma cell line). The analysis included hemoglobin, albumin, histone, pre-aggregated and complete medium. Protein adsorption differed little from protein to protein. Those

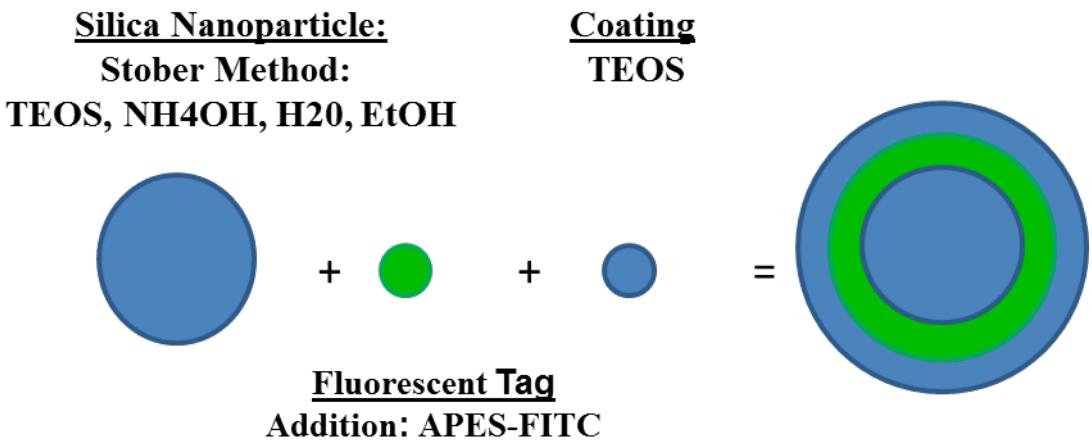

Figure 2.10: Fluorescent labeling of silica nanoparticles. Abbreviations: tetraethoxysilane (TEOS), ammonium hydroxide (NH4OH), water (H2O), ethanol (EtOH), 3-aminopropyltriethoxysilane (APES) and fluorescein isothiocyanate (FITC). Modified from Blaaderen, 1992 (250).

cultures incubated with single proteins tended to form particle aggregates, while bare particles had a higher degree of uptake. Additionally, those particles adsorbed with histone tended to have a reduced zeta potential which appeared to correlate with faster uptake. The investigators also created particles with a cadmium surface modification which appear to reduce toxicity and uptake (260). Furthermore, polymer coatings have shown to increase circulation, and significantly reduced particle toxicity on certain cell lines (24, 229). It is important to note that proteins adsorbed on the surface of silica nanoparticles have significant effect on cellular uptake and distribution (2, 93, 261, 262). The protein itself could potentially interact with cell surfaces and thus initiate adverse events. For example Chen et al. (263), suggested that nucleoplasmic protein aggregation significantly impaired nuclear function, leading to the inhibition of proliferation, transcription and replication. Surface modification can alter significantly the interactions and thus the protein association with the nanoparticle surface(264). Thus it will be important to pay attention to protein adsorption onto silica nanoparticles in the context of their biocompatibility, biodistribution and cellular uptake.

Targeting motifs have also been displayed on the surface of these particles to aid in active localized targeting to tumor sites and reduction in nonspecific uptake. Kumar et al. (254) created fluorescently labeled particles with transferrin surface modification which showed cell internalization within Mia-PaCa (pancreatic cancer cell line) and without modification showed no internalization. Additionally, Liong et al. (265) utilized a folic acid targeting motif and saw a significant increase in uptake of multimodial silica nanoparticles in PANC-1 (pancreatic cancer cell line).

Surface modification can also play a key role in the development of stimuli

sensitive materials. Stimuli sensitivity is a unique property that could provide an additional versatility to drug delivery systems. For example, porous silica nanoparticles can be utilized to trap drug molecules or imaging agents that are usually systemically toxic (265-267). These can be capped with materials such as cadmium sulfate, gold nanoparticles, dendrimers, or polymeric supports until they reach the intended site. The polymeric support can then initiate release dependent on changes in the local environment such as pH or reactive species (Figure 2.11) (268-275). For example, Nguyen et al. (273) have developed such a nanovalve for mesoporous nanomaterials where the valve is opened and closed via oxidation and reduction reactions. Additionally these materials can incorporate enzymatic identification markers to facilitate cleavage of the polymeric support (270, 276). These stimuli sensitive nanoparticles have also utilized mechanical processes such as magnetic fields to open magnetically capped porous materials (277). Stimuli-responsive silica composites can be used in delivery of bioactive and imaging agents, or theranostics, where release and/or imaging at the target site is desired.

2.2.1.5 Ability to control encapsulation of molecules of interest

In addition to exceptional surface modification characteristics, one is able to utilize the silica sol-gel chemical properties to dope and control encapsulation of other molecular agents. Similar to the synthesis of hollow spheres and rods, it is possible to stimulate nucleation off of other materials and encapsulate them within silica constructs. Such examples are iron oxide, quantum dots and gold (208, 278, 279). These doped materials provide useful alternative methods of detection such as fluorescence for

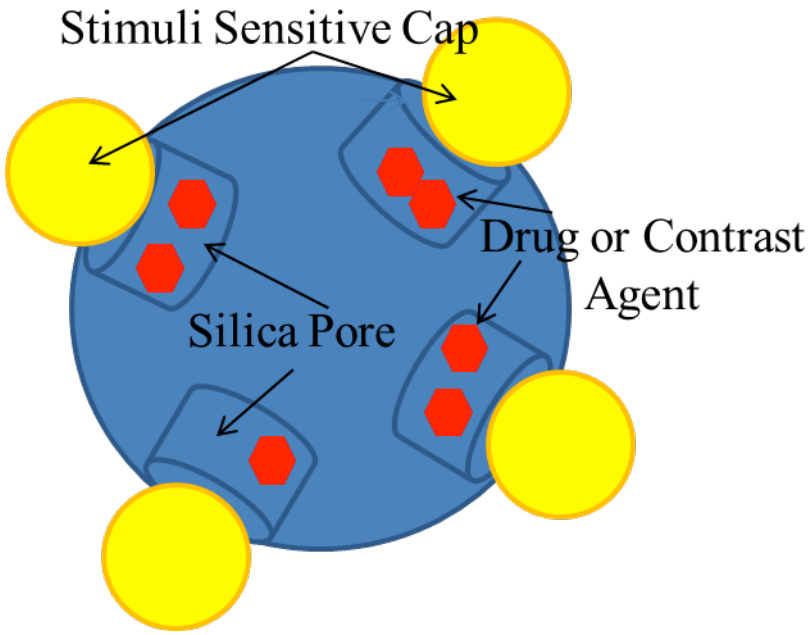

Figure 2.11: Encapsulation of payloads by porous silica nanoparticles. Payload (contrast agent or drug) can be released depending on environmental stimuli. Modified from Slowing 2008 (215).

confocal imaging or magnetic dipole capabilities for magnetic resonance imaging (MRI), but still retain the benefits of silica properties. Initial toxicity profiles on these materials have also proven to be similar to bare silica constructs, however it is important to note that some of these materials have shown leaching from the silica core (271). In the development of these materials it will be important to ensure that the silica constructs not retain toxicity but also any encapsulated leachable material. In addition to the encapsulation of imaging agents within these systems, therapeutic molecules have also been incorporated (144, 209, 280, 281).

Composite materials have also been formed utilizing silica (282). These composite materials have provided a unique capability of composite silica degradation, something that traditional silica nanoparticles do not offer. Park et al. (283) developed a complex of several 3-5 nm silica particles within a dextran coating. This composite created 130-180 nm constructs that could then be degraded to release the 3-5 nm particles which can subsequently be cleared(283). With the development of degradable materials the utilization of silica in drug delivery systems is significantly more promising, as clearance mechanisms of current silica constructs have still not been devolved.

Additionally, these composite materials have encapsulated proteins and immobilized enzymes within the silica nanoparticle. Investigators have done so by prehydrolyzing the silicon alkoxide and then simply adjusting and maintaining a stable pH range for which the protein retains stability. This process has provided effective doping capabilities without altering the conformation or shape upon release, which is extremely important to retaining function. This material provides an interesting approach to drug delivery as it helps to reduce degradation potential in circulation (284, 285).

These degradation profiles are promising as they provide evidence that inorganic materials could be developed with the ability to specify doping and enhanced control over therapeutic release rates.

2.2.1.6 Economic affordability and ease of scale up

Silica nanoparticle systems can be generated and purified with ease in large quantities at low cost. This is essential in clinical translation of these materials. Pharmaceutical and biomedical corporations are looking to invest in materials which are easy to produce and have the capability to present both an enhanced therapeutic benefit, as well as economic turnaround. Even with the ease in the synthetic chemistry and purification, some additional factors such as characterization and sterilization remain.

2.2.2 Silica nanoparticle characterization

Once silica nanoparticles are synthesized it is essential to effectively characterize the constructs. Size, charge, chemical core and surface composition all need to be validated and verified in order to successfully assess and re-evaluate the efficacy and the impact on delivery of these constructs. Presented here are only a few methods of characterization to illustrate each technique's pros and cons. Thus the key point is that validation must be made through multiple sources.

2.2.2.1 Size

Size characterization is essential because as previously mentioned factors such as cellular uptake, biodistribution and toxicity are dependent on size and surface area.

2.2.2.1.1 Dynamic light scattering (DLS) or photon correlation spectroscopy

This method shines a light source at a solution that contains a colloidal dispersion of the sample. The particles in the sample undergo Brownian motion, which creates interference in light penetration and introduces scattering of light. The light that is scattered is detected and translated into a velocity, which can be back calculated into a size. The measurement itself does not serve as a complete characterization of size, as it only provides the polydispersity over the total sample and measures the hydrodynamic radius rather than the actual particle radius. It is however a less expensive option to assess and quantify the size and polydispersity of a nanoparticle sample. The method is also helpful in the identification of aggregation of particles, due to surface modification or charge instability on the surface (286).

2.2.2.1.2 Transmission electron microscopy (TEM)

This method is a highly sensitive method that utilizes a beam of electrons emitted and passed through a dried sample on a copper grid. An image is generated via the detection of the electrons through the sample. These images can then be manually or electronically measured to assess the actual size of the particles. Due to the sensitivity of the instrument, particles in the single nanometer range can be detected. It is important to note that once particles are dried, most nonrigid surface modifications such as polymers or peptides are not displayed, due to collapse and nonexistent interaction with a solvent system. Thus, the actual size of the particle could potentially be much different than the representative image. Additionally, it is extremely difficult to ascertain surface topography or visualize porosity of dense materials due to electron penetration (287).

2.2.2.1.3 Scanning electron microscopy (SEM)

SEM utilizes a beam of electrons and detects the secondary or backscattered electrons of a metallic coated sample, introduced post sample drying. Due to the detection method it is difficult to provide effective resolution for particles much below 50 nm. However, surface topography can be resolved. Similar to TEM, soft organic modifications or materials are undetectable (288).

2.2.2.1.4 Atomic force microscopy (AFM)

AFM utilizes a dragging probe to probe the surface of a material and detects small vibrations, due to surface topography, utilizing a piezo electrode. This method can be performed in solution and thus can provide size information on both rigid and nonrigid materials. AFMs have been utilized to detect and image at the molecular scale, asserting topographical changes within 5 nm (289). However, changes in instrumentation set-up and sample preparation can significantly affect resolution (290).

2.2.2.2 Charge

As stated earlier, charge density plays an important role in directing uptake, distribution and toxicity. By controlling charge it is possible to direct the biological fate and toxicity of silica nanoparticles.

2.2.2.2.1 Zeta potential

This is a fast, efficient measurement of the electric potential of a colloidal suspension. By passing an electric field through the solution, one is able to detect zeta

potential at the interfacial double layer which can then be compared to a point in the bulk solution calculating a relative charge solution value. This number is extremely useful in the identification of the stability of the solution. Generally zeta potential values between -20 to +20 do not have enough electrostatic repulsion to be stable colloids, and thus they aggregate to create solution stability. Additionally, it can be a useful measurement to provide charge interaction comparison between particles and cell surfaces. It is important to note that this value is highly dependent on pH and salt concentration, since it measures the ions in solution. Thus, when taking zeta potential measurements one must note that physiological environments differ significantly from measured values, so the number they provide is relative (291).

2.2.2.2.2 Surface composition

Cell-cell mediated interactions via viable, nonviable, native and foreign materials are generally through conformation arrangement or chemical identification. This also appears to be the case in nanoparticle interactions, thus surface composition will be key in characterization.

2.2.2.2.3 Thermogravimetric analysis (TGA)

This is measurement based on weight loss due to increases in temperature and effectively burning off attached surface materials (i.e., polymers). Modified silica samples are heated after a thorough drying process and data is extracted and compared to bare silica nanomaterials. Correlations can be drawn between weight loss and average amount of material located on surface. This measurement provides evidence that

compound(s) exist on the surface. However correlative information is limited to melting temperature of the sample, thus it is difficult to discern the actual material (292).

2.2.2.2.4 Nuclear magnetic resonance (NMR)

This measurement is obtained through the induction of a magnetic field on an object. This field provides spin ratios which can then be correlated back to chemical structural characteristics, and subsequent molecular identification. The method relies on heavy training and can be extremely time consuming based on the surface modification. However it provides some of the most accurate and quantifiable information (293).

2.2.2.2.5 Infrared spectroscopy (IR)

This measurement is obtained by emitting infrared band on a sample and recording the absorption of stretching and bending frequencies. This also can be correlated back to chemical structural characteristics and subsequent molecular identification; yet, limited in quantification (294).

2.2.2.2.6 Traditional fluorescent labeling or chemical substitution
reactions

One can tag the surface modification or utilize a reagent that reacts with the surface modification to create a product which can then be measured via absorbance or fluorescence. The generation of a calibration curve can provide quantification for surface modification (295).

2.2.3 Silica nanoparticle preparation for biological evaluation

Following synthesis and characterization it is essential to effectively sterilize the particles in order to validate and verify the safety and efficacy of the constructs. Again this proves to be a difficult task for inorganic nanoparticles as many traditional sterilization techniques are inefficient, ineffective, or impractical. Without sterilization, drug delivery and imaging devices could potentially be contaminated, leading to toxic side effects not due to the construct itself but the contamination within the suspension the construct exists. For a more comprehensive review detailing experiments evaluating the effects of sterilization on nanoparticles the reader is directed elsewhere (296). The following briefly outlines the pros and cons of traditional sterilization techniques.

2.2.3.1 Heat and autoclaving

Traditional silica inorganic particles can be heated at extremely high temperatures (~500 C). These temperatures are sufficient to both kill bacteria and burn away endotoxins. However, the temperature induced does have the potential to detrimentally degrade any surface modifications or molecular encapsulations. A lower temperature alternative is autoclavation. However most natural or mimics of natural materials still degrade at these temperatures or pressures.

2.2.3.2 Filtration

Filtration through traditional 200 nm pore filters are sufficient to remove most bacteria. However endotoxins still pose a significant problem. Additionally, 200 nm pores will only work for particles much smaller than the pore size range and many

nonspherical or geometric nanomaterials might be caught up and remain within pores themselves.

2.2.3.3 Gamma irradiation

Ionizing radiation is emitted on samples to destroy bacteria and alter endotoxin formation effectively reducing inflammatory response. However, irradiating samples can ionize the sample or destroy surface modifications, which are not desirable.

2.2.3.4 Ethanol

Soaking materials within ethanol effectively destroys bacteria. However endotoxins remain in solution. Sterilization is one of the determining factors behind utilization of any nanotechnology-based construct for clinical applications. Each sterilization technique provides both sufficient pros and cons, while a combination of the techniques may prove to be ideal. It is important to note that sterilization techniques could potentially alter size and agglomeration, so it will be key to ensure technical composition is maintained through this process.

2.2.4 Toxicity of silica nanoparticles

Limited toxicity profiles exist on amorphous silica nanoparticles. However for use of silica nanoparticles in a clinical setting it is imperative that their toxicity *in vitro* and *in vivo* is carefully evaluated. As previously discussed, size, shape, surface modification and composition have proven to affect toxicity, distribution and uptake of silica nanoparticle constructs. Outlined here is a brief overview of how these characteristics affect silica

nanoparticle interaction with *in vitro* and *in vivo* environments. By paying close attention to outcomes this review will also attempt to address modifications or utilization of particular characteristics to obtain better engineered silica nanoparticles for biomedical applications.

There are two distinct modes of cell death: apoptosis, programmed cell death, and necrosis, premature cell death. Cytotoxicity has been indirectly linked to markers of these modes of cell death and their subsequent initiation events. Such an example is caspase-3. This is an important marker of apoptosis and it has been shown to be up-regulated in macrophage cell lines following silica nanoparticle treatment (39). Additionally, other modes of cell death can be initiated by other cytotoxic cellular events. The current initiation modes of cell death remain uncertain. Is it however certain that if silica nanoconstructs are instigating these events, in order to engineer safe and effective constructs, causation and subsequent elimination of these events need to be addressed.

It is important to note that bare silica nanoconstruct toxicity is cell type dependent. Thus the route of administration influences alterations in toxicity as well. Epithelial cells show very little to no cytotoxic effects when treated with silica nanoparticles (Figure 2.12) (297, 298). However, fibroblast cell lines and those cell lines with longer population doubling times or lower metabolic rates have been shown to have a substantial increase in susceptibility to toxic effects (299). Cells with phagocytic activity such as macrophages, and to some degree endothelial cells, appear to be the most affected cell types (300). Thus it will be important to pay close attention to the cell type(s) which many of these assays are performed on and the mechanisms that induce

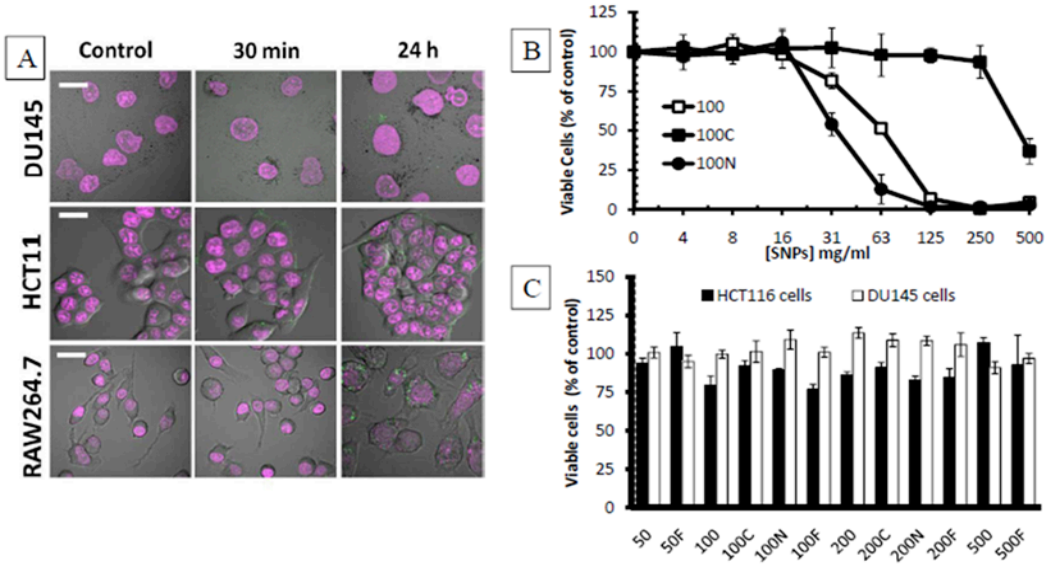

Figure 2.12: Influence of cell type and surface modification on toxicity. As shown, silica nanoparticle treatment does not induce HCT116 or DU145 epithelial cell toxicity, while it does induce RAW 264.7 macrophage toxicity. IC_{50} values in RAW 264.7 cells are heavily dependent on surface modification, as amine (N) modified particles are more toxic than unmodified and carboxyl modified particles (C). A) Confocal microscopy image of DU145, HCT11 and RAW264.7 cell nucleus stained with DRAQ5 and particles labeled with FITC. These images illustrate the relative uptake of these particles. RAW264.7 cells show a significant increase in relative uptake. B) RAW 264.7 WST-8 proliferation assay, 100nm plain, carboxyl and amine modified particles. C) HCT116 and DU145 WST-8 proliferation assay, 100nm plain, carboxyl and amine modified particles, little to no toxicity was observed. Modified from Malugin, 2010 (296).

toxic susceptibility (298). This can ensure that surface or material modifications are investigated to avoid cytotoxic mechanisms that are induced by processes like phagocytic activity. If toxicity has been identified or suggested it is crucial to determine the causation of cellular toxicity.

2.2.4.1 Toxicity via cellular internalization

Prior to discussion of potential toxicity mechanisms it will be important to address how nanoparticles can interact with cells and the most probable modes of internalization. Silica nanoparticles display on their surface approximately five hydroxyl functional groups per nanometer (301). The very nature of the particles is foreign to the human body and as such phagocytosis facilitates another uptake mechanism. Cells can also be internalized via caveolin and clathrin-mediated endocytosis, macropinocytosis or pinocyotsis (302). Each of these mechanisms generally has a size and surface dependent threshold (302).

The most probable mechanistic route of internalization is via endocytosis followed by encapsulation within lysosomal compartments (Figure 2.13) (298, 303, 304). It is important to note that the acidic pH of the lysosomal compartment is not sufficient to facilitate degradation of these particles. Thus after internalization these constructs have the potential to do irreversible cell damage if they are released from cellular compartments or internalized into important functional compartments such as the mitochrondria. Some literature sources have started to devolve potential silica nanoparticle escape routes as well as cellular compartment recycling. It has been suggested that silica nanoparticles remain within cellular compartments long enough to

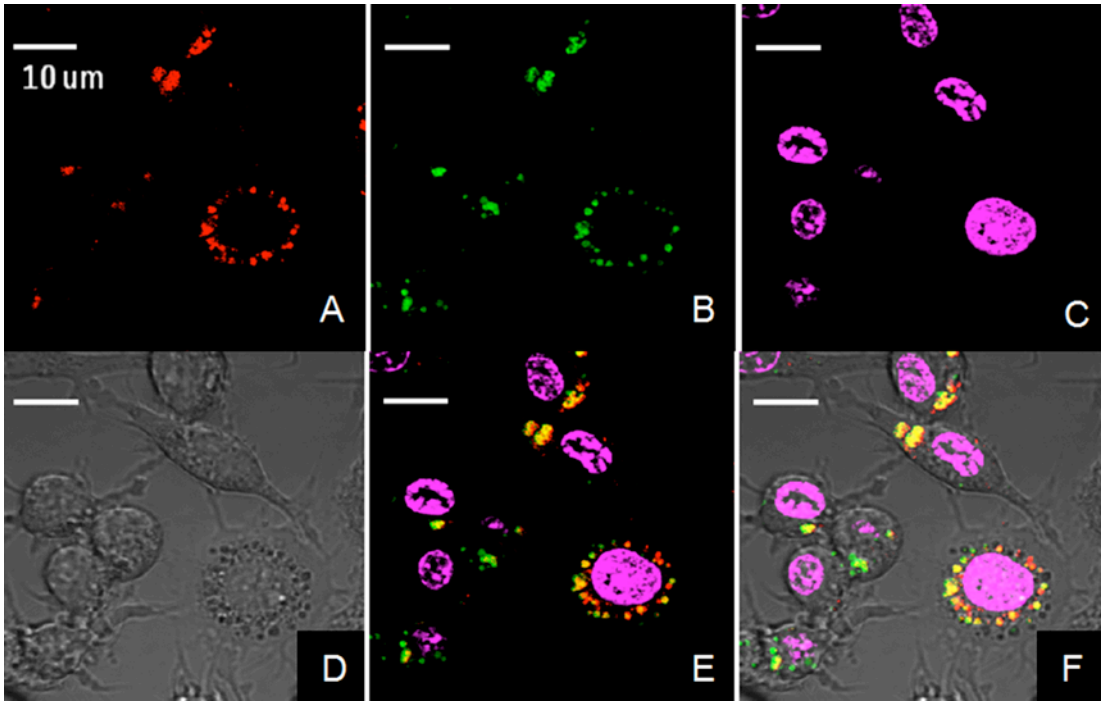

Figure 2.13: Confocal images of silica nanoparticle uptake in RAW 264.7 macrophages. Silica nanoparticles are colocalized in lysosomal compartments (yellow color in figures E and F). A. Lysosomes are stained with lysotracker. B. Particles are stained with FITC. C. Nucleus is stained with DRAQ5. D. Transmitted image of RAW 264.7 cells. E. Fluorescence overlay. F. Transmitted and fluorescence overlay. Modified Data from Malugin, 2010(296).

be released from late stage lysosomes into the cytoplasm. This has been confirmed via fluorescent microscopy and the delocalization of silica nanoparticles with lysosomal or endocytic compartments (305).

Increased cytoplasmic presence can increase cellular compartmental encapsulation and damage. One such example is the mitochondria. Chang et al. (299) compared the results of an (4,5-Dimethylthiazol-2-Yl)-2,5-Diphenyltetrazolium Bromide (MTT), mitochondrial function assay of ~80 nm bare silica to chitosan silica nanoparticles, on WS1, CCD-966sk (human skin adherent fibroblasts), MRC-5 (human lung adherent fibroblast), A549, MKN-28 (human cancer gastric epithelial), and HT-29 (human caner colon epithelial) cells. The results indicate that cancer mitochondrial function was more resilient to silica nanoparticle treatment. Fibroblast cell lines were susceptible to functional damage and chitosan modification significantly reduced toxicity. Julien et al. (306), Choi et al. (307) and Malugin et al. (298) found similar toxicity results.

2.2.4.2 Toxicity via particle-cell interaction

Cellular internalization however is not the only possible mechanistic route of toxicity. Silica nanoparticle cell interaction could potentially be sufficient to induce inflammatory or coagulation cascades, triggering signaling pathways and subsequent damage. Some investigators believe that nonspecific silica nanoparticle interaction with cells is sufficient to create membrane damage. Lactate dehydrogenase (LDH) or membrane integrity assays have supported this hypothesis (299, 308). It however remains unclear what initiates this damage. Also the influence of surface functional groups,

charge, hydrophobicity and contaminants need to be examined in detail.

The hydroxyl groups on the surface of the silica nanoparticle can also react with native species, such as iron in the Fenton reaction, or cellular receptors. Both modes create radicals which induce oxidative stress and reactive oxygen species (ROS) (140). Increase in ROS levels can cause oxidation of deoxyribonucleic acid (DNA), protein and lipids, induce mitochondrial dysfunction and significantly alter the genes related to the inflammatory and apoptotic response. Certain markers play a key role in indication of oxidative stress and suggest functional cell damage, such as increases in malondialdehyde (MDA) and Thiobarbituric Acid Reactive Substance (TBARS) and decreases in glutathione (GSH). MDA and TBARS indicate amplified lipid peroxidation and GSH is a ubiquitous sulfhydryl-containing molecule that is responsible for maintaining oxidative homeostasis, and does so by reducing cellular oxidation species within the cell. Oxidative stress induction via bare silica nanoparticles has been shown to be a potential mechanism of cellular toxicity in macrophage, embryonic kidney and bronchoalveolar carcinoma cell lines (13, 141, 283). Wang et al. have linked a potential apoptotic cell death mechanism, as a result of oxidative stress, with a flow cytometric analysis, by proving that the sub-G1 population of HEK293 (human embryonic kidney cell) increased, with a G2/M phase arrest (309).

Nanoparticle cellular interaction can also stimulate the release of primary and secondary inflammatory mediators, such as cytokines, chemokines, nitric oxide (NO) and expression of inflammatory genes (283). Increases in interleukins (such as IL-1beta, IL-6, IL-8, IL-10, etc.), tumor necrosis factor alpha (TNF-alpha), transforming growth factor (TGF), monocyte chemoattractant proteins (MCP-1), macrophage and inflammatory

proteins (MIP-1, MIP-2, etc) and their respective messenger ribonucleic acid (mRNA), have been shown to be up-regulated in cell lines in environments post *in vivo* and *in vitro* with silica nanoparticle treatment (35, 189, 283). Many of these represent inflammatory signaling factors which induce cellular migration, proliferation, differentiation and apoptosis within the biological environment. Direct correlations can be drawn between increases in these inflammatory mediators and increased levels of inflammatory or immunological cells (T, B, NK cells) in the local environment post silica nanoparticle treatment (34, 283). All of these events are hallmark indications of larger developing inflammatory events. Additionally, inflammatory events along with direct particle interaction with cell environments can adversely enhance cellular activation and subsequently induce thromobogenicity (310). If the induction of these mediators is indeed due to surface interaction, covering the surface or hydroxyl groups of the particle with a biocompatible material could potentially provide a safe alternative.

Circulation of bare and modified particles can induce additional interactions with other circulating blood cells and investigators have begun to study these implications. As stated previously, evidence suggests that bare silica nanoparticles cause the lysis of erythrocytes (140). Modes or mechanisms of cell death that have been proposed include the induction of reactive oxygen species, or surface electrostatic binding interactions with tetra-alkyl ammonium groups (218). It has been shown that the density of hydroxyl groups on the surface of silica nanoparticles is directly correlated with the rate of hemolysis (140, 311). Slowing et al. (219) reported that mesoporous silica nanoparticles maintain safe levels of biocompatibility, with low hemolysis activity. However contradictory these reports appear to be, it is interesting to note the impact of surface

density and charge on the safety of particular constructs. When designing drug delivery or imaging systems, it is important to attempt to minimize hemolysis via surface, bulk or geometric modifications to reduce side effects.

2.2.4.3 Toxicity via a combination of particle internalization and cellular interaction

Genotoxicity, chromosomal aberrations and mutagenicity are also extremely important factors to consider both in the long term health of the patient and in development of these particles. Waters et al. (142) performed a transcriptional analysis on a variety of different size ranges of particles, utilizing microarrays on RAW 264.7 (murine macrophage cell line). This provided evidence of adverse amplification effects on the expression of genes that are implicated in inflammatory and stress inducing events, such as chemokines and cytokines. Surface area was directly correlated with the level of gene expression abnormalities, which suggests inflammatory stimulation rather than genotoxicity induction. Similarly, Jin et al. (312) showed that luminescent DNA nanomaterials presented little DNA damage, which did not necessarily correlate with cytotoxicity levels within A549 cells, suggesting cell death occurs through other mechanisms. Similarly Barnes et al. (313) reported that 3T3-L1 (fibroblast like cells) incubated with silica nanoparticles produced no genotoxicity evidence within a reproducible comet assay which assesses breaks in both single and double stranded DNA. These results provide a positive outlook for the application of these materials in drug and imaging systems.

2.2.4.4 Toxicity via biodistribution and clearance mechanisms

Due to silica's inherent inability to degrade, clearance mechanisms and organ accumulation are extremely important to evaluate, to ensure the safety of these constructs. Borchardt et al. (314) investigated the biodistribution of a variety of different surface modified spherical nanoparticles, and found that increasing the hydrophilicity of the coatings led to increased intestinal delivery and lower uptake via liver and spleen, while increasing the chain length and attaching a butyltrichlorosilane increased muscle accumulation and bone marrow delivery, respectively. These investigators have proposed that alteration in biodistribution is due to both the hydrophilicity and steric inability for proteins or opsins to adsorb to the surface of the silica constructs. Additionally, the study introduced the aspect that bare silica has a much slower liver absorption than most common drug carriers. It will be important to keep these results in mind in development of silica nanoparticles, as this study suggests that size, geometry and surface modification could potentially provide directed targeting and initiate elimination in toxicity.

An important issue is clearance of nanoparticles. Ideally, particles should be excreted via the kidney so local liver accumulation does not occur. Liver clearance however is acceptable if particles are cleared through hepatobiliary mechanisms. Nevertheless, toxicity due to prolonged particle accumulation can still pose a significant threat. Burns et al. (278) were able to develop labeled silica nanoparticles of diameters 3.3 and 6.0 nm and showed complete clearance within 48 hours. He et al. (24) demonstrated that 45 nm silica nanoparticles with free hydroxyl, carboxyl and PEG modifications were cleared mainly through liver excretion with a high circulation rate for PEGylated particles. Additional data pointed to removal via renal routes in addition to

hepatobiliary mechanisms, suggesting that particles are statistically able to accumulate renally and with modification. Hudson et al. (238) examined rat subcutaneous biodistribution and clearance of 180 nm-4 um silica nanoparticles at four days, two- and three- months. Significant particle accumulation was found in the subcutaneous nodule at four days. However two- and three- month time points showed little to no accumulation. Following i.v. injection into mouse models doses above 1 mg per animal were lethal.

2.2.5 Applications of silica nanoparticles in drug delivery and imaging

2.2.5.1 Drug delivery

Drug delivery is defined by the ability to effectively attach or encapsulate a therapeutic payload, deliver the respective payload to a site of interest and finally release it at an appropriate therapeutic release rate. Silica nanoconstructs as outlined within the chapter have three distinct advantages over traditional delivery constructs: 1. the construct itself provides protective stability with which one can both protect and encapsulate therapeutics; 2. the physiochemical characteristics of the construct can be manipulated to facilitate controlled release rates; and 3. alterations in physiochemical characteristics and surface attachment can facilitate targetability and effective biocompatibility.

2.2.5.1.1 Protective stability

Silica nanoparticles provide a unique thermally and chemically stable nondegradable environment, which can potentially encapsulate therapeutics. Compared to

drug delivery systems such as polymeric micelles, liposomes and water-soluble polymeric carriers, silica nanoparticles have some advantages. Unlike silica nanoparticles, polymeric carriers may lack masking capabilities, while micelles and liposomes suffer from inherent potential dissociative properties due to critical concentrations and diminished physiochemical interactions (225). Silica nanoparticles provide a means by which to encapsulate hydrophobic molecules that would normally be insoluble. Such an example was produced by Liong et al. (265) where a mesoporous multimodal imaging phosphonate coated silica nanoparticle with a folic acid targeting motif was used to help deliver loaded hydrophobic chemotherapeutics, specifically camptothecin and paclitaxel. A significant cellular reduction in viability at 20 ug/mL and enhanced cellular uptake with the addition of a folic acid motif were demonstrated. Additionally, silica nanoconstructs can provide a platform to stabilize bioactive agents. As stated earlier, enzymes have been linked to the surface of silica to help maintain activity and facilitate a reduction in degradation. Similarly lipids have been stabilized on the surface of these materials. Silica nanoparticle-lipid emulsions were created for oral delivery where the silica component provided protection against lipase digestion in the gastrointestinal tract and a 15-fold increase in digestion was observed compared to lipid emulsions alone (315).

It is important to note, however, that silica stability also comes with inherent draw backs, including but not limited to lack of degradation, and aggregation. The key question in the design of novel silica systems for drug delivery will be how they will be cleared after systemic administration. As reported earlier investigators are looking at degradation chemistries that can help solve this elimination problem. Additionally, because these

particles are colloidal suspensions there could potentially be modes of aggregation or agglomeration. These could counteract alterations in physiochemical characteristics that facilitate directed targeting, such as size or geometry.

2.2.5.1.2 Manipulation of the construct to facilitate controlled release rates

While encapsulating the materials is the first step, release and maintenance of effective levels of therapeutics are keys to a successful delivery. Mesoporous silica constructs provide a means by which to manipulate drug release rates. Unlike traditional polymers which rely on cleavage of therapeutics or complete disassociation via hydrolysis or enzymatic mechanisms of micelles or liposomes, mesoporous materials rely on physiochemical interactions and their effects on basic diffusion or mass transport phenomena. These porous materials can have interconnected large networks of pores that can create different diffusion length paths and thus alter diffusion release rates. For example, Trewyn et al. (240) and Stromme et al. (234) utilized both spherical and rod like mesoporous silica nanoparticles. The spherical particle had ordered aligned pores while the rod like particle had a tortuous array of pores. These different constructs were loaded with an antibacterial agent that facilitates the destruction of both gram positive and gram negative bacteria. The altered pore structures significantly altered the release rates of the drug in *in vitro* bacterial cultures, as the spheres had an enhanced delivery at 48 hours after inoculation. This research suggested that pore geometry influences release rates where more interconnected networks could allow for longer diffusion paths and thus potentially longer release kinetics (240). Additionally, Brohede et al. (233) studied the

difference between cylindrical and spherical pores. It was found that diffusion through spherical pores was enhanced suggesting that the interconnected pores of cylindrical particles facilitate longer diffusion paths.

2.2.5.1.3 Physiochemical characteristics

Surface functionality is one of the most important aspects in enhancing biocompatibility, targeting and release of drugs from silica nanoconstructs. With surface functionalization one can potentially reduce or eliminate unwanted toxicity, and influence cellular uptake. For example, silica nanoconstructs have been modified with cationic residues to facilitate nucleic acid adsorption. These constructs have proven to be effective in increasing transfection efficiency of nucleic acids both *in vitro* and *in vivo* (316-321). Additionally, systemic side effects may be potentially avoided with the addition of specific functionalities. Mal et al. (322) have utilized coumarin to coat the pores of the mesoporous material and UV light emission at 310 nm to release cholestane and phenanthrene. Several groups have utilized redox alternatives, such as gold and poly(amido amine) dendrimers (PAMAM) to stimulate pore opening capabilities (269, 271, 274). Extensive work has been done with spherical mesoporous nanoparticles, where the attachment of a variety of different types of stimuli sensitive materials were explored that will only initiate release upon specified stimuli within certain physiological environments (240). For example a cadmium sulfide cap was utilized to encapsulate neurotransmitters within mesoporous silica nanoparticles and as a result of a reducing environment disulfide bonds where cleaved and drug was released into circulation (271).

Active targeting, through the attachment of specified ligand on the surface of the

particles has the potential to enhance the delivery of silica nanoparticles. As illustrated earlier the attachment of specific ligands (transferrin and folic acid) and their subsequent interactions with pancreatic cell receptors have facilitated preferential uptake (254, 265). Additionally, as stated earlier in the text, Nan (244) and Trewyn (251) demonstrated that geometry can potentially provide preferential uptake. One can extrapolate this *in vitro* data to translation, as more work is done to understand how these active targeting characteristics facilitate preferential uptake that reduce systemic side effects. Ultimately, combinations of silica with other materials can assist in the creation of an ideal synthetic system that combines appropriate biocompatibility, diffusivity, encapsulation and release.

2.2.5.2 Imaging contrast agents

Noninvasive methods utilizing contrast agents can effectively aid in earlier detection of disease states and result in better prognosis for patients. The contrast agents need to preferentially differentiate abnormal tissue environments from normal physiology, thus enhancing the local signal. As such, successful new imaging agents are defined by their capability to enhance sensitivity and resolution. Some challenges in toxicity, degradation and stability limit the use of traditional signal enhancing imaging constructs. However, if the constructs are concealed in a protective environment, translation to human use can be facilitated. Silica nanoparticles show promise in the development of contrast agent doped particles, such as those utilized in MRI and optical imaging applications. Silica nanoparticles provide a platform which can aid in developing these modalities by encapsulating specialized imaging materials, thereby protecting both the material and the body, and by enhancing the signal yield.

2.2.5.2.1 Encapsulating specialized imaging materials

Silica nanoparticle synthetic doping provides an ideal platform by which contrast agents can be doped into particles. Current contrast agents such as gadolinium (MRI) and quantum dots (optical), have an inherent toxicity when placed in physiological environments. However, if the material is encapsulated within an environment that prevents physiological contact, imaging agents can be developed with improved safety and signal intensity. As outlined earlier, gadolinium, iron oxide, quantum dots, gold, along with several different types of materials have been successfully incorporated or doped within silica constructs (208, 251, 265, 278, 279, 323, 324). Liong et al. (265) doped iron oxide constructs within silica nanoparticles and produced tumor localization in mouse models. This technology has also been utilized to track single stem cells to aid in the identification of the distribution of such cells after injection. Chung et al. (252) showed that uptake in mesenchymal stem cells does not alter proliferation, function or differentiation and they were able to subsequently image and track single cell migration through systemic circulation. Multimodal particles utilizing a combination of doped gadolinium and gold nanoparticles provided both MRI and photoacoustic imaging (optical) modalities. These systems were studied via uptake in J 774 macrophage cells to illustrate the proof of concept. However, as stated earlier, occasional reports have suggested that the materials can leak from silica materials (271). As a consequence better conjugation or incorporation methods are needed.

Is it important to note that in addition to being able to protect the body from potentially toxic materials, silica nanoparticles can actually enhance and protect the contrast agent. For example, as stated earlier, the incorporation of fluorophores within

these materials have protected them from degradation and reduced photobleaching (253-255). Additionally, the incorporation of MRI agents, such as gadolinium, within these materials could also reduce the potential dissociation of the agent from the carrier.

2.2.5.2.2 Enhancing the signal yield

The very premise of contrast agent is to enhance localized signal. Silica nanoparticles have two properties that enhance signal generation. The first is the capability to incorporate multiple contrast agents within one particle. The second is the ability to introduce changes in physiochemical characteristics and surface functionality that provide enhanced delivery potential. By delivering contrast agents in high payloads to a particular site of interest one can enhance the signal significantly. For example Kim et al. (323) developed silica nanoparticles containing gadolinium and a luminescent particle, with an attached arginine-glycine-aspartic acid (RGD) functionality. They showed little or no uptake in HT-29 (human colon cancer) cells when incubated with particles without RGD and a significant amount of uptake when incubated with particles with RGD. Additionally, Bickford et al. (325) developed a combination of gold and silica to produce a particle with near-infrared light scattering capabilities and attached human epidermal growth factor-2 (Her-2) targeting ligand. This nanoparticle proved efficacious to both target and image three separate cancer cell lines over expressing Her-2.

2.2.5.3 Theranostics

Dual modalities are useful in that both treatments and diagnostics can be delivered simultaneously. This aids not only in time and cost reduction, but also in identification of

localization of each construct. These materials maintain the same advantages and limitations outlined in drug delivery and imaging agent sections. The following will highlight a few of the examples with the utilization of silica as a theranostic platform. Lee et al. (326) combined doxorubicin with iron oxide and dye doped in mesoporous silica nanoparticles. Following subcutaneous injection passive targeting of these particles led to delivery and successful terminal deoxynucleotidyl transferase dUTP nick end labeling (TUNEL) staining or appearance of apoptotic cells within the tumor site. Similarly, Park et al. (283) were able to create a luminescent degradable silica nanocomposite that incorporated doxorubicin. The relatively nontoxic construct facilitated chemotherapeutic release, allowed for optical imaging and assessment of the location of the particles, and subsequently degraded which allowed for clearance of the particles.

The above examples provide evidence of the potential of silica nanoconstructs as drug delivery systems, imaging agents, or theranostics.

2.2.6 Unresolved issues and future directions

As outlined throughout this chapter, silica nanoparticles provide an opportunity for drug delivery and imaging. However, it remains unclear what exactly the implications are of introducing an inorganic material in a biological environment. A key challenge is limited knowledge about mechanisms of toxicity of silica nanoparticles. To facilitate clinical translation it will be important to define how silica interacts with the biological environment. As with any biomaterial, biocompatibility remains the hallmark concern. The material should elicit an appropriate response without adverse effects, locally or systemically. Taking this into consideration, the traditional definition of toxicity is only

part of this larger picture. As highlighted throughout the chapter these materials do not seem to produce much initial or immediate adverse effects, but *in vitro* and *in vivo* data are not without concerns, as the long term effects still remain unclear.

The initiation of inflammatory or thrombogenic events could potentially possess the greatest risks. It is worth noting that this will be important to understanding the total picture of these materials, as their crystalline counterparts, which are considered highly toxic, usually do not induce their effects for months to years. So, as one looks to the future of silica as a biomedical material, it will be key to maintaining safety, efficacy, and degradability while still affording the robust physiochemical properties. To translate these materials to clinical applications it is necessary to define a mode of transport, a mode of clearance, and a mode of treatment.

2.2.6.1 A defined mode of transport

Drug delivery and imaging systems are defined by their capacity to accumulate locally within diseased tissue. The utilization of SNPs to target these sites via alterations in geometry, size, surface modifications, including targeting ligands is still dependent on one key factor which is the ability to be transported via the blood stream. This transport process is not by any means simplistic or easy to effectively define. Silica nanomaterials must circulate long enough to allow targeting mechanisms to be effective. Thus, they must inherently escape traditional biological removal mechanisms, such as the innate immune system, while still not interfering with the local environment. What is essential here is that a surface or structural modification be made so that these materials evade phagocytic uptake, protein adsorption, and cellular activation. Overcoming hemolytic

concerns is imperative to effective maintenance of circulation and affording accumulation at the treatment site. Studies will need to focus on altering the surface chemistry via polymeric, protein or mesoporous modification that will aid in this endeavor.

2.2.6.2 A defined mode of clearance

As has already been stated, it is impossible to create a material that will elicit no adverse biological response. However one can create a material that provides limits to the induction of such response. One can do so by developing a material that provides quick access, treatment and subsequent removal. The previous section reviewed how to provide access with limited activation via surface modification. Here the focus will be on how to modify these materials so that they can be quickly cleared from the system. This can be done via the development of a degradation chemistry or utilization of small particles that can be excreted readily through renal or hepatobiliary mechanisms. In engineering and developing the chemical degradation of these systems, it will be helpful to consider and exploit native biological environments, such as acidic lysosomal compartments. After the system has performed its function, it should be removed so that the biological environment can return to its functioning hemostatic balance.

2.2.6.3 A defined mode of treatment

This is probably the most difficult and promising aspect of the design. One must carefully investigate the cellular uptake and biodistribution profiles of these systems. Rather than tailoring silica nanoparticles to a disease state or mechanism, it might be potentially useful to utilize their inherent properties as advantageous. For example since

silica nanoparticles appear to be able to escape lysosomal compartments, they could potentially help to deliver drugs to the cytoplasm of a cell (305). Or the fact that they appear to be taken up preferentially in certain cell types and completely ignored by others could potentially be utilized as a delivery advantage rather than a disadvantage (298). Additionally, dosing mechanisms of nanoparticle systems may also need to be altered, as it is clear that surface area and particle number have significantly different outcomes in toxicity profiles.

2.2.7 Silica nanoparticle concluding remarks

Silica nanoparticles show great promise for biomedical applications. However, if these materials are to be clinically translated there is a great need for in depth systematic evaluations of the implications of size, geometry, surface and core composition. It will be important to delineate and introduce possible solutions for modes of clearance, evasion of phagocytic activity, reduction in inflammatory mediator expression, elimination of thrombogenicity, etc. Each characteristic poses a unique solution for these potential problems.

2.3 References

1. Etheridge ML, Campbell SA, Erdman AG, Haynes CL, Wolf SM, McCullough J. The big picture on nanomedicine: the state of investigational and approved nanomedicine products. Nanomedicine: Nanotechnology, Biology, and Medicine. 2013;9(1):1-14.

2. Aggarwal P, Hall JB, McLeland CB, Dobrovolskaia MA, McNeil SE. Nanoparticle interaction with plasma proteins as it relates to particle biodistribution, biocompatibility and therapeutic efficacy. Adv Drug Deliv Rev. 2009;61(6):428-37.

3. Albanese A, Tang PS, Chan WC. The effect of nanoparticle size, shape, and surface chemistry on biological systems. Annu Rev Biomed Eng. 2012;14:1-16.

4. Dobrovolskaia MA, McNeil SE. Understanding the correlation between in vitro and in vivo immunotoxicity tests for nanomedicines. J Control Release. 2013;172(2):456-66.

5. Greish K, Thiagarajan G, Ghandehari H. In vivo methods of nanotoxicology. Methods Mol Biol. 2012;926:235-53.

6. Karmali PP, Simberg D. Interactions of nanoparticles with plasma proteins: implication on clearance and toxicity of drug delivery systems. Expert Opin Drug Deliv. 2011;8(3):343-57.

7. Walkey CD, Chan WC. Understanding and controlling the interaction of nanomaterials with proteins in a physiological environment. Chem Soc Rev. 2012;41(7):2780-99.

8. Dobrovolskaia MA, Aggarwal P, Hall JB, McNeil SE. Preclinical studies to understand nanoparticle interaction with the immune system and its potential effects on nanoparticle biodistribution. Mol Pharm. 2008;5(4):487-95.

9. Fubini B, Hubbard A. Reactive oxygen species (ROS) and reactive nitrogen species (RNS) generation by silica in inflammation and fibrosis. Free Radic Biol Med. 2003;34(12):1507-16.

10. Zhu M, Nie G, Meng H, Xia T, Nel A, Zhao Y. Physicochemical properties determine nanomaterial cellular uptake, transport, and fate. Acc Chem Res. 2013;46(3):622-31.

11. Khan MI, Mohammad A, Patil G, Naqvi SA, Chauhan LK, Ahmad I. Induction of ROS, mitochondrial damage and autophagy in lung epithelial cancer cells by iron oxide nanoparticles. Biomaterials. 2012;33(5):1477-88.

12. Lunov O, Syrovets T, Loos C, Nienhaus GU, Mailander V, Landfester K, et al.

Amino-functionalized polystyrene nanoparticles activate the NLRP3 inflammasome in human macrophages. ACS Nano. 2011;5(12):9648-57.

13. Wang F, Gao F, Lan M, Yuan H, Huang Y, Liu J. Oxidative stress contributes to silica nanoparticle-induced cytotoxicity in human embryonic kidney cells. Toxicol in Vitro. 2009;23(5):808-15.

14. Xia T, Kovochich M, Brant J, Hotze M, Sempf J, Oberley T, et al. Comparison of the abilities of ambient and manufactured nanoparticles to induce cellular toxicity according to an oxidative stress paradigm. Nano Lett. 2006;6(8):1794-807.

15. Chao Y, Karmali PP, Mukthavaram R, Kesari S, Kouznetsova VL, Tsigelny IF, et al. Direct recognition of superparamagnetic nanocrystals by macrophage scavenger receptor SR-AI. ACS Nano. 2013;7(5):4289-98.

16. Lunov O, Syrovets T, Loos C, Beil J, Delacher M, Tron K, et al. Differential uptake of functionalized polystyrene nanoparticles by human macrophages and a monocytic cell line. ACS Nano. 2011;5(3):1657-69.

17. Lunov O, Zablotskii V, Syrovets T, Rocker C, Tron K, Nienhaus GU, et al. Modeling receptor-mediated endocytosis of polymer-functionalized iron oxide nanoparticles by human macrophages. Biomaterials. 2011;32(2):547-55.

18. Orr GA, Chrisler WB, Cassens KJ, Tan R, Tarasevich BJ, Markillie LM, et al. Cellular recognition and trafficking of amorphous silica nanoparticles by macrophage scavenger receptor A. Nanotoxicology. 2011;5(3):296-311.

19. Gratton SE, Ropp PA, Pohlhaus PD, Luft JC, Madden VJ, Napier ME, et al. The effect of particle design on cellular internalization pathways. Proc Natl Acad Sci U S A. 2008;105(33):11613-8.

20. Champion JA, Mitragotri S. Role of target geometry in phagocytosis. Proc Natl Acad Sci U S A. 2006;103(13):4930-4.

21. Sharma G, Valenta DT, Altman Y, Harvey S, Xie H, Mitragotri S, et al. Polymer particle shape independently influences binding and internalization by macrophages. J Control Release. 2010;147(3):408-12.

22. Caron WP, Song G, Kumar P, Rawal S, Zamboni WC. Interpatient pharmacokinetic and pharmacodynamic variability of carrier-mediated anticancer agents. Clinical Pharmacology and Therapeutics. 2012;91(5):802-12.

23. Caron WP, Lay JC, Fong AM, La-Beck NM, Kumar P, Newman SE, et al. Translational studies of phenotypic probes for the mononuclear phagocyte system and liposomal pharmacology. J Pharmacol Exp Ther. 2013;347(3):599-606.

24. He X, Nie H, Wang K, Tan W, Wu X, Zhang P. In vivo study of biodistribution and urinary excretion of surface-modified silica nanoparticles. Anal Chem. 2008;80(24):9597-603.

25. Huang X, Li L, Liu T, Hao N, Liu H, Chen D, et al. The shape effect of mesoporous silica nanoparticles on biodistribution, clearance, and biocompatibility in vivo. ACS Nano. 2011;5(7):5390-9.

26. Kumar R, Roy I, Ohulchanskky TY, Vathy LA, Bergey EJ, Sajjad M, et al. In vivo biodistribution and clearance studies using multimodal organically modified silica nanoparticles. ACS Nano. 2010;4(2):699-708.

27. Liu T, Li L, Teng X, Huang X, Liu H, Chen D, et al. Single and repeated dose toxicity of mesoporous hollow silica nanoparticles in intravenously exposed mice. Biomaterials. 2011;32(6):1657-68.

28. Liu Y, Hu Y, Huang L. Influence of polyethylene glycol density and surface lipid on pharmacokinetics and biodistribution of lipid-calcium-phosphate nanoparticles. Biomaterials. 2014;35(9):3027-34.

29. Ohno K, Akashi T, Tsujii Y, Yamamoto M, Tabata Y. Blood clearance and biodistribution of polymer brush-afforded silica particles prepared by surface-initiated living radical polymerization. Biomacromolecules. 2012;13(3):927-36.

30. Owens DE, 3rd, Peppas NA. Opsonization, biodistribution, and pharmacokinetics of polymeric nanoparticles. Int J Pharm. 2006;307(1):93-102.

31. Albanese A, Sykes EA, Chan WC. Rough around the edges: the inflammatory response of microglial cells to spiky nanoparticles. ACS Nano. 2010;4(5):2490-3.

32. Bonilla DL, Bhattacharya A, Sha Y, Xu Y, Xiang Q, Kan A, et al. Autophagy regulates phagocytosis by modulating the expression of scavenger receptors. Immunity. 2013;39(3):537-47.

33. Carter JM, Driscoll KE. The role of inflammation, oxidative stress, and proliferation in silica-induced lung disease: a species comparison. J Environ Pathol Toxicol Oncol. 2001;20 Suppl 1:33-43.

34. Cho WS, Choi M, Han BS, Cho M, Oh J, Park K, et al. Inflammatory mediators induced by intratracheal instillation of ultrafine amorphous silica particles. Toxicol Lett. 2007;175(1-3):24-33.

35. Driscoll KE. TNFalpha and MIP-2: role in particle-induced inflammation and regulation by oxidative stress. Toxicol Lett. 2000;112-113:177-83.

36. Gazi U, Martinez-Pomares L. Influence of the mannose receptor in host immune

responses. Immunobiology. 2009;214(7):554-61.

37. Nishanth RP, Jyotsna RG, Schlager JJ, Hussain SM, Reddanna P. Inflammatory responses of RAW 264.7 macrophages upon exposure to nanoparticles: role of ROS-NFκB signaling pathway. Nanotoxicology. 2011;5(4):502-16.

38. Pajarinen J, Kouri VP, Jamsen E, Li TF, Mandelin J, Konttinen YT. The response of macrophages to titanium particles is determined by macrophage polarization. Acta Biomater. 2013;9(11):9229-40.

39. Park EJ, Park K. Oxidative stress and pro-inflammatory responses induced by silica nanoparticles in vivo and in vitro. Toxicol Lett. 2009;184(1):18-25.

40. Velard F, Braux J, Amedee J, Laquerriere P. Inflammatory cell response to calcium phosphate biomaterial particles: an overview. Acta Biomater. 2013;9(2):4956-63.

41. Duncan R, Gaspar R. Nanomedicine(s) under the microscope. Mol Pharm. 2011;8(6):2101-41.

42. Yang Q, Jones SW, Parker CL, Zamboni WC, Bear JE, Lai SK. Evading immune cell uptake and clearance requires PEG grafting at densities substantially exceeding the minimum for brush conformation. Mol Pharm. 2014;Epub ahead of print.

43. Mortimer GM, Butcher NJ, Musumeci AW, Deng ZJ, Martin DJ, Minchin RF. Cryptic epitopes of albumin determine mononuclear phagocyte system clearance of nanomaterials. ACS Nano. 2014.

44. Zreiqat H, Kumar RK, Markovic B, Zicat B, Howlett CR. Macrophages at the skeletal tissue-device interface of loosened prosthetic devices express bone-related genes and their products. J Biomed Mater Res A. 2003;65(1):109-17.

45. Garrigues GE, Cho DR, Rubash HE, Goldring SR, Herndon JH, Shanbhag AS. Gene expression clustering using self-organizing maps: analysis of the macrophage response to particulate biomaterials. Biomaterials. 2005;26(16):2933-45.

46. Wynn TA, Chawla A, Pollard JW. Macrophage biology in development, homeostasis and disease. Nature. 2013;496(7446):445-55.

47. Satpathy AT, Wu X, Albring JC, Murphy KM. Re(de)fining the dendritic cell lineage. Nat Immunol. 2012;13(12):1145-54.

48. Cassetta L, Cassol E, Poli G. Macrophage polarization in health and disease. The Scientific World Journal. 2011;11:2391-402.

49. Shibata Y, Foster LA, Metzger WJ, Myrvik QN. Alveolar macrophage priming by

intravenous administration of chitin particles, polymers of N-acetyl-D-glucosamine, in mice. Infection and Immunity. 1997;65(5):1734-41.

50. Moghimi SM, Hedeman H, Christy NM, Illum L, Davis SS. Enhanced hepatic clearance of intravenously administered sterically stabilized microspheres in zymosan-stimulated rats. J Leukoc Biol. 1993;54(6):513-7.

51. Davidson WS, Jonas A, Clayton DF, George JM. Stabilization of α-synuclein secondary structure upon binding to synthetic membranes. Journal of Biological Chemistry. 1998;273(16):9443-9.

52. Vertegel AA, Siegel RW, Dordick JS. Silica nanoparticle size influences the structure and enzymatic activity of adsorbed lysozyme. Langmuir. 2004;20(16):6800-7.

53. Roach P, Farrar D, Perry CC. Surface tailoring for controlled protein adsorption: effect of topography at the nanometer scale and chemistry. Journal of the American Chemical Society. 2006;128(12):3939-45.

54. Deng ZJ, Liang M, Monteiro M, Toth I, Minchin RF. Nanoparticle-induced unfolding of fibrinogen promotes Mac-1 receptor activation and inflammation. Nat Nanotechnol. 2011;6(1):39-44.

55. Lord MS, Foss M, Besenbacher F. Influence of nanoscale surface topography on protein adsorption and cellular response. Nano Today. 2010;5(1):66-78.

56. Dolatshahi-Pirouz A, Rechendorff K, Hovgaard MB, Foss M, Chevallier J, Besenbacher F. Bovine serum albumin adsorption on nano-rough platinum surfaces studied by QCM-D. Colloids Surf B Biointerfaces. 2008;66(1):53-9.

57. Zhu ZJ, Posati T, Moyano DF, Tang R, Yan B, Vachet RW, et al. The interplay of monolayer structure and serum protein interactions on the cellular uptake of gold nanoparticles. Small. 2012;8(17):2659-63.

58. Walkey CD, Olsen JB, Guo H, Emili A, Chan WC. Nanoparticle size and surface chemistry determine serum protein adsorption and macrophage uptake. J Am Chem Soc. 2012;134(4):2139-47.

59. Kumagai Y, Akira S. Identification and functions of pattern-recognition receptors. The Journal of Allergy and Clinical Immunology. 2010;125(5):985-92.

60. Singh H. Damage-associated Molecular Patterns. Encyclopedia of Systems Biology. 2013:517-.

61. Collier MA, Gallovic MD, Peine KJ, Duong AD, Bachelder EM, Gunn JS, et al. Delivery of host cell-directed therapeutics for intracellular pathogen clearance. Expert Rev Anti Infect Ther. 2013;11(11):1225-35.

62. Moon JJ, Suh H, Polhemus ME, Ockenhouse CF, Yadava A, Irvine DJ. Antigen-displaying lipid-enveloped PLGA nanoparticles as delivery agents for a Plasmodium vivax malaria vaccine. PLoS One. 2012;7(2):e31472.

63. Delgado MA, Elmaoued RA, Davis AS, Kyei G, Deretic V. Toll-like receptors control autophagy. EMBO J. 2008;27(7):1110-21.

64. Anand PK, Tait SW, Lamkanfi M, Amer AO, Nunez G, Pages G, et al. TLR2 and RIP2 pathways mediate autophagy of Listeria monocytogenes via extracellular signal-regulated kinase (ERK) activation. J Biol Chem. 2011;286(50):42981-91.

65. Yang M, Flavin K, Kopf I, Radics G, Hearnden CH, McManus GJ, et al. Functionalization of carbon nanoparticles modulates inflammatory cell recruitment and NLRP3 inflammasome activation. Small. 2013;9(24):4194-206.

66. Lu J, Li Z, Zink JI, Tamanoi F. In vivo tumor suppression efficacy of mesoporous silica nanoparticles-based drug-delivery system: enhanced efficacy by folate modification. Nanomedicine: Nanotechnology, Biology and Medicine. 2012;8(2):212-20.

67. Schroder K, Tschopp J. The inflammasomes. Cell. 2010;140(6):821-32.

68. Demento SL, Eisenbarth SC, Foellmer HG, Platt C, Caplan MJ, Mark Saltzman W, et al. Inflammasome-activating nanoparticles as modular systems for optimizing vaccine efficacy. Vaccine. 2009;27(23):3013-21.

69. Qu G, Liu S, Zhang S, Wang L, Wang X, Sun B, et al. Graphene oxide induces toll-like receptor 4 (TLR4)-dependent necrosis in macrophages. ACS Nano. 2013;7(7):5732-45.

70. Chen GY, Yang HJ, Lu CH, Chao YC, Hwang SM, Chen CL, et al. Simultaneous induction of autophagy and toll-like receptor signaling pathways by graphene oxide. Biomaterials. 2012;33(27):6559-69.

71. Weis WI, Drickamer K. Trimeric structure of a C-type mannose-binding protein. Structure. 1994;2(12):1227-40.

72. Connaris H, Crocker PR, Taylor GL. Enhancing the receptor affinity of the sialic acid-binding domain of Vibrio cholerae sialidase through multivalency. J Biol Chem. 2009;284(11):7339-51.

73. Turner MW. Mannose-binding lectin: the pluripotent molecule of the innate immune system. Immunology Today. 1996;17(11):532-40.

74. Chavez-Santoscoy AV, Roychoudhury R, Pohl NL, Wannemuehler MJ, Narasimhan B, Ramer-Tait AE. Tailoring the immune response by targeting C-type lectin

receptors on alveolar macrophages using "pathogen-like" amphiphilic polyanhydride nanoparticles. Biomaterials. 2012;33(18):4762-72.

75. Joshi MD, Unger WW, van Beelen AJ, Bruijns SC, Litjens M, van Bloois L, et al. DC-SIGN mediated antigen-targeting using glycan-modified liposomes: formulation considerations. Int J Pharm. 2011;416(2):426-32.

76. Yuan H, Li J, Bao G, Zhang S. Variable nanoparticle-cell adhesion strength regulates cellular uptake. Physical Review Letters. 2010;105(13):138101.

77. Jain SK, Gupta Y, Jain A, Saxena AR, Khare P, Jain A. Mannosylated gelatin nanoparticles bearing an anti-HIV drug didanosine for site-specific delivery. Nanomedicine: Nanotechnology, Biology and Medicine. 2008;4(1):41-8.

78. Kaur A, Jain S, Tiwary AK. Mannan-coated gelatin nanoparticles for sustained and targeted delivery of didanosine: in vitro and in vivo evaluation. Acta Pharm. 2008;58(1):61-74.

79. Luo Y, Zhou H, Krueger J, Kaplan C, Lee S-H, Dolman C, et al. Targeting tumor-associated macrophages as a novel strategy against breast cancer. Journal of Clinical Investigation. 2006;116(8):2132-41.

80. Keler T, Ramakrishna V, Fanger MW. Mannose receptor-targeted vaccines. Expert Opinion on Biological Therapy. 2004;4(12):1953-62.

81. Gary Bobo M, Mir Y, Rouxel C, Brevet D, Basile I, Maynadier M, et al. Mannose Functionalized Mesoporous Silica Nanoparticles for Efficient Two-Photon Photodynamic Therapy of Solid Tumors. Angewandte Chemie. 2011;123(48):11627-31.

82. Peiser L, Mukhopadhyay S, Gordon S. Scavenger receptors in innate immunity. Current Opinion in Immunology. 2002;14(1):123-8.

83. Canton J, Neculai D, Grinstein S. Scavenger receptors in homeostasis and immunity. Nature Reviews Immunology. 2013;13(9):621-34.

84. Pluddemann A, Neyen C, Gordon S. Macrophage scavenger receptors and host-derived ligands. Methods. 2007;43(3):207-17.

85. Kanno S, Furuyama A, Hirano S. A murine scavenger receptor MARCO recognizes polystyrene nanoparticles. Toxicol Sci. 2007;97(2):398-406.

86. Le Duc G, Vander Elst L, Colet JM, Roch A, Gillis P, Le Bas JF, et al. Ultrasmall particulate iron oxides as contrast agents for magnetic resonance spectroscopy: a dose-effect study. J Magn Reson Imaging. 2001;13(4):619-26.

87. Bell NC, Minelli C, Shard AG. Quantitation of IgG protein adsorption to gold

nanoparticles using particle size measurement. Anal Methods. 2013;5(18):4591-601.

88. Khlebtsov N, Bogatyrev V, Khlebtsov B, Dykman L, Englebienne P. A multilayer model for gold nanoparticle bioconjugates: application to study of gelatin and human IgG adsorption using extinction and light scattering spectra and the dynamic light scattering method. Colloid Journal. 2003;65(5):622-35.

89. Bee JS, Chiu D, Sawicki S, Stevenson JL, Chatterjee K, Freund E, et al. Monoclonal antibody interactions with micro- and nanoparticles: adsorption, aggregation, and accelerated stress studies. J Pharm Sci. 2009;98(9):3218-38.

90. Gupta AK, Gupta M, Yarwood SJ, Curtis AS. Effect of cellular uptake of gelatin nanoparticles on adhesion, morphology and cytoskeleton organisation of human fibroblasts. Journal of Controlled Release. 2004;95(2):197-207.

91. Taylor PR, Martinez-Pomares L, Stacey M, Lin HH, Brown GD, Gordon S. Macrophage receptors and immune recognition. Annu Rev Immunol. 2005;23:901-44.

92. Lesniak A, Fenaroli F, Monopoli MP, Åberg C, Dawson KA, Salvati A. Effects of the presence or absence of a protein corona on silica nanoparticle uptake and impact on cells. ACS Nano. 2012;6(7):5845-57.

93. Dutta D, Sundaram SK, Teeguarden JG, Riley BJ, Fifield LS, Jacobs JM, et al. Adsorbed proteins influence the biological activity and molecular targeting of nanomaterials. Toxicol Sci. 2007;100(1):303-15.

94. Aderem A, Underhill DM. Mechanisms of phagocytosis in macrophages. Annu Rev Immunol. 1999;17(1):593-623.

95. de Jonge MR, Koymans LH, Guillemont JE, Koul A, Andries K. A computational model of the inhibition of Mycobacterium tuberculosis ATPase by a new drug candidate R207910. PROTEINS: Structure, Function, and Bioinformatics. 2007;67(4):971-80.

96. Gratton SEA, Napier ME, Ropp PA, Tian S, DeSimone JM. Microfabricated particles for engineered drug therapies: elucidation into the mechanisms of cellular internalization of PRINT particles. Pharm Res. 2008;25(12):2845-52.

97. Herd H, Daum N, Jones AT, Huwer H, Ghandehari H, Lehr CM. Nanoparticle geometry and surface orientation influence mode of cellular uptake. ACS Nano. 2013;7(3):1961-73.

98. Arnida, Janat-Amsbury MM, Ray A, Peterson CM, Ghandehari H. Geometry and surface characteristics of gold nanoparticles influence their biodistribution and uptake by macrophages. European Journal of Pharmaceutics and Biopharmaceutics: Official Journal of Arbeitsgemeinschaft fur Pharmazeutische Verfahrenstechnik eV. 2011;77(3):417-23.

99. Champion JA, Katare YK, Mitragotri S. Making polymeric micro- and nanoparticles of complex shapes. Proc Natl Acad Sci U S A. 2007;104(29):11901-4.

100. Decuzzi P, Ferrari M. The receptor-mediated endocytosis of nonspherical particles. Biophysical Journal. 2008;94(10):3790-7.

101. Decuzzi P, Ferrari M. The role of specific and non-specific interactions in receptor-mediated endocytosis of nanoparticles. Biomaterials. 2007;28(18):2915-22.

102. Chithrani BD, Chan WC. Elucidating the mechanism of cellular uptake and removal of protein-coated gold nanoparticles of different sizes and shapes. Nano Letters. 2007;7(6):1542-50.

103. Jiang W, Kim BYS, Rutka JT, Chan WCW. Nanoparticle-mediated cellular response is size-dependent. Nature Nanotechnology. 2008;3(3):145-50.

104. Haensler J, Szoka Jr FC. Polyamidoamine cascade polymers mediate efficient transfection of cells in culture. Bioconjugate Chemistry. 1993;4(5):372-9.

105. Fischer D, Bieber T, Li Y, Elsässer H-P, Kissel T. A novel non-viral vector for DNA delivery based on low molecular weight, branched polyethylenimine: effect of molecular weight on transfection efficiency and cytotoxicity. Pharmaceutical Research. 1999;16(8):1273-9.

106. Roser M, Fischer D, Kissel T. Surface-modified biodegradable albumin nano-and microspheres. II: effect of surface charges on in vitro phagocytosis and biodistribution in rats. European Journal of Pharmaceutics and Biopharmaceutics. 1998;46(3):255-63.

107. Chellat F, Merhi Y, Moreau A, Yahia LH. Therapeutic potential of nanoparticulate systems for macrophage targeting. Biomaterials. 2005;26(35):7260-75.

108. Davis ME, Zuckerman JE, Choi CH, Seligson D, Tolcher A, Alabi CA, et al. Evidence of RNAi in humans from systemically administered siRNA via targeted nanoparticles. Nature. 2010;464(7291):1067-70.

109. Sankhala K, Mita A, Adinin R, Wood L, Beeram M, Bullock S, et al. A phase I pharmacokinetic (PK) study of MBP-426, a novel liposome encapsulated oxaliplatin. J Clin Oncol. 2009;27(15S):2535.

110. Leamon CP, Reddy JA. Folate-targeted chemotherapy. Advanced Drug Delivery Reviews. 2004;56(8):1127-41.

111. Hymel D, Peterson BR. Synthetic cell surface receptors for delivery of therapeutics and probes. Advanced Drug Delivery Reviews. 2012;64(9):797-810.

112. Wingard JR, White MH, Anaissie E, Raffalli J, Goodman J, Arrieta A, et al. A

randomized, double-blind comparative trial evaluating the safety of liposomal amphotericin B versus amphotericin B lipid complex in the empirical treatment of febrile neutropenia. L Amph/ABLC Collaborative Study Group. Clin Infect Dis. 2000;31(5):1155-63.

113. Hamilton RF, Jr., Thakur SA, Mayfair JK, Holian A. MARCO mediates silica uptake and toxicity in alveolar macrophages from C57BL/6 mice. J Biol Chem. 2006;281(45):34218-26.

114. Petrovski G, Zahuczky G, Majai G, Fesus L. Phagocytosis of cells dying through autophagy evokes a pro-inflammatory response in macrophages. Autophagy. 2007;3(5):509-11.

115. Fiuza C, Bustin M, Talwar S, Tropea M, Gerstenberger E, Shelhamer JH, et al. Inflammation-promoting activity of HMGB1 on human microvascular endothelial cells. Blood. 2003;101(7):2652-60.

116. Zhang Y, Morgan MJ, Chen K, Choksi S, Liu ZG. Induction of autophagy is essential for monocyte-macrophage differentiation. Blood. 2012;119(12):2895-905.

117. Li JJ, Hartono D, Ong CN, Bay BH, Yung LY. Autophagy and oxidative stress associated with gold nanoparticles. Biomaterials. 2010;31(23):5996-6003.

118. Vercauteren D, Deschout H, Remaut K, Engbersen JF, Jones AT, Demeester J, et al. Dynamic colocalization microscopy to characterize intracellular trafficking of nanomedicines. ACS Nano. 2011;5(10):7874-84.

119. Herd HL, Malugin A, Ghandehari H. Silica nanoconstruct cellular toleration threshold in vitro. J Control Release. 2011;153(1):40-8.

120. Perez-Carrion MD, Perez-Martinez FC, Merino S, Sanchez-Verdu P, Martinez-Hernandez J, Lujan R, et al. Dendrimer-mediated siRNA delivery knocks down Beclin 1 and potentiates NMDA-mediated toxicity in rat cortical neurons. J Neurochem. 2012;120(2):259-68.

121. Vernon PJ, Tang D. Eat-me: autophagy, phagocytosis, and reactive oxygen species signaling. Antioxid Redox Signal. 2013;18(6):677-91.

122. Wu L, Zhang Y, Zhang C, Cui X, Zhai S, Liu Y, et al. Tuning cell autophagy by diversifying carbon nanotube's surface chemistry. ACS Nano. 2014;8(3):2087-99.

123. Gupta A, Pant G, Mitra K, Madan J, Chourasia MK, Misra A. Inhalable particles containing rapamycin for induction of autophagy in macrophages infected with mycobacterium tuberculosis. Mol Pharm. 2014.

124. Kruth HS, Chang J, Ifrim I, Zhang W-Y. Characterization of patocytosis:

endocytosis into macrophage surface-connected compartments. European Journal of Cell Biology. 1999;78(2):91-9.

125. Kruth HS, Skarlatos SI, Lilly K, Chang J, Ifrim I. Sequestration of acetylated LDL and cholesterol crystals by human monocyte-derived macrophages. The Journal of Cell Biology. 1995;129(1):133-45.

126. Motskin M, Müller KH, Genoud C, Monteith AG, Skepper JN. The sequestration of hydroxyapatite nanoparticles by human monocyte-macrophages in a compartment that allows free diffusion with the extracellular environment. Biomaterials. 2011;32(35):9470-82.

127. Kirchhausen T. Adaptors for clathrin-mediated traffic. Annual Review of Cell and Developmental Biology. 1999;15(1):705-32.

128. Benjaminsen RV, Mattebjerg MA, Henriksen JR, Moghimi SM, Andresen TL. The possible "proton sponge " effect of polyethylenimine (PEI) does not include change in lysosomal pH. Mol Ther. 2013;21(1):149-57.

129. Szewczyk A, Wojtczak L. Mitochondria as a Pharmacological Target. Pharmacological Reviews. 2002;54(1):101-27.

130. Boddapati SV, D'Souza GG, Erdogan S, Torchilin VP, Weissig V. Organelle-targeted nanocarriers: specific delivery of liposomal ceramide to mitochondria enhances its cytotoxicity in vitro and in vivo. Nano Lett. 2008;8(8):2559-63.

131. Mukhopadhyay A, Weiner H. Delivery of drugs and macromolecules to mitochondria. Advanced Drug Delivery Reviews. 2007;59(8):729-38.

132. Hoshino A, Fujioka K, Oku T, Nakamura S, Suga M, Yamaguchi Y, et al. Quantum dots targeted to the assigned organelle in living cells. Microbiology and Immunology. 2004;48(12):985-94.

133. Pouton CW, Wagstaff KM, Roth DM, Moseley GW, Jans DA. Targeted delivery to the nucleus. Advanced Drug Delivery Reviews. 2007;59(8):698-717.

134. Murphy MP, Smith RA. Drug delivery to mitochondria: the key to mitochondrial medicine. Advanced Drug Delivery Reviews. 2000;41(2):235-50.

135. Pulskamp K, Diabaté S, Krug HF. Carbon nanotubes show no sign of acute toxicity but induce intracellular reactive oxygen species in dependence on contaminants. Toxicol Lett. 2007;168(1):58.

136. Petri-Fink A, Steitz B, Finka A, Salaklang J, Hofmann H. Effect of cell media on polymer coated superparamagnetic iron oxide nanoparticles (SPIONs): colloidal stability, cytotoxicity, and cellular uptake studies. European Journal of Pharmaceutics and

Biopharmaceutics: Official Journal of Arbeitsgemeinschaft fur Pharmazeutische Verfahrenstechnik eV. 2008;68(1):129-37.

137. Malugin A, Ghandehari H. Caspase 3 independent cell death induced by amorphous silica nanoparticles. Nanoscience and Nanotechnology Letters. 2011;3(3):309-13.

138. Joshi GN, Knecht DA. Silica phagocytosis causes apoptosis and necrosis by different temporal and molecular pathways in alveolar macrophages. Apoptosis. 2013;18(3):271-85.

139. Winterbourn CC. Toxicity of iron and hydrogen peroxide: the Fenton reaction. Toxicol Lett. 1995;82-83:969-74.

140. Dalal NS, Shi XL, Vallyathan V. Role of free radicals in the mechanisms of hemolysis and lipid peroxidation by silica: comparative ESR and cytotoxicity studies. J Toxicol Environ Health. 1990;29(3):307-16.

141. Lin W, Huang YW, Zhou XD, Ma Y. In vitro toxicity of silica nanoparticles in human lung cancer cells. Toxicol Appl Pharmacol. 2006;217(3):252-9.

142. Waters KM, Masiello LM, Zangar RC, Tarasevich BJ, Karin NJ, Quesenberry RD, et al. Macrophage responses to silica nanoparticles are highly conserved across particle sizes. Toxicol Sci. 2009;107(2):553-69.

143. Shahbazi M-A, Hamidi M, Mäkilä EM, Zhang H, Almeida PV, Kaasalainen M, et al. The mechanisms of surface chemistry effects of mesoporous silicon nanoparticles on immunotoxicity and biocompatibility. Biomaterials. 2013;34(31):7776-89.

144. Lee S, Yun H-S, Kim S-H. The comparative effects of mesoporous silica nanoparticles and colloidal silica on inflammation and apoptosis. Biomaterials. 2011;32(35):9434-43.

145. Miousse IR, Chalbot MC, Aykin-Burns N, Wang X, Basnakian A, Kavouras IG, et al. Epigenetic alterations induced by ambient particulate matter in mouse macrophages. Environ Mol Mutagen. 2014;Epub ahead of print.

146. Fischer HC, Hauck TS, Gómez Aristizábal A, Chan WC. Exploring primary liver macrophages for studying quantum dot interactions with biological systems. Advanced Materials. 2010;22(23):2520-4.

147. Bregoli L, Chiarini F, Gambarelli A, Sighinolfi G, Gatti AM, Santi P, et al. Toxicity of antimony trioxide nanoparticles on human hematopoietic progenitor cells and comparison to cell lines. Toxicology. 2009;262(2):121-9.

148. Hauck TS, Anderson RE, Fischer HC, Newbigging S, Chan WC. In vivo quantum

dot toxicity assessment. Small. 2010;6(1):138-44.

149. Naito M, Hasegawa G, Ebe Y, Yamamoto T. Differentiation and function of Kupffer cells. Medical Electron Microscopy. 2004;37(1):16-28.

150. Wake K, Decker K, Kirn A, Knook D, McCuskey R, Bouwens L, et al. Cell biology and kinetics of Kupffer cells in the liver. International Review of Cytology. 1988;118:173-229.

151. Baffy G. Kupffer cells in non-alcoholic fatty liver disease: the emerging view. Journal of Hepatology. 2009;51(1):212-23.

152. Moghimi SM, Hunter AC, Murray JC. Long-circulating and target-specific nanoparticles: theory to practice. Pharmacological Reviews. 2001;53(2):283-318.

153. Moghimi S. Mechanisms of splenic clearance of blood cells and particles: towards development of new splenotropic agents. Advanced Drug Delivery Reviews. 1995;17(1):103-15.

154. Cho M, Cho WS, Choi M, Kim SJ, Han BS, Kim SH, et al. The impact of size on tissue distribution and elimination by single intravenous injection of silica nanoparticles. Toxicol Lett. 2009;189(3):177-83.

155. Hirst SM, Karakoti A, Singh S, Self W, Tyler R, Seal S, et al. Biodistribution and in vivo antioxidant effects of cerium oxide nanoparticles in mice. Environmental Toxicology. 2013;28(2):107-18.

156. Hardonk M, Harms G, Koudstaal J. Zonal heterogeneity of rat hepatocytes in the in vivo uptake of 17 nm colloidal gold granules. Histochemistry. 1985;83(5):473-7.

157. Sadauskas E, Danscher G, Stoltenberg M, Vogel U, Larsen A, Wallin H. Protracted elimination of gold nanoparticles from mouse liver. Nanomedicine: Nanotechnology, Biology and Medicine. 2009;5(2):162-9.

158. Gad SC, Sharp KL, Montgomery C, Payne JD, Goodrich GP. Evaluation of the toxicity of intravenous delivery of auroshell particles (gold–silica nanoshells). International Journal of Toxicology. 2012;31(6):584-94.

159. He Q, Zhang Z, Gao F, Li Y, Shi J. In vivo biodistribution and urinary excretion of mesoporous silica nanoparticles: effects of particle size and PEGylation. Small. 2011;7(2):271-80.

160. Liu Z, Davis C, Cai W, He L, Chen X, Dai H. Circulation and long-term fate of functionalized, biocompatible single-walled carbon nanotubes in mice probed by Raman spectroscopy. Proceedings of the National Academy of Sciences. 2008;105(5):1410-5.

161. Zhang X-D, Wu D, Shen X, Liu P-X, Fan F-Y, Fan S-J. In vivo renal clearance, biodistribution, toxicity of gold nanoclusters. Biomaterials. 2012;33(18):4628-38.

162. Arvizo RR, Miranda OR, Moyano DF, Walden CA, Giri K, Bhattacharya R, et al. Modulating pharmacokinetics, tumor uptake and biodistribution by engineered nanoparticles. PLoS One. 2011;6(9):e24374.

163. Souris JS, Lee C-H, Cheng S-H, Chen C-T, Yang C-S, Ho J-aA, et al. Surface charge-mediated rapid hepatobiliary excretion of mesoporous silica nanoparticles. Biomaterials. 2010;31(21):5564-74.

164. Gaucher G, Asahina K, Wang J, Leroux J-C. Effect of poly (N-vinyl-pyrrolidone)-block-poly (D, L-lactide) as coating agent on the opsonization, phagocytosis, and pharmacokinetics of biodegradable nanoparticles. Biomacromolecules. 2009;10(2):408-16.

165. Kim ST, Saha K, Kim C, Rotello VM. The role of surface functionality in determining nanoparticle cytotoxicity. Accounts of Chemical Research. 2013;46(3):681-91.

166. Sarparanta M, Bimbo LM, Rytkönen J, Mäkilä E, Laaksonen TJ, Laaksonen Pi, et al. Intravenous delivery of hydrophobin-functionalized porous silicon nanoparticles: stability, plasma protein adsorption and biodistribution. Mol Pharm. 2012;9(3):654-63.

167. Monopoli MP, Åberg C, Salvati A, Dawson KA. Biomolecular coronas provide the biological identity of nanosized materials. Nature Nanotechnology. 2012;7(12):779-86.

168. Nishimori H, Kondoh M, Isoda K, Tsunoda S, Tsutsumi Y, Yagi K. Silica nanoparticles as hepatotoxicants. European Journal of Pharmaceutics and Biopharmaceutics. 2009;72(3):496-501.

169. Mossman BT, Churg A. Mechanisms in the pathogenesis of asbestosis and silicosis. Am J Respir Crit Care Med. 1998;157(5 Pt 1):1666-80.

170. Rimal B, Greenberg AK, Rom WN. Basic pathogenetic mechanisms in silicosis: current understanding. Curr Opin Pulm Med. 2005;11(2):169-73.

171. Choi HS, Ashitate Y, Lee JH, Kim SH, Matsui A, Insin N, et al. Rapid translocation of nanoparticles from the lung airspaces to the body. Nat Biotechnol. 2010;28(12):1300-3.

172. Neun BW, Dobrovolskaia MA. Qualitative analysis of total complement activation by nanoparticles. Methods Mol Biol. 2011;697:237-45.

173. Thomas SN, van der Vlies AJ, O'Neil CP, Reddy ST, Yu SS, Giorgio TD, et al.

Engineering complement activation on polypropylene sulfide vaccine nanoparticles. Biomaterials. 2011;32(8):2194-203.

174. Szebeni J, Baranyi L, Savay S, Milosevits J, Bunger R, Laverman P, et al. Role of complement activation in hypersensitivity reactions to doxil and hynic PEG liposomes: experimental and clinical studies. J Liposome Res. 2002;12(1-2):165-72.

175. Pedersen MB, Zhou X, Larsen EKU, Sørensen US, Kjems J, Nygaard JV, et al. Curvature of synthetic and natural surfaces is an important target feature in classical pathway complement activation. The Journal of Immunology. 2010;184(4):1931-45.

176. Ross GD, Reed W, Dalzell JG, Becker SE, Hogg N. Macrophage cytoskeleton association with CR3 and CR4 regulates receptor mobility and phagocytosis of iC3b-opsonized erythrocytes. J Leukoc Biol. 1992;51(2):109-17.

177. Moghimi S, Szebeni J. Stealth liposomes and long circulating nanoparticles: critical issues in pharmacokinetics, opsonization and protein-binding properties. Progress in Lipid Research. 2003;42(6):463-78.

178. Greish K, Thiagarajan G, Herd H, Price R, Bauer H, Hubbard D, et al. Size and surface charge significantly influence the toxicity of silica and dendritic nanoparticles. Nanotoxicology. 2012;6(7):713-23.

179. Radomski A, Jurasz P, Alonso Escolano D, Drews M, Morandi M, Malinski T, et al. Nanoparticle induced platelet aggregation and vascular thrombosis. British Journal of Pharmacology. 2005;146(6):882-93.

180. Movat HZ, Weiser WJ, Glynn MF, Mustard JF. Platelet phagocytosis and aggregation. The Journal of Cell Biology. 1965;27(3):531-43.

181. Jones CF, Campbell RA, Brooks AE, Assemi S, Tadjiki S, Thiagarajan G, et al. Cationic PAMAM dendrimers aggressively initiate blood clot formation. ACS Nano. 2012;6(11):9900-10.

182. Jones CF, Campbell RA, Franks Z, Gibson CC, Thiagarajan G, Vieira-de-Abreu A, et al. Cationic PAMAM dendrimers disrupt key platelet functions. Mol Pharm. 2012;9(6):1599-611.

183. Ilinskaya AN, Dobrovolskaia MA. Nanoparticles and the blood coagulation system. Part II: safety concerns. Nanomedicine: Nanotechnology, Biology, and Medicine. 2013;8(6):969-81.

184. Park J, Lim D-H, Lim H-J, Kwon T, Choi J-s, Jeong S, et al. Size dependent macrophage responses and toxicological effects of Ag nanoparticles. Chem Commun. 2011;47(15):4382-4.

185. Zhang Q, Hitchins VM, Schrand AM, Hussain SM, Goering PL. Uptake of gold nanoparticles in murine macrophage cells without cytotoxicity or production of pro-inflammatory mediators. Nanotoxicology. 2011;5(3):284-95.

186. Kunzmann A, Andersson B, Vogt C, Feliu N, Ye F, Gabrielsson S, et al. Efficient internalization of silica-coated iron oxide nanoparticles of different sizes by primary human macrophages and dendritic cells. Toxicology and Applied Pharmacology. 2011;253(2):81-93.

187. Lim D-H, Jang J, Kim S, Kang T, Lee K, Choi I-H. The effects of sub-lethal concentrations of silver nanoparticles on inflammatory and stress genes in human macrophages using cDNA microarray analysis. Biomaterials. 2012;33(18):4690-9.

188. Wilbourn JD, McGregor DB, Partensky C, Rice JM. IARC reevaluates silica and related substances. Environ Health Perspect. 1997;105(7):756-9.

189. Ovrevik J, Refsnes M, Namork E, Becher R, Sandnes D, Schwarze PE, et al. Mechanisms of silica-induced IL-8 release from A549 cells: initial kinase-activation does not require EGFR activation or particle uptake. Toxicology. 2006;227(1-2):105-16.

190. Lenz AG, Krombach F, Maier KL. Oxidative stress in vivo and in vitro: modulation by quartz dust and hyperbaric atmosphere. Free Radic Biol Med. 1992;12(1):1-10.

191. Kleinman MT, Araujo JA, Nel A, Sioutas C, Campbell A, Cong PQ, et al. Inhaled ultrafine particulate matter affects CNS inflammatory processes and may act via MAP kinase signaling pathways. Toxicol Lett. 2008;178(2):127-30.

192. Lacasse Y, Martin S, Gagne D, Lakhal L. Dose-response meta-analysis of silica and lung cancer. Cancer Causes Control. 2009;20(6):925-33.

193. Hnizdo E, Vallyathan V. Chronic obstructive pulmonary disease due to occupational exposure to silica dust: a review of epidemiological and pathological evidence. Occup Environ Med. 2003;60(4):237-43.

194. Cocco P, Dosemeci M, Rice C. Lung cancer among silica-exposed workers: the quest for truth between chance and necessity. Med Lav. 2007;98(1):3-17.

195. Iler RK. The chemistry of silica: John Wiley and Sons, Inc; 1979.

196. Garay RP, El-Gewely R, Armstrong JK, Garratty G, Richette P. Antibodies against polyethylene glycol in healthy subjects and in patients treated with PEG-conjugated agents. Expert Opinion on Drug Delivery. 2012;9(11):1319-23.

197. Moghimi SM, Andersen AJ, Ahmadvand D, Wibroe PP, Andresen TL, Hunter AC. Material properties in complement activation. Advanced Drug Delivery Reviews.

2011;63(12):1000-7.

198. Burger P, Hilarius-Stokman P, de Korte D, van den Berg TK, van Bruggen R. CD47 functions as a molecular switch for erythrocyte phagocytosis. Blood. 2012;119(23):5512-21.

199. Weiskopf K, Ring AM, Ho CCM, Volkmer J-P, Levin AM, Volkmer AK, et al. Engineered SIRPα variants as immunotherapeutic adjuvants to anticancer antibodies. Science. 2013;341(6141):88-91.

200. Smith CA, Wiley S, Kaykas A, Probst P. CD47 related compositions and methods for treating immunological diseases and disorders. CA2652570 A1(Patent)2007.

201. Rodriguez PL, Harada T, Christian DA, Pantano DA, Tsai RK, Discher DE. Minimal" Self" peptides that inhibit phagocytic clearance and enhance delivery of nanoparticles. Science. 2013;339(6122):971-5.

202. Fujimura N. Pathology and pathophysiology of pneumoconiosis. Curr Opin Pulm Med. 2000;6(2):140-4.

203. Byrne JD, Baugh JA. The significance of nanoparticles in particle-induced pulmonary fibrosis. Mcgill J Med. 2008;11(1):43-50.

204. Shive MS, Anderson JM. Biodegradation and biocompatibility of PLA and PLGA microspheres. Adv Drug Deliv Rev. 1997;28(1):5-24.

205. Basaraba RJ. Experimental tuberculosis: the role of comparative pathology in the discovery of improved tuberculosis treatment strategies. Tuberculosis (Edinb). 2008;88 Suppl 1:S35-47.

206. Chuankrerkkul N, Sangsuk S. Current status of nanotechnology consumer products and nano-safety issues Journal of Metals, Materials and Minearals. 2008;18(1):75-9.

207. Cameron NMdS, Mitchell ME. Nanoscale: issues and perspectives for the nano century. Hoboken, New Jersey John Wiley and Sons Inc; 2007.

208. Knopp D, Tang D, Niessner R. Review: bioanalytical applications of biomolecule-functionalized nanometer-sized doped silica particles. Anal Chim Acta. 2009;647(1):14-30.

209. Slowing, II, Vivero-Escoto JL, Wu CW, Lin VS. Mesoporous silica nanoparticles as controlled release drug delivery and gene transfection carriers. Adv Drug Deliv Rev. 2008;60(11):1278-88.

210. Sharma P, Brown S, Walter G, Santra S, Moudgil B. Nanoparticles for

bioimaging. Adv Colloid Interface Sci. 2006;123-126:471-85.

211. Martin KR. The chemistry of silica and its potential health benefits. J Nutr Health Aging. 2007;11(2):94-7.

212. Richmond KE, Sussman M. Got silicon? The non-essential beneficial plant nutrient. Curr Opin Plant Biol. 2003;6(3):268-72.

213. Epstein E. The anomaly of silicon in plant biology. Proc Natl Acad Sci U S A. 1994;91(1):11-7.

214. Crookes-Goodson WJ, Slocik JM, Naik RR. Bio-directed synthesis and assembly of nanomaterials. Chem Soc Rev. 2008;37(11):2403-12.

215. Perry CC. An overview of silica in biology: its chemistry and recent technological advances. Prog Mol Subcell Biol. 2009;47:295-313.

216. Gillette Guyonnet S, Andrieu S, Vellas B. The potential influence of silica present in drinking water on Alzheimer's disease and associated disorders. J Nutr Health Aging. 2007;11(2):119-24.

217. Sahin K, Onderci M, Sahin N, Balci TA, Gursu MF, Juturu V, et al. Dietary arginine silicate inositol complex improves bone mineralization in quail. Poult Sci. 2006;85(3):486-92.

218. Depasse J, Warlus J. Relation between the toxicity of silica and its affinity for tetraalkylammonium groups. Comparison between Si02 and Ti02. Journal of Colloid and Interface Science. 1976;56(3):618-21.

219. Slowing, II, Wu CW, Vivero-Escoto JL, Lin VS. Mesoporous silica nanoparticles for reducing hemolytic activity towards mammalian red blood cells. Small. 2009;5(1):57-62.

220. Mizutani T, Nagase H, Fujiwara N, Ogoshi H. Silicic acid polymerization catalyzed by amines and polyamines. Bulletin of the Chemical Society of Japan. 1998;71 (8):2017-22.

221. Stöber W, Fink A, Bohn E. Controlled growth of monodisperse silica spheres in the micro size range. Journal of Colloids and Interface Science. 1968;26:62-9.

222. He Q, Cui X, Cui F, Guo L, Shi J. Size-controlled synthesis of monodispersed mesoporous silica nano-spheres under a neutral condition. Microporous and Mesoporous Materials. 2009;117:609-16.

223. Brinker CJ, Scherer GW. Sol-gel science: the physics and chemistry of sol-gel processing. San Diego, CA: Academic Press; 1990.

224. Ostro MJ. Liposomes: from biophysics to therapeutics. New York, New York: Marcel Dekker Inc; 1987.

225. Kwon GS, Kataoka K. Block copolymer micelles as long circulating drug vehicles. Adv Drug Deliv Rev. 1995;16(2-3):295-309.

226. Carrstensen H, Muller RH, Muller BW. Particle size, surface hydrophobicity and interaction with serum of parenteral fat emulsions and model drug carriers as parameters related to RES uptake. Clin Nutr. 1992;11(5):289-97.

227. Bogush GH, Tracy MA, Zukoski CF. Preparation of monodisperse silica particles: control of size and mass fraction. Journal of Non-Crystalline Solids. 1988;104:95-106.

228. Limbach LK, Li Y, Grass RN, Brunner TJ, Hintermann MA, Muller M, et al. Oxide nanoparticle uptake in human lung fibroblasts: effects of particle size, agglomeration, and diffusion at low concentrations. Environ Sci Technol. 2005;39(23):9370-6.

229. Clift MJ, Rothen-Rutishauser B, Brown DM, Duffin R, Donaldson K, Proudfoot L, et al. The impact of different nanoparticle surface chemistry and size on uptake and toxicity in a murine macrophage cell line. Toxicol Appl Pharmacol. 2008;232(3):418-27.

230. Beck JS, Vartuli JC, Roth WJ, Leonowicz ME, Kresge CT, Schmitt KD, et al. A new family of mesoporous molecular sieves prepared with liquid crystal templates. Journal of American Chemical Society 1992;114:10834-43.

231. Kobler J, Moller J, Bein T. Colloidal suspensions of functionalized mesoporous silcia nanoparticles. ACS Nano. 2008;2(4):791-9.

232. Naik SP, Sokolov I. Room temperature synthesis of nanoporous silica spheres and their formation mechanism. Solid State Communications. 2007;144:437-40.

233. Brohede U, Atluri R, Garcia-Bennett AE, Stromme M. Sustained release from mesoporous nanoparticles: evaluation of structural properties associated with release rate. Curr Drug Deliv. 2008;5(3):177-85.

234. Stromme M, Brohede U, Atluri R, Garcia-Bennett AE. Mesoporous silica-based nanomaterials for drug delivery: evaluation of structural properties associated with release rate. Wiley Interdiscip Rev Nanomed Nanobiotechnol. 2009;1(1):140-8.

235. Huh S, Wiench JW, Yoo J-C, Pruski M, Lin VS-Y. Organic functionalization and morphology control of mesoporous silicas via a co-condensation synthesis method. Chem Mater. 2003;15:4247-56.

236. Nandiyanto ABD, Kim S-G, Iskandar F, Okuyama K. Synthesis of spherical

mesoporous silica nanoparticles with nanometer-size controllable pores and outer diameters Microporous and Mesoporous Materials. 2009;120(3):447-53.

237. Yu T, Hubbard D, Ray A, Ghandehari H. In vivo biodistribution and pharmacokinetics of silica nanoparticles as a function of geometry, porosity and surface characteristics. J Control Release. 2012;163(1):46-54.

238. Hudson SP, Padera RF, Langer R, Kohane DS. The biocompatibility of mesoporous silicates. Biomaterials. 2008;29(30):4045-55.

239. Li Z-Z, Wen L-X, Shao L, Chen J-F. Fabrication of porous hollow silica nanoparticles and their applications in drug release control. Journal of Controlled Release. 2004;98(2):245-54.

240. Trewyn BG, Whitman CM, Lin VS. Morphological control of room-temperature ionic liquid templated mesoporous silica nanoparticles for controlled release of antibacterial agents. Nano Lett. 2004;4(11):2139-43.

241. Zhang Q, Lu F, Li C, Wang Y, Huilin W. An efficient synthesis of helical mesoporous silica nanorods. Chemistry Letters. 2006;35(2):190-1.

242. Nuraje N, Su K, Matsui H. Catalytic growth of silica nanoparticles in controlled shapes at planar liquid/liquid interfaces. New Journal of Chemistry. 2007;31(11):1895-8.

243. Son SJ, Bai X, Nan A, Ghandehari H, Lee SB. Template synthesis of multifunctional nanotubes for controlled release. J Control Release. 2006;114(2):143-52.

244. Nan A, Bai X, Son SJ, Lee SB, Ghandehari H. Cellular uptake and cytotoxicity of silica nanotubes. Nano Lett. 2008;8(8):2150-4.

245. Obare SO, Jana NR, Murphy CJ. Preparation of polystyrene- and silica-coated gold nanorods and their use as templates for the synthesis of hollow nanotubes. Nano Lett. 2001;1(11):601-3.

246. Caruso F, Caruso RA, Möhwald H. Nanoengineering of inorganic and hybrid hollow spheres by colloidal templating Science. 1998;282(5391):1111 - 4.

247. Lu Y, McLellan J, Xia Y. Synthesis and crystallization of hybrid spherical colloids composed of polystyrene cores and silica shells. Langmuir. 2004;20(8):3464–70.

248. Chen J-F, Ding H-M, Wang J-X, Shao L. Preparation and characterization of porous hollow silica nanoparticles for drug delivery application Biomaterials 2004;25(4):723-7.

249. Mitragotri S, Lahann J. Physical approaches to biomaterial design. Nature Materials 2009;8(1):15-23.

250. Nelson SM, Mahmoud T, Beaux M, 2nd, Shapiro P, McIlroy DN, Stenkamp DL. Toxic and teratogenic silica nanowires in developing vertebrate embryos. Nanomedicine: Nanotechnology, Biology, and Medicine. 2009.

251. Trewyn BG, Nieweg JA, Zhao Y, Lin VS-Y. Biocompatible mesoporous silica nanoparticles with different morphologies for animal cell membrane penetration. Chemical Engineering Journal. 2008;137(1):23-9.

252. Chung TH, Wu SH, Yao M, Lu CW, Lin YS, Hung Y, et al. The effect of surface charge on the uptake and biological function of mesoporous silica nanoparticles in 3T3-L1 cells and human mesenchymal stem cells. Biomaterials. 2007;28(19):2959-66.

253. Blaaderen Av, Vrij A. Synthesis and characterization of colloidal dispersions of fluorescent silica spheres. Langmuir. 1992;8:2921-31.

254. Kumar R, Roy I, Ohulchanskyy TY, Goswami LN, Bonoiu AC, Bergey EJ, et al. Covalently dye-linked, surface-controlled, and bioconjugated organically modified silica nanoparticles as targeted probes for optical imaging. ACS Nano. 2008;2(3):449-56.

255. Jin Y, Kannan S, Wu M, Zhao JX. Toxicity of luminescent silica nanoparticles to living cells. Chem Res Toxicol. 2007;20(8):1126-33.

256. Guo ZX, Liu WF, Li Y, Yu J. Grafting of poly(ethylene glycol)s onto nanometer silica surface by a one-step procedure. Journal of Macromolecular Science Part A- Pure and Applied Chemistry. 2005;42:221-30.

257. Xu H, Yan F, Monson EE, Kopelman R. Room-temperature preparation and characterization of poly (ethylene glycol)-coated silica nanoparticles for biomedical applications. J Biomed Mater Res A. 2003;66(4):870-9.

258. Thierry B, Zimmer L, McNiven S, Finnie K, Barbe C, Griesser HJ. Electrostatic self-assembly of PEG copolymers onto porous silica nanoparticles. Langmuir. 2008;24:8143-50.

259. Wang L, Reis A, Seifert A, Philippi T, Ernst S, Jia M, et al. A simple procedure for the covalent grafting of triphenylphosphine ligands on silica: application in the palladium catalyzed Suzuki reaction. Dalton Trans. 2009(17):3315-20.

260. Stayton I, Winiarz J, Shannon K, Ma Y. Study of uptake and loss of silica nanoparticles in living human lung epithelial cells at single cell level. Anal Bioanal Chem. 2009;394(6):1595-608.

261. Cedervall T, Lynch I, Foy M, Berggard T, Donnelly SC, Cagney G, et al. Detailed identification of plasma proteins adsorbed on copolymer nanoparticles. Angew Chem Int Ed Engl. 2007;46(30):5754-6.

262. Cedervall T, Lynch I, Lindman S, Berggard T, Thulin E, Nilsson H, et al. Understanding the nanoparticle-protein corona using methods to quantify exchange rates and affinities of proteins for nanoparticles. Proc Natl Acad Sci U S A. 2007;104(7):2050-5.

263. Chen M, von Mikecz A. Formation of nucleoplasmic protein aggregates impairs nuclear function in response to SiO2 nanoparticles. Exp Cell Res. 2005;305(1):51-62.

264. Karlsson M, Carlsson U. Protein adsorption orientation in the light of fluorescent probes: mapping of the interaction between site-directly labeled human carbonic anhydrase II and silica nanoparticles. Biophys J. 2005;88(5):3536-44.

265. Liong M, Lu J, Kovochich M, Xia T, Ruehm SG, Nel AE, et al. Multifunctional inorganic nanoparticles for imaging, targeting, and drug delivery. ACS Nano. 2008;2(5):889-96.

266. Tasciotti E, Liu X, Bhavane R, Plant K, Leonard AD, Price BK, et al. Mesoporous silicon particles as a multistage delivery system for imaging and therapeutic applications. Nat Nanotechnol. 2008;3(3):151-7.

267. Sharma P, Brown SC, Bengtsson N, Zhang Q, Walter GA, Grobmyer SR, et al. Gold-speckled multimodal nanoparticles for noninvasive bioimaging. Chem Mater. 2008;20(19):6087-94.

268. Aznar E, Marcos MD, Martinez-Manez R, Sancenon F, Soto J, Amoros P, et al. pH- and photo-switched release of guest molecules from mesoporous silica supports. J Am Chem Soc. 2009;131(19):6833-43.

269. Gruenhagen JA, Lai CY, Radu DR, Lin VS, Yeung ES. Real-time imaging of tunable adenosine 5-triphosphate release from an MCM-41-type mesoporous silica nanosphere-based delivery system. Appl Spectrosc. 2005;59(4):424-31.

270. Klichko Y. Mesostructured silica for optical functionality, nanomachines, and drug delivery. Journal of the American Ceramic Society. 2008;92(1, Suppl.):S2.

271. Lai CY, Trewyn BG, Jeftinija DM, Jeftinija K, Xu S, Jeftinija S, et al. A mesoporous silica nanosphere-based carrier system with chemically removable CdS nanoparticle caps for stimuli-responsive controlled release of neurotransmitters and drug molecules. J Am Chem Soc. 2003;125(15):4451-9.

272. Nguyen TD, Leung KC, Liong M, Pentecost CD, Stoddart JF, Zink JI. Construction of a pH-driven supramolecular nanovalve. Org Lett. 2006;8(15):3363-6.

273. Nguyen TD, Tseng HR, Celestre PC, Flood AH, Liu Y, Stoddart JF, et al. A reversible molecular valve. Proc Natl Acad Sci U S A. 2005;102(29):10029-34.

274. Radu DR, Lai CY, Jeftinija K, Rowe EW, Jeftinija S, Lin VS. A polyamidoamine dendrimer-capped mesoporous silica nanosphere-based gene transfection reagent. J Am Chem Soc. 2004;126(41):13216-7.

275. Radu DR, Lai CY, Wiench JW, Pruski M, Lin VS. Gatekeeping layer effect: a poly(lactic acid)-coated mesoporous silica nanosphere-based fluorescence probe for detection of amino-containing neurotransmitters. J Am Chem Soc. 2004;126(6):1640-1.

276. Patel K, Angelos S, Dichtel WR, Coskun A, Yang YW, Zink JI, et al. Enzyme-responsive snap-top covered silica nanocontainers. J Am Chem Soc. 2008;130(8):2382-3.

277. Angelos S, Liong M, Choi E, Zink JI. Mesoporous silicate materials as substrates for molecular machines and drug delivery. Chemical Engineering Journal 2008;137:4-13.

278. Burns AA, Vider J, Ow H, Herz E, Penate-Medina O, Baumgart M, et al. Fluorescent silica nanoparticles with efficient urinary excretion for nanomedicine. Nano Letters. 2009;9(1):442-8.

279. Insin N, Tracy JB, Lee H, Zimmer JP, Westervelt RM, Bawendi MG. Incorporation of iron oxide nanoparticles and quantum dots into silica microspheres ACS Nano. 2008;2(2):197-202.

280. Brevet D, Gary-Bobo M, Raehm L, Richeter S, Hocine O, Amro K, et al. Mannose-targeted mesoporous silica nanoparticles for photodynamic therapy. Chemical Communications. 2009(12):1475-7.

281. Radin S, Ducheyne P, Kamplain T, Tan BH. Silica sol-gel for the controlled release of antibiotics. I. Synthesis, characterization, and in vitro release. J Biomed Mater Res. 2001;57(2):313-20.

282. Satishkumar BC, Doorn SK, Baker GA, Dattelbaum AM. Fluorescent single walled carbon nanotube/silica composite materials. ACS Nano. 2008;2(11):2283-90.

283. Park JH, Gu L, von Maltzahn G, Ruoslahti E, Bhatia SN, Sailor MJ. Biodegradable luminescent porous silicon nanoparticles for in vivo applications. Nature Materials. 2009;8(4):331-6.

284. Qhobosheane M, Santra S, Zhang P, Tan W. Biochemically functionalized silica nanoparticles. Analyst. 2001;126(8):1274-8.

285. Lei C, Shin Y, Liu J, Ackerman EJ. Entrapping enzyme in a functionalized nanoporous support. J Am Chem Soc. 2002;124(38):11242-3.

286. Berne BJ, Pecora R. Dynamic light scattering: with applications to chemistry, biology, and physics. Mineola, NY: Dover Publications, Inc. ; 2000.

287. Williams DB, Carter CB. Transmission electron microscopy: a textbook for materials science. 2nd ed. New York: Plenum Publishing Corporation; 2009. 694 p.

288. Goldstein J, Newbury DE, Joy DC, Echlin P, Lyman CE, Lifshin E, et al. Scanning electron microscopy and x-ray microanalysis. 3rd ed. New York, NY: Kluwer Academic/Plenum Publishers; 2003.

289. McLean S, Sauer BB. Tapping-mode AFM studies using phase detection for resolution of nanophases in segmented polyurethanes and other block copolymers. Macromolecules. 1997;30(26):8314-7.

290. Gross L, Mohn F, Moll N, Liljeroth P, Meyer G. The chemical structure of a molecule resolved by atomic force microscopy. Science. 2009;325:1110-4.

291. Hunter RJ. Zeta potential in colloid science: Principles and applications. London: Academic Press; 1988.

292. Coats AW, Redfern JP. Thermogravimetric analysis. A review. Analyst. 1963;88(1053):906-24.

293. Engelhardt GM, D. High-resolution solid-state NMR of silicates and zeolites. New York, NY: John Wiley and Sons; 1987.

294. Ferrari M, Mottola L, Quaresima V. Principles, techniques, and limitations of near infrared spectroscopy. Can J Appl Physiol. 2004;29(4):463-87.

295. Corrie SR, Lawrie GA, Trau M. Quantitative analysis and characterization of biofunctionalized fluorescent silica particles. Langmuir. 2006;22(6):2731–7.

296. Franca A, Pelaz B, Moros M, Sanchez-Espinel C, Hernandez A, Fernandez-Lopez C, et al. Sterilization matters: consequences of different sterilization techniques on gold nanoparticles. Small. 2010;6(1):89-95.

297. Lanone S, Rogerieux F, Geys J, Dupont A, Maillot-Marechal E, Boczkowski J, et al. Comparative toxicity of 24 manufactured nanoparticles in human alveolar epithelial and macrophage cell lines. Part Fibre Toxicol. 2009;6:14.

298. Malugin A, Herd H, Ghandehari H. Differential toxicity of amorphous silica nanoparticles toward phagocytic and epithelial cells. Journal of Nanoparticle Research. 2011;13(10):5381-96.

299. Chang JS, Chang KL, Hwang DF, Kong ZL. In vitro cytotoxicitiy of silica nanoparticles at high concentrations strongly depends on the metabolic activity type of the cell line. Environ Sci Technol. 2007;41(6):2064-8.

300. Hamilton RF, Jr., Thakur SA, Holian A. Silica binding and toxicity in alveolar macrophages. Free Radic Biol Med. 2008;44(7):1246-58.

301. Rahman IA, Vejayakumaran P, Sipaut CS, Ismail J, Chee CK. Size-dependent physiochemical and optical properties of silica nanoparticles. Materials Chemistry and Physics 2009;114:328-32.

302. Muhlfeld C, Gehr P, Rothen-Rutishauser B. Translocation and cellular entering mechanisms of nanoparticles in the respiratory tract. Swiss Med Wkly. 2008;138(27-28):387-91.

303. Sun W, Fang N, Trewyn BG, Tsunoda M, Slowing, II, Lin VS, et al. Endocytosis of a single mesoporous silica nanoparticle into a human lung cancer cell observed by differential interference contrast microscopy. Anal Bioanal Chem. 2008;391(6):2119-25.

304. Xing X, He X, Peng J, Wang K, Tan W. Uptake of silica-coated nanoparticles by HeLa cells. J Nanosci Nanotechnol. 2005;5(10):1688-93.

305. Huang DM, Hung Y, Ko BS, Hsu SC, Chen WH, Chien CL, et al. Highly efficient cellular labeling of mesoporous nanoparticles in human mesenchymal stem cells: implication for stem cell tracking. FASEB J. 2005;19(14):2014-6.

306. Julien DC, Richardson CC, Beaux MF, 2nd, McIlroy DN, Hill RA. In vitro proliferating cell models to study cytotoxicity of silica nanowires. Nanomedicine: Nanotechnology, Biology, and Medicine. 2009.

307. Choi SJ, Oh JM, Choy JH. Toxicological effects of inorganic nanoparticles on human lung cancer A549 cells. J Inorg Biochem. 2009;103(3):463-71.

308. Yu KO, Grabinski CM, Schrand AM, Murdock RC, Wang W, Gu B, et al. Toxicity of amorphous silica nanoparticles in mouse ketatinocytes. J Nanopart Res. 2009;11:15-24.

309. Wang W, Gu B, Liang L, Hamilton W. Fabrication of two and three-dimensional silica nanocolloidal particle arrays. Journal of Physical Chemistry. 2003;107(15):3400-4.

310. Nemmar A, Hoylaerts MF, Hoet PH, Nemery B. Possible mechanisms of the cardiovascular effects of inhaled particles: systemic translocation and prothrombotic effects. Toxicol Lett. 2004;149(1-3):243-53.

311. Murashov V, Harper M, Demchuk E. Impact of silanol surface density on the toxicity of silica aerosols measured by erythrocyte haemolysis. J Occup Environ Hyg. 2006;3(12):718-23.

312. Jin H, Heller DA, Strano MS. Single-particle tracking of endocytosis and exocytosis of single-walled carbon nanotubes in NIH-3T3 cells. Nano Lett.

2008;8(6):1577-85.

313. Barnes CA, Elsaesser A, Arkusz J, Smok A, Palus J, Lesniak A, et al. Reproducible comet assay of amorphous silica nanoparticles detects no genotoxicity. Nano Lett. 2008;8(9):3069-74.

314. Borchardt G, Brandriss S, Kreuter J, Margel S. Body distribution of 75Se-radiolabeled silica nanoparticles covalently coated with omega-functionalized surfactants after intravenous injection in rats. J Drug Target. 1994;2(1):61-77.

315. Tan A, Simovic S, Davey AK, Rades T, Boyd BJ, Prestidge CA. Silica nanoparticles to control the lipase-mediated digestion of lipid-based oral delivery systems. Mol Pharm. 2010.

316. Bharali DJ, Klejbor I, Stachowiak EK, Dutta P, Roy I, Kaur N, et al. Organically modified silica nanoparticles: a nonviral vector for in vivo gene delivery and expression in the brain. Proc Natl Acad Sci U S A. 2005;102(32):11539-44.

317. Kneuer C, Sameti M, Bakowsky U, Schiestel T, Schirra H, Schmidt H, et al. A non-viral DNA delivery system based on surface modified silica-nanoparticles can efficiently transfect cells in vitro. Bioconjugate Chem. 2000;11(6):926-32.

318. Kneuer C, Sameti M, Haltner EG, Schiestel T, Schirra H, Schmidt H, et al. Silica nanoparticles modified with aminosilanes as carriers for plasmid DNA. Int J Pharm. 2000;196:257-61.

319. Roy I, Ohulchanskyy TY, Bharali DJ, Pudavar HE, Mistretta RA, Kaur N, et al. Optical tracking of organically modified silica nanoparticles as DNA carriers: a nonviral, nanomedicine approach for gene delivery. Proc Natl Acad Sci U S A. 2005;102(2):279-84.

320. Sameti M, Bohr G, Ravi Kumar MN, Kneuer C, Bakowsky U, Nacken M, et al. Stabilisation by freeze-drying of cationically modified silica nanoparticles for gene delivery. Int J Pharm. 2003;266(1-2):51-60.

321. Shang W, Nuffer JH, Dordick JS, Siegel RW. Unfolding of ribonuclease A on silica nanoparticle surfaces. Nano Lett. 2007;7(7):1991-5.

322. Mal NK, Fujiwara M, Tanaka Y. Photocontrolled reversible release of guest molecules from coumarin-modified mesoporous silica. Nature. 2003;421(6921):350-3.

323. Kim JS, Rieter WJ, Taylor KM, An H, Lin W, Lin W. Self-assembled hybrid nanoparticles for cancer-specific multimodal imaging. J Am Chem Soc. 2007;129(29):8962-3.

324. Wang F, Liu J, Yang H, Luo Z, Lv W, Li C, et al. Spherical particles from

tetraorthosilicate (TEOS) sol–gel process with dimethyldiethoxysilane (DDS) and diphenyldiethoxysilane (DPDS) addition. Journal of Non-Crystalline Solids. 2008;354(45):5047-52.

325. Bickford LR, Agollah G, Drezek R, Yu TK. Silica-gold nanoshells as potential intraoperative molecular probes for HER2-overexpression in ex vivo breast tissue using near-infrared reflectance confocal microscopy. Breast Cancer Res Treat. 2010;120(3):547-55.

326. Lee JE, Lee N, Kim H, Kim J, Choi SH, Kim JH, et al. Uniform mesoporous dye-doped silica nanoparticles decorated with multiple magnetite nanocrystals for simultaneous enhanced magnetic resonance imaging, fluorescence imaging, and drug delivery. J Am Chem Soc. 2009;132(2):552-7.

CHAPTER 3

SILICA NANOCONSTRUCT CELLULAR TOLERATION THRESHOLD *IN VITRO*

Heather L Herd, Alexander Malugin,
Hamidreza Ghandehari

The Journal of Controlled Release, 2011;153:40-48

Journal of Controlled Release 153 (2011) 40–48

Contents lists available at ScienceDirect

Journal of Controlled Release

journal homepage: www.elsevier.com/locate/jconrel

Silica nanoconstruct cellular toleration threshold in vitro

Heather L. Herd [a,c], Alexander Malugin [b,c], Hamidreza Ghandehari [a,b,c,*]

[a] Department of Bioengineering, University of Utah, 20 South 2030 East, Salt Lake City, UT, 84112, USA
[b] Department of Pharmaceutics and Pharmaceutical Chemistry, University of Utah, 30 South 2000 East, Salt Lake City, UT 84112, USA
[c] Utah Center for Nanomedicine, Nano Institute of Utah, University of Utah, Salt Lake City, UT, USA

ARTICLE INFO

Article history:
Received 20 December 2010
Accepted 11 February 2011
Available online 20 February 2011

Keywords:
Silica nanoparticles
Cellular uptake
Autophagy
Nanotoxicity
Nanomedicine

ABSTRACT

The influence of geometry of silica nanomaterials on cellular uptake and toxicity on epithelial and phagocytic cells was studied. Three types of amine-terminated silica nanomaterials were prepared and characterized via the modified Stober method, namely spheres (178 ± 27 nm), worms (232 ± 22 nm × 1348 ± 314 nm) and cylinders (214 ± 29 nm × 428 ± 66 nm). The findings of the study suggest that in this size range and for the cell types studied, geometry does not play a dominant role in the modes of toxicity and uptake of these particles. Rather, a concentration threshold and cell type dependent toxicity of all particle types was observed. This correlated with confocal microscopy observations, as all nanomaterials were observed to be taken up in both cell types, with a greater extent in phagocytic cells. It must be noted that there appears to be a concentration threshold at ~100 μg/mL, below which there is limited to no impact of the nanoparticles on membrane integrity, mitochondrial function, phagocytosis or cell death. Analysis of cell morphology by transmission electron microscopy, colocalization experiments with intracellular markers and Western Blot results provide evidence of potential involvement of lysosomal escape, autophagic like activity, compartmental fusion and recycling in response to intracellular nanoparticle accumulation. These processes could be involved in cellular coping or defense mechanisms. The manipulation of physicochemical properties to enhance or reduce toxicity paves the way for the safe design of silica-based nanoparticles for use in nanomedicine.

1. Introduction

Silica nanoparticles are an appealing biomedical platform for nanomedicine since ease in physicochemical modification, economic affordability and potential for reasonably simplistic scale up provide the feasibility of rapid translation. This has led to an increased academic and industrial interest in the creation of new silica nanomaterials for therapeutic, diagnostic, prognostic and combinatory applications.

The chemistry and science of nanomaterials has drastically improved over the last several decades, facilitating the development of silica nanoparticles with significantly different physicochemical characteristics such as surface functionalization and alterations in geometry [1–16]. Silica nanoparticles can be engineered to facilitate controlled release rates, targetability, biocompatibility, and protective stability with which one can encapsulate therapeutics or contrast agents [1,2,8–13]. New mesoporous silica chemistries have allowed for the development of nanoconstructs with variations in nanopore geometry [1,2]. Such variations provide different mechanisms and path lengths for small molecule encapsulation, which is shown to significantly alter their diffusion patterns [1,2]. Additionally, mesoporous silica can have stimuli sensitive capabilities, where encapsulated drug content can remain protected in the nanoparticle until it reaches the desired delivery site where release can take place via changes in the local environment such as pH, reactive species or magnetic fields [3–7]. Investigators have utilized capping agents such as gold nanoparticles, polymeric supports, dendrimers, cadmium sulfide and magnetic nanoparticles to facilitate encapsulation [3–7]. Additionally, the sol–gel chemistries can facilitate the enclosure of a variety of non-releasing molecular agents, such as organic dyes, iron oxide, quantum dots and gold [8–13]. These doped materials can be utilized in optical, magnetic resonance or photonic imaging and evidence suggests an increase in biocompatibility and signal yields [14–16].

With the development of new nanoscale silica-based materials however, comes the necessity to fully understand how they interact with the biological environment to ensure safety. Evidence suggests that both the material's physicochemical properties and the cell type which the experiments are performed on alter the mode and mechanisms of induced cellular toxicity. For example, epithelial cells treated with silica nanoparticles show very little to no cytotoxic effects [17], while cells with longer population doubling times (i.e., fibroblasts), or phagocytic capabilities (i.e., macrophages and

* Corresponding author at: Utah Center for Nanomedicine, Nano Institute of Utah, University of Utah, 383 Colorow Dr, Salt Lake City, UT 84108, USA. Tel.: +1 801 587 1566; fax: +1 801 585 0575.
E-mail address: hamid.ghandehari@pharm.utah.edu (H. Ghandehari).

0168-3659/$ – see front matter © 2011 Elsevier B.V. All rights reserved.
doi:10.1016/j.jconrel.2011.02.017

endothelial cell types) have a substantial increase in toxicity [18,19]. Nanoparticle size, geometry and surface modification have also proven to alter uptake and toxicity patterns. For example, smaller nanoparticles are widely thought of as having an increased uptake and thus toxicity, mostly contributed to their increase in surface area and exposure to cell surfaces [20,21]. Likewise, tubular silica nanostructures showed a decrease in uptake when compared to their spherical counter parts [22]. Mesenchymal stem cells have been shown to endocytose positively charged silica nanoparticles to a greater extent than their unmodified systems [23].

To provide validity to these existing and future investigations it will be imperative to correlate physicochemical properties with specified induced biological mechanisms in a systematic fashion. This can lead to the development of safer nanoconstructs, and further lead to the potential for effective manipulation of these properties to facilitate better bioengineered materials for use in nanomedicine. In this work, we set out to investigate the safety and biocompatibility of three silica nanoconstructs, namely spherical, worm-like and cylindrical nanoparticles. The induced biological mechanisms following in vitro treatment of these constructs on model epithelial and phagocytic cell lines is further elucidated.

2. Materials and methods

2.1. Silica nanoparticle synthesis and characterization

Spherical silica nanoparticles, nanoworms, and nanocylinders were prepared utilizing previously reported modified Stober methods [24,25]. Changes in geometry were facilitated by altering the ratios during synthesis of cetyltrimethylammonium bromide (CTAB), tetraethyl orthosilicate (TEOS), sodium hydroxide (NaOH), aminopropyltrimethoxysilane (APTMS) and water respectively. The following ratios were used respectively to synthesize the worm-like (1.0:8.16:3.85:2.55:4857), cylinder-like (1.0:8.16:1.28:2.55:4857) and sphere-like (1.0:8.16:0:2.55:4857) particles. Following synthesis, CTAB was removed via acid hydrolysis and extensive washing. 3-aminopropyltriethoxysilane (3-APES) was coupled to the surface of silica nanoparticles by procedures described before [16]. All particles were fluorescently labeled with fluorescein isothiocyanate (FITC) to assess cellular uptake [16]. The constructs were sterilized by dry autoclavation. Transmission electron microscopy (TEM) images were taken on a Phillips, TECHAI F2 (Hillsboro, OR) at an accelerating voltage of 80 kV. TEM samples were created by evaporating droplets of particles suspended in deionized water off copper grids. After micrograph collection nanoconstruct size was measured utilizing Adobe Photoshop's pixilation ruler measurement tool (Adobe, San Jose, CA). The sizes of at least 300 particles of each type were measured. Particle zeta potential of SNPs dispersed in DI water at a concentration of 1.0 mg/mL was measured using a Malvern Instruments Zetasizer Nano ZS (Westborough, MA). SNPs (50 or 25 mg/mL) were sonicated, vortexed and the final particle dispersions were prepared immediately before use from common stock in cultured medium and vortexed before application to the culture cells. With the exception of fluorescent microscopy and flow cytometry studies, all experiments were carried out with unlabeled SNPs. The absence of CTAB and presence of primary amines after acid hydrolysis was ascertained by a Nicolet 740 FT-IR spectrometer (West Palm Beach, FL) and TA Instruments TGA2950 thermogravimetric analyzer (New Castle, DE).

2.2. Cell culture

Human adenocarcinoma alveolar basal epithelial A549 cells, and RAW 264.7 murine macrophages were obtained from ATCC (Manassas, Virginia) and maintained in the recommended media supplemented with 10% FBS. Cell cultures were incubated at 37 °C in 5% CO2 and 95% humidified air and kept in logarithmic phase of growth throughout all experiments.

2.3. Measurement of cell viability and proliferation

Cells were exposed to a range of concentrations (.0001–1000 ug/mL) of silica nanoparticles for 72 h. They were subsequently washed with phosphate buffer saline (PBS) and relative cell viability was assessed by utilizing a water-soluble tetrazolium salt, WST-8 [2-(2-methoxy-4-nitrophenyl)-3-(4-nitrophenyl)-5-(2,4-disulfophenyl)-2H-tetrazolium, monosodium salt], the key component in the Cell Counting Kit-8 from Dojindo Molecular Technologies, Inc (Rockville, Maryland). IC50 values were calculated utilizing GraphPad Prism software (La Jolla, CA). To assess plasma membrane integrity, cells were exposed to various concentrations of silica constructs for 24 h and assayed for lactate dehydrogenase (LDH) or leakage with the CytoScan LDH leakage cytotoxicity assay from G-Bioscience (Madison, WI). Maximum LDH was assessed via total control cell lysis induced by 0.1% Triton X-100, and a diluted series of LDH enzymes (supplied with the kit) were utilized as positive control.

2.4. Cellular uptake

The uptake of silica nanoparticles by cultured cells was visualized by confocal microscopy. Cells were grown on 35-mm glass bottom microwell dishes (MatTek, Ashland, MA) and incubated for 24 h with 50 μg/mL FITC labeled silica nanoconstructs. Cell nuclei were stained with 2.5 μM DRAQ5 (Biostatus Ltd.) according to the manufacturer's protocol. Fluorescent images of live cells were taken under a confocal laser scanning microscope (CLSM) Olympus FluoView® FV1000 (Olympus America Corp., Center Valley, PA). The intensity of the laser beam and the photodetector sensitivity were kept constant in order to compare the relative fluorescence intensities between experiments. Z stacks were collected and used for 3D reconstruction and visualization of intracellular particle localization. All image acquisitions and analyses were performed using FluoView 2.0 software.

2.5. Colocalization of nanoconstructs with intracellular compartments

The colocalization of silica nanoparticles with acidic and basic lysosomes by cultured cells was assessed by confocal microscopy. Cells were grown on 35-mm glass bottom microwell dishes (MatTek, Ashland, MA) and incubated for 24 h with 50 μg/mL FITC labeled silica nanoconstructs. Lysosomes were stained with 2.5 μM LysoSensor Yellow/Blue DND-160 or 50 μg/mL Transferrin Alexa Fluor 546 (Invitrogen Corp., Carlsbad, CA). Fluorescent images of live cells were taken by CLSM as described above.

2.6. Annexin V/Propidium Iodine (PI) staining

Cells were grown for 24 h on 35-mm glass bottom microwell dishes (MatTek, Ashland, MA) and incubated for 24 h with 50 μg/mL FITC labeled silica nanoconstructs. Annexin V/PI staining was used for detection of the mode of cell death according to the Vybrant Apoptosis Kit #3 (Invitrogen) manufacturer's instructions.

2.7. Transmission electron microscope analysis

The uptake of silica constructs by cultured cells was assessed by transmission electron microscopy. Cells were seeded on 6 well plates containing 1×cm ACLAR plastic at 2×10^5 cells per well. After an overnight incubation, 50 μg/mL of silica nanoconstructs was added and cells were incubated for 24 h after which cells were washed with PBS and fixed with a 2.5% glutaraldehyde and 1% formaldehyde in 0.1 M sodium cacodylate buffer with sucrose and calcium chloride. Cells were

stained with uranyl acetate for 45 min at room temperature and TEM images were taken with a Phillips, TECHAI F2 TEM (Hillsboro, OR, USA) at an accelerating voltage of 80 kV.

2.8. Phagocytic activity

Relative levels of phagocytic activity were assessed utilizing IgG-FITC coated beads, obtained from Caymen Chemicals (Ann Arbor, Michigan). A 96 well plate was seeded with 10,000 cells per well, 24 h prior to being incubated for 24 h with 62.5 μg/mL and 250 mg/mL of silica nanoparticles and a 1:10 dilution in cell culture medium of IgG-FITC coated beads, according to manufactures instructions. The relative bead uptake was assessed utilizing a Molecular Device's Spectramax M2 (Sunnyvale, CA).

2.9. Caspase 3 induction

Relative levels of caspase 3 induction were assessed utilizing Caspase 3 cell lysate kit, obtained from Caymen Chemicals (Ann Arbor, Michigan). RAW 264.7 and A549 cells were plated in a 96 well plate at 10,000 cells per well, 24 h prior to being incubated with 62.5 μg/mL and 250 μg/mL of each silica nanoparticle for 24 h. Incubation with adipocyte was utilized as a positive control. Cells were lysed, supernatant removed and incubated with caspase 3 detection protein, according to the manufacturer's instructions. The relative levels of caspase 3 induction were assessed utilizing a Molecular Device's Spectramax M2 (Sunnyvale, CA).

2.10. Western blot

The relative levels of LC-3 I, LC-3 II, ATG9a, ATG5, and beclin induction were assessed utilizing standard western blot techniques. Cells were plated in a 6 well plate at 500,000 cells per well, incubated for 2.5 h with particle concentrations of 62.5 μg/mL and 250 mg/mL. Tamoxifen and Rapamycin were utilized as positive controls. Following incubation, cells were washed with phosphate buffered saline (PBS), incubated for 10 min with Radio-Immunoprecipitation Assay (RIPA) buffer supplemented with protease inhibitor cocktail (Sigma) and protein was harvested after a 15 min centrifugation at 14,000 ×g. Sodium dodecyl sulfate polyacrylamide gel electrophoresis was performed with a loading of 50 μg of protein per well. Protein immunobloting was performed via gel transfer to a Polyvinylidene Fluoride membrane. The membrane was blocked with a 5% milk, PBS, 0.5% Tween-20 (Sigma) solution and incubated with primary antibodies obtained from Novus Biologicals for 1 h and then incubated with a peroxidase conjugated secondary stabilized goat anti-rabbit antibody (Pierce) for 1 h. Proteins were detected with western blotting luminal reagent (Santa Cruz) and imaged utilizing UVP Biospectrum Multispectral Imaging System (Upland, CA).

2.11. Statistical analysis

All experiments were performed in triplicate, and the results were presented as mean ± standard deviation. Student's *t*-test (two tailed, unpaired) was performed between samples of nanoparticle-treated cells vs controls, unless stated otherwise. The difference between values was considered significant at the level of $p<0.05$.

Table 1
Physicochemical characteristics of silica nanoparticles.

Nanoparticle	Size (TEM)	Zeta potential
Worms	232 ± 22 nm by 1348 ± 314 nm	87 mV
Cylinders	214 ± 29 nm by 428 ± 66 nm	79 mV
Spheres	178 ± 27 nm	58 mV

3. Results and discussion

3.1. Particle synthesis and characterization

Three silica nanoparticle types with various geometries were synthesized; worms, cylinders, and spheres. Each construct had a common dimension of approximately 200 nm, with an average

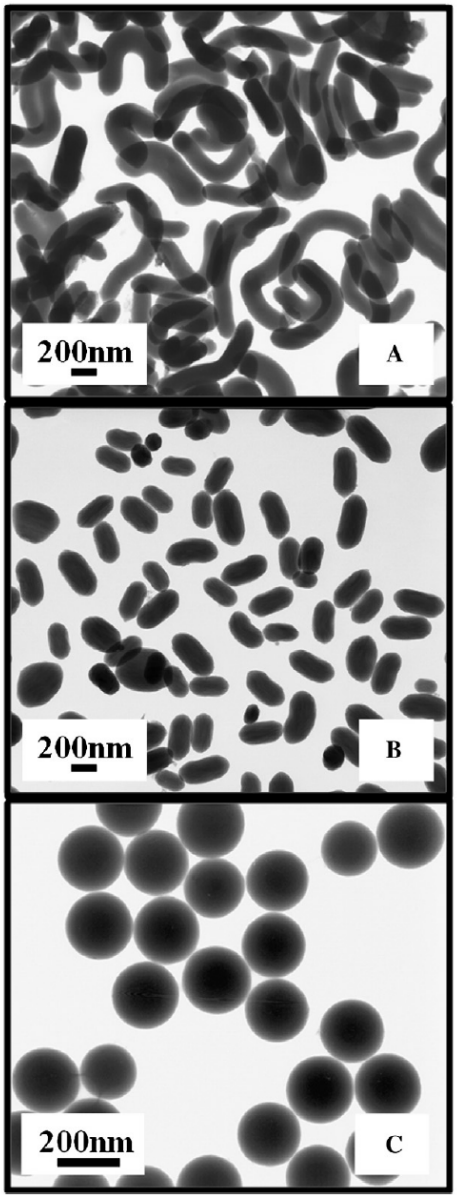

Fig. 1. Transmission Electron Microscope (TEM) images of aqueous suspensions of silica nanoconstructs. A) Worms; B) Cylinders; C) Spheres.

equivalent positive charge density and an approximate 20% variation in the size of the nanoparticle (Table 1, Fig. 1).

Variations in nanoparticle geometries were due to alterations in incorporated APTMS and CTAB ratios. CTAB is a surfactant and self associates at a critical concentration, facilitating the formation of micelles that serve as nucleation sites, from which TEOS hydrolyzes to create the solid nanoparticle. Variations in geometry were initiated by altering the critical concentration of the CTAB micelles. In this work APTMS was utilized in various ratios, which altered the degree of association, shape of the micelles and the resulting geometry. This synthetic process can create long micelles that can wiggle in solution and obtain various conformations. When nucleation occurs, these conformations lock, and longer micelles can form additional conformations. Thus, nanoworm constructs had significant variations in length elongation or geometry, while nanocylinders and nanoparticles maintained a relatively uniform geometry. CTAB was removed via acid hydrolysis and confirmation of complete removal was obtained from IR and TGA analysis (data not shown). Following removal of CTAB, APES was added, to ensure total equivalent exposure of the relative level of primary amines across all constructs. This was done so that the surfaces of the particles remained consistent across all geometries. It is important to note that fluorescence labeling did not significantly alter the shape of the constructs (data not shown), and affected zeta potential, minimally.

3.2. Cellular toleration threshold

3.2.1. Cellular viability, proliferation and function

The materials were designed with a highly positive surface charge to promote cellular uptake [23] and facilitate the assessment and correlation of changes in geometry on uptake and toxicity. RAW 264.7 and A549 cells were chosen as representative in vitro models of cells of the reticulo-endothelial system (RES) and epithelial cell types, in which silica nanoparticles have previously been evaluated and shown a cell type dependent toxicity, with an increased toxicity observed in macrophages [26]. This is not surprising, as one of the primary functions of RES cells is to remove foreign materials from the biological environment. It is important to note, however that while macrophages have an inherent advantage of engulfing nanoconstructs due to their primary phagocytic nature, epithelial cells do occasionally present with phagocytic capabilities [26].

Following synthesis and characterization of silica nanoconstructs, their abilities to interfere with cell proliferation and to compromise plasma membrane integrity were evaluated. All the constructs inhibited cell proliferation in a dose-dependent manner. The toxicity of nanoconstructs was cell-type dependent, showing that macrophages were more susceptible to treatment than epithelial cells (Table 2).

This observation correlated well with cellular uptake results in which particles exhibited a greater accumulation in macrophages when compared to epithelial cells (Fig. 2).

Proliferative functional damage presented in macrophages at approximately 80 μg/mL while epithelial cells did not present with damage until 200 μg/mL, both with minimal geometric impact (Supplemental Figs. 1 and 2). The particles appear to have no affect on cell proliferative function up until a specific concentration at which point cell proliferation drops off rapidly. Additionally, limited plasma membrane damage, as was manifested with minimal LDH release, was observed in both cell lines, with the exception of very high nanoparticle concentrations (Fig. 3). Nanoparticle geometry played little to no significant role in the relative release of LDH in both cell

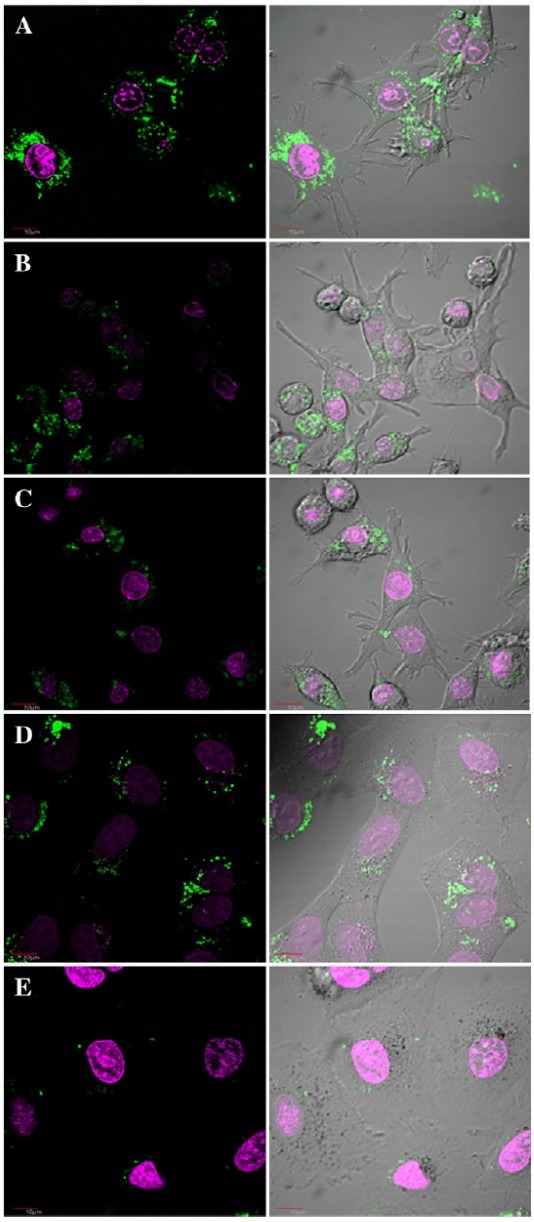

Fig. 2. Internalization of 50 μg/mL FITC labeled (green) silica nanoconstructs after 24 h of incubation with RAW264.7 and A549 cells. Nuclei are stained with DRAQ5 (pink). RAW 264.7 cells incubated with worms (A), cylinders (B), or spheres (C); A549 incubated with worms (D), cylinders (E), or spheres (F).

Table 2
IC_{50} values (μg/mL) for silica nanoparticles.[a]

Nanoparticle	A549	RAW 264.7
Cylinders	141 ± 5	82 ± 3
Spheres	N/A	113 ± 9
Worms	324 ± 13	73 ± 19

[a] Concentrations leading to the death of 50% of cell population after 72 h incubation. The values (mean +/− SD, μg/mL) of 3 independent experiments are shown.

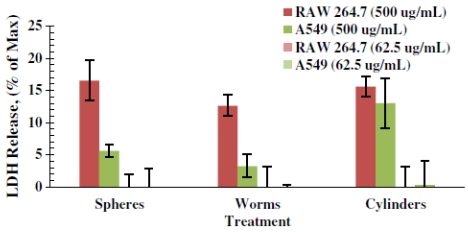

Fig. 3. Effect of nanoconstructs on plasma membrane integrity measured by LDH release.

lines. These results suggest that the membrane integrity of the particles is maintained up to ~250 μg/mL in both cell lines, however the proliferative function of RAW 264.7 cells initiated a higher release of LDH at those concentrations. While the data presents a cell type dependent toxicity, it does not seem to present with a significant difference when comparing changes in construct geometry within a particular cell type. It is important to note, however, that the design of these constructs was such that they had similar surface characteristics and common dimensionality. It is well known that nanoparticle protein adsorption helps to facilitate cellular internalization and uptake dictating modes and mechanisms of toxicity [27–30]. The highly positive charge associated with these particles could potentially provide an enhanced protein association negating geometric implications. Very slight variations in surface chemistry have proven to present drastic differences in protein absorption on silica nanoconstructs [31]. This could provide a reason for variations, or the lack there of, in results with regards to nanoconstruct geometry. This phenomenon however needs further detailed investigation and can depend on both surface characteristics and cell type.

3.2.2. Mechanisms of cell death

To assess the mode of cell death induced by the nanoparticles, the phosphatidyl serine translocation and activation of key enzymes of apoptotic cascade were examined.

Annexin V has high affinity to phosphatidylserine which is translocated from the inner layer to the outer layer of the plasma membrane during apoptosis. Propidium Iodide (PI) is an intercalating agent which stains DNA and can only penetrate cells that have compromised membrane integrity. Positive staining with PI is indicative of necrotic cell death. The staining patterns present at higher concentrations (500 μg/mL, Fig. 4 and Supplemental Fig. 3), are either red or a combination of red and green, which is indicative of late stage apoptotic or necrotic cell death. Little to no Annexin V or PI positive staining was observed when cells were treated with low concentrations (62.5 μg/mL, data not shown) of nanoconstructs. This observation correlates with LDH release, as membrane integrity appears to be intact up to 250 μg/mL. In an attempt to differentiate between apoptotic and necrotic cell death, cell lysates were evaluated for relative levels of active caspase 3. Activation of caspase 3, which present in the cytoplasm as an active proenzyme, plays a central role in the execution phase of apoptosis. No significant activation of the enzyme was observed in treated or control cells, however caspase 3 activation was observed in adipocyte treated cells, which were used as the positive control (Fig. 5 and Supplemental Fig. 4). These results seem to suggest that cells are able to survive and proliferate up to a certain concentration threshold, at which point cells are overwhelmed with the nanoparticles and undergo necrotic cell death due to membrane rupture. It must be noted that nanoparticle geometry played little to no role in caspase activation or observable increases in Annexin V or PI positive staining.

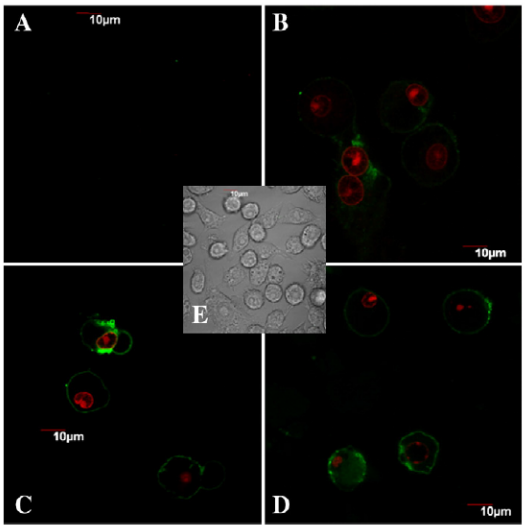

Fig. 4. Mode of cell death induced in RAW264.7 cells after 24 h of incubation with 500 μg/mL of silica nanoparticles. Annexin V (green) staining provides evidence of apoptotic cell death and PI (red) staining provides evidence of necrotic cell death. A) Control; B) Spheres; C) Worms; D) Cylinders.

3.3. Cellular coping mechanisms

3.3.1. Cellular uptake and internalization

Validation of cellular concentration toleration thresholds claims was attempted utilizing cellular uptake visualization methods. Both cell types did uptake these constructs to a significant extent (Fig. 2). However constructs were taken up to a greater extent by RAW 264.7 cells. Particle geometry again, did not appear to have a significant impact on relative nanoparticle uptake, in both cell lines. Increased relative fluorescene in Fig. 2 could be due to the depicted focal plane or the fact that the relative fluorescence per particle was not normalized facilitating variations in relative emissions.

Transferrin is a blood plasma glycoprotein utilized in iron transport. Because of well established intracellular transport mechanism, transferrin is often used as a marker of receptor-mediated endocytosis. Co-incubation of transferrin and nanoconstructs, appeared to provide evidence that geometry plays little to no role in the uptake of particles. However, co-localization of transferrin was only observed in RAW 264.7 cells and appeared to be absent in A549

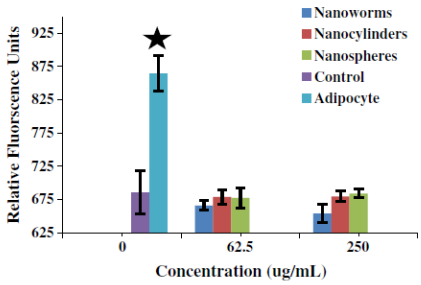

Fig. 5. Relative levels of activated caspase 3 by silica nanoparticles treated with RAW 264.7 cells. The star indicates a statistically significant increase in caspase activation when compared to control.

cells (representative image, Supplemental Fig. 5). This suggests that receptor mediated endocytosis mechanisms may potentially be responsible for some RAW 264.7 cell particle internalization and cellular trafficking, while such mechanisms are improbable for A549 cells. This phenomenon has previously been confirmed as the most probable mechanistic route of internalization of spherical silica nanoparticles [32–34]. Furthermore, phagocytic activity of Ig-G microparticles was assessed to help rule out interference with phagocytic uptake mechanisms. As expected, all concentrations and particle types did not appear to interfere with Ig-G microparticle uptake (Supplemental Fig. 6). This suggests that nanoparticles do not interfere with phagocytic activity of microparticles, and could further indicate the possibility of endocytosis. However other modes of uptake, including phagocytosis, could potentially be involved. Two concentrations of particles were studied; 62.5 μg/mL and 250 μg/mL. Incubation of cells with both concentrations presented with similar results. A549 cells may have internalized particles via another mechanism of endocytosis. Further studies will need to be performed to assess the detailed modes of internalization of silica nanoparticles.

3.3.2. Lysosomal colocalization, escape, and compartmental recycling

Uptaken particles were further analyzed with lysosensor co-localization. Lysosensor dyes accumulate and fluoresce in acidic compartments due to protonation of the basic side chains and are commonly utilized as a colocalization tool to assess relative lysosomal encapsulation. A specific lysosensor that exhibits two different spectral fluorescence peaks dependent on the relative acidity of the compartment was chosen. Particles were incubated for 24 h and lysosomes were stained with lysosensor to assess the relative lysosomal compartmentalization. Results indicate that constructs were not always co-localized with lysosomes and some appeared to be free within the cytoplasm. However, when co-localized they appear to reside within more highly acidic lysosomal compartments. All particles within A549 and RAW 264.7 cells presented with similar results, suggesting similar cellular sequestering mechanisms despite the variations in geometry (representative results, Supplemental Fig. 7). These results suggest lysosomal escape from basic compartments, acidic compartmental fusion or an indication of different stages of lysosome maturation.

Transmission electron microscopy was utilized to validate co-localization via confocal microscopy. Similar to lysosomal co-localization results, particles were observed both in membrane-bound organelles and in cytoplasm (representative image, Fig. 6).

Cytoplasmic content could help support lysosomal escape mechanisms suggested by delocalized particles in lysosensor colocalization results.

Previous studies have suggested that silica nanoparticles can be trafficked to lysosomal compartments [35], however the lysosomal environment was not sufficient to facilitate degradation of these particles. Thus, it has been suggested that these particles can remain within these compartments through late stage lysosomal digestion and then release into the cytoplasm [35]. Additionally, investigations have provided evidence that these materials remain within these compartments for a sufficient period of time to be involved in compartmental recycling, where the particles are trafficked from the lysosome to the surface of the cell and released extracellularly [36]. These mechanisms could be a process by which cells are attempting to cope with the internalization of a material that they are both unfamiliar with and unable to digest.

3.3.3. Autophagic activity

If compartmental recycling and lysosomal escape are indeed playing a role in these coping mechanisms, it would not be unusual to suggest that other native cell mechanisms that help to remove foreign pathogens or misfolded proteins from cells could be at play. Evidence suggests that other nanoconstructs such as dendrimers, quantum dots and gold nanoparticles also induce autophagic mechanisms [37–39]. Autophagy is the process in which materials that cells cannot digest are trafficked and sequestered into membrane bound vesicles, which

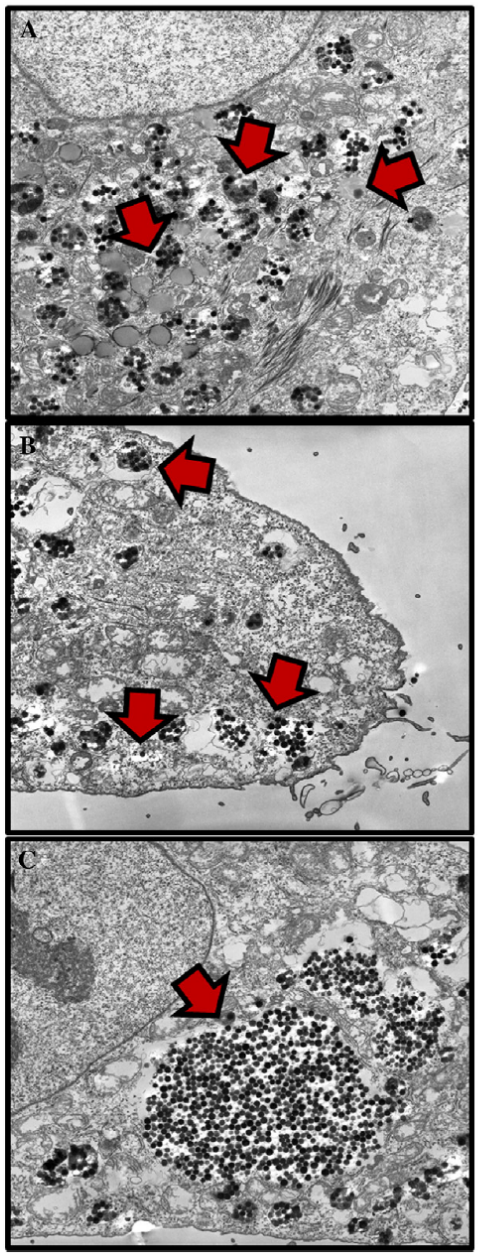

Fig. 6. Representative TEM images of the uptake of spherical particles by A549 cells at 50 μg/mL concentration and over 24 h incubation. A) and B) Depict numerous vacuoles with particles encapsulated within them. Additionally, numerous lysosomes were observed, while several vacuoles and lysosomes appear to be fusing with one another. Futhermore, a few particles appear to be isolated without vacuole encapsulation within the cytoplasm. C) Depicts an apparent larger vacuole formation after vesicle fusion. No differences were observed across all particle types.

isolate them from the rest of the cell and promote degradation (Fig. 7). In this work we confirm the autophagic activity by assessing traditional morphological features indicated in TEM images and overexpressed proteins in western blot analysis.

Transmission electron microscopy images of all particle and cell types were evaluated for hallmark autophagic morphological features [40]. Both cell types and all particle treatments, presented with similar morphological features. Particles appear to be co-localized in double membrane vesicles that contain other whole or remnants of cellular organelles (Fig. 8).

Additionally, particles appear to be uptaken in small quantities, which are then later sequestered in larger vacuoles containing multiple particles (Fig. 6). This is enhanced by apparent increased lysosomal fusion, when compared to control cells. Furthermore, when compared to control cells, the relative size is increased and mitochondria appear to have swollen features.

Autophagic activity was confirmed by assessing the presence of and the expression level of several characteristic marker proteins, namely: LC-3 I, LC-3 II, ATG9a, ATG5, and beclin. LC-3 protein component in the development of autophagic vesicles. LC-3 I is a cytosolic form and is converted to LC-3 II when it is incorporated in the membrane of autophagic vesicles. The upregulation of this conversion can be quantitatively correlated with the number of autophagic vesicles formed [41,42]. The presence and upregulation of Beclin, ATG9a, and ATG5 correlate but are not specific to autophagic activity [41,42]. However the presence of these proteins is essential to the development of autophagic vesicles and provides evidence of tracking the autophagic process from initiation to complete development. Beclin is an important regulator of the selective turnover of proteins involved in cell growth and proliferation and participates in the nucleation of the autophagic membrane, ATG-5 is involved in an ubiquitin like conjugated system that facilitates the growth of the membrane, and ATG9a facilitates the last stage of vesicle expansion. The results of protein immunoblot indicate that incubation with nanoconstructs resulted in the upregulation of LC-3 I, LC-3 II, ATG9a, ATG5, ATG16, and beclin, in both cell lines (representative image, Fig. 9 and Supplement Fig. 8).

Overall these findings suggest that cells are able to uptake silica nanoparticles and cope with them up to a certain concentration threshold. They utilize native cellular processes including autophagic mechanisms and potentially lysosomal recycling and escape to facilitate this coping. At a certain concentration cells are no longer able to handle nanoparticle internalization, and it appears that the particles consume the extracellular space and facilitate membrane damage and cause cells to undergo necrotic cell death. In the size and shape range studied, geometry in this case, seems to play little to no role in the induced biological toxicity. However surface charge, size and relative curvature might significantly alter uptake and toxicity patterns, which is a subject of further studies. Additionally, it is important to note that geometry might play a significant role in vivo when one accounts for the transport of particles through the blood stream and across endothelial barriers.

4. Conclusion

This work demonstrates cell type dependent toxicity of cationic silica nanoparticles and illustrates limited geometric dependence in biological results across the two cell lines, and in the size range studied. Evidence collected suggests the existence of a cellular toleration concentration threshold and the involvement of autophagic processes in cellular coping mechanisms for silica nanoparticles.

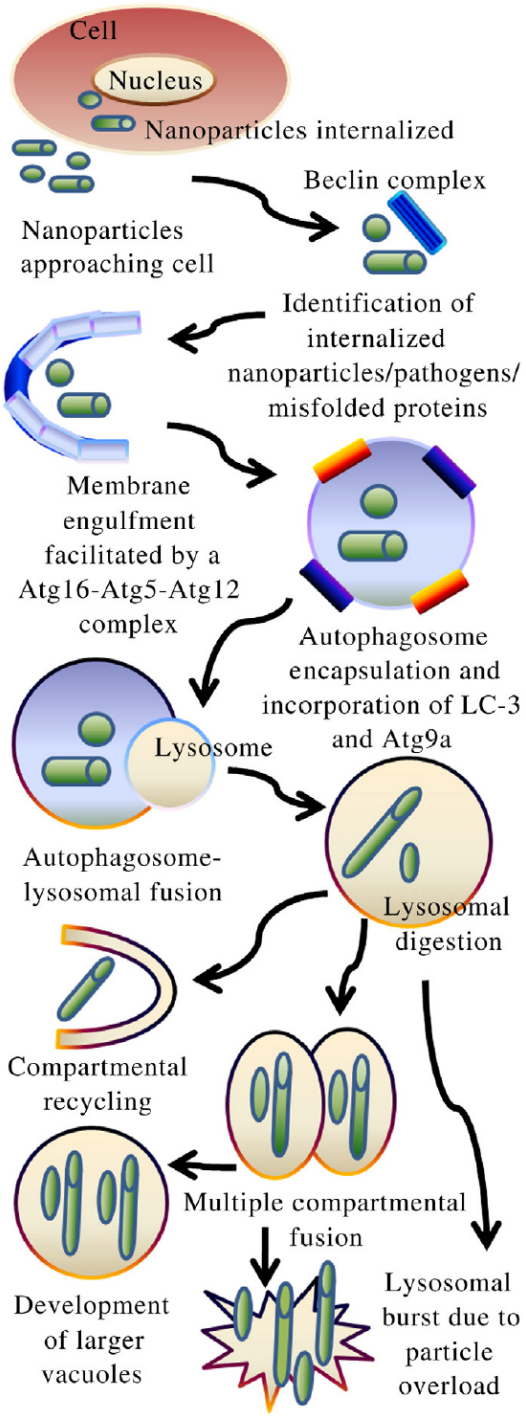

Fig. 7. Illustration of native autophagic vesicle formation. It is hypothesized that the nanoparticles initiate progression and virulence of autophagic processes within the in-vitro cellular environment.

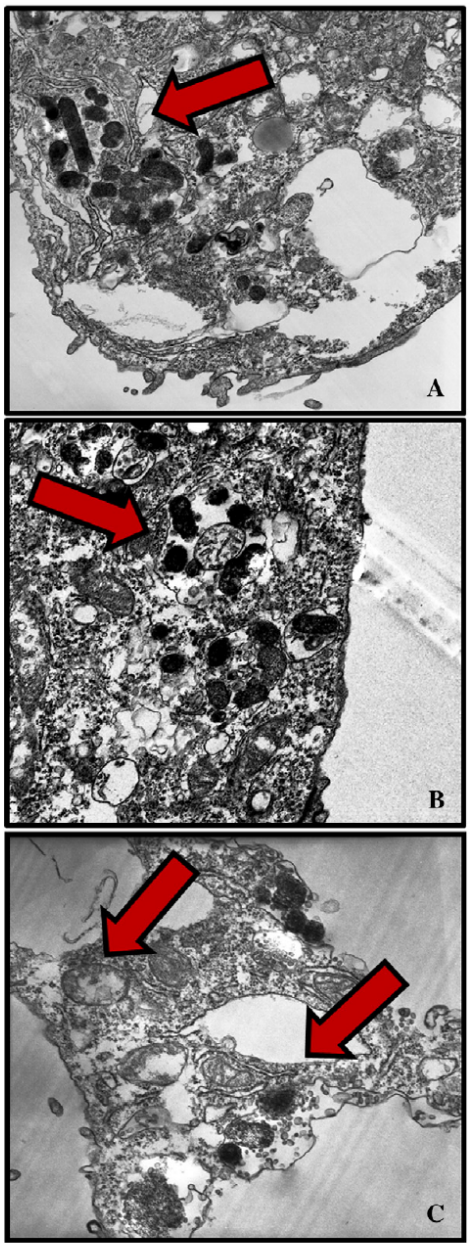

Fig. 8. Representative TEM images of the uptake of cylindrical and worm-like particles at 50 μg/mL and 24 h incubation in A549 cells (B), and RAW 264.7 (A and C). Particles appear to be co-localized in double membrane lysosome-like vesicles (A), some of which contain whole (B) or remnants (C) of cellular organelles. Treated cell size is much larger and the mitochondria appear to be swollen, when compared to control (C). No differences were observed as a function of particle geometry.

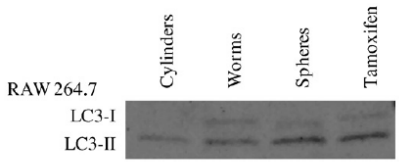

Fig. 9. Representative western blot image of LC3-I and LC3-II protein expression. 6 well plates of RAW 264.7 cells were treated with 250 μg/mL of particles and incubated for 2.5 h before harvesting. Expression was also seen in A549 but to a much lesser extent (data not shown). Control cells did express LC3-I but did not express LC3-II. Tamoxifen was utilized as a positive control to validate methodology. Limited changes in protein expression was seen when cells were treated with 50 μg/mL of particles.

Acknowledgments

This research was supported by the National Institutes of Health (R01-DE19050), National Science Foundation (NSF-NIRT: 0835342) and the Utah Science Technology and Research (USTAR) Initiative. The authors would also like to thank Nancy Chandler from the Health Sciences Center Research Microscopy Facility at the University of Utah for her help with transmission electron microscopy.

Appendix A. Supplementary data

Supplementary data to this article can be found online at doi:10.1016/j.jconrel.2011.02.017.

References

[1] M. Stromme, U. Brohede, R. Atluri, A.E. Garcia-Bennett, Mesoporous silica-based nanomaterials for drug delivery: evaluation of structural properties associated with release rate, Wiley interdisciplinary reviews 1 (1) (2009) 140–148.
[2] U. Brohede, R. Atluri, A.E. Garcia-Bennett, M. Stromme, Sustained release from mesoporous nanoparticles: evaluation of structural properties associated with release rate, Current Drug Delivery 5 (3) (2008) 177–185.
[3] D.R. Radu, C.Y. Lai, J.W. Wiench, M. Pruski, V.S. Lin, Gate keeping layer effect: a poly(lactic acid)-coated mesoporous silica nanosphere-based fluorescence probe for detection of amino-containing neurotransmitters, Journal of the American Chemical Society 126 (6) (2004) 1640–1641.
[4] E. Aznar, M.D. Marcos, R. Martinez-Manez, F. Sancenon, J. Soto, P. Amoros, C. Guillem, pH- and photo-switched release of guest molecules from mesoporous silica supports, Journal of the American Chemical Society 131 (19) (2009) 6833–6843.
[5] J.A. Gruenhagen, C.Y. Lai, D.R. Radu, V.S. Lin, E.S. Yeung, Real-time imaging of tunable adenosine 5-triphosphate release from an MCM-41-type mesoporous silica nanosphere-based delivery system, Applied Spectroscopy 59 (4) (2005) 424–431.
[6] C.Y. Lai, B.G. Trewyn, D.M. Jeftinija, K. Jeftinija, S. Xu, S. Jeftinija, V.S. Lin, A mesoporous silica nanosphere-based carrier system with chemically removable CdS nanoparticle caps for stimuli-responsive controlled release of neurotransmitters and drug molecules, Journal of the American Chemical Society 125 (15) (2003) 4451–4459.
[7] J.E. Lee, N. Lee, H. Kim, J. Kim, S.H. Choi, J.H. Kim, T. Kim, I.C. Song, S.P. Park, W.K. Moon, T. Hyeon, Uniform mesoporous dye-doped silica nanoparticles decorated with multiple magnetite nanocrystals for simultaneous enhanced magnetic resonance imaging, fluorescence imaging, and drug delivery, Journal of the American Chemical Society 132 (2) (2009) 552–557.
[8] A.A. Burns, J. Vider, H. Ow, E. Herz, O. Penate-Medina, M. Baumgart, S.M. Larson, U. Wiesner, M. Bradbury, Fluorescent silica nanoparticles with efficient urinary excretion for nanomedicine, Nano letters 9 (1) (2009) 442–448.
[9] D. Knopp, D. Tang, R. Niessner, Review: bioanalytical applications of biomolecule-functionalized nanometer-sized doped silica particles, Analytica Chimica Acta 647 (1) (2009) 14–30.
[10] Q. Wang, D.F. Shantz, Ordered mesoporous silica-based inorganic nanocomposites, Journal of Solid State Chemistry 181 (2008) 1659–1669.
[11] M. Liong, J. Lu, M. Kovochich, T. Xia, S.G. Ruehm, A.E. Nel, F. Tamanoi, J.I. Zink, Multifunctional inorganic nanoparticles for imaging, targeting, and drug delivery, ACS Nano 2 (5) (2008) 889–896.
[12] N. Insin, J.B. Tracy, H. Lee, J.P. Zimmer, R.M. Westervelt, M.G. Bawendi, Incorporation of iron oxide nanoparticles and quantum dots into silica microspheres, ACS Nano 2 (2) (2008) 197–202.
[13] P. Sharma, S. Brown, G. Walter, S. Santra, B. Moudgil, Nanoparticles for bioimaging, Advances in Colloid and Interface Science 123–126 (2006) 471–485.
[14] R. Kumar, I. Roy, T.Y. Ohulchanskky, L.A. Vathy, E.J. Bergey, M. Sajjad, P.N. Prasad, In vivo biodistribution and clearance studies using multimodal organically modified silica nanoparticles, ACS Nano 4 (2) (2010) 699–708.
[15] Y. Jin, S. Kannan, M. Wu, J.X. Zhao, Toxicity of luminescent silica nanoparticles to living cells, Chemical Research in Toxicology 20 (8) (2007) 1126–1133.
[16] A.V. Blaaderen, A. Vrij, Synthesis and characterization of colloidal dispersions of fluorescent silica spheres, Langmuir 8 (1992) 2921–2931.
[17] S. Lanone, F. Rogerieux, J. Geys, A. Dupont, E. Maillot-Marechal, J. Boczkowski, G. Lacroix, P. Hoet, Comparative toxicity of 24 manufactured nanoparticles in human alveolar epithelial and macrophage cell lines, Particle and Fibre Toxicology 6 (2009) 14.

[18] J.S. Chang, K.L. Chang, D.F. Hwang, Z.L. Kong, In vitro cytotoxicitiy of silica nanoparticles at high concentrations strongly depends on the metabolic activity type of the cell line, Environmental Science & Technology 41 (6) (2007) 2064–2068.
[19] R.F. Hamilton Jr., S.A. Thakur, A. Holian, Silica binding and toxicity in alveolar macrophages, Free Radical Biology & Medicine 44 (7) (2008) 1246–1258.
[20] K.M. Waters, L.M. Masiello, R.C. Zangar, B.J. Tarasevich, N.J. Karin, R.D. Queesenberry, S. Bandyopadhyay, J.G. Teeguarden, J.G. Pounds, B.D. Thrall, Macrophage responses to silica nanoparticles are highly conserved across particle sizes, Toxicological Science 107 (2) (2009) 553–569.
[21] M.J. Clift, B. Rothen-Rutishauser, D.M. Brown, R. Duffin, K. Donaldson, L. Proudfoot, K. Guy, V. Stone, The impact of different nanoparticle surface chemistry and size on uptake and toxicity in a murine macrophage cell line, Toxicology and Applied Pharmacology 232 (3) (2008) 418–427.
[22] B.G. Trewyn, J.A. Nieweg, Y. Zhao, V.S.-Y. Lin, Biocompatible mesoporous silica nanoparticles with different morphologies for animal cell membrane penetration, Chemical Engineering Journal 137 (1) (2008) 23–29.
[23] T.H. Chung, S.H. Wu, M. Yao, C.W. Lu, Y.S. Lin, Y. Hung, C.Y. Mou, Y.C. Chen, D.M. Huang, The effect of surface charge on the uptake and biological function of mesoporous silica nanoparticles in 3 T3-L1 cells and human mesenchymal stem cells, Biomaterials 28 (19) (2007) 2959–2966.
[24] W. Wang, B. Gu, L. Liang, W. Hamilton, Fabrication of two and three-dimensional silica nanocolloidal particle arrays, Journal of Physical Chemistry 107 (15) (2003) 3400–3404.
[25] S. Huh, J.W. Wiench, J.-C. Yoo, M. Pruski, V.S.-Y. Lin, Organic functionalization and morphology control of mesoporous silicas via a co-condensation synthesis method, Chemistry of Materials 15 (2003) 4247–4256.
[26] J. Monks, D. Rosner, F. Jon Geske, L. Lehman, L. Hanson, M.C. Neville, V.A. Fadok, Epithelial cells as phagocytes: apoptotic epithelial cells are engulfed by mammary alveolar epithelial cells and repress inflammatory mediator release, Cell Death Differ 12 (2) (2005) 107–114.
[27] P. Aggarwal, J.B. Hall, C.B. McLeland, M.A. Dobrovolskaia, S.E. McNeil, Nanoparticle interaction with plasma proteins as it relates to particle biodistribution, biocompatibility and therapeutic efficacy, Advanced Drug Delivery Reviews 61 (6) (2009) 428–437.
[28] T. Cedervall, I. Lynch, S. Lindman, T. Berggard, E. Thulin, H. Nilsson, K.A. Dawson, S. Linse, Understanding the nanoparticle-protein corona using methods to quantify exchange rates and affinities of proteins for nanoparticles, Proceedings of the National Academy of Sciences of the United States of America 104 (7) (2007) 2050–2055.
[29] D. Dutta, S.K. Sundaram, J.G. Teeguarden, B.J. Riley, L.S. Fifield, J.M. Jacobs, S.R. Addleman, G.A. Kaysen, B.M. Moudgil, T.J. Weber, Adsorbed proteins influence the biological activity and molecular targeting of nanomaterials, Toxicological Sciences 100 (1) (2007) 303–315.
[30] M. Chen, A. von Mikecz, Formation of nucleoplasmic protein aggregates impairs nuclear function in response to SiO2 nanoparticles, Experimental Cell Research 305 (1) (2005) 51–62.
[31] M. Karlsson, U. Carlsson, Protein adsorption orientation in the light of fluorescent probes: mapping of the interaction between site-directly labeled human carbonic anhydrase II and silica nanoparticles, Biophysical Journal 88 (5) (2005) 3536–3544.
[32] W. Sun, N. Fang, B.G. Trewyn, M. Tsunoda, I.I. Slowing, V.S. Lin, E.S. Yeung, Endocytosis of a single mesoporous silica nanoparticle into a human lung cancer cell observed by differential interference contrast microscopy, Analytical and Bioanalytical Chemistry 39 (6) (2008) 2119–2125.
[33] X. Xing, X. He, J. Peng, K. Wang, W. Tan, Uptake of silica-coated nanoparticles by HeLa cells, Journal of Nanoscience and Nanotechnology 5 (10) (2005) 1688–1693.
[34] C. Muhlfeld, P. Gehr, B. Rothen-Rutishauser, Translocation and cellular entering mechanisms of nanoparticles in the respiratory tract, Swiss Med Wkly 138 (27–28) (2008) 387–391.
[35] D.M. Huang, Y. Hung, B.S. Ko, S.C. Hsu, W.H. Chen, C.L. Chien, C.P. Tsai, C.T. Kuo, J.C. Kang, C.S. Yang, C.Y. Mou, Y.C. Chen, Highly efficient cellular labeling of mesoporous nanoparticles in human mesenchymal stem cells: implication for stem cell tracking, FASEB J 19 (14) (2005) 2014–2016.
[36] Z. Tao, B.B. Toms, J. Goodisman, T. Asefa, Mesoporosity and functional group dependent endocytosis and cytotoxicity of silica nanomaterials, Chemical Research in Toxicology 22 (11) (2009) 1869–1880.
[37] C. Li, H. Liu, Y. Sun, H. Wang, F. Guo, S. Rao, J. Deng, Y. Zhang, Y. Miao, C. Guo, J. Meng, X. Chen, L. Li, D. Li, H. Xu, H. Wang, B. Li, C. Jiang, PAMAM nanoparticles promote acute lung injury by inducing autophagic cell death through the Akt-TSC2-mTOR signaling pathway, Journal of Molecular Cell Biology 1 (1) (2009) 37–45.
[38] O. Seleverstov, O. Zabirnyk, M. Zscharnack, L. Bulavina, M. Nowicki, J.M. Heinrich, M. Yezhelyev, F. Emmrich, R. O'Regan, A. Bader, Quantum dots for human mesenchymal stem cells labeling. A size-dependent autophagy activation, Nano letters 6 (12) (2006) 2826–2832.
[39] J.J. Li, D. Hartono, C.N. Ong, B.H. Bay, L.Y. Yung, Autophagy and oxidative stress associated with gold nanoparticles, Biomaterials 31 (23) (2010) 5996–6003.
[40] M. Baba, K. Takeshige, N. Baba, Y. Ohsumi, Ultrastructural analysis of the autophagic process in yeast: detection of autophagosomes and their characterization, The Journal of Cell Biology 124 (1994) 903–913.
[41] A. Longatti, S.A. Tooze, Vesicular trafficking and autophagosome formation, Cell Death Differ 16 (7) (2009) 956–965.
[42] C. He, D.J. Klionsky, Regulation mechanisms and signaling pathways of autophagy, Annual Review of Genetics 43 (2009) 67–93.

CHAPTER 4

NANOPARTICLE GEOMETRY AND SURFACE ORIENTATION INFLUENCE MODE OF CELLULAR UPTAKE

Heather L Herd, Nicole Daum, Arwyn T. Jones,
Hanno Huwer, Hamidreza Ghandehari,
Claus Michael-Lehr

ACS Nano, 2013;7(3):1961-1973

Nanoparticle Geometry and Surface Orientation Influence Mode of Cellular Uptake

Heather Herd,[†,‡,§] Nicole Daum,[§] Arwyn T. Jones,[⊥] Hanno Huwer,[∥] Hamidreza Ghandehari,[†,‡,#,*] and Claus-Michael Lehr[§,△,*]

[†]Utah Center for Nanomedicine, Nano Institute of Utah, University of Utah, 36 S. Wasatch Drive, Salt Lake City, Utah 84112, United States , [‡]Department of Bioengineering, University of Utah, United States, [§]Helmholtz Centre for Infection Research, Helmholtz-Institute for Pharmaceutical Research Saarland, Saarland University, Campus, Building A4_1, D-66123 Saarbruecken, Germany, [⊥]Cardiff School of Pharmacy and Pharmaceutical Sciences, Cardiff University, Cardiff Wales, CF10 3NB, United Kingdom, [∥]Cardiothoracic Surgery, Heart Center Voelklingen, Germany, [#]Department of Pharmaceutics and Pharmaceutical Chemistry, University of Utah, United States, and [△]Biopharmaceutics and Pharmaceutical Technology, Saarland University, Campus, Building A4_1, D-66123 Saarbruecken, Germany

ABSTRACT In order to engineer safer nanomaterials, there is a need to understand, systematically evaluate, and develop constructs with appropriate cellular uptake and intracellular fates. The overall goal of this project is to determine the uptake patterns of silica nanoparticle geometries in model cells, in order to aid in the identification of the role of geometry on cellular uptake and transport. In our experiments we observed a significant difference in the viability of two phenotypes of primary macrophages; immortalized macrophages exhibited similar patterns. However, both primary and immortalized epithelial cells did not exhibit toxicity profiles. Interestingly uptake of these geometries in all cell lines exhibited very different time-dependent patterns. A screening of a series of chemical inhibitors of endocytosis was performed to isolate the uptake mechanisms of the different particles. The results show that all geometries exhibit very different uptake profiles and that this may be due to the orientation of the nanoparticles when they interact with the cell surface. Additionally, evidence suggests that these uptake patterns initialize different downstream cellular pathways, dependent on cell type and phenotype.

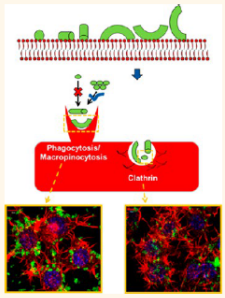

KEYWORDS: silica nanoparticle · nanotoxicity · endocytosis · cellular uptake · intracellular fate

The biomedical and engineering world has seen a drastic increase in the use of nanomaterials for therapeutic and diagnostic applications. However, it remains uncertain how nanomaterials interact with biological interfaces such as the plasma membrane of cells. Studies suggest that small alterations in physicochemical characteristics can drastically influence interactions of nanoparticles with the biological environment, affecting the mechanisms of cellular uptake and ultimately intracellular fate.[1,2] These changing interactions may also produce unintentional adverse effects, such as the induction of chronic inflammatory cascades. In order to engineer safe, efficient drug delivery systems, there is a need to develop a higher level of understanding of the mechanisms of uptake and intracellular fate of these constructs. Identification and systematic evaluation of the cellular uptake of nanomaterials will afford the development of target-specific constructs that deliver through a defined entry pathway leading to an appropriate intracellular fate with resultant bioactivity of the associated pharmacologically active ingredient.

It is generally appreciated that vesicular processes occurring at the cell membrane represent the prevailing route of uptake for these systems. For example, the accumulation of localized lipid raft domains induced by cell membrane interactions can be responsible for local membrane invaginations, facilitating nanoparticle uptake. Numerous endocytic routes exist, and some require activation *via* cell surface interactions to mediate receptor-mediated internalization.[3,4] For example, when conjugated to small nanoparticles, platelet endothelial cell adhesion molecule 1 (PECAM-1) and intercellular adhesion molecule 1 (ICAM-1) demonstrated increased uptake and transfection when compared to unconjugated ligand and large nanoparticle attachment.[5,6] However mechanisms such as

* Address correspondence to (H.G.) hamid.ghandehari@pharm.utah.edu; (C.M.L.) lehr@mx.uni-saarland.de.

Received for review August 12, 2012 and accepted February 12, 2013.

Published online February 12, 2013
10.1021/nn304439f

macropinocytosis and phagocytosis are nonspecific internalization modalities utilizing membrane ruffling to engulf nanoparticulates. Generally macropinocytosis and phagocytosis require membrane ruffling with actin polymerization, leading to enclosure of fluid or a physical entity such as a bacterium or particle.[7] It has been previously shown that shape modulates phagocytic potential, where the flexibility and curvature of a particle and cell membrane dictate the capability for internalization.[8] Endocytosis however is not always the only mechanism of internalization, as membrane association of nanoparticles can induce physical interactions that allow particle internalization, such as that observed with highly cationic dendrimer lipid bilayer disruption, which is hypothesized to induce transient cell holes and needle-like materials that stab membranes for internalization.[9,10] In general there is little consensus in the literature as to what uptake mechanism is used by most nanoparticles, a product of the limited availability of appropriate techniques to characterize internalization and diverse nanoconstructs. Recent literature suggests that alterations in characteristics of nanomaterials such as the radius of curvature, surface functionalization, size, geometry, and charge, can drastically affect uptake mechanisms and the intracellular fate of nanoparticles.[11−16] Investigations showed that highly positively charged polyplexes associated with negatively charged cell surface heparan sulfate proteoglycans, for example, were essential for inducing phagocytic-like mechanisms to internalize these constructs.[11] Additionally, geometric variations in silica nanoconstructs facilitated different levels of macropinocytosis uptake due to differences in cell surface GTPase interactions.[12] Small nanoparticle systems were shown to have reduced rates of uptake and variations in mechanisms of uptake with variations in surface properties. The authors suggested these slight changes significantly altered the protein corona and thus mechanistic internalization.[17] Mathematical analyses and experimental confirmations have been done to show that clathrin-mediated invaginations are due to elastic deformation of the membrane dependent on a critical nanoconstruct radius that provides essential energy minimization.[13,14,18] It is hypothesized that when a particle has a radius above this critical value, the cell membrane is unable to invaginate the particle,[13,14] facilitating a decrease in clathrin-mediated mechanisms. Additionally, evidence suggests that spherical particles with a size range around 200 nm or less are internalized *via* clathrin-mediated endocytosis.[15] Gratton *et al.* have suggested that cationic polymeric PRINT particles exhibited a high degree of uptake *via* macropinocytic and clathrin-mediated mechanisms, with a kinetic increase in rod-like particle uptake.[19,20] Other groups have shown geometric-dependent kinetic uptake, surface orientation, and toll-like receptor 2 upregulation, which enhanced the uptake of nonspherical particles.[21−23] Additionally, the unique orientation of rod-like nanoparticles into vesicular compartments in the perinuclear region has also been demonstrated, when compared to their spherical counterparts.[24] This evidence suggests that orientation of materials due to differences in geometry results in entering cells through separate mechanisms, which may potentially dictate the ultimate fate of the particles intracellularly.

The objectives of this study were to determine the uptake patterns of three different silica nanoparticle geometries, namely, spheres, cylinders, and worms, in model cells. These translationally relevant cell models were primary human alveolar macrophages, primary human tissue macrophages, primary human alveolar epithelial cells, immortalized RAW 264.7 mouse macrophages, and A549 human lung tumor epithelial cells. The cells were used to aid in the identification of the role of geometry on cellular uptake and intracellular transport. Our findings reveal that geometry plays a role in the defined mechanism of intracellular uptake and may potentially lead to a specified intracellular fate.

RESULTS AND DISCUSSION

Silica Nanopartide Synthesis and Characterization. Three silica nanoparticle constructs were synthesized and characterized, as previously described:[25] worm-like, cylindrical, and spherical. Each construct was created such that charge, one dimension, fluorescence, and polydispersity were held constant (Supplemental Table 1 and Supplemental Figure 1). Polydispersity and the dimensions of the constructs were determined by the adjustment of the surfactant concentration while holding the stirring rate and heating of the solution constant. Charge and fluorescence attachment were determined by altering the ratio of surface modification to the number of particles in the solution.

Vialight Assay, Relative Nanoparticle Toxicity, and Cellular Uptake. To assess relative toxicity of the nanoparticles, cell viability at different concentrations was evaluated utilizing a measurement of the relative level of cellular adenosine triphosphate (ATP), an essential metabolic component in living cells. Relative nanoparticle cellular association and uptake was also assessed *via fluorescence-activated cell sorting* (FACS) and confirmed *via* confocal microscopy. No relative toxicity or nanoparticle uptake was observed in primary epithelial cells even at the highest concentration studied, and similar results were observed with the cell line A549 (Figure 1b and d, Supplement Figures 2d−f, 3b, and 4b and d). These results are corroborated with our previous findings that limited to no toxicity in epithelial cells following silica nanoparticle treatment was observed.[26] Additionally, these cells themselves serve primarily as a protective barrier and do not generally take up foreign material through phagocytic processes like

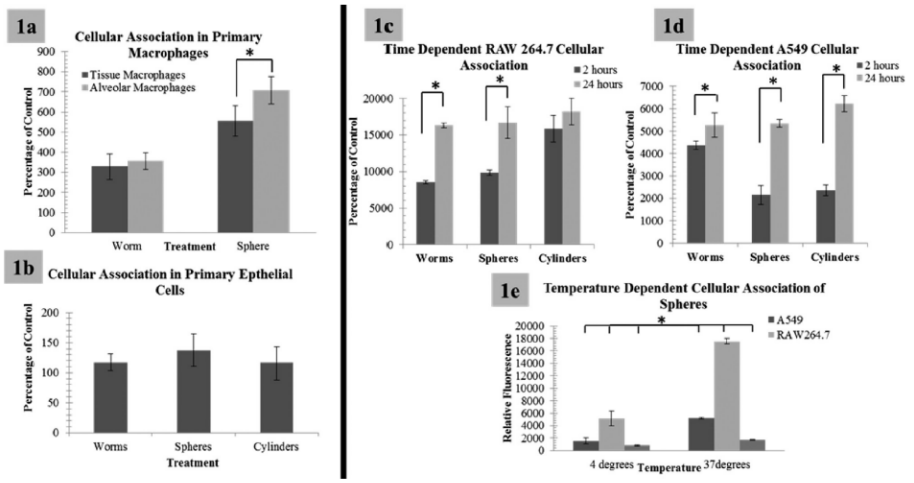

Figure 1. Basal uptake of geometrically defined nanoparticles. Relative uptake of 75 μg/mL of nanoparticles at specified time points assessed *via* FACS. (a) Macrophages exhibit significant uptake. However, both the phenotype of the macrophage and the geometry (at this time point, 1.5 h) appear to play important roles in the degree of uptake. It is also important to note that alveolar macrophages treated with spherical nanoparticles when compared to worm-like nanoparticles appear to have a greater degree of nanoparticle uptake, at this time point. This suggests a phenotypic and geometric implication. (b) Epithelial cells exhibit little to no nanoparticle uptake when compared to control. (c, d) Relative uptake of 75 μg/mL of nanoparticles at specified time points assessed *via* FACS. As shown, initial time point analysis shows a variation in the uptake rate of nanoparticles, dependent upon geometry, while later time points appear to have an equivalent rate of cellular association (for clarity some time points have been removed; please see Supplemental Figure 5 for all time points). (e) Representative graph of the relative uptake of spherical nanoparticles as a function of temperature in model cells. Alveolar macrophages are depicted by their increased uptake potential. The graph provides confirmation of energy-dependent mechanisms of uptake. Please note: graphs are represented as percentage of control or the background provided by FACS analysis of cells incubated without nanoparticles; so 100% would be 100% of control. Low levels of autofluorescence were indicated for immortalized lines, while high levels were indicated for primary cells due to donor variations including unknown patient treatment (chemotherapeutics, smoker or nonsmoker, other diseases/treatments, *etc.*) *Indicates statistical significance *p* value <0.05.

macrophages. Primary macrophages however were observed to follow a trend similar to RAW 264.7 cells (Figure 1a, Supplemental Figures 2–4), where high concentrations of nanoparticles exhibited toxicity (Supplemental Figure 4a and c) and a high degree of uptake (Figure 1a and c) was observed, while lower concentrations did not appear to exhibit a toxic effect. Interestingly, macrophage phenotypic variations did show differences in nanoparticle uptake (Figure 1a, Supplemental Figure 3a), suggesting that not only cell type but also cell phenotype have implications on toxicity and uptake of nanoparticles.

Time-Dependent Uptake. In an attempt to assess the relative mode of uptake of these geometries, a time point assay to determine the uptake saturation point was performed. During these experimental analyses it was observed that initially cells had variations in the rates of uptake that appeared to be dependent on the geometry of the nanoparticle, while at later time points, labeling became saturated and equilibrated to a level that was irrespective of geometry (Figure 1c and d, Supplemental Figure 5). These slight variations in the rates of uptake could potentially be due to differences in the internalization mechanisms of the nanoparticles, where some could be harnessing multiple or faster endocytic mechanisms.

Energy-Dependent Mechanisms of Uptake. To determine if mechanisms of uptake were due to endocytosis (or other energy-dependent mechanisms) or membrane association, cells were incubated at 4 and 37 °C to evaluate the relative level of particle internalization. This method provides a reduction in the relative energy-dependent processes within cell models, effectively eliminating endocytosis. It was observed that there was a greater degree of cellular association at 37 °C when compared to 4 °C, suggesting energy-dependent or endocytic mechanisms of uptake (Figure 1e and Supplemental Figure 6). It does appear that some amount of nanoparticle uptake occurs at 4 °C, suggesting that they could interact with the membrane of the cell and facilitate uptake independent of energy active processes. It is also conceivable that this fraction is associated with the plasma membrane and not internalized. It is important to note that a majority of this nonspecific uptake occurs in A549 cells, rather than RAW 264.7 cells, suggesting that it could be a cell-dependent phenomenon. Since the majority of uptake was energy dependent, we then proceeded to further investigate what endocytic processes the nanoparticles were using to gain access to the cells.

Mechanisms of Uptake. A preliminary screening of a series of inhibitors was performed to isolate the initial

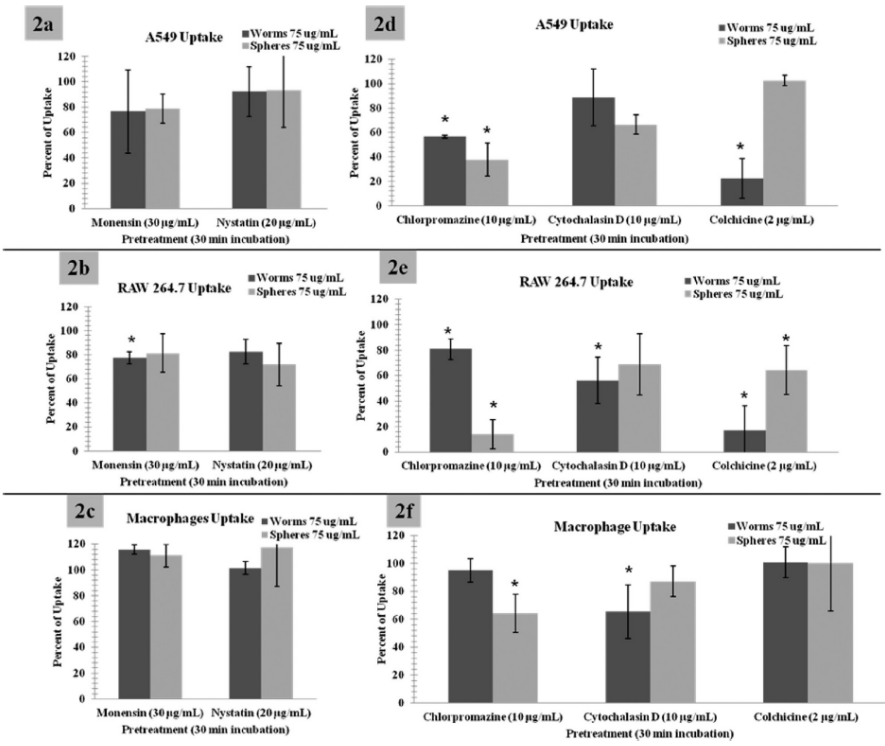

Figure 2. (a–c) Relative level of nanoparticle uptake when incubated with monensin (clathrin- and caveolin-independent endocytosis inhibitor) and nystatin (caveolin endocytosis inhibitor). This suggests that caveolin-mediated endocytosis is not involved in the internalization of these nanoparticle systems. (d–f) Cytochalasin D and colchicine are phagocytic and macropinocytosis inhibitors, while chlorpromazine inhibits clathrin-mediated mechanisms. The results show that there is a statistically significant reduction in nanoparticle uptake for these three inhibitors, but all geometries show very different uptake profiles. This suggests that the mechanisms by which these particles are entering the cells vary and are dependent on the relative shape (or size). For clarity and due to the significant similarities of worms and cylinders, cylindrical data have been moved to the Supporting Information. Please note: graphs are represented as percentage of uptake or the background provided by FACS analysis of cells incubated with spheres or worms without the respective inhibitor. *Indicates statistical significance from control p value <0.05. Macrophages are alveolar macrophages.

uptake mechanisms of the different particles. Nystatin was used to increase membrane fluidity *via* the depletion of cholesterol and reduce the formation of lipid caveolar rafts.[27] Monensin was used as an ionophore that facilitates an increased exchange of sodium ions and is generally considered an inhibitor of caveolae and clathrin-independent endocytosis.[28] Both of these inhibitors did not show a significant decrease in nanoparticle uptake (Figure 2a–c). This is a predictable result, as the nanoparticles are much larger in size than what is considered to be "normally" taken up by caveolae rafts.[29] It is important to note while epithelial cells normally express caveolae rafts, little is known about similar expression in macrophages. However, inflammatory phenotypes of macrophages including mouse macrophages and alveolar macrophages have been shown to express and in some cases overexpress caveolin.[30,31]

Three more inhibitors were involved in this initial screen, namely, cytochalasin D, colchicine, and chlorpromazine. Cytochalasin D and colchicine are phagocytic and macropinocytosis inhibitors. Cytochalasin D prevents actin polymerization, and colchicine inhibits microtubule polymerization, both of which reduce membrane ruffling.[32–34] Chlorpromazine reduces invaginations *via* clathrin-mediated endocytosis by depleting the plasma membrane of clathrin and adaptor proteins and sequestering them on intracellular vesicles. The results in Figure 2d–f show that there is a statistically significant reduction in nanoparticle uptake for these three inhibitors. However, all geometries show very different uptake profiles. Clathrin-mediated inhibitors appear to be reducing the amount of spherical uptake, while macropinocytosis and phagocytic inhibitors appear to be reducing worm-like nanoparticle uptake. These observations suggest that the mechanisms by which the particles are entering the cells vary and are dependent on their relative shape (or size). We did however detect some variations in observations,

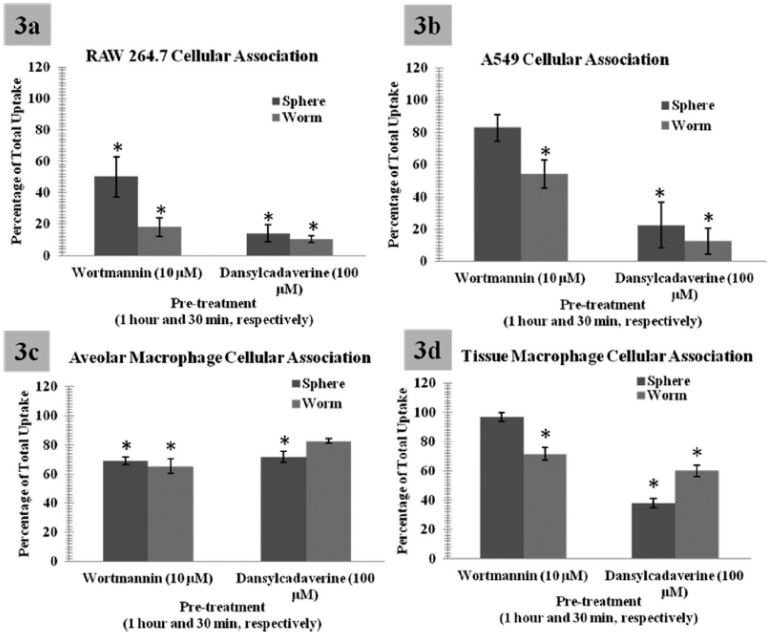

Figure 3. Flow cytometry analysis to quantitatively assess the uptake of nanoparticles. Due to low specificity in endocytic inhibitors, dansylcadaverine (a clathrin inhibitor) and wortmannin (a phagocytic and macropinocyotsis inhibitor) were utilized to confirm the apparent variations in uptake due to changes in geometry. As shown, dansylcadaverine blocks both sphere and worm uptake, but to a more significant degree spherical uptake. However, wortmannin is observed to block worm-like uptake to a more significant degree, supporting geometric variations in cellular uptake. Additionally, differences in uptake due to the cell phenotype were observed. For clarity and due to the significant similarities of worms and cylinders, cylindrical data hasve been moved to the Supporting Information. Please note: graphs are represented as percentage of uptake or the background provided by FACS analysis of cells incubated with spheres or worms without the respective inhibitor. *Indicates statistical significance from control p value <0.05.

as shown in Figure 2, where cytochalasin D did not exhibit the same degree of inhibition as colchicines induced, suggesting that microtubules may play a more important role in the polymerization pathways responsible for the extravasations. It is interesting to note that similar results with colloidal gold have been observed previously.[35]

Due to this variability, and because endocytic inhibitors can induce toxicity (Supplemental Figure 7) and lack specificity and efficacy,[11] dansylcadaverine and wortmannin were utilized to confirm the apparent variations in uptake due to differences in geometry. Dansylcadaverine treatment blocked the formation of coated pits by inhibiting transglutaminase in the cell membrane, which will reduce receptor-mediated endocytosis (clathrin mediated).[36] Wortmannin prevents fluid phase endocytosis (macropinocytosis) by inhibiting multiple isoforms of PI 3-kinase (phosphatidyl inositol-3-kinases).[32] As shown in Figure 3 dansylcadaverine blocked both sphere and worm uptake. Wortmannin blocked worm uptake to a greater extent. Additionally, to some degree both cell type and phenotypic differences were observed. Confocal image analysis confirmed all FACS results within all pharmacological screens (data not shown). Two concentrations of wortmannin were tested, in an attempt to discern between macropinocytosis and phagocytic uptake;[37,38] however neither showed significant difference from one another (Supplemental Figure 8).

These pharmacological inhibitor results are indicative of geometrically specific mechanism(s) of uptake, primarily clathrin-mediated endocytosis for spherical particles and macropinocytosis or phagocytosis for worm particles. It is hypothesized that this phenomena is due to the orientation of the nanoparticles when they interact with the cell surface (Figure 4) and that geometry provides a unique advantage because alteration in this parameter allows for the design of multiple approach mechanisms. For example, a spherical nanoparticle has only one face that can interact with the cell surface, while cylindrical and worm-like nanoparticles have multiple faces with large variations in size in each dimension. If one draws a correlation between the physicochemical characteristics (or dimensions) of these nanoparticles and endocytic mechanisms, one can identify or predict their primary mode of uptake (Figure 4). For example spheres have one dimension of approximately 200 nm, which may be expected to be

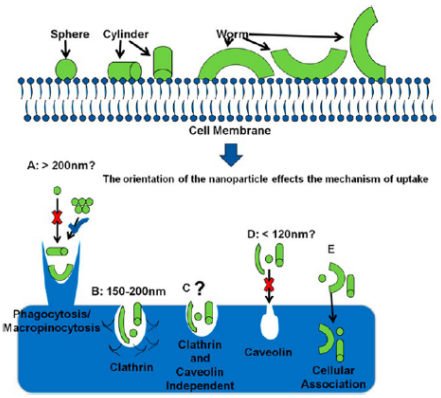

Figure 4. Cartoon depicting the hypothesis that the orientation of the nanoparticle influences the mechanism of uptake. (A) Macropinocytosis has been shown to occur at the microscale, fitting with one dimension of cylinders and worms. However, spheres, unless aggregated, do not fit this criterion. (B) Theoretically if oriented properly, all particles could be taken up *via* clathrin-mediated mechanisms. (C, E) Other mechanisms of uptake not readily identifiable are plausible. (D) Caveolin-mediated invaginations are theoretically much too small for the nanoparticle size range tested here.[29]

within the size range of clathrin-mediated endocytosis. It is important however to note that this dimension is on the larger end of normal clathrin invaginations.[39] This dimension however is too large for caveolin-mediated endocyotsis and too small for phagocytosis unless the spheres are aggregated. However, evidence does suggest that macropinocytosis can occur in small size ranges.[7] Thus, it is hypothesized that clathrin-mediated endocytosis is the primary mechanism of uptake for the spherical nanoparticle systems. Worms and cylinders however had one dimension of approximately 200 nm, within the clathrin limits, and another dimension (~400 and 1300 nm) that was within the limits of macropinocytosis and phagocytosis. Thus, it is possible that both the end of the particle and the longitudinal rotation of the particle could interact with the cell surface, effectively harnessing both mechanisms of uptake. It is more probable that macropinocytosis and or phagocytosis are the mechanisms of uptake of these particles due to their relatively large size. Additionally, when comparing the transversal (small) axis of the nanoparticle to the longitudinal axis, it is more likely that the longitudinal axis will have a higher positive charge. Thus, it is more probable that there will be an axial rotational association of the particle with the net negative charge of the cell membrane, leading to an energy maximum. Similar observations were made previously for microparticles at the nucleus and surface.[24,40,41]

Dextran and Transferrin Co-localization. To further confirm uptake pathways, we utilized traditional markers for co-localization. Transferrin is a well-characterized marker of clathrin-mediated uptake, and dextran is primarily used as a marker for fluid phase uptake and macropinocytosis.[39] As observed in the pharmacological inhibition experiments, a greater degree of transferrin co-localization was observed with spherical nanoparticles, while colocalization with dextran appears to be equivalent (Figure 5A and C, transferrin and dextran, respectively) when compared to worm-like nanoparticles (Figure 5B and D, transferrin and dextran, respectively) in both RAW 264.7 and A549 cells. It is important to note however that in both cases co-localization did occur in the worm-like nanoparticle conditions, suggesting that clathrin- and fluid-phase-mediated mechanisms may both play a role in the uptake of these particles.

Actin Polymerization. To provide further visual evidence of endocytosis and to prove the involvement of actin polymerization mechanisms, a phalloidin stain was used to label the cell lines studied. As observed in Figure 6, A and D, spherical and worm nanoparticle treatment, respectively, have very different actin polymerization patterns. The apparent actin polymerization patterns include polymerization into bowl-like structures just below the surface of the cell (B, C, E, and F) and extravasations polymerizing above the surface of the cell. Both of these patterns appear to be associated with the nanomaterials. The polymerization patterns could be suggestive of the involvement of clathrin-mediated, macropinocytic, and phagocytic mechanisms.

Transmission Electron Microscopy of Endocytosis. From experiments with labeled actin showing the involvement of surface protrusions we performed further ultrastructural analysis of cells incubated with these nanoparticles. Here, following 15 min of incubation with worm and spherical nanoparticles, cells were imaged *via* TEM. Visualization suggests that worm-like particles were mostly associated with extravasations from the membrane (Figure 7E and G), as well as particle wrapping like protrusions (Figure 7F). Invaginations where spherical particles seemed to be associated with the cellular membrane were observed (Figure 7A and B). Particles were also observed in the intracellular space within 15 min (Figure 7G for worms and C for spheres), an unusually rapid internalization for nanoparticle systems. Additionally, several nanoparticles appear to be clumped, suggesting that particles are entering through similar pathways or being sequestered by the cell. It is important to note that spherical particles appear to be internalized and associate with the plasma membrane much more rapidly than worm particles. More particles reside within the intracellular space and around the membrane within that time frame, correlating with the time-dependent FACS cellular uptake results. However, as observed previously, nanoparticle content does reach an equivalence at later time points.[25] This suggests that spherical

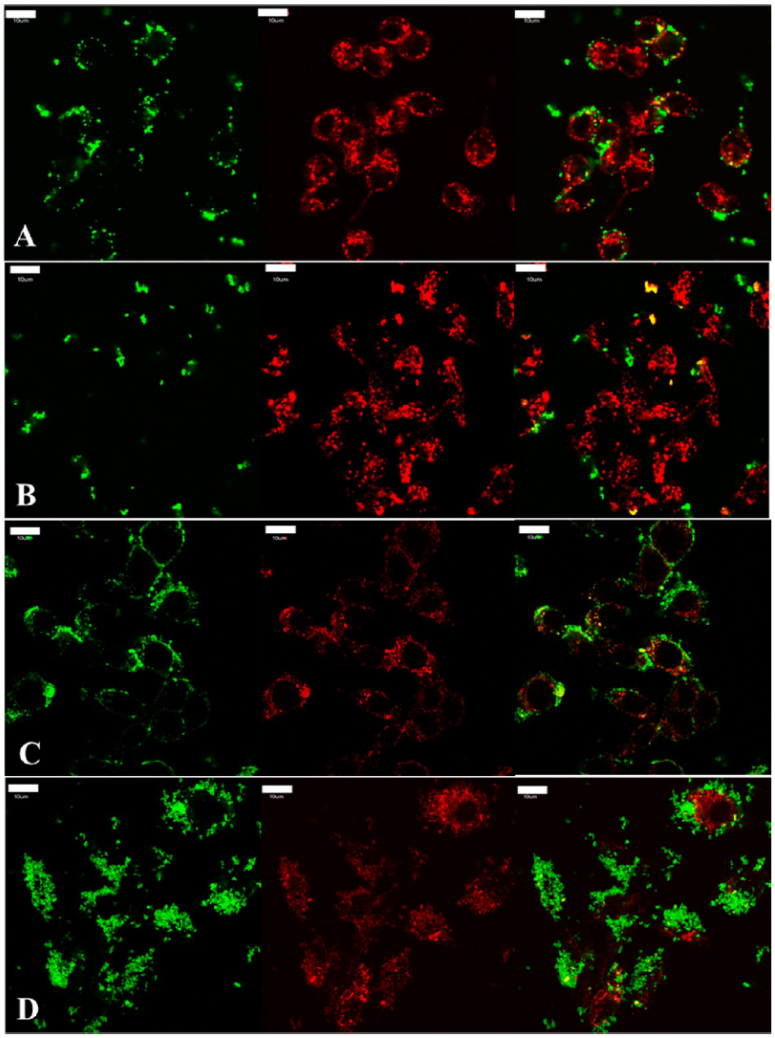

Figure 5. Transferrin and dextran, intracellular markers of clathrin-mediated endocytosis and fluid phase endocytosis, respectively, were co-incubated with silica nanoparticles to investigate the degree of co-localization to confirm clathrin- and fluid-phase-mediated mechanisms; RAW 264.7 cells shown. (A, B) A single focal plane and the respective channels of live cells after 15 min of incubation. Transferrin is labeled in red, nanoparticles are labeled in green (A is spherical treatment and B is worm-like treatment, both at 75 μg/mL), and the co-localization is depicted in yellow between particles and transferrin. (C, D) Fluorescence from all Z stacks and respective channels of fixed cells after 30 min of incubation. Dextran is labeled in red, particles are labeled in green (C is spherical treatment and D is worm-like treatment at 75 μg/mL), and yellow represents the co-localization between nanoparticles and dextran. There appears to be a higher degree of co-localization of both these cellular internalization markers with spherical nanoparticles when compared to worm-like nanoparticles, suggesting that a higher degree of clathrin- and fluid-phase-mediated endocytosis occurs with these systems. It is important to note that the co-localization (yellow) in all images suggests that clathrin- and fluid-phase-mediated endocytosis is at play for all geometries tested. For clarity and due to the significant similarities of worms and cylinders, cylindrical data have been moved to the Supporting Information. Scale bars: 10 μm.

particles are internalized more rapidly, due to either their relative size or the internalization mechanism. Worm-like particles and spherical particles are completely internalized at 24 h, as depicted in Figure 7D and H.[25] These sequestering mechanisms appear to continue at 24 h.

PI 3-Kinase Pathway Upregulation after Nanoparticle Uptake. In an attempt to begin to understand the cues behind this sequestering mechanism, initial gene expression levels were analyzed after a 1.5 h incubation period with nanoparticles. As briefly introduced earlier, PI 3-kinase is an essential protein in the formation and

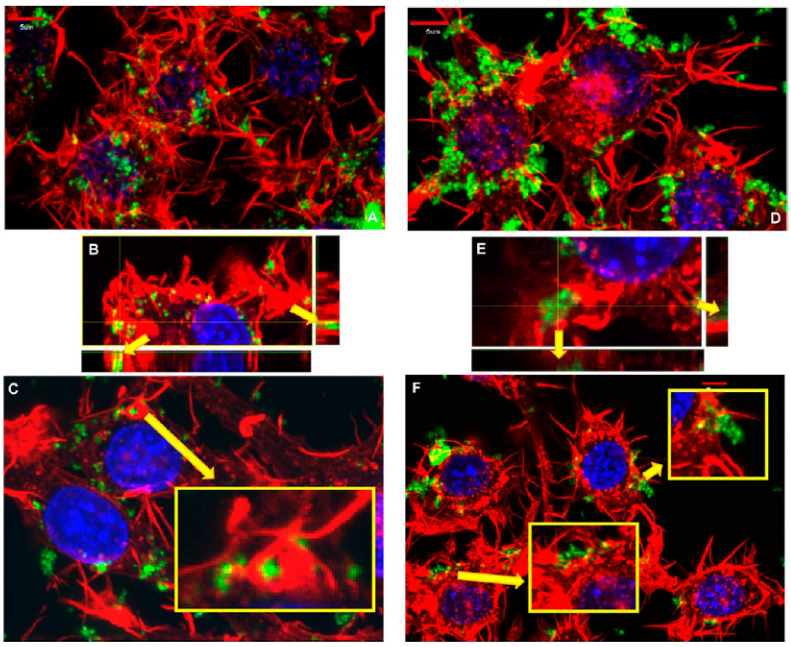

Figure 6. Actin polymerization staining in RAW 264.7 cells, involved in mechanisms of endocytosis, is depicted to visualize the hallmark endocytic process involved in the internalization of these particles. Red: phalloidin stain of actin polymerization, green: nanoparticle FITC attachment, and blue: DAPI nucleus stain. (A–C) Spherical nanoparticle and (D–F) worm nanoparticle treatment after 15 min. Spherical nanoparticle treatment (A) and worm nanoparticle treatment (D) appear to induce very different polymerization patterns. The polymerization patterns observed in treated cells include invaginations within the membrane associated with nanomaterials, identified in the zoomed inset in C and in the depiction of the Z stack in B, while other polymerization patterns appear to be extravasations from the membrane associated with nanomaterials, marked in the zoomed insets in F and the Z stack in E. These polymerization patterns could suggest the involvement of clathrin-mediated, macropinocytic, and phagocytic mechanisms. For clarity and due to the significant similarities of worms and cylinders, cylindrical data have been moved to the Supporting Information.

budding of macropinosomes in the intracellular environment,[38] and our results indicated that PI 3-kinase inhibition with wortmannin facilitated a reduction in the nanoparticle uptake and potentially the formation of macropinosomes in tissue macrophages (Figure 3). This led us to believe that downstream gene expression levels within the PI 3-kinase pathway could potentially provide insights into how cells cope with the intracellular uptake of these nanoparticles. Thus, following the incubation period, the RNA from tissue and alveolar macrophages was isolated and subjected to a PI 3-kinase signaling PCR array from SABiosciences (Qiagen, Valencia, CA, USA). This array is complete with 84 genes that are either directly or closely related to this signaling cascade and could potentially provide some additional insight into genes that might cause downstream intracellular signaling and ultimate intracellular fate. While all treatments caused a regulation of these genes, a greater degree of regulation was observed with worm-like treatments when compared to spherical treatments (Figure 8). This suggests that PI 3-kinase may potentially be affected to a greater degree in worm-like treatments when compared to spherical counterparts; however all nanoparticle treatments may induce this cascade. It is important to note that there is a significant difference between the affects in tissue and alveolar macrophages, suggesting that tissue macrophages might have an increased fluid phase or macropinocytic function. Or alternatively an increase in phagocytic activity could be present in alveolar cells due to their native physiological function, which may operate independently of PI 3-kinase.

The regulated genes were further processed *via* data mining bioinformatics online freeware services (GATHER)[42] to identify other pathways that could potentially be responsible for the observed regulation. It was seen that a majority of the genes were interconnected and regulated cell size and growth, phosphorylation, focal adhesion, cell signaling, cell surface receptors, toll-like receptor signaling, insulin signaling, and ribosomal protein S6 kinases (Supplemental Table 2).

In our previous observations, cells appeared to take up and eventually sequester a certain concentration of nanoparticles in autophagic compartments. Below this threshold the cells were able to proliferate and function "normally", while above it they underwent what

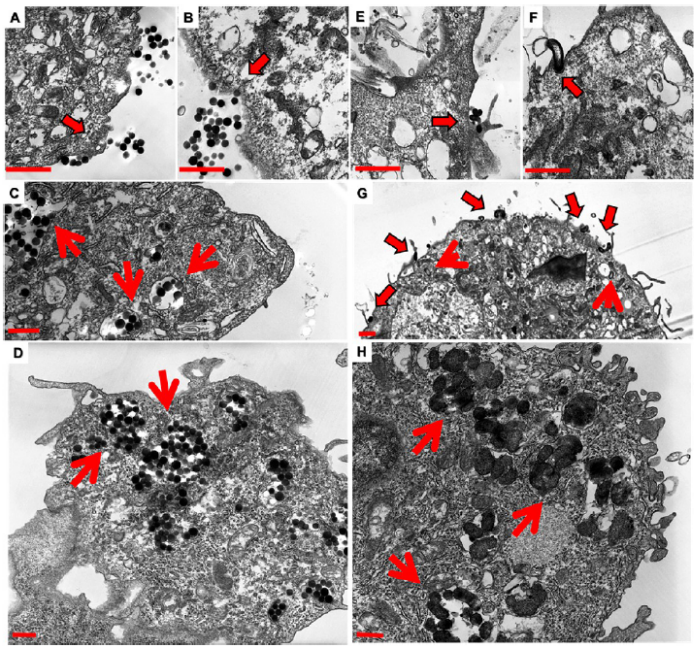

Figure 7. Following 15 min of incubation with both worm and spherical nanoparticles, cells were fixed and imaged *via* TEM. Membrane invaginations are associated with spherical particles (A and B). Membrane extravasations however are observed to be associated with worm particles (E and G), and membrane wrapping associated with worm-like particles (F and G) is observed. Both nanoparticles are observed within the cytoplasm of these cells at 15 min (C and G), while there is a greater degree of uptake of spherical nanoparticles at this time point. This suggests that spherical particles are taken up more rapidly than worm nanoparticles. However, a greater amount of both nanoparticles is internalized at 24 h time points, as we observed previously (D and H).[25] Additionally, there appears to be some type of sequestering mechanism at play. For clarity and due to the significant similarities of worms and cylinders, cylindrical data have been moved to the Supporting Information. Scale bars: 1 μm.

appeared to be necrotic cell death.[25] This threshold mechanism appeared to be independent of geometric variations at a 24 h time point.[25] Using similar nanoparticles, in this study we observed that variations in the mechanisms of and the accumulation rate of uptake are dependent on the geometry. Yet, at later time points, we still observe a threshold mechanism in both immortalized and primary cells.

If we connect this gene expression to our previous findings, we might be able to link the initial gene expression to the ultimate intracellular fate of these nanoparticles. In our PCR analysis we identified the presence of cell size and growth, phosphorylation, focal adhesion, cell signaling, cell surface receptors, and toll-like receptor signaling gene regulation pathways (Supplemental Table 2). However we also identified the involvement of insulin signaling and ribosomal protein S6 kinase pathways (Supplemental Table 2). While it is expected that the former signaling cascades would be induced due to local interactions of the nanoparticles with the cell surface, the latter seems surprising. One would expect that with an increase in macropinocytosis activity one would see an increase in the relative cell size, leading to an increase in the amount of material that could be taken up by the cells. Additionally, focal adhesions might need to be initiated to induce cellular internalization and surface receptors would be initiated with nanoparticle interactions. However, the latter two signaling cascades are surprising. Yet, if one takes a look at previously reported data, it can be seen that nanoparticles including silica nanoparticles[25] have been implicated in an intracellular trafficking and signaling event called autophagy. Not only does PI 3-kinase signaling play an important role in the initiation of these events, but so do the insulin and ribosomal protein S6 kinase signaling cascades.[43−45] The potential implication of these cascades could suggest that internalization is inducing intracellular signaling gene cascades, leading to ultimate intracellular fate or sequestering within autophagic compartments.

If intracellular fate is determined upon cellular internalization, it means that the manipulation of these uptake patterns could provide enhanced specific delivery properties. Thus, it will be important in further research to identify specific patterns in the biological response in both protein and gene

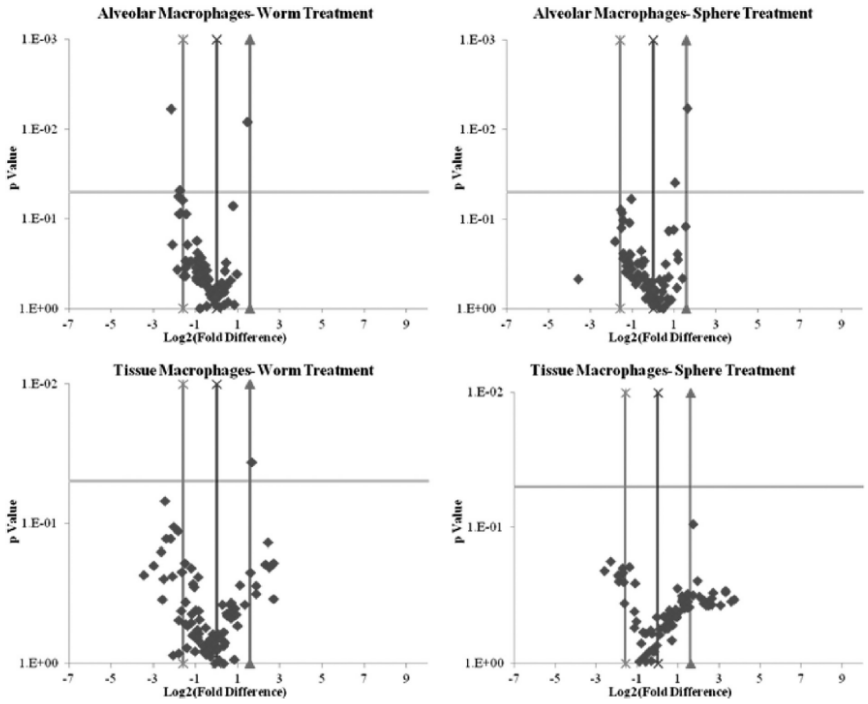

Figure 8. PI 3-kinase array analysis volcano plots of primary macrophages regulated genes. More regulation is observed in tissue macrophages when compared to alveolar macrophages, suggesting a different pattern of uptake due to phenotypic differences. This could also potentially play an important role in toxicity. Additionally, worms regulate genes to a more significant extent than spheres do in both tissue and alveolar macrophages. However, it is plausible that particle treatment itself could induce this regulation.

expression and correlate that to the physicochemical characteristics.

CONCLUSIONS

In summary, in this report we have shown that geometry plays an important role in the uptake of nanoparticles. Nanoparticle uptake was induced *via* a variety of different endocytic and cellular association mechanisms, dependent on the geometry. Within this size range with highly positively charged materials, it appears that clathrin-mediated endocytosis was the primary mechanism of uptake for spherical particles, while those materials with a larger dimension appear to be taken up primarily through macropinocytosis or phagocytic mechanisms. However, all materials to some degree were taken up *via* both mechanisms. Additionally, we have shown that phenotypic differences within cell types can lead to very different uptake profiles, suggesting that cell function plays an important role in nanoparticle toxicity.

EXPERIMENTAL METHODS

Silica Nanoparticle Synthesis and Characterization. Silica nanoparticles were synthesized and characterized as described previously.[25] Briefly porous silica nanoworms, -spheres, and -cylinders were synthesized utilizing modified Stober methods.[3,46] 3-Aminopropyltriethoxysilane was coupled to the surface of the silica nanoparticles by procedures described earlier.[47] All particles were fluorescently labeled with fluorescein isothiocyanate (FITC) to assess cellular uptake (~2.9, 3.5, and 6.5 mg of FITC per 100 mg of worms, cylinders, and spheres, respectively). The constructs were sterilized by dry autoclavation. Following synthesis the size and shape of the particles were determined by transmission electron microscopy (TEM). Zeta potential of the constructs was measured using a Malvern Instruments Zetasizer Nano ZS. The absence of cetyltrimethylammonium bromide and presence of primary amine after acid hydrolysis was ascertained by infrared spectroscopy and thermogravimetric analysis.

Cell Culture. Human adenocarcinoma alveolar basal epithelial A549 cells and RAW 264.7 murine macrophages were obtained from ATCC (Manassas, VA, USA) and maintained in the recommended media supplemented with 10% FBS. Cell cultures were incubated at 37 °C in 5% CO_2 and 95% humidified air and kept in logarithmic phase of growth throughout all experiments. In general, cells were seeded at ~15000 cells per cm^2.

Primary epithelial cells and macrophages were isolated and cultivated, as described previously.[48,49] Briefly, human lung tissue was obtained from patients undergoing lung resections. The tissue was sliced and washed repeatedly with a balanced

salt solution. The tissue slices were collected, pelleted, and incubated with hypotonic buffer to isolate alveolar macrophages. The remaining tissue slices were digested with a trypsin−elastase combination and filtered prior to an incubation of the resulting fluid in a Petri dish for 90 min to allow for tissue macrophage attachment. Unattached cells in the Petri dish underwent a Percoll density gradient and cell sorting with magnetic beads to isolate purified human alveolar epithelial type II cells. Both macrophages and epithelial cells were seeded at 500 000 cells in a 12-well plate. Macrophages were cultivated in MΦ medium (RPMI 1640, 5% FCS, 100 U/mL penicillin G, 100 μg/mL streptomycin, 2 mM glutamine) for 4−5 days to ensure appropriate receptor expression. Epithelial cells were cultivated in SAGM small airway epithelial cell growth medium (SAGM Airway Bullet Kit, CC-3118), with supplements including bovine pituitary extract, hydrocortisone, human epidermal growth factor, epinephrine, insulin, triiodothyronine, transferrin, gentamicin/amphotericin B, retinoic acid, and BSA-FAF (Lonza, Verviers, Belgium) supplemented with penicillin (100 units/mL), streptomycin (100 μg/mL), and 1% fetal calf serum and were maintained for 10 days until confluence. All cultures were kept at 37 °C in a 5% CO_2 humidified atmosphere.

Measurement of Cell Viability. Cells were exposed to a range of concentrations (30−500 μg/mL) of silica nanoparticles for 2 and 24 h. They were subsequently washed with phosphate buffer saline (PBS), and relative cell viability was assessed by utilizing a luciferase enzyme, which is converted to a bioluminescent molecule *via* ATP, a required element in living cells. The luciferase enzyme is the key component in the Vialight Assay (Lonza,Verviers, Belgium), and assessment of relative cell viability was obtained using manufacturer's protocols. Light intensity measurements were performed using an Infinite M200 microplate reader (Tecan, Crailsheim, Germany). IC_{50} values were calculated utilizing GraphPad Prism software (La Jolla, CA, USA).

Cellular Uptake Visualization, Quantification, and Time Point Analysis. The uptake of silica nanoparticles by cultured cells was visualized by confocal microscopy. Cells were grown on 24-well imaging plates at a density of ~9000 cells/cm^2 and incubated for 24 h with 75 μg/mL FITC-labeled silica nanoconstructs. After incubation, cell membranes were stained with rhodamine-labeled wheat germ agglutinin (rhodamine-WGA) and fixed with 4% formalin in PBS. Cell nuclei were stained with 2.5 μM 4′,6-diamidino-2-phenylindole (DAPI) according to the manufacturer's protocol. Fluorescent images of fixed cells were taken under a confocal laser scanning microscope (LSM510; Zeiss, Jena, Germany). The intensity of the laser beam and the photodetector sensitivity were kept constant in order to compare the relative fluorescence intensities between experiments. Z stacks were collected and localization was assessed utilizing the LSM510 software package. 3D reconstruction, visualization of intracellular particles, image acquisitions, and analyses were performed using Velocity (Improvisions, Lexington, MA, USA).

Flow cytometry analysis was used to quantify the amount of nanoparticle uptake. Cells were grown on 12-well plates at a density of ~15 000 cells/cm^2 and incubated with 75 μg/mL FITC-labeled silica nanoconstructs for various time points (0.5, 1, 2, 4, 6, 12, and 24 h). Following incubation, cells were trypsinized (epithelial cells) or scraped (macrophage cells) to obtain a single-cell suspension. Cells were suspended in PBS containing 1% BSA, and analysis was performed on a FACSCalibur (BD Biosciences, Heidelberg, Germany). Emitted light resulting from FITC-labeled nanoparticles was detected by the FL-2 detector. To calculate the background fluorescence of unlabeled cells, cells without any addition of nanoparticles were carried along as a negative control in every measurement. For whole-cell analysis 10 000 cells were counted. Data analysis was performed with BD CellQuest Pro (BD Biosciences, Heidelberg, Germany).

Energy-Dependent Mechanisms. Flow cytometry analysis was used to quantify the amount of nanoparticle uptake. Cells were grown on 12-well plates at a density of ~15 000 cells/cm^2 and incubated with 75 μg/mL FITC-labeled silica nanoconstructs for 2 h at 4 and 37 °C. Analysis and quantification methods were identical to quantification and time point analyses.

Studies with Chemical Inhibitors of Endocytosis. The relative level of nanoparticle uptake was assessed *via* confocal microscopy and flow cytometry. Cells were grown on 24-well imaging and 12-well cell culture plates (confocal and FACS, respectively) at a density of ~15 000 cells/cm^2. They were preincubated with endocytosis inhibitors prior to a 1.5 h incubation with 75 μg/mL FITC-labeled silica nanoconstructs. Following incubation, confocal and FACS analysis (as outlined previously) were performed. Nanoparticle-only treated cells were utilized as positive controls and compared to inhibitor plus nanoparticle-treated cells. Caveolin-dependent endocytosis was assessed utilizing nystatin at a 30 min preincubation at 20 μg/mL. Clathrin-dependent endocytosis was assessed utilizing a 30 min preincubation with either 100 μM dansylcadaverine or 10 μg/mL chlorpromazine. Clathrin- and caveolin-independent endocytosis were assessed utilizing a 30 min pretreatment with 30 μg/mL monensin. Phagocytosis and macropinocytosis were assessed utilizing a single inhibitor; the following were used: 1 h incubation with 10 μM or 10 nM concentrations of Wortmannin or a 30 min preincubation with 10 μg/mL cytochalasin D or 2 μg/mL of colchicine. Concentrations were obtained from reported literature values.[50,51] Cell viability was tested for all concentrations of each inhibitor after 3 h of incubation.

Dextran and Transferrin Co-localization. The co-localization of silica nanoparticles with Alexa Fluor 633-labeled dextran and transferrin (Invitrogen Corp., Carlsbad, CA, USA) by cultured cells was assessed by confocal microscopy. Cells were grown on 35 mm glass bottom microwell dishes at a density of ~9000 cells/cm^2 (MatTek, Ashland, MA, USA) and incubated with either a 15 min co-incubation with 75 μg/mL FITC-labeled silica nanoconstructs and Alex Fluor 633-labeled transferrin or 30 min with 75 μg/mL FITC-labeled silica nanoconstructs and 50 μg/mL Alex Fluor 633-labeled dextran. Fluorescent images of fixed cells were taken by CLSM as described above.

Actin Labeling with Rhodamine Phalloidin. To assess the relative proximity of silica nanoparticles to polymerized actin, following fixation cells were assessed *via* confocal microscopy. First, cells were grown on 35 mm glass bottom microwell dishes at a density of ~9000 cells/cm^2 (MatTek, Ashland, MA, USA) and incubated for 15 min with 75 μg/mL FITC-labeled silica nanoconstructs. Following incubation with the nanoparticles the actin cytoskeleton was labeled essentially according to the manufacturer's instructions. Briefly cells were washed with PBS, fixed with 3.7% formaldehyde solution for 10 min, washed with PBS, and permeabilized by 0.1% Triton X-100 in PBS. The cells were then washed with PBS and incubated for 20 min with 5 μL of rhodamine phalloidin from a 200 units/mL methanolic stock. Cells were washed a final time, fixed, and mounted for CLSM imaging.

Transmission Electron Microscopy. The uptake of silica constructs by cultured cells was assessed by transmission electron microscopy. Cells were seeded on six-well plates containing 1 × 1 cm ACLAR plastic at 2 × 10^5 cells per well. After an overnight incubation, 50 μg/mL of silica nanoconstructs was added, and cells were incubated for 15 min, after which they were washed with PBS and fixed with a 2.5% glutaraldehyde and 1% formaldehyde in 0.1 M sodium cacodylate buffer with sucrose and calcium chloride. Cells were stained with uranyl acetate for 45 min at room temperature, and TEM images were taken with a Phillips TECHAI F2 TEM (Hillsboro, OR, USA) at an accelerating voltage of 80 kV.

Real-Time PI3K-AKT Signaling PCR Array. RNA was isolated from three separate patient samples of primary alveolar and tissue macrophages using an RNeasy Mini Kit (Qiagen), and genomic DNA was removed utilizing an RNase-Free DNase Set (Qiagen, Valencia, CA, USA). Total RNA was converted to cDNA using the RT^2 First strand kit (SABiosciences, Qiagen) and mixed with RT^2 qPCR SYBR Green Mastermix (SABiosciences, Qiagen, Valencia, CA, USA). Samples were loaded and read *via* manufactures' instructions into a 384-well PI3K-AKT signaling PCR array (SABiosciences, Valencia, CA, USA) on a Roche Light Cycler 480. The melt curves and threshold cycle values were determined utilizing the Roche Light Cycler program. The 84 genes that were assessed in the array were related to the PI3K-AKT signaling pathway, after analysis utilizing RT^2 Profiler PCR Array data analysis software (http://pcrdataanalysis.sabiosciences.com/pcr/arrayanalysis.php, SABiosciences, Qiagen, Valencia,

CA, USA). Following the array data analysis software investigation and identification, the genes that were regulated were processed utilizing online data mining software tools, by GATHER,[42] to provide information on other pathway regulations.

Statistical Analysis. All experiments were performed in triplicate, and the results were presented as mean ± standard deviation. Student's *t* test (two tailed, unpaired) was performed for samples of nanoparticle-treated cells *vs* controls, unless stated otherwise. The difference between values was considered significant at the level of $p < 0.05$.

Conflict of Interest: The authors declare no competing financial interest.

Acknowledgment. We would like to thank Dr. Chris Rodesh and Nancy Chandler from the University of Utah Core Facilities for help with confocal microscopy and TEM imaging, respectively. This research was supported by a predoctoral Whitaker Foundation fellowship, Department of Defense Breast Cancer predoctoral fellowship (W81XWH-11-1-0057), National Institutes of Health (R01-DE19050), the Utah Science Technology and Research (USTAR) Initiative, and the Helmholtz Institute for Pharmaceutical Research Saarland (HIPS), Germany.

Supporting Information Available: Physicochemical characterization and TEM images of silica nanomaterials, confocal images of silica nanoparticles in immortalized and primary cells, viability data, time-dependent uptake data, energy-dependent mechanism data, inhibitor cell viability data, wortmannin data, and GATHER analysis. This material is available free of charge *via* the Internet at http://pubs.acs.org.

REFERENCES AND NOTES

1. Nel, A. E.; Madler, L.; Velegol, D.; Xia, T.; Hoek, E. M.; Somasundaran, P.; Klaessig, F.; Castranova, V.; Thompson, M. Understanding Biophysicochemical Interactions at the Nano-Bio Interface. *Nat. Mater.* **2009**, *8*, 543–557.
2. Jones, A. T.; Gumbleton, M.; Duncan, R. Understanding Endocytic Pathways and Intracellular Trafficking: A Prerequisite for Effective Design of Advanced Drug Delivery Systems. *Adv. Drug Delivery Rev.* **2003**, *55*, 1353–1357.
3. Wang, L. H.; Rothberg, K. G.; Anderson, R. G. Mis-Assembly of Clathrin Lattices on Endosomes Reveals a Regulatory Switch for Coated Pit Formation. *J. Cell Biol.* **1993**, *123*, 1107–1117.
4. Pelkmans, L.; Burli, T.; Zerial, M.; Helenius, A. Caveolin-Stabilized Membrane Domains as Multifunctional Transport and Sorting Devices in Endocytic Membrane Traffic. *Cell* **2004**, *118*, 767–780.
5. Wiewrodt, R.; Thomas, A. P.; Cipelletti, L.; Christofidou-Solomidou, M.; Weitz, D. A.; Feinstein, S. I.; Schaffer, D.; Albelda, S. M.; Koval, M.; Muzykantov, V. R. Size-Dependent Intracellular Immunotargeting of Therapeutic Cargoes into Endothelial Cells. *Blood* **2002**, *99*, 912–922.
6. Muro, S.; Garnacho, C.; Champion, J. A.; Leferovich, J.; Gajewski, C.; Schuchman, E. H.; Mitragotri, S.; Muzykantov, V. R. Control of Endothelial Targeting and Intracellular Delivery of Therapeutic Enzymes by Modulating the Size and Shape of Icam-1-Targeted Carriers. *Mol. Ther.* **2008**, *16*, 1450–1458.
7. Jones, A. T. Macropinocytosis: Searching for an Endocytic Identity and Role in the Uptake of Cell Penetrating Peptides. *J. Cell Mol. Med.* **2007**, *11*, 670–684.
8. Champion, J. A.; Mitragotri, S. Shape Induced Inhibition of Phagocytosis of Polymer Particles. *Pharm. Res.* **2009**, *26*, 244–249.
9. Hong, S.; Bielinska, A. U.; Mecke, A.; Keszler, B.; Beals, J. L.; Shi, X.; Balogh, L.; Orr, B. G.; Baker, J. R., Jr.; Banaszak Holl, M. M. Interaction of Poly(Amidoamine) Dendrimers with Supported Lipid Bilayers and Cells: Hole Formation and the Relation to Transport. *Bioconjugate Chem.* **2004**, *15*, 774–782.
10. Doshi, N.; Mitragotri, S. Needle-Shaped Polymeric Particles Induce Transient Disruption of Cell Membranes. *J. R. Soc., Interface* **2010**, *7*, S403–S410.
11. Vercauteren, D.; Vandenbroucke, R. E.; Jones, A. T.; Rejman, J.; Demeester, J.; De Smedt, S. C.; Sanders, N. N.; Braeckmans, K. The Use of Inhibitors to Study Endocytic Pathways of Gene Carriers: Optimization and Pitfalls. *Mol. Ther.* **2010**, *18*, 561–569.
12. Meng, H.; Yang, S.; Li, Z.; Xia, T.; Chen, J.; Ji, Z.; Zhang, H.; Wang, X.; Lin, S.; Huang, C.; *et al.* Aspect Ratio Determines the Quantity of Mesoporous Silica Nanoparticle Uptake by a Small Gtpase-Dependent Macropinocytosis Mechanism. *ACS Nano* **2011**, *5*, 4434–4447.
13. Decuzzi, P.; Ferrari, M. The Role of Specific and Non-Specific Interactions in Receptor-Mediated Endocytosis of Nanoparticles. *Biomaterials* **2007**, *28*, 2915–2922.
14. Decuzzi, P.; Ferrari, M. The Receptor-Mediated Endocytosis of Nonspherical Particles. *Biophys. J.* **2008**, *94*, 3790–3797.
15. Rejman, J.; Oberle, V.; Zuhorn, I. S.; Hoekstra, D. Size-Dependent Internalization of Particles *via* the Pathways of Clathrin- and Caveolae-Mediated Endocytosis. *Biochem. J.* **2004**, *377*, 159–169.
16. Rivera-Gil, P.; Jimenez De Aberasturi, D.; Wulf, V.; Pelaz, B.; Del Pino, P.; Zhao, Y.; De La Fuente, J. M.; Ruiz De Larramendi, I.; Rojo, T.; Liang, X. J.; *et al.* The Challenge to Relate the Physicochemical Properties of Colloidal Nanoparticles to Their Cytotoxicity. *Acc. Chem. Res.* **2012**.
17. Moros, M.; Hernaez, B.; Garet, E.; Dias, J. T.; Saez, B.; Grazu, V.; Gonzalez-Fernandez, A.; Alonso, C.; de la Fuente, J. M. Monosaccharides *versus* PEG-Functionalized NPs: Influence in the Cellular Uptake. *ACS Nano* **2012**, *6*, 1565–1577.
18. Chithrani, B. D.; Chan, W. C. W. Elucidating the Mechanism of Cellular Uptake and Removal of Protein-Coated Gold Nanoparticles of Different Sizes and Shapes. *Nano Lett.* **2007**, *7*, 1542–1550.
19. Gratton, S. E. A.; Napier, M. E.; Ropp, P. A.; Tian, S.; DeSimone, J. M. Microfabricated Particles for Engineered Drug Therapies: Elucidation into the Mechanisms of Cellular Internalization of Print Particles. *Pharm. Res.* **2008**, *25*, 2845–2852.
20. Gratton, S. E. A.; Ropp, P. A.; Pohlhaus, P. D.; Luft, J. C.; Madden, V. J.; Napier, M. E.; DeSimone, J. M. The Effect of Particle Design on Cellular Internalization Pathways. *Proc. Natl. Acad. Sci.* **2008**, *105*, 11613–11618.
21. Albanese, A.; Sykes, E. A.; Chan, W. C. W. Rough around the Edges: The Inflammatory Response of Microglial Cells to Spiky Nanoparticles. *ACS Nano* **2010**, *4*, 2490–2493.
22. Chithrani, B. D.; Ghazani, A. A.; Chan, W. C. W. Determining the Size and Shape Dependence of Gold Nanoparticle Uptake into Mammalian Cells. *Nano Lett.* **2006**, *6*, 662–668.
23. Doshi, N.; Mitragotri, S. Macrophages Recognize Size and Shape of Their Targets. *PLoS One* **2010**, *5*, e10051.
24. Yoo, J. W.; Doshi, N.; Mitragotri, S. Endocytosis and Intracellular Distribution of PLGA Particles in Endothelial Cells: Effect of Particle Geometry. *Macromol. Rapid Commun.* **2009**, *31*, 142–148.
25. Herd, H. L.; Malugin, A.; Ghandehari, H. Silica Nanoconstruct Cellular Toleration Threshold *in Vitro*. *J. Controlled Release* **2011**, *153*, 40–48.
26. Malugin, A.; Herd, H.; Ghandehari, H. Differential Toxicity of Amorphous Silica Nanoparticles toward Phagocytic and Epithelial Cells. *J. Nanopart. Res.* **2011**, *13*, 5381–5396.
27. Parton, R. G.; Richards, A. A. Lipid Rafts and Caveolae as Portals for Endocytosis: New Insights and Common Mechanisms. *Tra&c* **2003**, *4*, 724–738.
28. Pohlmann, R.; Kruger, S.; Hasilik, A.; von Figura, K. Effect of Monensin on Intracellular Transport and Receptor-Mediated Endocytosis of Lysosomal Enzymes. *Biochem. J.* **1984**, *217*, 649–658.
29. Kumari, S.; Mg, S.; Mayor, S. Endocytosis Unplugged: Multiple Ways to Enter the Cell. *Cell Res.* **2010**, *20*, 256–275.
30. Gargalovic, P.; Dory, L. Caveolin-1 and Caveolin-2 Expression in Mouse Macrophages. High Density Lipoprotein 3-Stimulated Secretion and a Lack of Significant Subcellular Co-Localization. *J. Biol. Chem.* **2001**, *276*, 26164–26170.
31. Xu, Y.; Krause, A.; Hamai, H.; Harvey, B. G.; Worgall, T. S.; Worgall, S. Proinflammatory Phenotype and Increased

Caveolin-1 in Alveolar Macrophages with Silenced CFTR mRNA. *PLoS One* **2010**, *5*, e11004.
32. Khalil, I. A.; Kogure, K.; Akita, H.; Harashima, H. Uptake Pathways and Subsequent Intracellular Trafficking in Non-viral Gene Delivery. *Pharmacol. Rev.* **2006**, *58*, 32–45.
33. Piasek, A.; Thyberg, J. Effects of Colchicine on Endocytosis of Horseradish Peroxidase by Rat Peritoneal Macrophages. *J Cell Sci.* **1980**, *45*, 59–71.
34. Piasek, A.; Oblakowski, P. Influence of Colchicine and Cytochalasin B on Pinocytosis, Phagocytosis, and Antibody-Dependent Cell-Mediated Cytotoxicity. *Haematol. Blood Transfus.* **1985**, *29*, 511–513.
35. Valberg, P. A.; Brain, J. D.; Kane, D. Effects of Colchicine or Cytochalasin B on Pulmonary Macrophage Endocytosis *in Vivo*. *J. Appl. Physiol.* **1981**, *50*, 621–629.
36. Davies, P. J.; Cornwell, M. M.; Johnson, J. D.; Reggianni, A.; Myers, M.; Murtaugh, M. P. Studies on the Effects of Dansylcadaverine and Related Compounds on Receptor-Mediated Endocytosis in Cultured Cells. *Diabetes Care* **1984**, *7*), 35–41.
37. Cox, D.; Tseng, C. C.; Bjekic, G.; Greenberg, S. A Requirement for Phosphatidylinositol 3-Kinase in Pseudopod Extension. *J. Biol. Chem.* **1999**, *274*, 1240–1247.
38. Araki, N.; Johnson, M. T.; Swanson, J. A. A Role for Phosphoinositide 3-Kinase in the Completion of Macropinocytosis and Phagocytosis by Macrophages. *J. Cell Biol.* **1996**, *135*, 1249–1260.
39. Doherty, G. J.; McMahon, H. T. Mechanisms of Endocytosis. *Annu. Rev. Biochem.* **2009**, *78*, 857–902.
40. Champion, J. A.; Walker, A.; Mitragotri, S. Role of Particle Size in Phagocytosis of Polymeric Microspheres. *Pharm. Res.* **2008**, *25*, 1815–1821.
41. Vacha, R.; Martinez-Veracoechea, F. J.; Frenkel, D. Receptor-Mediated Endocytosis of Nanoparticles of Various Shapes. *Nano Lett.* **2011**, *11*, 5391–5395.
42. Chang, J. T.; Nevins, J. R. Gather: A Systems Approach to Interpreting Genomic Signatures. *Bioinformatics* **2006**, *22*, 2926–2933.
43. Yamamoto, A.; Cremona, M. L.; Rothman, J. E. Autophagy-Mediated Clearance of Huntingtin Aggregates Triggered by the Insulin-Signaling Pathway. *J. Cell Biol.* **2006**, *172*, 719–731.
44. Chang, Y. Y.; Juhasz, G.; Goraksha-Hicks, P.; Arsham, A. M.; Mallin, D. R.; Muller, L. K.; Neufeld, T. P. Nutrient-Dependent Regulation of Autophagy through the Target of Rapamycin Pathway. *Biochem. Soc. Trans.* **2009**, *37*, 232–236.
45. Armour, S. M.; Baur, J. A.; Hsieh, S. N.; Land-Bracha, A.; Thomas, S. M.; Sinclair, D. A. Inhibition of Mammalian S6 Kinase by Resveratrol Suppresses Autophagy. *Aging (Albany NY)* **2009**, *1*, 515–528.
46. Huh, S.; Wiench, J. W.; Yoo, J. C.; Pruski, M.; Lin, V. Organic Functionalization and Morphology Control of Mesoporous Silicas *via* a Co-Condensation Synthesis Method. *Chem. Mater.* **2003**, *15*, 4247–4256.
47. Blaaderen, A.; Vrji, A. Synthesis and Characterization of Colloidal Dispersions of Fluorescent Silica Spheres. *Langmuir* **1992**, *8*, 2921–2931.
48. Daum, N.; Kuehn, A.; Hein, S.; Schaefer, U. F.; Huwer, H.; CM., L. Isolation, Cultivation, and Application of Human Alveolar Epithelial Cells. *Methods Mol. Biol.* **2012**, *806*, 31–42.
49. Hoppstadter, J.; Diesel, B.; Zarbock, R.; Breinig, T.; Monz, D.; Koch, M.; Meyerhans, A.; Gortner, L.; Lehr, C. M.; Huwer, H.; *et al*. Differential Cell Reaction Upon Toll-Like Receptor 4 and 9 Activation in Human Alveolar and Lung Interstitial Macrophages. *Respir. Res.* **2010**, *11*, 124.
50. Zaki, N. M.; Tirelli, N. Gateways for the Intracellular Access of Nanocarriers: A Review of Receptor-Mediated Endocytosis Mechanisms and of Strategies in Receptor Targeting. *Expert Opin. Drug Delivery* **2010**, *7*, 895–913.
51. Feng, S.-z.; Cao, W.-s.; Liao, M. The PI3K/Akt Pathway Is Involved in Early Infection of Some Exogenous Avian Leukosis Viruses. *J. Gen. Virol.* **2011**, *92*, 1688–1697.

CHAPTER 5

PHAGOCYTIC NANOPARTICLE RESPONSE IS PHENOTYPICALLY DEPENDENT

5.1 Introduction

Macrophages play an important role in nanomedicine processing, and are believed to be primarily responsible for uptake and *in vivo* trafficking. For example, increased clinical liposomal chemotherapeutic circulation times correlate with decreased monocyte counts at nadir, which suggests the role of macrophages in nanoparticle processing (1, 2). Macrophages have also shown an *in vivo* retention of approximately 75% of iron oxide nanoparticles administered (3). Finally, *in vitro* macrophage nanoparticle cytokine assays have direct correlation with the *in vivo* success of nanoparticle-based therapeutics (4).

Due to the role of macrophages in nanoparticle processing *in vivo*, macrophage targeting has been harnessed with few clinical examples. Iron oxide particle uptake by macrophages has been utilized to detect inflammatory phenotypes of macrophages both *in vivo* and clinically (3, 5). AmBisome, a lysosomal formulation of amphotericine B, is used clinically as a broad spectrum antifungal. The formulation primarily utilizes toll-like receptors to harness parasitophorous targeting mechanisms within macrophages (6).

Local microenvironmental factors and cues *in vivo* can alter the phenotype and differentiation state of macrophages, which can drastically influence how the cell

interacts with the surrounding environment including nanomaterial processing (7). Most successful clinically targeted macrophage examples are likely targeted specifically towards a classically activated macrophage phenotype (M1). For instance, in the clinical examples listed above M1s are generally up-regulated. However, M1 phenotypes are only one of an unknown number of phenotypes found *in vivo* (8). We lack a full understanding of which macrophage phenotype discovers and uptakes nanoparticle systems. A more complete understanding of this would be valuable in the design of new drug delivery systems, because one could facilitate a higher specificity towards payload targets.

The Th1/Th2 paradigm illustrates different activation states and different macrophage phenotypes, which could help identify the macrophage phenotype that discovers and uptakes nanoparticles (9). M1 macrophages are generally considered janitorial cells, responsible for clearing foreign materials, pathogens and, potentially, nanomaterials. M1 cells are induced by IFN-gamma and are generally characterized by high iNOS, IL-12 release, and high expression of CD80. M1s represent, in general, a Th1 response and, most likely, an inflammatory-mediated response (10). In contrast, a Th2 state generally has an up-regulation of alternatively activated (or M2) cells. M2 cells are considered wound healing cells, inducing basement membrane breakdown, angiogenesis and general tissue repair. These cells are induced by IL-4 and are characterized by high arginase, IL-10 release and high expression of CD206 (10). The Th1/Th2 paradigm is a simplified immunological model system. Many macrophage phenotypes *in vivo* lie in between these two states and may even reside outside of them (8). However, the Th1/Th2 model system does represent the complex *in vivo* biological environment more accurately than traditional unpolarized macrophage models. The model system helps to identify

which macrophage phenotype is responsible for nanoparticle processing and overall biological response. Additionally, this model may help explain whether a specific phenotype is responsible for nanomaterial processing and, if so, whether we can select for specific target phenotypes to harness therapeutic responses.

Evidence suggests variations in nanomaterial properties can alter macrophage uptake and initiate either Th1 or Th2 responses, which appear to be directly dependent on the nanomaterial property. Clinically, environmental exposure to nanomaterials correlates directly to induced autoimmune disorders such as scleroderma and rheumatoid arthritis. These disease states are generally classified as a Th1 response, suggesting the involvement of M1 phenotypes (11). In line with these findings, silica and titanium nanoparticles have been shown to induce M1 phenotypes *in vivo*, significantly regulating inflammatory mechanisms (12, 13). However, a recent study revealed that alternatively activated macrophage M2 phenotypes *in vitro* and *in vivo* took up 300nm PRINT™ nanoparticles to a higher extent than M1 phenotypes (14). In contrast, 200-600nm poly(lactic acid) particles induced a Th1 response while 2-8μm particles showed a Th2 response (15). Poly(lactic-co-glycolic) acid (PLGA) nanoparticles showed a Th1 response even after priming *in vivo* for a Th2 response (16). Interestingly, environmental exposure to crystalline silica has also been linked to silicosis, a disease characterized by fibrosis and a general Th2 response (17). Injection of silica has also shown increased levels of IgG2a and IgE within serum indicating increased presence of antibodies (18). The increased presence of antibodies suggests the adjuvant properties of these systems, an M2 mediated-response. However, research has shown an inability to induce an M2 activation state after macrophage incubation with SPIO (superparamagnetic iron oxide)

particles and, to a limited degree, this effect is observed with silica (19). In general, evidence suggests nanoparticle characteristics and testing environments can drastically affect the uptake and response within macrophage systems.

Direct correlations between nanoparticle surface modifications have altered macrophages responses, specifically with varied phenotypic uptake. Surface modification of iron oxide particles with CD86 and CD206 shows targeting of M1 and M2 macrophages, respectively (20). This modification and uptake shows nanoparticle characteristics can be altered to target specific macrophage phenotypes, which could be used in therapeutic applications. Surface alterations may also help explain the wide variations in reported literature in the systemic immunological response of nanoparticle systems. Surface properties may help to induce specific uptake and internalization.

A correlation should be drawn between variations in nanomaterial properties and how these properties interact with the biological environment to induce either a Th1 or Th2 response. We believe that stober silica nanoparticle systems, a commonly used pre-clinical nanomedical agent, interact with the biological environment and initiate an M1 phenotypic response *in vitro* and *in vivo*. Macrophage phenotype expression is dependent on disease state; understanding the phenotype that specific nanomaterial characteristics target will help to derive a better functional design platform for drug delivery systems.

5.2 Materials and Methods

5.2.1 Particle synthesis and characterization

Spherical silica nanoparticles were prepared by previously reported modified Stöber methods (21, 22). All particles were fluorescently labeled with fluorescein

isothiocyanate (FITC) to assess cellular uptake. The constructs were sterilized by dry autoclaving. Transmission electron microscopy (TEM) images were taken on a Phillips, TECHAI F2 (Hillsboro, OR) at an accelerating voltage of 80 kV. TEM samples were created by evaporating droplets of particles suspended in deionized water off copper grids. After micrograph collection, nanoconstruct size was measured utilizing Adobe Photoshop's pixilation ruler measurement tool (Adobe, San Jose, CA). At minimum the sizes of 300 particles of each type were measured. Particle zeta potential of SNPs dispersed in DI water at a concentration of 1.0 mg/ml was measured using a Malvern Instruments Zetasizer Nano ZS (Westborough, MA). SNPs (50 or 25 mg/ml) were sonicated, vortexed and the final particle dispersions were prepared immediately before use from common stock in culture medium and vortexed before application to the culture cells. All particles were tested for endotoxin levels prior to cellular incubation; levels were below FDA recommended .05 EU/mL.

5.2.2 *In vitro* methods

5.2.2.1 Cell culture

RAW 264.7 murine macrophages were obtained from ATCC (Manassas, Virginia) and maintained in RPMI media supplemented with 10% FBS, at passage numbers 5-25. Cell cultures were incubated at 37°C in 5% CO2 and 95% humidified air and kept in logarithmic phase of growth throughout all experiments, never reaching full confluency.

5.2.2.2 Cell polarization and confirmation

Cells were seeded and allowed to adhere overnight at 37°C in 5% CO2. The following day the cells were treated with a M1 cocktail that consisted of LPS (100ng/mL) and IFN-gamma (300 units/mL), a M2 cocktail of IL-4 (10 units/mL) or an unpolarized cocktail with no additives (Sigma-Aldrich, St. Louis, MO). All cocktails were diluted in fresh media. The cells were incubated for 18 hours to obtain sufficient polarization. To confirm polarization, IL-10 and IL-12 were quantified via BD Cytokine Flow Cytometry protocol and colormetrically for arginase and nitric oxide (described below).

5.2.2.3 Arginase and nitric oxide evaluation

Following cellular polarization in 96 well plates, cells were treated for 24 hours with a range of silica nanoparticle concentrations (5-250 ug/mL). The colorimetric protocols of Classen et al. for the Griess reagent (detection of nitric oxide) and a urea assay (detection of arginase) were followed (23).

5.2.2.4 Cellular proliferation

Following polarization, cells were exposed to a range of concentrations (5-250 ug/mL) of silica nanoparticles for 72 hours. Relative cell viability was assessed by utilizing a water-soluble tetrazolium salt, WST-8 [2-(2-methoxy-4-nitrophenyl)-3-(4-nitrophenyl)-5-(2,4-disulfophenyl)-2H-tetrazolium, monosodium salt], the key component in the Cell Counting Kit-8 from Dojindo Molecular Technologies, Inc. (Rockville, Maryland).

5.2.2.5 Cell uptake, visualization and quantification

The uptake of silica nanoparticles by cultured cells was visualized by confocal microscopy. Cells were grown on 24 well imaging plates at a density of ~9000 cells/cm^2 polarized and incubated for 24 hours with 37.5 μg/ml FITC labeled silica nanoconstructs. After incubation, cells were fixed with 4% formalin in PBS. Cell nuclei were stained with 2.5 μM 4′,6-diamidino-2-phenylindole (DAPI) according to the manufacturer's protocol. (CLSM) Olympus FluoView® FV1000 (Olympus America Corp., Center Valley, PA). The intensity of the laser beam and the photodetector sensitivity were kept constant in order to compare the relative fluorescence intensities between experiments. Z stacks were collected and used for 3D reconstruction and visualization of intracellular particle localization. All image acquisitions and analyses were performed using FluoView 2.0 software.

Flow cytometry was used to quantify the amount of nanoparticle uptake. Cells were grown on 12 well plates at a density of ~15,000 cells/cm^2 polarized and incubated with 37.5 μg/ml FITC labeled silica nanoconstructs for 24 hours. Following incubation, cells were scraped to obtain a single cell suspension. Cells were suspended in PBS containing 1% BSA and analysis was performed on a FACSCalibur (BD Biosciences). Emitted light resulting from FITC-labeled nanoparticles was detected by the FL-2 detector. To calculate the background fluorescence of unlabeled cells, cells without any addition of nanoparticles were carried along as a negative control in every measurement. For whole-cell analysis 10,000 cells were counted. Data analysis was performed with BD CellQuest Pro (BD Biosciences).

5.2.2.6 Cellular autophagy

Coverslips were seeded at a density of ~9000 cells/cm^2, polarized with polarization cocktails for 24 hours. Following polarization cells were incubated for 24 hours with 37.5 μg/ml FITC labeled silica nanoconstructs. After incubation cells were fixed, permeabilized via triton-X and stained intracellularly for LC3-IIb (Molecular Probes). Both colocalization and cellular internalization were visualized with confocal microscopy.

5.2.2.7 Cellular co-localization

Six well plates were seeded at a density of ~9000 cells/cm^2 and polarized to either M1 or M2 phenotypes. Following polarization, wells were scraped, 1 well containing M1 polarized cells and 1 well containing M2 polarized cells were seeded on glass coverslips and allowed to adhere overnight. Prior to scrapping M1 cells were preincubated with DiD (M1) to mark the phenotype and M2 cells were left unstained (Molecular Probes). Following adhesion these co-cultures were treated for 24 hours with 37.5 μg/ml FITC labeled silica nanoconstructs. After incubation cells were fixed, and stained with DAPI. Cellular internalization was visualized with confocal microscopy.

5.2.2.8 Transmission electron microscopy

The uptake of silica constructs by cultured cells was assessed by transmission electron microscopy. Cells were seeded on 6 well plates containing 1x1 cm ACLAR plastic at a density of ~9000 cells/cm^2, polarized and after an overnight incubation, 37.5 μg/mL of silica nanoconstructs were added. Subsequently, cells were incubated for 24

hours after which they were washed with PBS and fixed with a 2.5% glutaraldehyde and 1% formaldehyde in 0.1M sodium cacodylate buffer with sucrose and calcium chloride. Cells were stained with uranyl acetate for 45 minutes at room temperature and TEM images were taken with a Phillips, TECHAI F2 TEM (Hillsboro, OR, USA) at an accelerating voltage of 80 kV.

5.2.3 *In vivo* methods

5.2.3.1 Animal handing

All animal experiments were performed in accordance with the Institutional Animal Care and Use Committee (IACUC) guidelines of The University of Utah. Adult female CD-1 mouse injections were administered via the tail vein at 20 mg/kg of hydroxyl nanoparticle formulations with a max injection volume of 200 ul. Saline administration was used as a negative control. Mice were sacrificed at one- and four-week time points and organs analyzed. N=5 for all studies.

5.2.3.2 Biodistribution and clearance

At necropsy, organs were collected, isolated and weighed. Organs subsequently underwent acid digestion with aqua regia at 80 C. Following complete organic digestion, the solution was suspended in 5% trace metal-grade nitric acid and HF was added to the solution to dissolve and stabilize the silica content. This solution was analyzed via inductively coupled plasma mass spectrometry (ICP-MS), and quantified against a silica and internal standard. Urine and fecal matter was pooled to assess the total silica content.

5.2.3.3 Histology

Following necropsy organs were fixed in 4% fresh paraformaldehyde. Samples were dehydrated, paraffin-embedded and cut into 4μm thick sections. Sections were stained hematoxylin and eosin. Immunohistochemical staining was performed on air-dried room temperature sections, placed in a 60 C oven to melt the paraffin. Sections were deparaffinized with EZ Prep solution (Ventana Medical Systems). In the case of iNOS and Arginase sections were pretreated with CC1 (Cell Conditioner 1, pH 8.0) and F4/80 was digested with Protease 2. Primary antibodies were applied (iNOS: 1:50 for 2 hours, Arginase 1:800 for 1 hour, F4/80 1:200 for 2 hours) (Thermo Scientific and Abcam). Slides were detected using the IView DAB detection kit (Ventana Medical Systems), which is a Streptavidin-HRP system, utilizing DAB (3-3' diaminobenzidine) as the chromogen and counterstained with hematoxylin. Sections were washed with DI water, dipped in iodine followed by sodium thiosulfate and dehydrated in graded alcohols cleared with xylene and coverslipped. Immunofluorescence was similarly performed with primary antibody incubation (C68 1:100 for 2hours, CD206 1:50 for 2 hours, LC3-IIb 1:100 for 1 hour) and subsequent secondary detection (Alexa Fluor 647) (Molecular Probes).

Immunofluorescence was imaged on an Olympus 1×50 inverted microscope. Quantification and visualization were performed utilizing an ImageJ plug-in described elsewhere. Immunohistochemical staining was visualized utilizing an Aperio slide scanner. Quantification and visualization were performed utilizing Aperio ScanScope software.

5.2.3.4 Transmission electron microscopy

The uptake of silica constructs within organs was assessed by transmission electron microscopy. Organs were fixed with a 2.5% glutaraldehyde and 1% formaldehyde in 0.1M sodium cacodylate buffer with sucrose and calcium chloride. Cells were stained with uranyl acetate for 45 minutes at room temperature and TEM images were taken with a Phillips, TECHAI F2 TEM (Hillsboro, OR, USA) at an accelerating voltage of 80 kV.

5.3 Results

5.3.1 Silica nanoparticle synthesis and characterization

FITC-labeled silica nanoparticles 130nm in diameter were synthesized and characterized via DLS, zeta potential, IR and TGA (Table 5.1). Characterization of particle stability in serum was assessed and confirmed that nanoparticles were in suspension. After verification of synthesis and stability, the particles were utilized to investigate the influence of uptake in M1 and M2 polarized macrophages *in vitro* and *in vivo*.

5.3.2 Polarization of M1 and M2 macrophages *in vitro*

RAW 264.7 macrophages were polarized to M1 and M2 phenotypes utilizing traditional cytokine cocktails, IFN-gamma/LPS and IL-4, respectively (Figure 2.1). M1 polarized macrophages exhibited expected morphological changes such as enhanced intracellular vacuoles and 5x increase in size when compared to M2 cells which exhibited very little to no vacuolization and spindle like morphology (Figure 5.1a). Additionally,

Table 5.1. Characterization of silica nanoparticles.

Nanoconstruct	Particle Distance (TEM)	Size (TEM)	Size (DLS)	Zeta Potential	Zeta Potential in Media Containing Serum
Hydroxyl	130.67+/-14.05 nm	130+/-12 nm	158 +/-15 nm	-38.5 +/-4.8 mV	180 +/- 88mV

Hydroxyl Image Characterization	
TEM	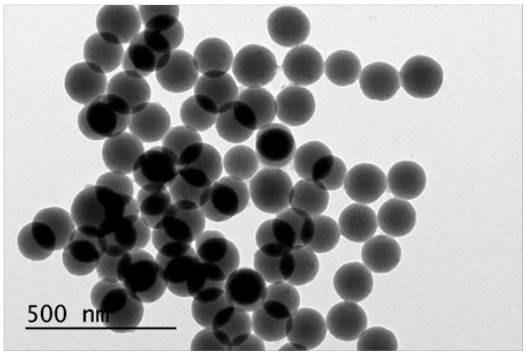
IR	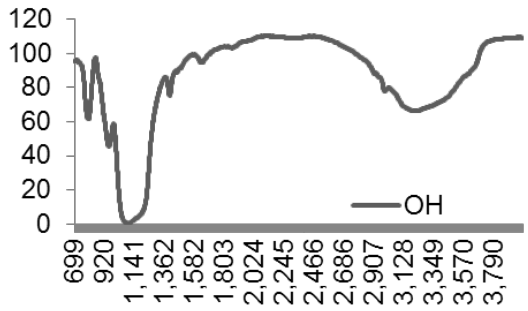
TGA	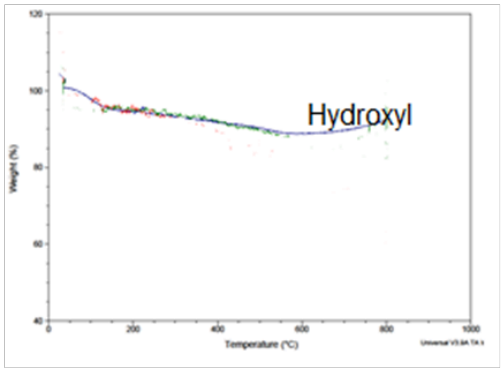

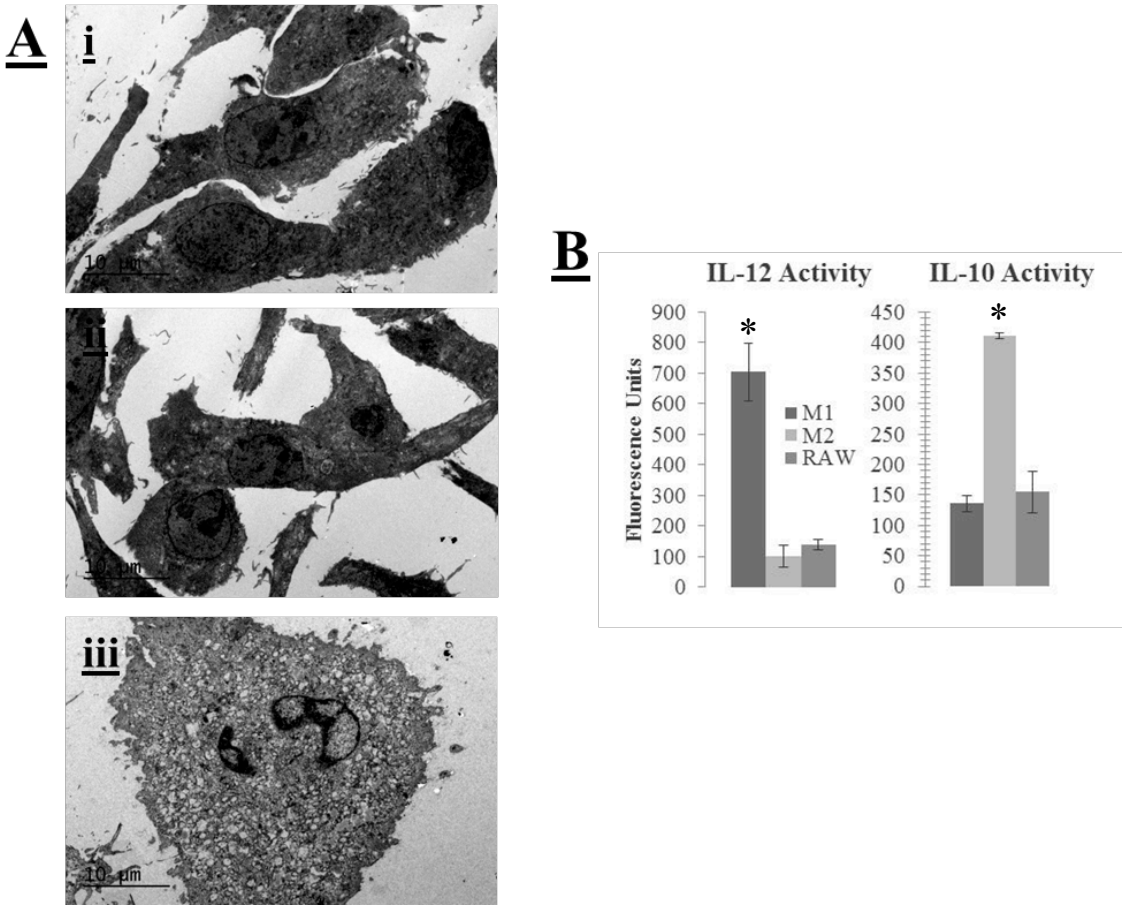

Figure 5.1. Confirmation of macrophage polarization. Macrophages were polarized into M1 and M2 phenotypes and this polarization was confirmed morphologically and by cytokine excretions. A) i) TEM images of the morphology of unpolarized macrophages. ii) TEM image of the morphology of M2 polarized macrophages. M2s retains a similar size to unpolarized macrophages with a spindle like morphology. iii) TEM image of the morphology of M1 polarized macrophages. M1s increase drastically in size (~2-5x) and has a drastic increase in vacuoles. B) Confirmation of hallmark M1 and M2 cytokines show a statistical significant increase in IL-12 in M1s and IL-10 in M2s when compared to their unpolarized and oppositely polarized counterparts, as expected. Statistical difference from control determined via paired t-test, p value < .05 are indicated by a *, p values > .05 were determined insignificant.

iNOS and IL-12 were present in M1 polarization states and absent in M2. M2 states exhibited arginase and IL-10 but these cytokines were absent in M1 polarization (Figure 5.1b and Figure 5.2b,c). The cytokine and morphological results confirmed RAW 264.7 polarization into M1 and M2 phenotypes. The confirmed polarized macrophages were utilized in *in vitro* testing.

Nanoparticles were incubated with unpolarized RAW 264.7 cells, M1, and M2 polarization states for 72 hours (~2 population doubling times) to assess the relative influence of nanoparticle treatment on overall function and proliferation capacity. Nanoparticle solutions affected proliferation status in M2 and unpolarized cells, with higher concentrations exhibiting more pronounced toxicity (Figure 5.2a). The nanoparticle concentrations tested did not appear to affect M1 proliferation.

We observed little to no effect on hallmark M1 and M2 markers, iNOS and arginase, after nanoparticle treatment at a variety of concentrations (Figure 5.2b and 5.2c).

In an attempt to understand proliferative effects, we sought to investigate and quantify the degree of nanoparticle uptake within these polarization states. As such, nanoparticles were incubated with M1, M2 and unpolarized macrophages, and the relative level of uptake was assessed and quantified via FACS, and confirmed via confocal microscopy (Figure 5.3 and 5.4). Nanoparticles were taken up to a greater extent in M1 macrophages when compared to M2 and unpolarized macrophage phenotypes. In order to compensate for potential data aberrations related to the significantly different cell size between M1 and M2 cells (40um vs. 10um, respectively), we normalized the FACS analysis to the size of each cell type, and still saw a statistical

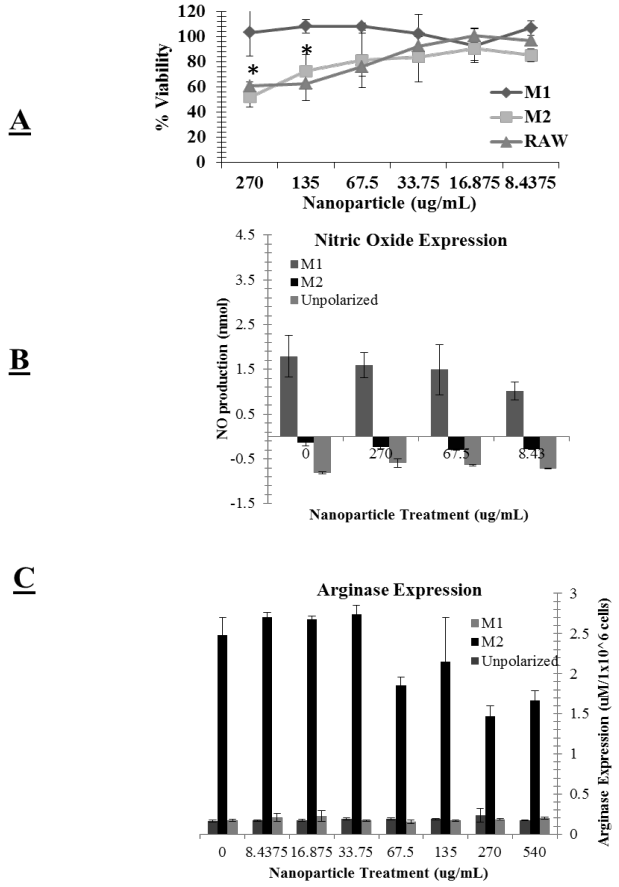

Figure 5.2. Macrophage viability and cytokine excretion after nanoparticle treatment. A) Macrophage viability following nanoparticle treatment. Unpolarized and M2 cells showed a statistically significant decreased viability with increasing nanoparticle concentration. M1 cells however appeared to be statistically unaffected by nanoparticle treatment. B) iNOS did not appear to be significantly affected by any nanoparticle treatment. M1 cells exhibited a statistically significant higher native expression, as expected. C) Arginase activity was not significantly affected by nanoparticle treatment. M2 cells exhibited a statistically significant higher native expression, as expected. Statistical difference from control determined via paired t-test, p value < .05 indicated with a *, p values > .05 were determined insignificant.

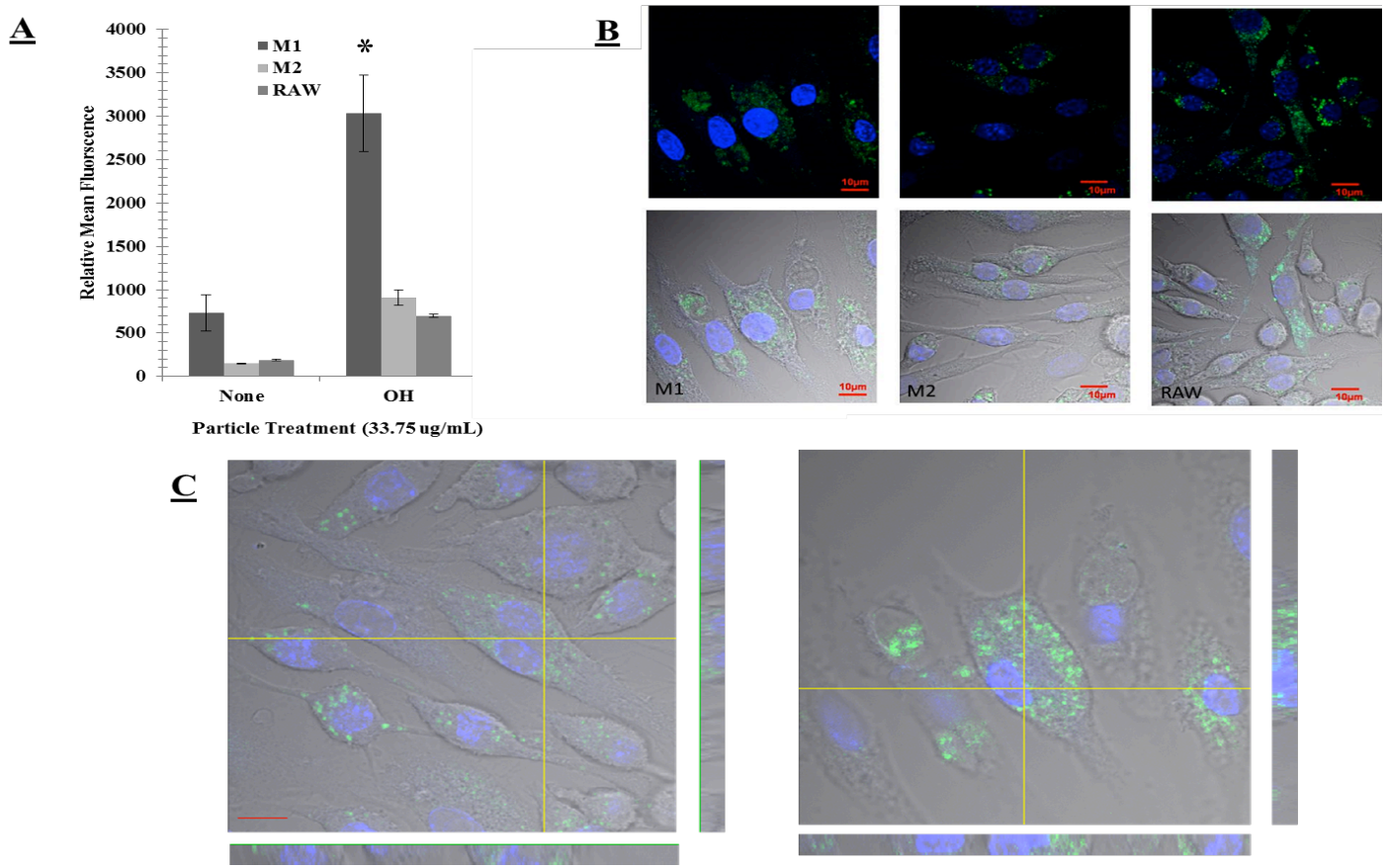

Figure 5.3. Uptake of nanoparticles in macrophages. A) Uptake of nanoparticles in different macrophage polarization states via FACS. M1 macrophages took up nanoparticles to the highest extent, statistically significant increase in uptake was shown. Statistical difference from control determined via paired t-test, p value < .05 indicated with a *, p values > .05 were determined insignificant. B) Confocal images confirming FACs analysis of nanoparticle uptake in polarized macrophages, with the highest degree of uptake in M1 cells. C) Z-stack images of cells showing internalization and not cellular surface association of particles.

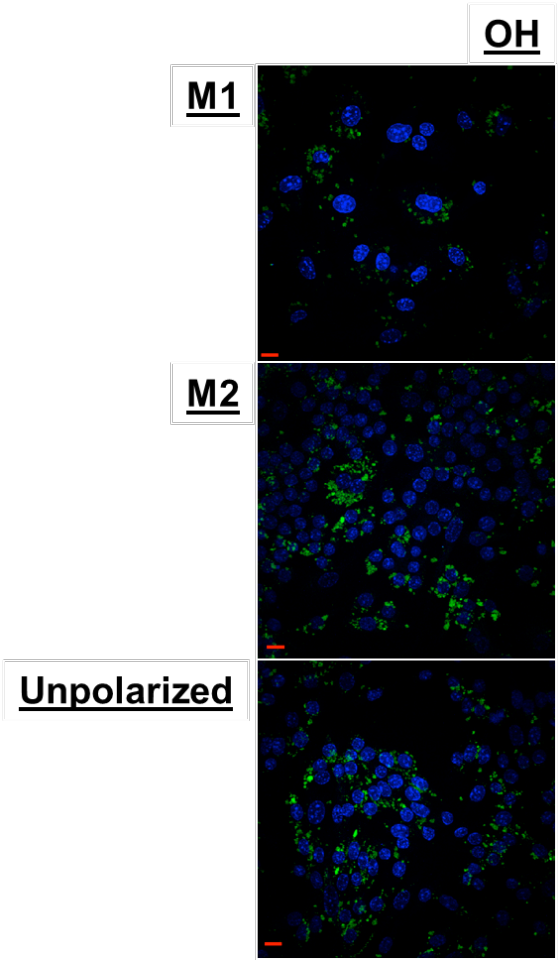

Figure 5.4. A more representative confocal image of nanoparticle uptake in polarized macrophages. Highest degree of uptake is in seen in M1 cells.

increase in overall uptake.

The conflicting uptake and proliferation results led us to ask if internalization mechanisms within these polarization states were altered. To visualize nanoparticle localization within polarization states, TEM images were taken of macrophages incubated with nanoparticles (Figure 5.5). A large accumulation of nanoparticles was observed in the vacuoles of M1 macrophages. Very few vacuoles were observed in M2 cells, and the vacuoles displayed reduced nanoparticle association and vesicular definition. Similar results to M2 macrophages were observed for unpolarized cells.

Mechanisms of particle intracellular fate were investigated in macropahges. We previously identified intracellular fate, consistent with autophagic activity after treatment with amine modified particles in unpolarized cells (24). We investigated whether similar internalization was observed in M1 and M2 polarized cells. A high upregulation of autophagic activity in M2 and unpolarized macrophages was observed (Figure 5.5, 5.6). M1 cells exhibited little to no autophagy in any treatment group.

M1 cells have a higher affinity for nanoparticles in isolated culture; however, *in vivo* polarization states are mixed and an investigation with a co-culture may mimic *in vivo* environments better. We investigated if both macrophages were cultured together whether an affinity for one macrophage over the other would still be present. We observed an increase in particle accumulation in M1 macrophages (Figure 5.7).

5.3.3 *In vivo* nanoparticle effect

After observing an increase in nanoparticle uptake in M1 macrophages in both isolated and co-culture systems, we investigated if we could correlate this *in vitro* effect

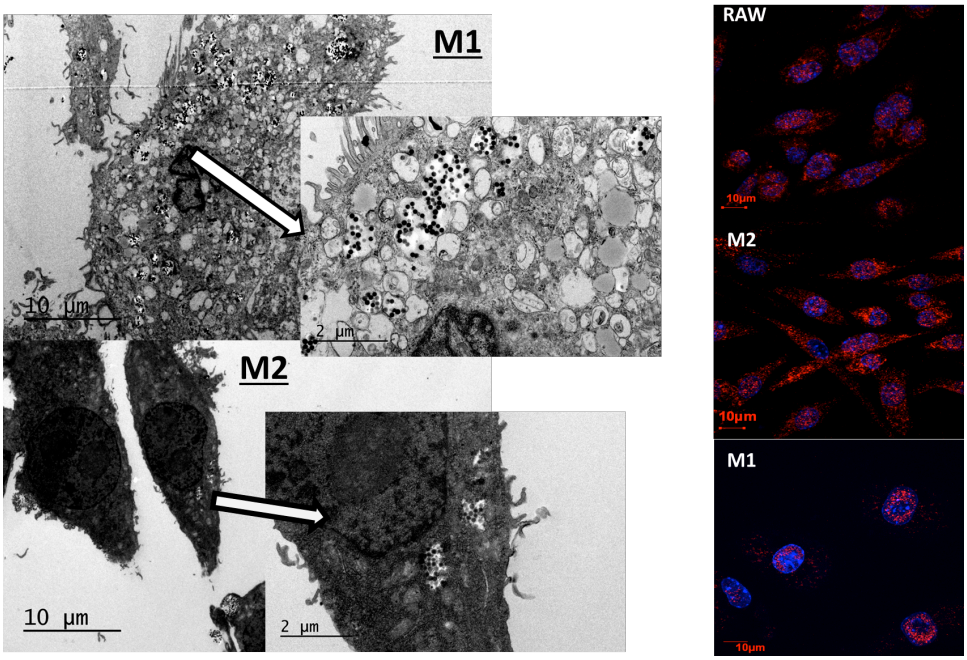

Figure 5.5. Morphological features of macrophages after nanoparticle treatment. Autophagy is observed within macrophage populations after nanoparticle treatment. Left) TEM images of nanoparticle uptake in M1 and M2 cells. Nanoparticles resided within increased vacuolization in M1 cells. M2 cells appeared to have less uptake and decreased vacuolization. Right) Levels of autophagic activation after nanoparticle treatment in polarized macrophage cells. M2 and unpolarized cells had drastic increases in autophagy, while M1 cells only showed a slight increase, suggesting differing internalization and intracellular fate of nanoparticles within different macrophage polarization states.

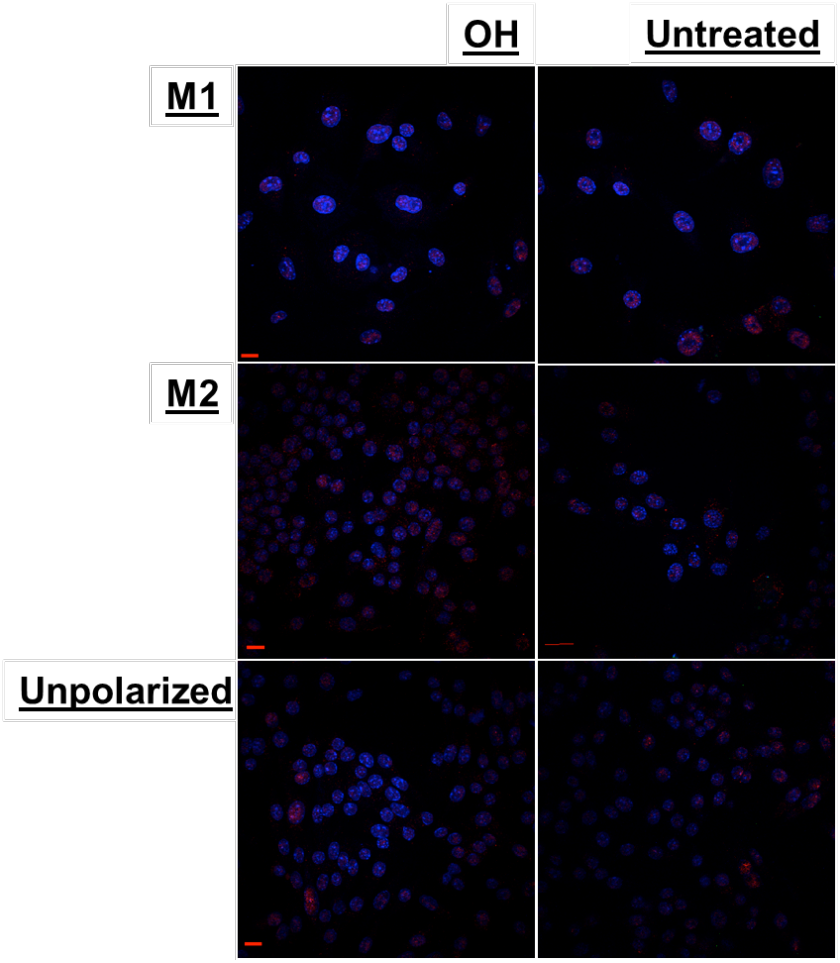

Figure 5.6. Confocal images of induction of autophagy after nanoparticle treatment. High amounts of autophagy were observed in M2 and unpolarized cells when compared to control and M1 cells. Staining is observed in the perinuclear region which may give the nucleus the appearance of localized stain. However it may also be concentrated within that region due to nonspecific staining.

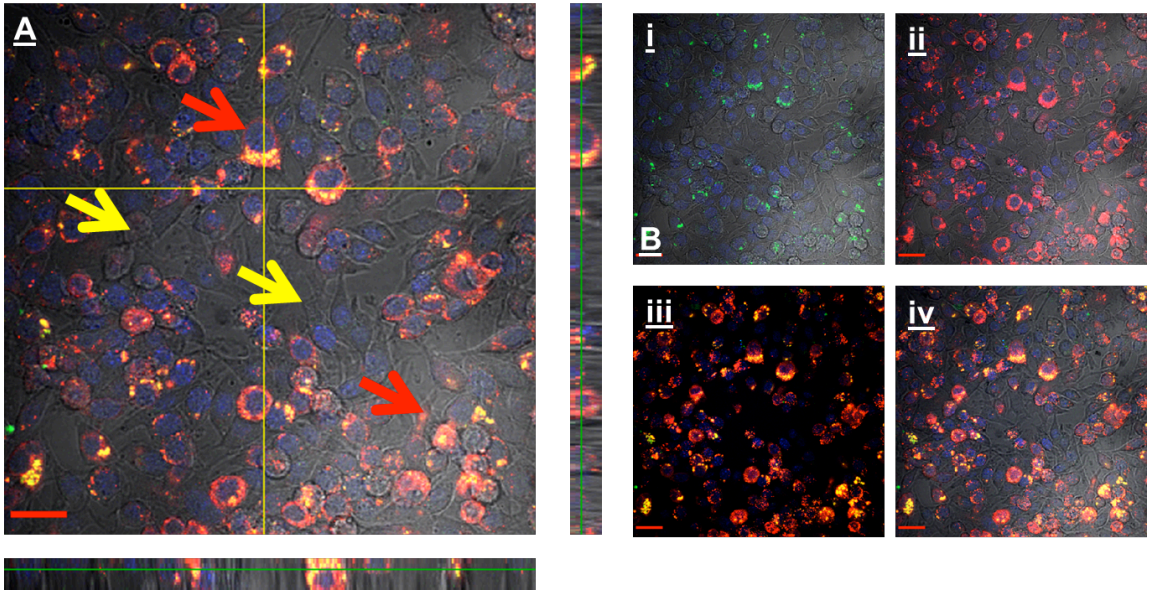

Figure 5.7 Co-culture of M1 and M2 macrophages. A) Z stack representing the uptake of hydroxyl nanoparticles within a co-culture of M1 and M2 cells. Red arrows: Nanoparticles (green) are nearly always co-localized (yellow) with M1 cells (red), providing evidence for M1 affinity towards nanoparticle uptake. Yellow arrows: Cells that are unlabeled represent an M2 phenotype, these cells appear to avoid nanoparticle uptake. B) For clarification dyes are separated out to help visualization. i) Nanoparticle label ii) M1 macrophage label iii) colocalization of M1 and nanoparticle label without DIC iv) DIC and co-localization.

with an *in vivo* system. Adult CD-1 mice were injected with each nanoparticle formulation, and the effects of these systems after 1 and 4 weeks were observed. As expected with nondegradable nanoparticle systems, we observed high accumulation in the liver and spleen and very little association with other organs (Figure 5.8). While uptake and residence of nanoparticles were significantly increased within the liver and spleen, animals did not have any weight loss or gain over time compared to control animals, suggesting minimal toxic effects of these systems (Figure 5.9).

Following these observations, we wanted to see if accumulation and residence of these nanoparticles within the spleen or liver caused any great duress on the tissue. H&E staining did not show toxicity (Figure 5.10); however, slight variations in cell content and morphology within the spleen and liver were observed. The spleen showed a slight but not significant increase in inflammatory cells, formation of multinucleated cells, and very slight destruction of lymphatic foci from 1 to 4 weeks (Figure 5.11). The liver showed a slight but not significant increase in hydropic degeneration or vacuolization and increased levels of inflammatory cells from 1 to 4 weeks (Figure 5.12). Overall, we observed little to no toxicity or induced inflammation *in vivo* after nanoparticle treatment.

The observation of a slight increase in inflammatory mediated cells in H&E staining led us to investigate the potential of increased levels of macrophages over time within these tissues. We observed a drastic increase in CD68 expression, a lysosomal marker within the liver from 1 to 4 weeks, suggesting the increase in residence of macrophages with lysosomal-like compartments (Figure 5.13).

Confirmation of increased macrophage residence and identification of the phenotype of the up-regulated *in vivo* macrophage population was performed through

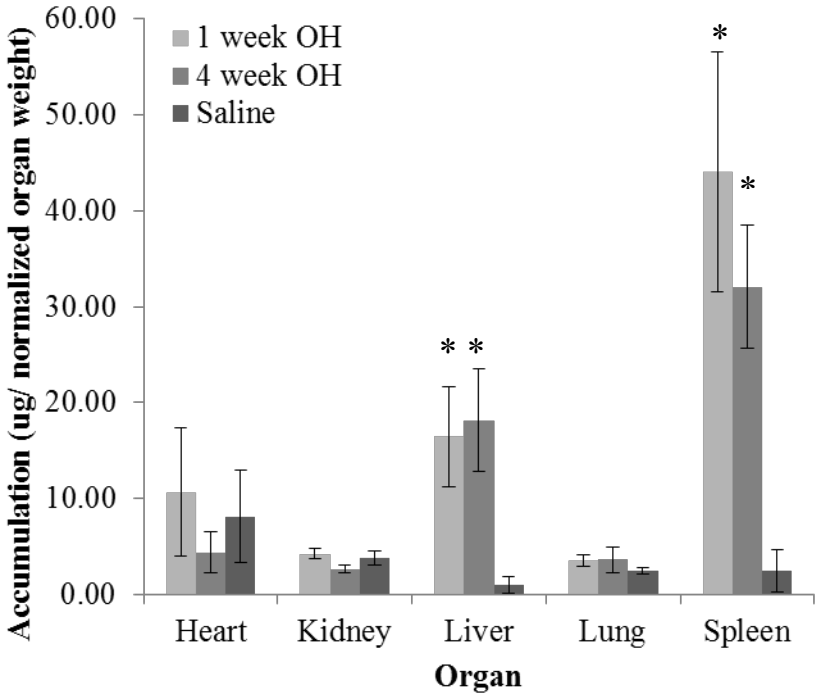

Figure 5.8 Silica nanoparticle organ accumulation, as determined via quantitative ICP-MS. Data have been normalized to organ weight to account for aberrations, and additionally were also normalized to brain weight and no observable differences occurred. We observed accumulation of silica nanoparticles primarily in splenic and hepatic tissues, with minimal accumulation in other organs. Silica was retained within these organs at statistically similar levels out to 4 week time points. Statistical difference from control determined via paired t-test, p value < .05 indicated with a *, p values > .05 were determined insignificant.

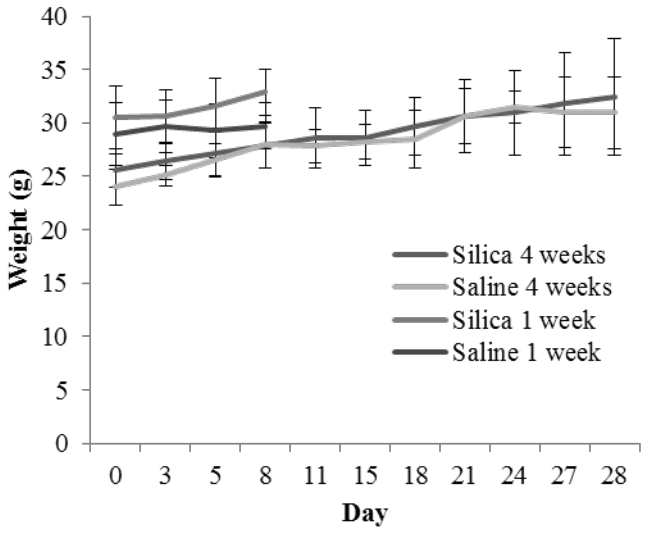

Figure 5.9. Animal weights as a function of silica nanoparticle treatment and time. Little to no change in overall animal weight was observed across groups when compared to saline control, suggesting minimal toxic effects due to silica treatment. Statistical difference from control determined via paired t-test, p value < .05, p values > .05 were determined insignificant.

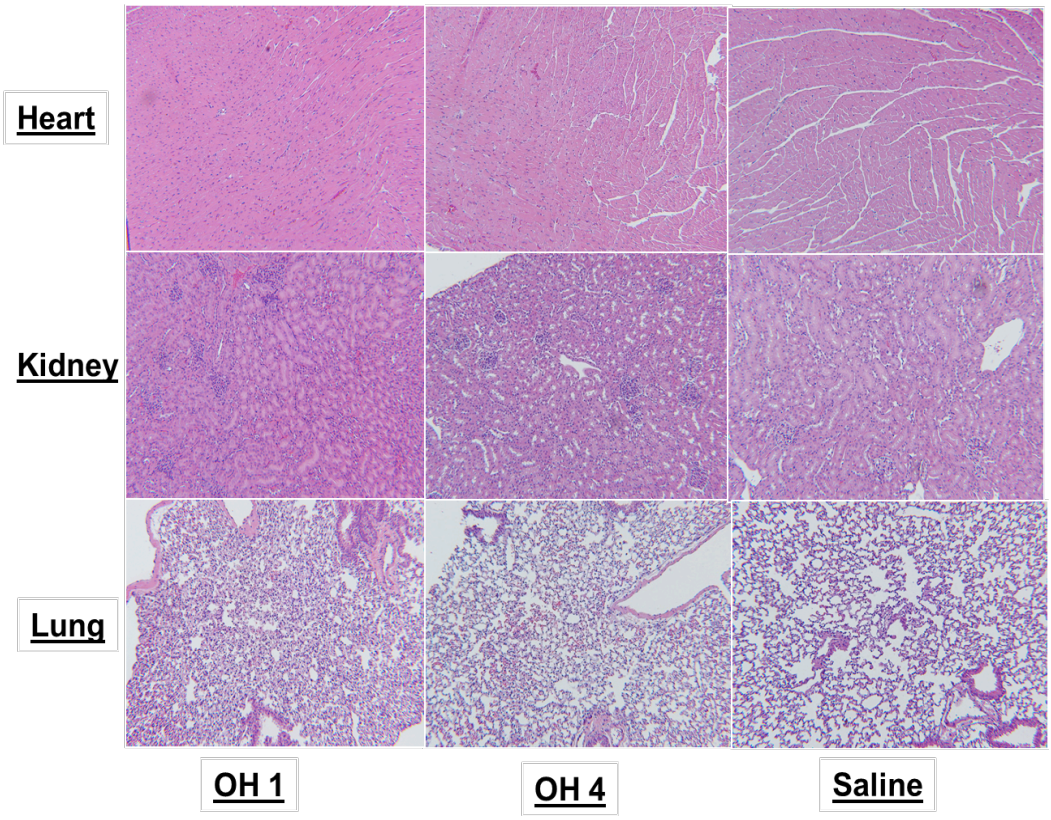

Figure 5.10 H&E images of heart (top), kidney (middle) and lung (bottom) tissues of animals treated with silica nanoparticles at 1 and 4 weeks. Tissue exhibited no response to silica treatment, suggesting limited toxicity within these organs as a function of silica nanoparticle treatment.

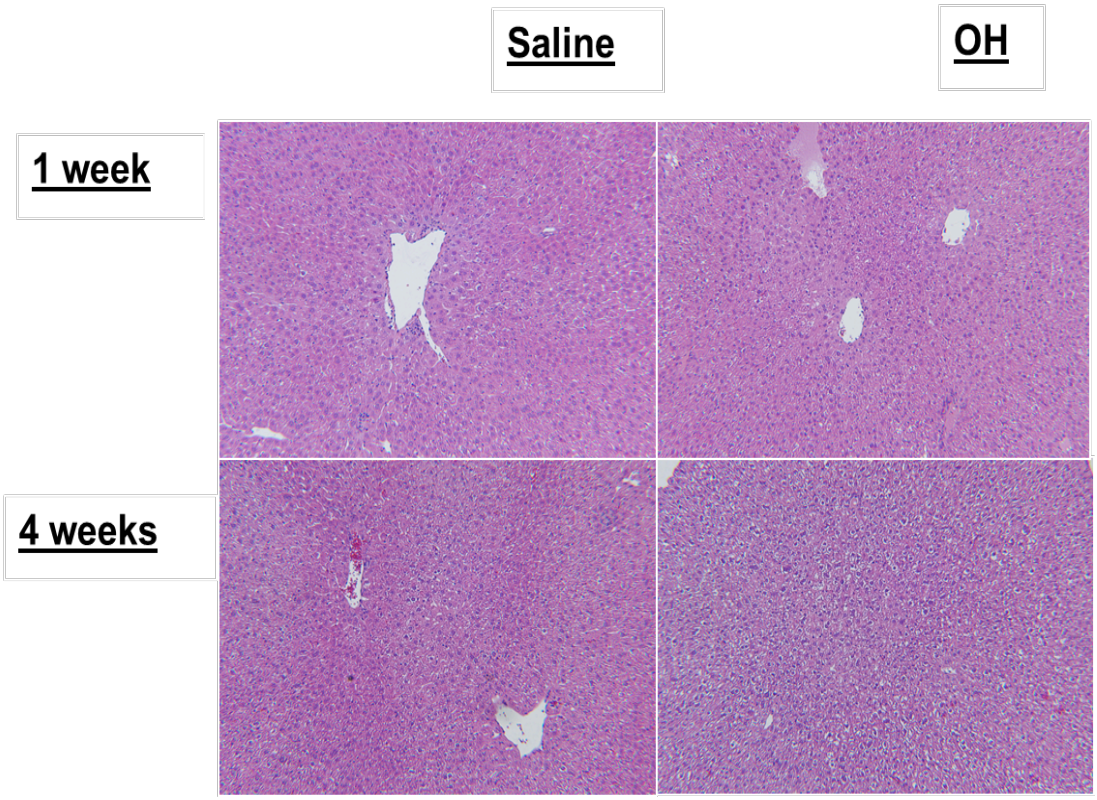

Figure 5.11 H&E images of liver tissue of animals treated with silica nanoparticles at 1 and 4 weeks. Increased levels of vacuolization (increased white space) are present in the liver at both 1 and 4 weeks. However, overall inflammatory effects are minimal as a result of silica nanoparticle treatment.

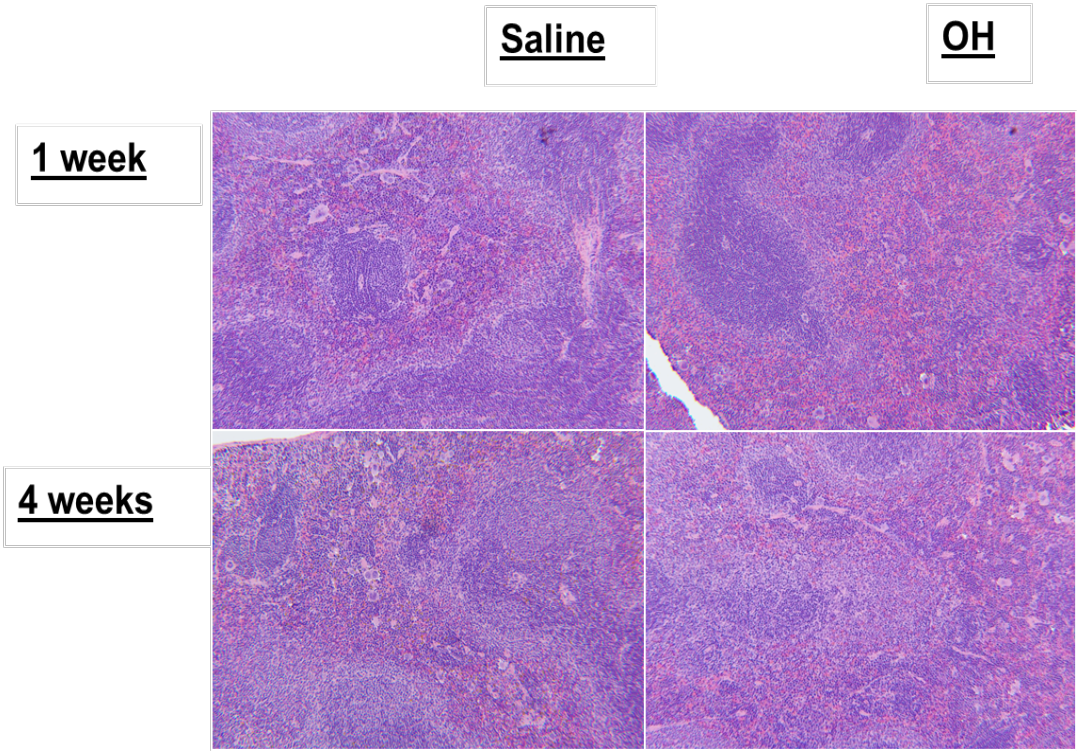

Figure 5.12 H&E images of spleen tissue of animals treated with silica nanoparticles at 1 and 4 weeks. Increased levels of macrophages and multinucleated cells are present in the spleen at both 1 and 4 weeks. However, overall inflammatory effects are minimal, as a function of silica nanoparticle treatment.

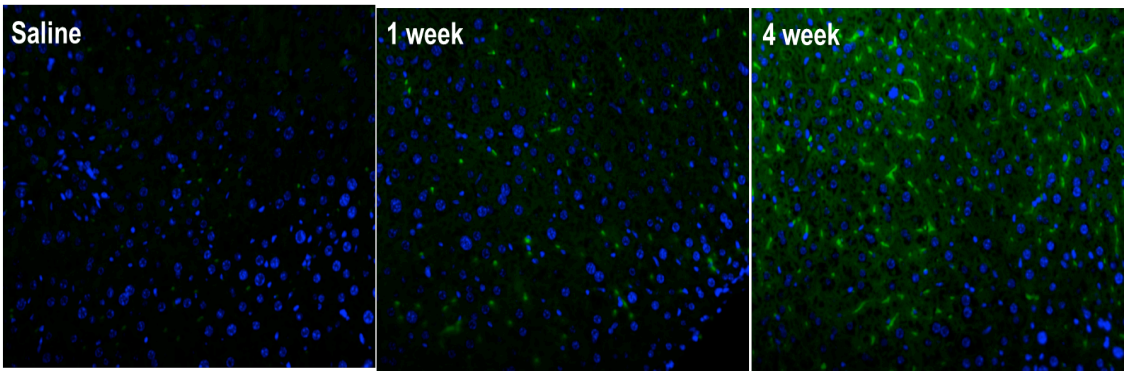

Figure 5.13 Immunofluorescence of liver tissues stained with CD68. CD68 is a lysosomal marker that is useful in identification of increased levels of macrophages. This image suggests that we have a drastic increase or recruitment of macrophages within the liver at 4 weeks.

tissue staining with F4/80 (an M1 marker), iNOS (an M1 marker) and arginase (an M2 marker). We observed an upregulation of F4/80 and iNOS in the liver and spleen (Figure 5.14 and Figure 5.15). These M1 markers were patchy; staining was not uniform throughout the tissue. To quantify the level of upregulation a complete organ slide scan and colorimetric deconvolution were performed, increased F4/80 and iNOS were observed in liver tissues. Increases in these M1 markers suggest that M1 macrophages play an important role in the response to these nanoparticle systems. We observed no upregulation in arginase (Figure 5.16) in any tissue. CD206 (M2 marker) and autophagic markers were also utilized, and we observed little to no overall increase in staining (data not shown).

We sought to determine whether M1 macrophage upregulation was a result of recruitment as a reaction to nanoparticle residence or if proliferation of macrophages was a direct result of macrophage uptake of nanoparticles. We performed TEM on liver and spleen tissues (Figure 5.17) and observed macrophage nanoparticle uptake in both organs.

5.4 Discussion

5.4.1 Polarization of M1 and M2 macrophages *in vitro*

M1 cells appear to show minimal toxic effects when treated with nanoparticles, even at very high concentrations. M1 cells also uptake nanoparticles to the greatest degree, despite showing the lowest toxicity. This may suggest that polarizing cells to an M1 state induces a coping mechanism, for foreign matter, which helps the cell to avoid interference with the rest of the cellular machinery and phenotypic state. This may be due to TLR4 induction as a result of treatment with LPS during the polarization protocol, as

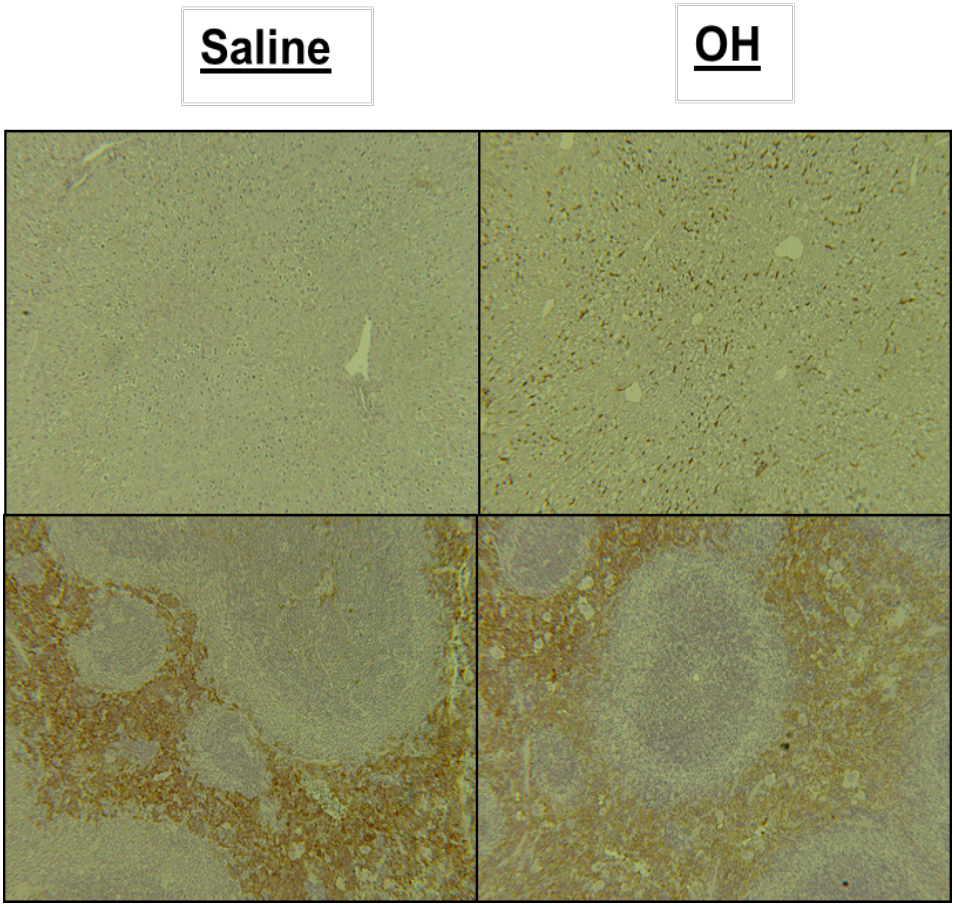

Figure 5.14 Liver and splenic tissues stained for F4/80. An observable increase is shown in treatment groups of the F4/80 stain. This is a macrophage marker stain suggesting an increase in the local recruitment of macrophages within these tissues.

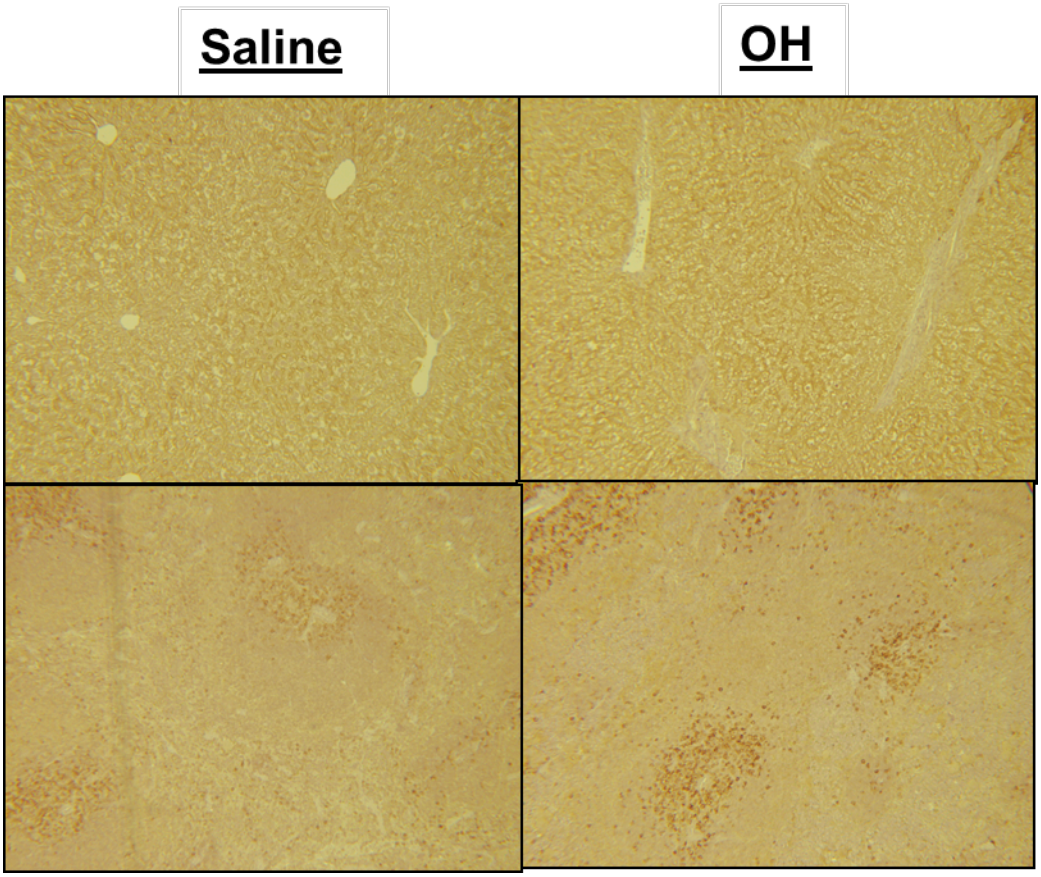

Figure 5.15 Liver and splenic tissues stained for iNOS. An observable increase is shown in treatment groups. This is a marker for M1 macrophages, and may suggest increased levels of macrophages present in the tissue, as observed via CD68 and F4/80 are M1 macrophages. However iNOS is present in other cell types and could be a function of their release, as well.

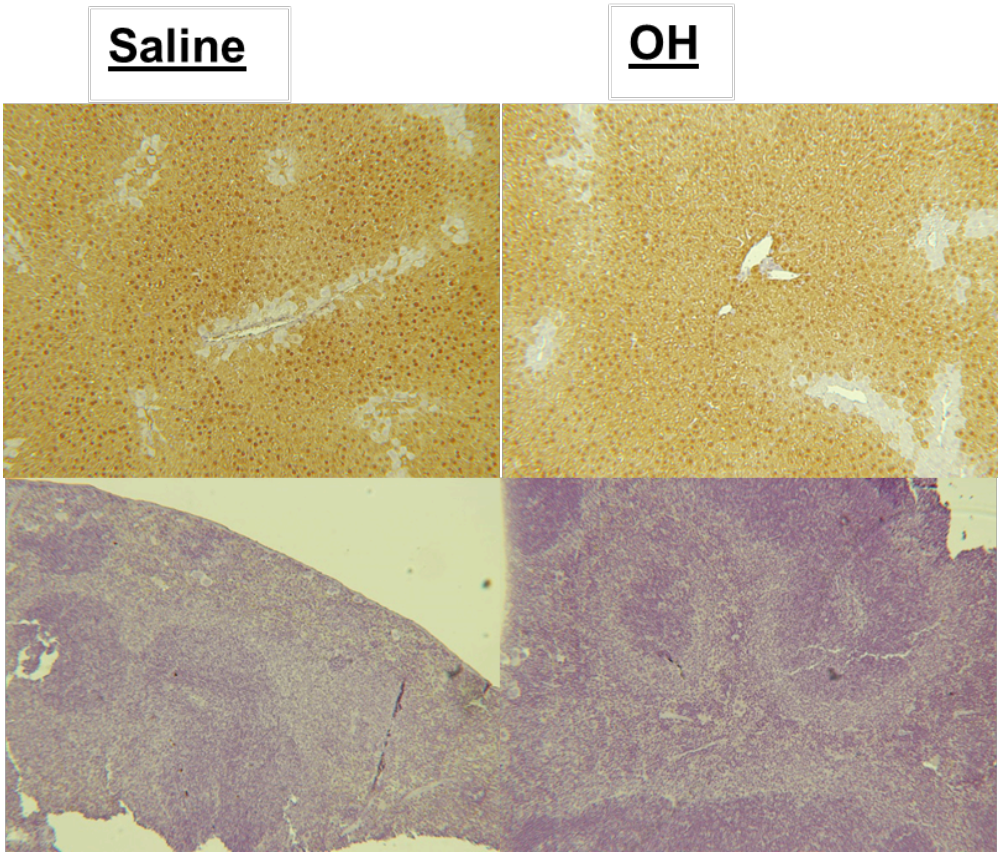

Figure 5.16 Liver and splenic tissues stained for arginase. No observable increase is seen across treatment groups. Arginase is a marker for M2 cells, which may suggest that M2 cells are not related to the macrophage response that we are visualizing.

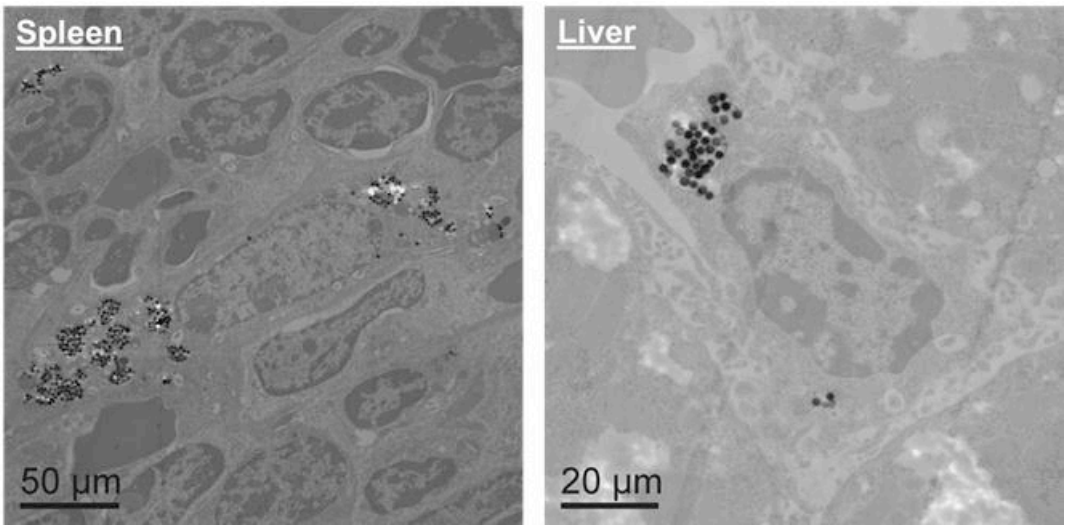

Figure 5.17. TEM images of nanoparticles residing within macrophages of the liver and the spleen.

this is thought to help support cell survival and increase phagocytosis (25). Globally, this behavior is not surprising, as characteristically the M1 phenotype is thought to remove foreign materials and pathogens from the local environment, which is likely to leave the cell, in most cases, unaffected.

Unlike M1 cells, M2 and unpolarized cells exhibit a toxic effect at higher nanoparticle treatment concentrations, despite reduction in overall uptake. The effect appears to be at consistent concentrations between M2 and unpolarized cells, which may suggest they process the materials in a similar manner. However, the mechanism of toxicity remains to be studied. Future analysis such as the use of RNAseq will be essential to understand how nanoparticles interact with the cellular machinery. These studies will help ensure that interactions do not alter the function and polarization states of these cell types, and to determine toxicity related mechanisms.

5.4.2 Uptake of nanoparticles in M1 and M2 cells

Clear M1-specific uptake suggests that M1 cells have a higher affinity for taking up these nanoparticle systems. This may be explained by increased levels of SR-AI/II and MARCO scavanger receptors on M1 macrophages, which are known to bind a variety of polyanionic materials promiscuously *in vivo* (26). The collagen-like domain incorporated within both SR-AI and SR-AII bind the anionic hydroxyl surface of silica (27). The SRCR domain of MARCO has also been implicated in silica binding (28). The increased levels of scavenger receptors and their high affinity for hydroxyl terminated groups may help explain why these hydroxyl-terminated particles were taken up to a greater degree in M1 cells.

The morphological features identified within the TEM images may suggest differing intracellular fate for nanoparticle systems within M1 and M2 cells. Previously, we have observed clathrin-mediated endocytosis for spherical particles of similar sizes in unpolarized cells (29). M2 cells may utilize similar internalization mechanisms. M1 cells, however, may harness phagocytic mechanisms. These two varied uptake mechanisms can lead to very different internalization fates and also varied capacity to reach internal cellular machinery. Phagocytic vacuoles tend to be an end stage, while clathrin-mediated endocytic vesicles can lead to variations in cellular organelle dispersion and, ultimately, intracellular fate. This may help to explain why we observe increased autophagic vesicles in unpolarized and M2 macrophages and decreased vesicles in M1 cells.

Varied LC-3II or autophagic expression levels might also be explained by phenotypic differences. Autophagy is also known to be decreased in cells with upregulated phagocytosis, a known feature of M1 macrophages (30). This decreased autophagic phenomenon in M1 cells may suggest that these macrophages mediate phagocytosis in M1 cells, while uptake via M2 and unpolarized macrophages is mediated through another mechanism. These variations in intracellular fate could help to explain variations in cellular nanoparticle processing behavior.

Intracellular fate may also help to explain variations in proliferation. Nanoparticles appear to be internalized and trafficked to autophagic vesicles in unpolarized and M2 cells. This internalization may alter proliferative capacity within M2 and unpolarized cells. M1 cells do not appear to utilize similar internalization or fate mechanisms and remain unaffected proliferatively. Further studies will need to be done to

understand if autophagy is a global effect for all nanoparticle surface modifications and if autophagy helps to facilitate toxicity related mechanisms.

Our results indicate that M1s clearly outcompete M2 uptake both in isolated, as well as co-culture. Understanding this phenomenon might be useful when designing future *in vitro* assays and globally understanding nanoparticle processing. The results may help to correlate *in vitro* results to a greater extent *in vivo*. Understanding that M1s are the primary phenotype which uptake these nanoparticle systems could help to explain downstream physiological effects, such as the induction of inflammation or the recruitment of other immunological cell types.

5.4.3 *In vivo* nanoparticle effect

We observed minimal toxic effects after nanoparticle treatment, which may suggest that the cells which ingest nanoparticles *in vivo* may potentially be providing a cellular coping effect helping to preserve the local tissue from further nanoparticle damage. We observed similar results with M1 systems *in vitro*. In future studies it will be important to investigate protein expression patterns within the liver and spleen to see if similar *in vitro* and *in vivo* protective profiles are observed. These protective profiles might also be initiating factors for more chronic inflammatory responses. Future directions should allow for increased time point analysis.

Increase levels of inflammatory cells, destruction of lympatics and increased vacuoles suggested the involvement of macrophages and potential induction of inflammatory mediated mechanisms. Hydropic degeneration is also a sign of mitochondrial dysfunction, a characteristic we have observed with nanoparticle exposure

in vitro and can be detrimental in longer terms (31). These studies were only carried out to 4 weeks, it will be essential in nanoparticle development to carry such studies out to at least a year to characteristically identify if inflammatory cell infiltration, tissue destruction and vacuolization persists and if it potentiates further downstream issues.

Drastic increases in lysosomes (CD68) in the liver may help to explain decreased levels of silica in some tissues and may help to support downstream inflammation. Silica may potentially be trafficked to this site, and cleared or stored in or around biliary tracts. It is important to note that CD68 is a lysosomal marker that is observed in cell types other than macrophages and one cannot discern between M1 and M2 polarization states with this marker. One can only assume that the macrophages or cells that have been stained are activated to a lysomal or inflammatory like state, which could potentially be harmful to the animal in chronic situations.

Increased levels of F4/80, iNOS and CD68 are indicative of primarily activated M1 macrophage involvement. Limited to no increase in arginase, CD206 or LC3-bII suggests M2 macrophages play little to no role in the overall response to these nanoparticle systems. However, local uptake of nanoparticles may potentiate a Th1 response and thus increased M1 cells. Increased M1 response may be a result of nanoparticle uptake and not necessarily completely responsible for uptake themselves.

Increased M1 and Th1 responses are not surprising, as M1 macrophages are traditionally involved in biological processing of nanoparticles. Crystalline silica has been linked as an adjuvant to induce autoimmune disorders (32) such as scleroderma, a Th1 response. Hydroxyl groups are also known to differentiate dendritic cells and upregulate CD80 and CD86 (F4/80), the markers utilized to show increased M1

phenotypes *in vivo* (33, 34). MARCO, a scavenger receptor found on M1 cells, has been shown to increase nanoparticle uptake. This is also a receptor that is overexpressed on the Kupffer cells of the liver and within the red pulp of the spleen. Scavenger receptor response has also been shown *in vivo* to increase M1 response, as SR-A knockouts have shown reduced inflammatory M1 phenotypes (35). TLRs have been shown to act in cooperation with scavenger receptors inducing inflammatory like phenotypes with increased levels of IL-12 and IFN-gamma (M1 cytokines). Induced M1 phenotypes have shown to be overloaded with iron oxide particles *in vivo* (36). Hydroxyl modifications induce complement mediated events which could facilitate specific uptake in M1 macrophages. The evidence presented here and within literature may suggest that silica could induce a Th1 response as a result of nanoparticle uptake within these tissues.

Our TEM results show images that provide clear evidence for nanoparticles affinity for macrophages *in vivo.* This may also suggest further that nanoparticles may have an affinity towards M1 phenotypes, however future quantification is necessary to draw these specific conclusions. Quantification of macrophage uptake versus other cell type uptake will be important in future studies.

5.5 Conclusions and Future Directions

Macrophage phenotype and the surface modification on nanoparticles both play an important role in *in vitro* and *in vivo* processing. Our research demonstrates that characteristics of stober silica nanoparticle systems, a commonly used preclinical nanomedical agent, interact with the biological environment and initiate an M1 phenotypic response *in vitro* and *in vivo*. We have shown that M1 macrophages have a

higher affinity for nanoparticles *in vitro* and may potentially regulate organ-level uptake and response *in vivo*. Uptake within M1 phenotypes may provide a protective effect or initiate long term chronic responses *in vitro* and *in vivo*. Coping and chronic response mechanisms will need further justification and mechanistic evaluation. Surface of nanoparticles may potentially play a role in cellular uptake, increased circulation, and clearance. The increased levels of M1 uptake *in vitro* and *in vivo* may also suggest that multiple macrophage phenotypic model systems must be used *in vitro* to understand potential effects of nanoparticles *in vivo*. Variations in nanoparticle physicochemical characteristics could alter how the nanoparticle interacts with macrophages, changing the phenotype that uptakes the nanoparticle and as a direct result of that phenotypic uptake changing the physiological response. For example, if M2 macrophages instead up took silica nanoparticles to a higher extent, it may have instead elicited a Th2 response and we would have observed very different physiological patterns. It will be imperative in the future to pay attention to which particles are taken up by which phenotypes, as nanoparticle processing could initiate detrimental chronic responses dependent on the phenotypic uptake. Additionally, this could have therapeutic implications as differing disease states have variations in macrophage phenotypic responses.

Macrophage phenotype targeting and response could be useful therapeutically. The results of this study may suggest that hydroxyl terminated silica nanoparticles could be utilized to target M1 macrophages *in vivo*. Such a strategy could potentially be utilized in the design of a treatment for neurodegenerative disorders, where an upregulation of M1 phenotypes is destructive to surrounding tissue. If one could target this phenotype and revert or change it to say an M2 phenotype it may resolve the disease state. For

example, in cases of spinal cord injury, an upregulation of M1 polarized macrophages is observed which could be preventing M2 cells from repairing the local environment (37). M1 phenotypes have been also implicated in the development of multiple sclerosis, and M2 suppression has been implicated in relapse of MS suggesting targeting of these phenotypes could present with therapeutic advantage (38). However, it is imperative even within disease states to understand the overall chronic implications of nanoparticle treatment and therefore the potential of these systems.

Overall, this research highlights the need to study nanoparticle uptake in a variety of macrophage phenotypes to help understand *in vivo* physiological responses. We have shown a drastic uptake in M1 phenotypes and an increase in macrophages *in vivo*. These studies have only been carried out to 4 weeks, and the early results here suggest that chronic studies will need to be performed to understand if immunological or chronic inflammatory cascades are being initiated as a result of nanoparticle treatment.

5.6 References

1. Caron WP, Lay JC, Fong AM, La-Beck NM, Kumar P, Newman SE, et al. Translational studies of phenotypic probes for the mononuclear phagocyte system and liposomal pharmacology. J Pharmacol Exp Ther. 2013;347(3):599-606.

2. Caron WP, Song G, Kumar P, Rawal S, Zamboni WC. Interpatient pharmacokinetic and pharmacodynamic variability of carrier-mediated anticancer agents. Clinical Pharmacology and Therapeutics. 2012;91(5):802-12.

3. Nahrendorf M, Zhang H, Hembrador S, Panizzi P, Sosnovik DE, Aikawa E, et al. Nanoparticle PET-CT imaging of macrophages in inflammatory atherosclerosis. Circulation. 2008;117(3):379-87.

4. Dobrovolskaia MA, McNeil SE. Understanding the correlation between in vitro and in vivo immunotoxicity tests for nanomedicines. J Control Release. 2013;172(2):456-66.

5. Trivedi R, U-King-Im J, Graves M, Kirkpatrick P, Gillard J. Noninvasive imaging of carotid plaque inflammation. Neurology. 2004;63(1):187-8.

6. Wingard JR, White MH, Anaissie E, Raffalli J, Goodman J, Arrieta A, et al. A randomized, double-blind comparative trial evaluating the safety of liposomal amphotericin B versus amphotericin B lipid complex in the empirical treatment of febrile neutropenia. L Amph/ABLC Collaborative Study Group. Clin Infect Dis. 2000;31(5):1155-63.

7. Cassetta L, Cassol E, Poli G. Macrophage polarization in health and disease. The Scientific World Journal. 2011;11:2391-402.

8. Wynn TA, Chawla A, Pollard JW. Macrophage biology in development, homeostasis and disease. Nature. 2013;496(7446):445-55.

9. Romagnani S. The Th1/Th2 paradigm. Immunology Today. 1997;18(6):263-6.

10. Mantovani A, Sica A, Locati M. Macrophage polarization comes of age. Immunity. 2005;23(4):344-6.

11. Cooper GS, Miller FW, Germolec DR. Occupational exposures and autoimmune diseases. International Immunopharmacology. 2002;2(2):303-13.

12. Lucarelli M, Gatti AM, Savarino G, Quattroni P, Martinelli L, Monari E, et al. Innate defense functions of macrophages can be biased by nano-sized ceramic and metallic particles. European Cytokine Network. 2004;15(4):339-46.

13. Schanen BC, Das S, Reilly CM, Warren WL, Self WT, Seal S, et al.

Immunomodulation and T helper TH(1)/TH(2) response polarization by CeO(2) and TiO(2) nanoparticles. PLoS One. 2013;8(5):e62816.

14. Jones SW, Roberts RA, Robbins GR, Perry JL, Kai MP, Chen K, et al. Nanoparticle clearance is governed by Th1/Th2 immunity and strain background. The Journal of Clinical Investigation. 2013;123(7):3061-73.

15. Kanchan V, Panda AK. Interactions of antigen-loaded polylactide particles with macrophages and their correlation with the immune response. Biomaterials. 2007;28(35):5344-57.

16. Lutsiak M, Kwon GS, Samuel J. Biodegradable nanoparticle delivery of a Th2 biased peptide for induction of Th1 immune responses. Journal of Pharmacy and Pharmacology. 2006;58(6):739-47.

17. Barbarin V, Xing Z, Delos M, Lison D, Huaux F. Pulmonary overexpression of IL-10 augments lung fibrosis and Th2 responses induced by silica particles. American Journal of Physiology-Lung Cellular and Molecular Physiology. 2005;288(5):L841-L8.

18. Granum B, Gaarder PI, Groeng E-C, Leikvold R-B, Namork E, Løvik M. Fine particles of widely different composition have an adjuvant effect on the production of allergen-specific antibodies. Toxicology Letters. 2001;118(3):171-81.

19. Kodali V, Littke MH, Tilton SC, Teeguarden JG, Shi L, Frevert CW, et al. Dysregulation of Macrophage Activation Profiles by Engineered Nanoparticles. ACS Nano. 2013;7(8):6997-7010.

20. Al Faraj A, Shaik AS, Afzal S, Al Sayed B, Halwani R. MR imaging and targeting of a specific alveolar macrophage subpopulation in LPS-induced COPD animal model using antibody-conjugated magnetic nanoparticles. International Journal of Nanomedicine. 2014;9:1491-9.

21. Stöber W, Fink A, Bohn E. Controlled growth of monodisperse silica spheres in the micro size range. Journal of Colloids and Interface Science. 1968;26:62-9.

22. Blaaderen A, Vrji A. Synthesis and characterization of colloidal dispersions of fluorescent silica spheres. Langmuir. 1992;8:2921-31.

23. Classen A, Lloberas J, Celada A. Macrophage activation: classical vs. alternative. Macrophages and Dendritic Cells: Springer; 2009. p. 29-43.

24. Herd HL, Malugin A, Ghandehari H. Silica nanoconstruct cellular toleration threshold in vitro. J Control Release. 2011;153(1):40-8.

25. Lu YC, Yeh WC, Ohashi PS. LPS/TLR4 signal transduction pathway. Cytokine. 2008;42(2):145-51.

26. Platt N, Gordon S. Scavenger receptors: diverse activities and promiscuous binding of polyanionic ligands. Chemistry & Biology. 1998;5(8):R193-R203.

27. Chao SK, Hamilton RF, Pfau JC, Holian A. Cell surface regulation of silica-induced apoptosis by the SR-A scavenger receptor in a murine lung macrophage cell line (MH-S). Toxicology and Applied Pharmacology. 2001;174(1):10-6.

28. Hamilton Jr RF, Thakur SA, Holian A. Silica binding and toxicity in alveolar macrophages. Free Radical Biology and Medicine. 2008;44(7):1246-58.

29. Herd H, Daum N, Jones AT, Huwer H, Ghandehari H, Lehr CM. Nanoparticle geometry and surface orientation influence mode of cellular uptake. ACS Nano. 2013;7(3):1961-73.

30. Shintani T, Klionsky DJ. Autophagy in health and disease: a double-edged sword. Science. 2004;306(5698):990-5.

31. Malugin A, Ghandehari H. Caspase 3 independent cell death induced by amorphous silica nanoparticles. Nanoscience and Nanotechnology Letters. 2011;3(3):309-13.

32. Haustein U-F, Ziegler V, Herrmann K, Mehlhorn J, Schmidt C. Silica-induced scleroderma. Journal of the American Academy of Dermatology. 1990;22(3):444-8.

33. Bartneck M, Keul HA, Wambach M, Bornemann J, Gbureck U, Chatain N, et al. Effects of nanoparticle surface-coupled peptides, functional endgroups, and charge on intracellular distribution and functionality of human primary reticuloendothelial cells. Nanomedicine: Nanotechnology, Biology and Medicine. 2012;8(8):1282-92.

34. Yang D, Zhao Y, Guo H, Li Y, Tewary P, Xing G, et al. [Gd@ C82 (OH) 22] n Nanoparticles Induce Dendritic Cell Maturation and Activate Th1 Immune Responses. ACS nano. 2010;4(2):1178-86.

35. Xu Y, Qian L, Zong G, Ma K, Zhu X, Zhang H, et al. Class A scavenger receptor promotes cerebral ischemic injury by pivoting microglia/macrophage polarization. Neuroscience. 2012;218:35-48.

36. Sindrilaru A, Peters T, Wieschalka S, Baican C, Baican A, Peter H, et al. An unrestrained proinflammatory M1 macrophage population induced by iron impairs wound healing in humans and mice. The Journal of Clinical Investigation. 2011;121(3):985.

37. Kigerl KA, Gensel JC, Ankeny DP, Alexander JK, Donnelly DJ, Popovich PG. Identification of two distinct macrophage subsets with divergent effects causing either neurotoxicity or regeneration in the injured mouse spinal cord. The Journal of

Neuroscience. 2009;29(43):13435-44.

38. Mikita J, Dubourdieu-Cassagno N, Deloire MS, Vekris A, Biran M, Raffard G, et al. Altered M1/M2 activation patterns of monocytes in severe relapsing experimental rat model of multiple sclerosis. Amelioration of clinical status by M2 activated monocyte administration. Multiple Sclerosis Journal. 2011;17(1):2-15.

CHAPTER 6

CONCLUSIONS AND FUTURE DIRECTIONS

This dissertation explores how the geometry, charge and surface modification of nanoparticles influence intracellular fate and uptake within macrophages.

6.1 Conclusions

6.1.1 Aim 1 conclusions

In Chapter 3, positively charged silica nanoparticles were shown to induce autophagy, a cellular toleration and coping mechanism, within RAW 264.7 macrophages. Inclusion in autophagic vesicles was irrespective of size and shape of the nanoparticle systems. Similar fates for other highly positively charged systems have been observed (1, 2). If payload delivery to a specific cellular compartment is required, autophagic compartmentalization will be detrimental. It will be imperative to keep this in mind especially when designing systems that require delivery to a specific intracellular compartment for efficacy.

6.1.2 Aim 2 conclusions

In Chapter 4, the influence of physicochemical characteristics on uptake mechanisms in macrophages was shown within RAW 264.7 cells and isolated primary lung tissue macrophages. Phenotype of the macrophage did influence the extent of uptake

of nanoparticle systems. Within this chapter the important role that geometry can play in the uptake of silica nanoparticle systems was also shown. Manipulation of geometry induced specific uptake mechanisms. Within the size ranges studied, highly positively charged materials appeared primarily to undergo clathrin-mediated endocytosis for ~200nm spherical nanoparticles, while adjusting the geometry and size of these systems to ~1 um switched the primary uptake mechanism to macropinocytosis or phagocytosis with limited uptake of all nanoparticles in both systems. This chapter illustrates the capability to manipulate geometry to facilitate specific uptake mechanisms. In the design of systems for drug delivery intracellular payload delivery is highly dependent on the initial stages of uptake. Ultimate fate of the nanoconstruct could be determined via sequestration into compartments early on, ending the fate of the payload in vesicles which do not provide opportunity for delivery.

6.1.3 Aim 3 conclusions

In Chapter 5, the impact of macrophage phenotype on uptake was explored *in vivo* and *in vitro*. This chapter illustrates the importance of macrophage polarization state on studying and understanding the interactions of physicochemical characteristics with biological systems. M1 polarized macrophages took up silica nanoparticles to a higher extent than unpolarized or M2 macrophages. Unlike M2 and unpolarized macrophages, M1 polarized cells did not exhibit toxicity after nanoparticle treatment. This was consistent with *in vivo* findings, as nanoparticles resided within macrophages of clearance organs, liver and spleen, with little to no observed toxicity. Markers specific for M1-type macrophages were upregulated in tissue and M2 macrophage markers appeared absent in

these organs, suggesting the proliferative role of this phenotype in processing of the nanoparticles. The importance of surface chemistry on aggregation potential and initial biodistribution was observed. However ultimately all silica nanoparticles underwent the same processing. The chapter highlights the importance of the *in vitro* macrophage model system on understanding the fate of nanoparticles.

Chapter 5 concludes by suggesting *in vitro* macrophage model systems may be capable of targeting specific phenotypes of macrophages, which may be useful in targeting pathogenically loaded macrophages or macrophages involved in immunological disorders. M1 phenotypes traditionally retain bacteria and pathogenic material within their cellular compartments. M1 targeting mechanisms may enhance the delivery of bactericidal materials. Additionally, M1 phenotypes are overexpressed in chronic debilitating immunological diseases such as MS and RA (3), targeted removal may provide therapeutic effect.

6.1.4 Dissertation conclusions

This dissertation illustrates the importance of macrophages in nanoparticle processing and suggests that M1 phenotypes of macrophages are more important than other phenotypes. This dissertation claims that macrophages not only uptake nanoparticles to a great extent but also appear to have global coping mechanisms to handle that uptake. Positively charged nanomaterials initiate autophagy within some macrophages to facilitate this coping mechanism. Physicochemical characteristics have been shown to drastically alter macrophage nanoparticle interactions. Finally, manipulation of physicochemical characteristics can direct intracellular uptake

mechanisms. In designing of nanomaterials for drug delivery it will be important to consider these conclusions.

6.2 Future directions

6.2.1 Outline and explanation of future directions

Early evidence suggests that innate immune functions, specifically cell autonomous processes utilized by cellular machinery in pathogen processing, are initiating inflammatory mediated events after systemic and oral nanoparticle treatments (4-15). Evidence in Chapters 3-5, as well as my lab's collaborative work, suggests that autophagic mechanisms in phagocytic lines are up-regulating inflammatory genes, affecting cellular machinery, initiating fibrotic-like encapsulation and chronic inflammation (16-20). The collaborative work also highlighted evidence demonstrating that NP surface characteristics significantly influence cellular *in vitro* and *in vivo* inflammatory responses (18-21). The ultimate goal of this future direction section is to understand how nanoparticles can be designed and modified to reduce inflammatory mediated events.

Our lab has yet to expand upon the evidence that demonstrates correlations between specific inflammatory mediated mechanisms and surface characteristics. I believe it is possible to modulate the levels and potentially the mechanisms of inducing inflammation by modulating the surface characteristics. In this chapter, I propose to modulate SNP surface curvature, surface functionality, porosity and degradability to influence inflammatory mechanisms (increase inflammatory protein cascades, autophagy, and immunological cell activation). Our evidence suggests that modulations of the SNP

surface curvature affect the protein adsorption to SNP, intracellular uptake mechanisms and the ultimate intracellular fate. Cellular trafficking mechanisms for particles that prompt inflammatory cascades facilitate chronic inflammatory endpoints. My lab has already shown significant alterations in hemolysis and biodistribution as a function of NP porosity (21, 22). Nonporous materials resided mostly in the spleen while porous materials were found in kidney (22). If certain mechanisms elicit specific localizations, they may also initiate different inflammatory cascades, due to differing interactions with the biological environment. Surface modifications, such as PEGylation, can impact inflammatory mediated results, as was shown in Chapter 5. Finally, silica itself, while nondegradable, cannot be cleared from the host tissue, and could initiate long-term fibrosis as a part of a host chronic response. Increased levels of immunological cells as a result of nanoparticle administration within tissues at 4 weeks described in Chapter 4 helps to support that nondegradable NP materials initiate acute inflammatory mechanisms. Inflammatory initiation may be resolved with degradable silica particles, which would be resorbed and cleared. To test this, I propose to exploit established methods to adjust silica nanoparticle curvature and develop new methods to adjust SNP porosity and degradability.

Chapters 3-5 and my lab's collaborative efforts illustrate *in vivo* and *in vitro* evidence supports primary uptake via phagocytic systems and accumulation in RES organs as a result nanoparticulate insults on tissue, or encapsulation within thrombus, initial events of inflammatory mediated chronic response (17, 19, 23-26). Chapter 3 and 5 also suggest that after phagocytic internalization, particles are trafficked to autophagic compartments where they continue to reside for the duration of the life of the cell. Cell

death and dysfunction appear to result from injurious response to the mitochondria and consequent ROS production. I propose that combinations of these intracellular processes initiate inflammatory cascades, leading to increased levels of gene expression and local induction of fibrosis responses. However, I cannot yet connect these mechanistic complications to develop requisite deeper understandings of how each process initiates another. Additionally, neither my lab nor I has yet to expand this understanding to specific NP surface characteristics, or to propose routes to induce or avoid specific cascades and mechanisms within these processes using NP designs. Additionally, I have not yet expanded these observations to other nanomaterials or examination of degradation products, to see if the results from these studies are universally applicable. As such I proposed to add the evaluation of PLGA particles, gold nanorods and G3.5 dendrimers to selected studies. I believe that the utilization of PLGA, as a polymer used in FDA-approved products, gold nanoparticles, currently in phase 2 clinical trials, and dendrimers, used extensively in preclinical studies, will help to supply clinical applicability and devolve platform development. Here, I propose strategies to assess how NPs are taken up, trafficked and influence phagocytic cellular responses *in vitro*. I propose to utilize neutrophils, macrophages and dendritic cells as model systems for NP processing. I aim to identify inflammatory gene and protein expression resulting from variations in NP surface modifications, NPs themselves and degradation products, in order to address reductions in local levels of inflammation. I also propose to assess local levels of autophagy and connect NP surface characteristics that initiate these mechanisms. Additionally, I propose to analyze the relative levels of blood component activation to determine what surface modifications activate coagulopathies and to provide

ways to mitigate thrombotic plugs. The ultimate goal is to connect intracellular uptake and trafficking to downstream cascades. Based on observations in Chapters 3 and 5, I propose that autophagic encapsulation induces mitochondrial damage and subsequent inflammatory gene induction. I also propose to investigate levels of protein adsorption and what proteins may initiate inflammatory mediation, utilizing 2D gel methods specific inflammatory proteins (TNF-alpha, IL-1beta, IL-6, IL-8, IL-2, IL-4, IL-5) can be investigated. I propose to correlate these levels of adsorption to levels of activation of the same proteins via quantification using western blots, ELISA and their subsequent gene regulation by qPCR. I propose to correlate these degrees of adsorption to the relative level of inflammatory mediation events, and believe that surface modifications can substantially influence protein as well as inflammatory events. I also believe that these two events will be directly correlated, due to protein interactions with the inflammatory biological environment. Additionally, I propose to assess the levels of *in vitro* and *in vivo* degradation, as well as degradation products and their associated toxicity.

Traditional chronic particle-associated inflammatory disease states, such as mesothelioma, pneumoconiosis, asbestos and silicosis, present 10-15 years after environmental particulate exposure. Gold, zinc and titanium particles have shown responses similar to silicosis (27, 28), suggesting that local nanoparticle encapsulation initiates acute inflammatory events that progress to chronic disease states due to the lack of NP resorption and clearance of the material. Currently, no long-term studies evaluate particles residence in tissues and what effects that residence has on the ultimate tissue inflammatory states. It is possible that NP residence induces autoimmune disorders. My lab's collaborative acute toxicity study shows significant increase in local thrombotic

events, fibrosis, and infiltration of PMNs suggesting downstream inflammatory cascades (22, 26, 29-34). This dissertation and my lab's collaborative efforts *in vitro* evidence support this theory (17-19, 21, 23, 26, 32). Because of this I propose to investigate how NPs and their surface modifications initiate local chronic responses and progression through the phases of chronic inflammation. I also propose to expand selected experiments with PLGA particles, dendrimers and gold nanomaterials. I believe that degradation products will not cause the same levels of activation as whole nanoparticles. I propose to study mechanisms used for pathogen processing such as autophagy that initiate local fibrosis and increased levels of inflammation. I propose to test for chronic inflammation with CD-1 mice models to assess local infiltration of innate and adaptive immunological cells including but not limited to PMNs, T cells, and B cells, degree of fibrosis, local levels of inflammatory gene, cytokine and chemokine expression. I also propose to assess local levels of tissue autophagy to correlate with our previous findings. Ideally, one should seek to correlate mechanistic studies to suggest how and why certain specific surface functionalities present with specific chronic inflammatory mechanisms. The ultimate goal is to understand how these NP materials can be designed and modified to reduce inflammatory mediated events.

6.2.1 Outline of future experiments

6.2.1.1 Synthesis and characterization

(This section was developed with the aid of Dr. Ilya Zharov.)

6.2.1.1.1 Surface curvature

Monodispersed silica spheres with diameters of 50,500 nm (35) should be prepared by hydrolysis of tetraethyl orthosilicate (TEOS) in the presence of water and ammonia in ethanol (36). Silica colloidal sphere sizes should be controlled by changing ammonium concentration at fixed TEOS and water concentrations (35). Smaller silica nanoparticles should be prepared using a similar procedure (37). Surface curvature should be modified systematically with these preparative methods. Pegylated gold nanoparticles of 50nm size will be synthesized/characterized as described by Bergen et al. (38), pegylated PLGA nanoparticles should be synthesized and characterized as described by Velcia et al. (39) and dendrimers should be purchased from dendritic and prepared as described in our lab previously (30, 31, 40).

6.2.1.1.2 Porosity and roughness

As my lab's collaborators have shown (41, 42), NP pore shape and size in silica nanoparticles are controlled by the size and nature of the porogen organic groups and by organic templates used during the nanoparticle formation. To establish relationships between the toxicity of silica nanoparticles and their porosity, one should prepare SNPs with different pore sizes and shapes, and with different porosities. To distinguish the effects of porosity based on altered adsorption of various biological molecules inside the pores from the effects based on the increased nanoparticle roughness, one should prepare SNPs with solid cores and mesoporous shells (43) and SNPs with varying degrees of surface roughness (44). The nanoparticle porosity should be examined using transmission electron microscopy (TEM). In addition, specific surface area and pore diameters should

be calculated from nitrogen adsorption/desorption isotherms.

6.2.1.1.3 Surface PEGylation

One should surface modify SNPs with a 5000 Da PEG with a terminal free amine, which will be conjugated to a N-hydroxysuccinimide (NHS) activated silane (Nanocs, Japan) via a reductive amidation chemistry. Following the conjugation, SNPs should be centrifuged and washed to remove excess reagents. Polymer conjugation to the surface will be confirmed by hydrodynamic radius measurements, Fourier transform infrared spectroscopy (FTIR) to confirm the presence of the PEG chains on the surface, and by thermogravimetric analysis (TGA) to determine the amount of the PEG attached to the surface.

6.2.1.1.4 Degradability

As shown by my lab's collaborators previously, novel approaches can be used to destabilize silica by incorporating cleavable organic linkers into SNPs (42). One should expand the set of linkers and will vary linker content in order to control the SNP degradability. These degradable silica nanoparticles should be characterized by scanning electron microscopy (SEM), dynamic light scattering (DLS) and TGA. The key characteristics to be examined will be SNP size, size distribution and composition. The latter is particularly important for toxicity prediction. While the starting materials for the synthesis are of intrinsically low toxicity (45-47), one should validate residual solvents within SNPs using TGA coupled with mass spectrometry (TGA-MS). If solvents are found, they should be removed by drying under reduced pressure and mildly elevated

temperature. SNP degradability studies as a function of the cleavable linker structure and content should be followed by measuring the amounts of the resulting product, $Si(OH)_4$, spectrophotometrically as a molybdenum blue complex (48). With this organosilica NP series in hand, one should perform degradation studies as a function of pH to obtain kinetic and thermodynamic data for the degradation process.

6.2.1.1.5 Additional characterization of SNPs

Since nanoparticles have the propensity to agglomerate depending on surface properties, one should utilize dynamic light scattering to evaluate the aggregation in cell culture media containing serum proteins. One should also use confocal microscopy to characterize aggregate localization and size within cells. Zeta-potentials will be measured for as-synthesized SNPs as a function of pH and also after equilibrating SNPs with cell culture media. The particles should be monitored for endotoxin contamination using LAL assay kits.

6.2.1.1.6 Anticipated results, potential pitfalls, and alternative strategies

In the event that SNPs do not degrade rapidly enough or not in response to sharp transitions in pH, one should augment destabilization by incorporating biodegradable, biocompatible polymer, poly(L-lactic acid), PLLA, as previously described (49). One should then study the influence of poly(L-lactic acid) molecular weight and amount on SNP degradation rates (49). One should incorporate PLLA also if insufficient porosity is obtained. If spherical systems (drastic changes in size and thus NP curvature) do not

produce increased changes in biological activity, triangular and cube-like silica nanoparticles should be prepared using reported procedures (50).

6.2.1.2 Investigation of effects on cellular and protein inflammatory mediated mechanisms.

6.2.1.2.1 NP stability in cell culture medium

One should evaluate NP aggregation and stability in physiological conditions with DLS and UV measurements. Particles should be suspended in DMEM and mouse serum at 50 and 100 ug/mL and the hydrodynamic diameter and OD should be estimated at 37 °C. All measurements should be performed in triplicate. I believe both nondegradable and degradable particles should be stable under these conditions.

6.2.1.2.2 Degradation in vitro

One should assess the relative levels of degradation of SNPs by enclosing known amounts (by weight) in dialysis bags (MW cut-off ~10000 Da) incubated in buffer solutions of pH values 4, 7.4, and 10. For determination of NP weight and size loss, NP samples will be removed from dialysis tubing medium at 1 day, 1 week, 1, 2, 4, 6 and 12 months. Weight differences should be measured between samples at zero time and time removed represent weight loss over time *t*. Recovered solid residues should then be dispersed in buffer and sizes analyzed via DLS (51).

6.2.1.2.3 Degradation *in vitro*

One should assess the relative levels of degradation of the silica nanoparticles by enclosing known amounts (by weight) in dialysis bags (cellulose membranes with a MW cut-off ~10000 Da). These bags should be incubated in several buffer solutions of pH values 4, 7.4, and 10. For the determination of the weight loss and size reduction from the nanoparticles, samples should be removed from the incubation medium at 1 day, 1 week, 1, 2, 4, 6 and 12 months. The solid residues should be weighed and the weight difference between the sample at zero time and time removed will represent the weight loss occurring until time *t*. The solid residues should then be dissolved in buffer and size will be analyzed via DLS, TEM and flow field fractionation to see the relative size, topography and degradation mechanisms (51). The degradation products should also be tested for associated toxicity via standard proliferation assays and in selected immunological processes. One should capture degradation products and assess toxicity and enhancement of inflammatory activation.

6.2.1.2.4 Immune cell processing

Blood-derived neutrophils are isolated by density centrifugation (Ficoll-Plaque Plus, Amersham) and purified from contaminating erythrocytes as described (52). Their production of superoxide anion upon NP incubation is used as an indicator of neutrophil activation, measured spectrophotometrically at 550nm by following ferricytochrome c reduction. PBMC should be cultured to produce monocyte-derived DC as described (53). Cells will be seeded; 2 hours later nonadherent cells will be removed. Adherent PBMC will be cultured in the presence of 800 U/mL GM-CSF and 500 U/mL IL-4 for 2 to 7

days. Monocytes should be obtained from whole CD-1 mouse blood utilizing a density gradient centrifugation and isolated utilizing anti-CD14 microbead. These should then be cultured for 6 days in RPMI-1640 supplemented with 20% FBS and 100 ng/mL of macrophage colony stimulating factor at a density of $1.5x10^5$ per cm^2. Inflammatory mediated cells should be obtained by culturing cells for an additional 72 hours in RPMI 1640 supplemented with 5% FBS and 100 ng/mL of LPS plus 20 ng/mL of IFN-gamma (54, 55).

6.2.1.2.5 Cell viability and proliferation

WST-1 assay should be used to assess the relative proliferative capacity and mitochondrial function. A base level of cellular toxicity should be assessed via a standard WST-1 (4-[3-(4-iodophenyl)-2-(4-nitrophenyl)-2H-5-tetrazolio]-1,3-benzene disulfonate) assay. Cells should be exposed to a range of concentrations (.0001-1000 ug/mL) of SNPs for 72 hours. IC50 values can be calculated using GraphPad Prism (La Jolla, CA). To assess plasma membrane integrity, cells should be exposed to various concentrations of NPs for 24 hrs and assayed for lactate dehydrogenase (LDH) or leakage with the CytoScan LDH leakage cytotoxicity assay (G-Bioscience, Madison, WI). Maximum LDH is assessed via total control cell lysis induced by 0.1% Triton X-100, and a diluted series of LDH supplied with the kit will be utilized as positive control. Degradation products should also be assessed to ensure safety.

6.2.1.2.6 Cellular uptake

SNP uptake by cultured cells is visualized by confocal microscopy. Cells should be incubated for 24 h with 50 μg/ml FITC-labeled SNPs. Cell nuclei should be stained with DRAQ5 (Biostatus Ltd.). Fluorescent images of live cells should be captured using confocal laser scanning microscopy. Laser beam intensity and photodetector sensitivity should be kept constant in order to compare relative fluorescence intensities between experiments. Z-stacks should be collected and used for 3D reconstruction and visualization of intracellular particle localization. Flow cytometry should be used to quantify SNP uptake. Cells should be grown and incubated with 75 μg/ml FITC-labeled SNPs for various time points (0.5, 1, 2, 4, 6, 12 and 24 h). Following incubation, analysis should be performed on a FACSCalibur (BD Biosciences, Germany). Emitted light resulting from FITC-labeled NPs should be detected and background fluorescence of unlabeled cells subtracted. Cells without any NP addition will be negative controls in every measurement. Data analysis should be performed with BD CellQuest Pro (BD Biosciences, Germany).

6.2.1.2.6 Co-localization in intracellular compartments

The co-localization of SNPs with acidic and basic lysosomes, as well as autophagosomes by cultured cells should be assessed by confocal microscopy. Cells should be grown and incubated for 24 hrs with 50 μg/ml FITC-labeled NPs. Lysosomes should be stained with 2.5 μM LysoSensor Yellow/Blue DND-160 or 50 μg/mL Transferrin Alexa Fluor 546 (Invitrogen Corp., Carlsbad, CA). Fluorescent images of live cells should be captured by CLSM.

6.2.1.2.7 Transmission electron microscopy (TEM)

Cell uptake of SNPs by cultured cells will be assessed by TEM. Cells should be seeded on 1x1 cm ACLAR plastic. After an overnight incubation, 50 μg/mL of SNPs should be added and cells incubated for 24 hr after which cells should be fixed. Cells should be stained with uranyl acetate for 45 min at room temperature and TEM images should be taken with a Phillips TECHAI F2 TEM (Hillsboro, USA) at an accelerating voltage of 80 kV.

6.2.1.2.8 Protein adsorption

A 2-D PAGE gel of the protein containing supernatants should be run before and after adsorption to nanoparticles (56, 57). 2-D PAGE separates proteins with respect to their isoelectric point in the first dimension and their molecular weight in the second dimension (58-61). The gels should be stained for proteins using high affinity quantitative silver staining. It has been shown that the 2-D PAGE adsorption method can analyze which plasma proteins simultaneously bind to particles both *in vivo* and *in vitro* (58, 60). The gel after adsorption should be compared to standards and specific spots should be excised and characterized individually. While gross surface adsorption should be determined via ellipsometry, circular dichroism, SPR, and optical waveguide lightmode spectroscopy, the specific proteins adsorbed to the surface should be determined from the 2-D gel excised spots via NMR, FTIR, MS, or Western blotting similar to previous procedures (62-65). Correlations between adsorption and Western blot/ELISA analysis should be determined**,** specifically one should investigate the presence of inflammatory proteins **(**TNF-alpha, IL-1beta, IL-6, IL-8, IL-2, IL-4, IL-5),

quantify the degree of adsorption and correlate that to the relative activation of inflammatory mediated mechanisms.

6.2.1.2.9 Assessment of inflammatory cytokine production

Fresh blood from CD-1 mice (6-8 weeks old) should be drawn into an appropriate anticoagulant-containing polypropylene container using gravity flow to prevent cell damage due to shear. Collected blood should be diluted to 25% with plasmalyte, a physiological dilutent used during surgical procedures. Aliquots (1 ml) of the blood should be added to 24-well cell culture plates. Stock concentrations of SNPs will be added to the blood (100 μL of synthesized SNP added to 1 mL of blood). The blood with the test compound should be incubated at 37 ^{o}C for 15 min. Following the initial incubation, 10 μg/mL of LPS (as a control treatment) and NPs below IC_{50} concentration should be added. The plate should be incubated for 2 h with shaking on an orbital shaker at 37°C. After incubation, plates should be spun down at 1300g and plasma extracted for inflammatory cytokine analysis using capture ELISA methods (BD Biosciences). For Inflammatory Capture ELISA (TNF-alpha, IL-1beta, IL-6, IL-8, IL-2, IL-4, IL-5) 96-well polystyrene microtiter plates should be coated with anti-inflammatory cytokine capture antibodies overnight at 4^{o}C. One hundred μl of plasma extracted from the same whole blood method should be added to the respective wells and incubated at room temperature for 1 h. Samples should be aspirated and incubated with inflammatory cytokine detection antibody conjugated to a horseradish peroxidase substrate for 1 h. Antibody solutions should be aspirated and the plate washed, developed with 3,3',5,5'-tetramethylbenzidine (TMB), and analyzed at OD 450nm.

6.2.1.2.10 Western blot and ELISA assessment of cell inflammatory and autophagic activation

Relative levels of LC3-I and II (traditional autophagic markers), MIP1, MIP2, MCP, iNOS (traditional inflammatory markers) should be assessed utilizing standard western blot and ELISA techniques. Cells should be lysed with Radio-Immunoprecipitation Assay (RIPA) buffer supplemented with protease inhibitor cocktail (Sigma) and sodium dodecyl sulfate polyacrylamide gel electrophoresis should be performed. Protein immunobloting should be performed via gel transfer to PVDF membranes. The membrane should be blocked and incubated with primary antibodies (Novus Biologicals) for 1 hr and then with peroxidase-conjugated secondary stabilized goat anti-rabbit antibodies (Pierce) for 1 hr. Proteins should be detected with western blotting. One should include degradation products of degradable silica systems, PLGA particles, gold nanorods and G3.5 dendrimers within this examination.

6.2.1.2.11 Inflammatory gene profiling

My lab's collaborators have considerable experience using the Agilent microarray platform (20) but RNAseq allows for more thorough gene expression analysis. Therefore, it is proposed to utilize RNAseq to generate transcriptional profiles of primary human cells exposed to nontoxic SNP doses. Following cell viability analysis, nontoxic amounts of NPs should be dosed to macrophages, dendritic cells and neutrophils. Total RNA should be collected following ~4 hrs of incubation with NPs (Qiagen RNeasy minikit protocol RNA), quantified (Nanodrop spectrophotometer), and assessed for quality. RNeasy methods provide high quality, uniform yields of total RNA from cells in culture

as monitored using the Experion (Bio-Rad) analyzer to ensure high quality RNA is used for the expression analysis. One should utilize Illumina TruSeq RNA sample preparation to generate barcoded sample libraries. Supervised strategies should be used to identify genes with greatest significant differences among NP treatments and compared to untreated controls. Since RNAseq has considerable costs, a focus should be on ensuring reasonable sequencing depth. A maximum of 8 multiplexed samples per HiSeq 2000 lane to ensure that the depth of sequencing should be sufficient (currently, typical results from one HiSeq lane at our institution is between 150-200 million reads or approximately 7.5 to 10 billion bases, so for 8 multiplexed samples, we anticipate >16 million reads/sample). The samples should be processed using the Genomic Analyzer Pipeline and mapped to the genome using GNUMAP. The differential gene expression profiles are used for pathway analysis where a focus on gene ontology, transcriptional regulation (TRANSFAC) and KEGG analysis of the differentially expressed genes should be accomplished with GATHER(66). Degradation products of degradable silica systems, PLGA particles, gold nanorods and G3.5 dendrimers will be included within this examination.

6.2.1.2.12 Validate select genes by quantitative PCR

Microarray expression analysis is generally a semiquantitative method. Hence select genes that may serve as potential biomarkers will be evaluated by quantitative PCR procedures. Should the transcriptional profiling identify genes involved in inflammatory cascades or other pathways, these pathways may help with selection of candidate biomarkers.

6.2.1.2.13 Platelet aggregation

Platelet-rich plasma (PRP) and platelet-poor plasma (PPP) should be prepared from citrated CD-1 mice, 6 - 8 weeks old (67). Various concentrations (50-500 μg/mL) of blank nanoparticles should be incubated at 37°C for 10 min with PRP containing 10^6 platelets/ml under constant stirring. Platelet aggregation in the presence of various nanoparticle concentrations should be measured turbidimetrically from absorbance at 500nm. Collagen (2 ug/ml) and epinephrine (2.5 μmol/L) should be used as positive controls. Platelet aggregation by the positive controls added to PRP (10^6 cells/ml) should be measured in the absence or presence of NPs.

6.2.1.2.14 Neutrophil activation studies

Neutrophils should be isolated by density centrifugation (Ficoll-Plaque Plus, Amersham) and purified from contaminating erythrocytes as described previously (68). The production of superoxide anion upon NP incubation with neutrophils is used as an indicator of neutrophil activation and measured spectrophotometrically at 550nm by following ferricytochrome c reduction (68). The reduction of ferricytochrome c as a result of NP incubation with neutrophils should be carried out in the presence and absence of superoxide dismutase (SOD; free radical scavenger). The superoxide production should be determined in supernatants from AU550 of samples without SOD minus samples with SOD. The results obtained from NP suspensions should be presented with respect to the amounts of superoxide production from neutrophil incubation with phorbol 12-myristate 13-acetate (PMA; positive control). The criteria for selection of biocompatible NPs should be based on standard values that show absorbance values less

than 5% of positive controls (in both platelet aggregation and neutrophil activation).

6.2.1.2.15 Thrombin assays

Platelet-rich plasma (PRP) should be obtained via centrifugation of whole mouse blood for 20 min at 150 x g. Prior to PRP isolation the whole blood will need to be incubated with SNP samples for 30 min or 4 hr. A Synergy HT multi Detection Microplate Reader (Bio-Tek Instruments, Winooski, USA) will be utilized to determine thrombin generation at excitation/emission wavelength of 360 nm/460 nm.

6.2.1.3 Investigation of chronic inflammatory mechanisms *in vivo* as a function of NP surface properties

6.2.1.3.1 Animal models and treatments

CD-1 mice, 6 - 8 weeks old, should be purchased from Jackson Laboratories (USA). Synthesized SNPs should be injected via tail vein into these mouse models at 20 mg/kg (a concentration previously showing acute toxicity and fibrosis as well as physiologically relevant in drug delivery applications (35 mg/kg, Nanomedicine: Nanotechnology, Biology, and Medicine 8 (2012) 212–220) (21, 29, 53)). Saline should be utilized as a negative control and crystalline silica known to induce silicosis as a positive control. Each treatment method should have 10 mice per time point, for a total of 280 mice; 5 mice should be utilized to assess histology/immunohistochemistry and for protein, RNA and DNA assessment and 5 for biodistribution. At Day=0, mice receive intravenous injection of NPs at maximum concentration in 25 μL of media (approximately 150 μg/mL). On weeks 1, 4, 24 and 60, mice cohorts will be euthanized

by CO_2 asphyxiation. One should include degradation products of degradable silica systems, PLGA particles, gold nanorods and G3.5 dendrimers within this examination to ensure universal applicability, but reduce assessment to 2-, 24- and 60- week time points to reduce animal sacrifice increasing animals by 90 for a total of 370 mice. Large numbers of animal cohorts are necessary since these experiments have previously been unperformed and we are unable to complete a proper power analysis.

6.2.1.3.2 Histology, foreign body response and immunological cell infiltration

Five mice from each time point and treatment will be utilized. Primary accumulation organs (lung, spleen, kidney, liver) should be excised and placed in histological cassettes, fixed in formaline-free zinc fixative (BD PharMingen, San Diego, USA) for 48 hours. Tissue should be embedded in paraffin, stained with hematoxylin and eosin, masson's trichrome to assess the level of macrophage fusion or presence of foreign body giant cells and extent of local fibrosis. The fusion of local macrophages should be determined by counting total numbers of cells with fused nuclei, with foreign body giant cells defined as having three or more nuclei. Immunohistochemical analysis should be performed with the sliced paraffin-embedded blocks, the paraffin should be removed from the tissue sections utilizing EZDeWax solution (Biogenex Lab, San Ramon, CA). Staining should be done with F4/80 and CD11b (for macrophages), CD3 (for T cell infiltration), B220 (for B cell infiltration), IL-3, IL-4, IL-10 and TGF-beta (immunoregulatory cytokines and chemokines), IL-6, TNF-alpha, IFN-gamma, MCP-1 (Th1 type immune response). The slides should then be counterstained with hematoxylin

QS (Vector Laboratories) and observed under the microscope. In gross blinded pathological examination one should look for hard nodules, with enlarged lymphatic nodes. Statistical significance should be determined using one way ANOVA with Bonferroni's multiple comparison post test ($p<0.05$).

6.2.1.3.3 Accumulation, residence and degradation rates of SNPs

Five mice from each time point and treatment should be utilized to assess the relative level of accumulation over time of silica in residence organs. Inductively coupled plasma mass spectrometry should be utilized to quantify silica retention in tissues and blood. After sacrifice, blood should be collected using a heparinized needle from the inferior vena cava and the animals should be perfused with at least 20 mL of saline by cardiac puncture. Blood and organs such as the liver, spleen, lungs, heart and kidneys should be collected and weighed. Each sample should be refluxed in 4 ml of fresh trace-metal grade aqua regia at 90 °C for 24 hrs, and then dried at 130 °C. Subsequently, samples should be dissolved in 4 ml of 5% trace-metal grade nitric acid before quantification of silica content by ICP-MS against a silica internal standard. Statistical significance should be determined using one way ANOVA with Bonferroni's multiple comparison post test ($p<0.05$). The relative level of degradation of the newly developed silica nanoparticles should be assessed via increased clearance rates.

6.2.1.3.4 PK analysis for early degradation of silica nanomaterials

CD-1 mice, 6 - 8 weeks old, will need to be purchased from Jackson Laboratories (Bar Harbor, USA) Synthesized SNPs (1 particles should be tested: 50 nm degradable

particles) should be injected into these mouse models at 20 mg/kg (a concentration previously evaluated to show acute toxicity and fibrosis and is significantly less than recent therapeutic levels of *in vivo* treatments of silica (35 mg/kg, Nanomedicine: Nanotechnology, Biology, and Medicine 8 (2012) 212–220) (21, 29, 53)), saline should be utilized as a negative control and 50 nm Stöber nanoparticles, as a positive control. Each treatment method should have 5 mice per time point, with a total of 90 mice. At Day=0 mice receive intravenous injection of NPs at maximum concentration in 25 μL of solution which should be approximately 20 mg/kg. At 0, 1, 12, 24, 48, and 72 hours mice cohorts should be euthanized by CO2 asphyxiation. Blood and major organs should be collected and ICP-MS should be utilized to assess relative levels of silica accumulation. Metabolic cages should be utilized to extract and quantify the concentration excreted through renal or hepatic means. The relative level of degradation of the newly developed silica nanoparticles can be assessed via increased clearance rates.

6.2.1.3.5 Phases of chronic inflammation

The phase of chronic inflammation should be evaluated utilizing analysis from the histological slides outlined above. Since limited to no evidence has been provided for nanoparticle chronic evaluation, one will assess the levels based on previously reported microspheres (69). One should assess local/chronic inflammation characterized by the pre-defined inflammatory phases outlined below (69). A significant temporal variation in the acute, chronic and developed granulation, foreign body and fibrous encapsulation response should be observed (outlined in the phases).

6.2.1.3.5.1 Phase 1. One should look for minimal inflammatory reaction within the first 2 weeks of treatment with the presence of PMNs, leukocytes, lymphocytes, plasma cell and monocytes. One should expect to see edema, transient myositis and initial injury or damage to local tissue due to deposition of the particles. High levels of monocytes will infiltrate and adopt local macrophage phenotype.

6.2.1.3.5.2 Phase 2. The persistence of this phase depends on the length of time of residence of NPs in the tissue. One should look for creation of foreign body giant cells or highly activated macrophages, as well as the presence of the initial stages of fibrosis and infiltration of fibroblasts. Staining for collagen should also be done at this point to assess the local levels of fibrous capsule formation. One should also assess the local levels of neoangiogenesis and formation of blood capillaries. I believe, as happens in microparticle cases, that we will see this development within 4-20 weeks after the initial acute phase reaction.

6.2.1.3.5.3 Phase 3. Enhancement of the fibrous capsule will take place with large increases in local inflammatory response, including increased neovascularization, collagen deposition, and fibroblast infiltration. The rate of NP degradation will facilitate the time length that NPs reside within this phase. I propose that it is possible with nondegradable systems to continue to maintain this phase for the animal's life due to the inability to secrete the local nanomaterials. During each phase, at least two people should assess local histological sections, utilizing a scoring system to assess the levels of infiltration, extent of collagen deposition and levels of local vascularization. One should utilize a blind evaluation with a rating system of - = no infiltration and ++++ will = extensive infiltration. Statistical significance should be determined using one-way

ANOVA with Bonferroni's multiple comparison post test ($p<0.05$).

6.2.1.3.6 Connecting fibrosis and autophagic activation

6.2.1.3.6.1 Immunohistochemistry and Western blot. Five mice should be used from each time point. One should stain for autophagic markers (i.e., LC3 transition from I to II), to verify autophagy at each time point. Sections should be washed with phosphate-buffered saline (PBS; pH 7.4) and blocked. They should be incubated overnight at 4°C with primary antibody and the following day the slices should be incubated for 2 h with fluorochrome-coupled secondary antibody at room temperature. A confocal microscope should detect the following autophagic immunohistochemistry markers: anti-microtubule-associated protein 1 light chain 3, anti- beclin-1, anti-caspase-3 and anti-p62. Western blot should be run on digested samples with similar primary markers to quantify levels in tissue over time to back correlate autophagic markers to phases of chronic inflammation and levels of fibrosis. Statistical significance should be determined using one way ANOVA with Bonferroni's multiple comparison post test ($p<0.05$).

6.2.1.3.6.2 Real time PCR analysis. One should further refine the induction of inflammatory genes that are obtained from aim two and assess the local tissue levels for inflammatory and fibrotic markers to help correlate stages of inflammation to fibrotic levels. Statistical significance should be determined using one way ANOVA with Bonferroni's multiple comparison post test ($p<0.05$).

6.3 References

1. Perez-Carrion MD, Perez-Martinez FC, Merino S, Sanchez-Verdu P, Martinez-Hernandez J, Lujan R, et al. Dendrimer-mediated siRNA delivery knocks down Beclin 1 and potentiates NMDA-mediated toxicity in rat cortical neurons. J Neurochem. 2012;120(2):259-68.

2. Vercauteren D, Deschout H, Remaut K, Engbersen JF, Jones AT, Demeester J, et al. Dynamic colocalization microscopy to characterize intracellular trafficking of nanomedicines. ACS Nano. 2011;5(10):7874-84.

3. Murray PJ, Wynn TA. Protective and pathogenic functions of macrophage subsets. Nature Reviews Immunology. 2011;11(11):723-37.

4. Albanese A, Sykes EA, Chan WC. Rough around the edges: the inflammatory response of microglial cells to spiky nanoparticles. ACS Nano. 2010;4(5):2490-3.

5. Kleinman MT, Araujo JA, Nel A, Sioutas C, Campbell A, Cong PQ, et al. Inhaled ultrafine particulate matter affects CNS inflammatory processes and may act via MAP kinase signaling pathways. Toxicol Lett. 2008;178(2):127-30.

6. Lim D-H, Jang J, Kim S, Kang T, Lee K, Choi I-H. The effects of sub-lethal concentrations of silver nanoparticles on inflammatory and stress genes in human macrophages using cDNA microarray analysis. Biomaterials. 2012;33(18):4690-9.

7. Monks J, Rosner D, Geske FJ, Lehman L, Hanson L, Neville M, et al. Epithelial cells as phagocytes: apoptotic epithelial cells are engulfed by mammary alveolar epithelial cells and repress inflammatory mediator release. Cell Death & Differentiation. 2005;12(2):107-14.

8. Nishanth RP, Jyotsna RG, Schlager JJ, Hussain SM, Reddanna P. Inflammatory responses of RAW 264.7 macrophages upon exposure to nanoparticles: role of ROS-NFκB signaling pathway. Nanotoxicology. 2011;5(4):502-16.

9. Park EJ, Park K. Oxidative stress and pro-inflammatory responses induced by silica nanoparticles in vivo and in vitro. Toxicol Lett. 2009;184(1):18-25.

10. Petrovski G, Zahuczky G, Majai G, Fesus L. Phagocytosis of cells dying through autophagy evokes a pro-inflammatory response in macrophages. Autophagy. 2007;3(5):509-11.

11. Sindrilaru A, Peters T, Wieschalka S, Baican C, Baican A, Peter H, et al. An unrestrained proinflammatory M1 macrophage population induced by iron impairs wound healing in humans and mice. The Journal of Clinical Investigation. 2011;121(3):985.

12. Velard F, Braux J, Amedee J, Laquerriere P. Inflammatory cell response to calcium phosphate biomaterial particles: an overview. Acta Biomater. 2013;9(2):4956-63.

13. Xu Y, Krause A, Hamai H, Harvey BG, Worgall TS, Worgall S. Proinflammatory phenotype and increased caveolin-1 in alveolar macrophages with silenced CFTR mRNA. PLoS One. 2010;5(6):e11004.

14. Yang M, Flavin K, Kopf I, Radics G, Hearnden CH, McManus GJ, et al. Functionalization of carbon nanoparticles modulates inflammatory cell recruitment and NLRP3 inflammasome activation. Small. 2013;9(24):4194-206.

15. Zhang Q, Hitchins VM, Schrand AM, Hussain SM, Goering PL. Uptake of gold nanoparticles in murine macrophage cells without cytotoxicity or production of pro-inflammatory mediators. Nanotoxicology. 2011;5(3):284-95.

16. Kim J, Seok YM, Jung KJ, Park KM. Reactive oxygen species/oxidative stress contributes to progression of kidney fibrosis following transient ischemic injury in mice. Am J Physiol Renal Physiol. 2009;297(2):F461-70.

17. Herd HL, Malugin A, Ghandehari H. Silica nanoconstruct cellular toleration threshold in vitro. J Control Release. 2011;153(1):40-8.

18. Malugin A, Ghandehari H. Caspase 3 independent cell death induced by amorphous silica nanoparticles. Nanoscience and Nanotechnology Letters. 2011;3(3):309-13.

19. Malugin A, Herd H, Ghandehari H. Differential toxicity of amorphous silica nanoparticles toward phagocytic and epithelial cells. Journal of Nanoparticle Research. 2011;13(10):5381-96.

20. Moos PJ, Honeggar M, Malugin A, Herd H, Thiagarajan G, Ghandehari H. Transcriptional responses of human aortic endothelial cells to nanoconstructs used in biomedical applications. Mol Pharm. 2013;10(8):3242-52.

21. Yu T, Malugin A, Ghandehari H. Impact of silica nanoparticle design on cellular toxicity and hemolytic activity. ACS Nano. 2011;5(7):5717-28.

22. Yu T, Greish K, McGill LD, Ray A, Ghandehari H. Influence of geometry, porosity, and surface characteristics of silica nanoparticles on acute toxicity: their vasculature effect and tolerance threshold. ACS Nano. 2012;6(3):2289-301.

23. Herd H, Daum N, Jones AT, Huwer H, Ghandehari H, Lehr CM. Nanoparticle geometry and surface orientation influence mode of cellular uptake. ACS Nano. 2013;7(3):1961-73.

24. Herd H, Ghandehari H. Synthetic and toxicological characteristics of silica nanomaterials for imaging and drug delivery applications. Sitharaman B, editor. Boca Raton, FL: CRC Press; 2011.

25. Herd H, Ghandehari H. Phagocytic silica nanoparticle response is phenotypically dependent. Submitted to Biomaterials.

26. Jones CF, Campbell RA, Brooks AE, Assemi S, Tadjiki S, Thiagarajan G, et al. Cationic PAMAM dendrimers aggressively initiate blood clot formation. ACS Nano. 2012;6(11):9900-10.

27. Churg A, Wright JL. Small-airway lesions in patients exposed to nonasbestos mineral dusts. Hum Pathol. 1983;14(8):688-93.

28. Moriyama H, Kobayashi M, Takada T, Shimizu T, Terada M, Narita J, et al. Two-dimensional analysis of elements and mononuclear cells in hard metal lung disease. Am J Respir Crit Care Med. 2007;176(1):70-7.

29. Yu T, Hubbard D, Ray A, Ghandehari H. In vivo biodistribution and pharmacokinetics of silica nanoparticles as a function of geometry, porosity and surface characteristics. J Control Release. 2012;163(1):46-54.

30. Thiagarajan G, Sadekar S, Greish K, Ray A, Ghandehari H. Evidence of oral translocation of anionic G6.5 dendrimers in mice. Mol Pharm. 2013;[Epub ahead of print].

31. Thiagarajan G, Greish K, Ghandehari H. Charge affects the oral toxicity of poly(amidoamine) dendrimers. European Journal of Pharmaceutics and Biopharmaceutics: Official Journal of Arbeitsgemeinschaft fur Pharmazeutische Verfahrenstechnik eV. 2013;[Epub ahead of print].

32. Jones CF, Campbell RA, Franks Z, Gibson CC, Thiagarajan G, Vieira-de-Abreu A, et al. Cationic PAMAM dendrimers disrupt key platelet functions. Mol Pharm. 2012;9(6):1599-611.

33. Greish K, Thiagarajan G, Herd H, Price R, Bauer H, Hubbard D, et al. Size and surface charge significantly influence the toxicity of silica and dendritic nanoparticles. Nanotoxicology. 2012;6(7):713-23.

34. Greish K, Thiagarajan G, Ghandehari H. In vivo methods of nanotoxicology. Methods Mol Biol. 2012;926:235-53.

35. Wang L, Reis A, Seifert A, Philippi T, Ernst S, Jia M, et al. A simple procedure for the covalent grafting of triphenylphosphine ligands on silica: application in the palladium catalyzed Suzuki reaction. Dalton Trans. 2009(17):3315-20.

36. Stöber W, Fink A, Bohn E. Controlled growth of monodisperse silica spheres in the micron size range. Journal of Colloid and Interface Science. 1968;26(1):62-9.

37. Hiramatsu H, Osterloh FE. pH-controlled assembly and disassembly of electrostatically linked CdSe-SiO2 and Au-SiO2 nanoparticle clusters. Langmuir. 2003;19(17):7003-11.

38. Bergen JM, Von Recum HA, Goodman TT, Massey AP, Pun SH. Gold nanoparticles as a versatile platform for optimizing physicochemical parameters for targeted drug delivery. Macromolecular Bioscience. 2006;6(7):506-16.

39. Valencia PM, Hanewich-Hollatz MH, Gao W, Karim F, Langer R, Karnik R, et al. Effects of ligands with different water solubilities on self-assembly and properties of targeted nanoparticles. Biomaterials. 2011;32(26):6226-33.

40. Sadekar S, Ghandehari H. Transepithelial transport and toxicity of PAMAM dendrimers: implications for oral drug delivery. Adv Drug Deliv Rev. 2012;64(6):571-88.

41. Brozek EM, Zharov I. Internal functionalization and surface modification of vinylsilsesquioxane nanoparticles. Chem Mater. 2009;21(8):1451-6.

42. Gao Z. 2013;University of Utah, Ph.D. Thesis.

43. Yoon SB, Kim J-Y, Kim JH, Park YJ, Yoon KR, Park S-K, et al. Synthesis of monodisperse spherical silica particles with solid core and mesoporous shell: mesopore channels perpendicular to the surface. J Mater Chem. 2007;17(18):1758-61.

44. Zhao B, Collinson MM. Well-defined hierarchical templates for multimodal porous material fabrication. Chemistry of Materials. 2010;22(14):4312-9.

45. Souza D, Andrade A, Fabris J, Valério P, Góes A, Leite M, et al. Synthesis and in vitro evaluation of toxicity of silica-coated magnetite nanoparticles. Journal of Non-Crystalline Solids. 2008;354(42):4894-7.

46. Nieto A, Areva S, Wilson T, Viitala R, Vallet-Regi M. Cell viability in a wet silica gel. Acta Biomater. 2009;5(9):3478-87.

47. Khonina T, Chupakhin O, Larionov L, Boyakovskaya T, Suvorov A, Shadrina E. Synthesis, toxicity, and percutaneous activity of silicon glycerolates and related hydrogels. Pharmaceutical Chemistry Journal. 2008;42(11):609-13.

48. Czuryszkiewicz T, Areva S, Honkanen M, Lindén M. Synthesis of sol–gel silica materials providing a slow release of biphosphonate. Colloids and Surfaces A: Physicochemical and Engineering Aspects. 2005;254(1):69-74.

49. Zalzberg L, Avnir D. Biocompatible hybrid particles of poly (L-lactic acid)@

silica. Journal of Sol-Gel Science and Technology. 2008;48(1):47-50.

50. Nuraje N, Su K, Matsui H. Catalytic growth of silica nanoparticles in controlled shapes at planar liquid/liquid interfaces. New Journal of Chemistry. 2007;31(11):1895-8.

51. Beletsi A, Leontiadis L, Klepetsanis P, Ithakissios DS, Avgoustakis K. Effect of preparative variables on the properties of poly(dl-lactide-co-glycolide)-methoxypoly(ethyleneglycol) copolymers related to their application in controlled drug delivery. Int J Pharm. 1999;182(2):187-97.

52. Ottonello L, Frumento G, Arduino N, Dapino P, Tortolina G, Dallegri F. Immune complex stimulation of neutrophil apoptosis: investigating the involvement of oxidative and nonoxidative pathways. Free Radic Biol Med. 2001;30(2):161-9.

53. Zupke O, Distler E, Baumann D, Strand D, Meyer R, Landfester K, et al. Preservation of dendritic cell function upon labeling with amino functionalized polymeric nanoparticles. Biomaterials. 2010;31(27):7086-95.

54. Martinez FO, Helming L, Gordon S. Alternative activation of macrophages: an immunologic functional perspective. Annual Review of Immunology. 2009;27:451-83.

55. Tjiu J-W, Chen J-S, Shun C-T, Lin S-J, Liao Y-H, Chu C-Y, et al. Tumor-associated macrophage-induced invasion and angiogenesis of human basal cell carcinoma cells by cyclooxygenase-2 induction. Journal of Investigative Dermatology. 2009;129(4):1016-25.

56. Ehrenberg MS, Friedman AE, Finkelstein JN, Oberdorster G, McGrath JL. The influence of protein adsorption on nanoparticle association with cultured endothelial cells. Biomaterials. 2009;30(4):603-10.

57. Higuchi A, Sugiyama K, Yoon BO, Sakurai M, Hara M, Sumita M, et al. Serum protein adsorption and platelet adhesion on pluronic-adsorbed polysulfone membranes. Biomaterials. 2003;24(19):3235-45.

58. Gessner A, Lieske A, Paulke B, Muller R. Influence of surface charge density on protein adsorption on polymeric nanoparticles: analysis by two-dimensional electrophoresis. European Journal of Pharmaceutics and Biopharmaceutics: Official Journal of Arbeitsgemeinschaft fur Pharmazeutische Verfahrenstechnik eV. 2002;54(2):165-70.

59. Gessner A, Waicz R, Lieske A, Paulke B, Mader K, Muller RH. Nanoparticles with decreasing surface hydrophobicities: influence on plasma protein adsorption. Int J Pharm. 2000;196(2):245-9.

60. Ho CH, Hlady V, Nyquist G, Andrade JD, Caldwell KD. Interaction of plasma proteins with heparinized gel particles studied by high-resolution two-dimensional gel

electrophoresis. J Biomed Mater Res. 1991;25(4):423-41.

61. Luck M, Paulke BR, Schroder W, Blunk T, Muller RH. Analysis of plasma protein adsorption on polymeric nanoparticles with different surface characteristics. J Biomed Mater Res. 1998;39(3):478-85.

62. Höök F, Vörös J, Rodahl M, Kurrat R, Böni P, Ramsden J, et al. A comparative study of protein adsorption on titanium oxide surfaces using in situ ellipsometry, optical waveguide lightmode spectroscopy, and quartz crystal microbalance/dissipation. Colloids and Surfaces B: Biointerfaces. 2002;24(2):155-70.

63. Lundqvist M, Sethson I, Jonsson BH. Protein adsorption onto silica nanoparticles: conformational changes depend on the particles' curvature and the protein stability. Langmuir. 2004;20(24):10639-47.

64. Moirangthem RS, Chang YC, Wei PK. Ellipsometry study on gold-nanoparticle-coated gold thin film for biosensing application. Biomed Opt Express. 2011;2(9):2569-76.

65. Mrksich M, Sigal GB, Whitesides GM. Surface plasmon resonance permits in situ measurement of protein adsorption on self-assembled monolayers of alkanethiolates on gold. Langmuir. 1995;11(11):4383-5.

66. Chang JT, Nevins JR. GATHER: a systems approach to interpreting genomic signatures. Bioinformatics. 2006;22(23):2926-33.

67. Yang L, Yatomi Y, Satoh K, Ozaki Y. Inhibitory effects of beraprost on platelet aggregation: comparative study utilizing two methods of aggregometry. Thromb Res. 1999;94(1):25-32.

68. Xue JM, Tan CH, Lukito D. Biodegradable polymer-silica xerogel composite microspheres for controlled release of gentamicin. J Biomed Mater Res B Appl Biomater. 2006;78(2):417-22.

69. Shive MS, Anderson JM. Biodegradation and biocompatibility of PLA and PLGA microspheres. Adv Drug Deliv Rev. 1997;28(1):5-24.

APPENDIX A

SUPPLEMENTAL INFORMATION FOR: SILICA NANOCONSTRUCT CELLULAR TOLERATION THRESHOLD *IN VITRO*

Heather L Herd, Alexander Malugin,
Hamidreza Ghandehari

The Journal of Controlled Release, 2011;153: Appendix A(1-5)

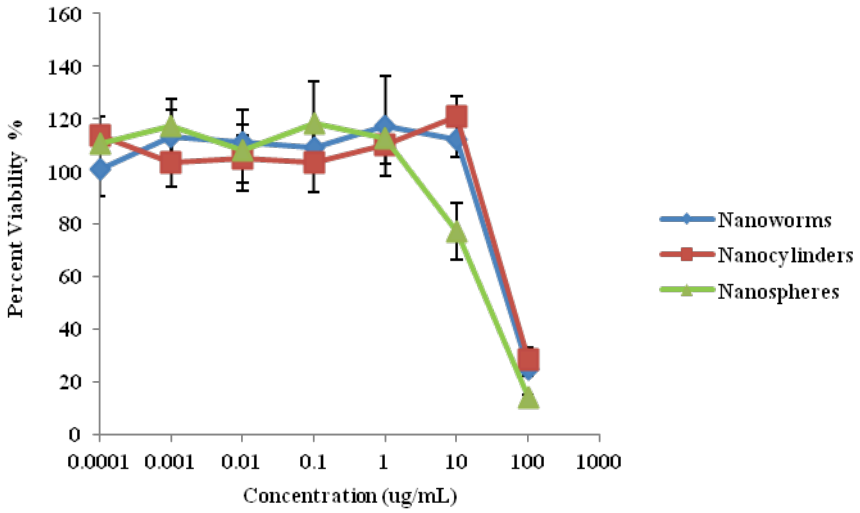

Figure A.1: RAW 264.7 cellular viability profiles after 72 hour incubation with various concentrations of silica nanoconstructs. The values of 3 different experiments are shown. Proliferative functional alteration was not observed up to approximately 50 ug/mL at which point there was a rapid fall off in proliferation, suggesting a threshold level of activation.

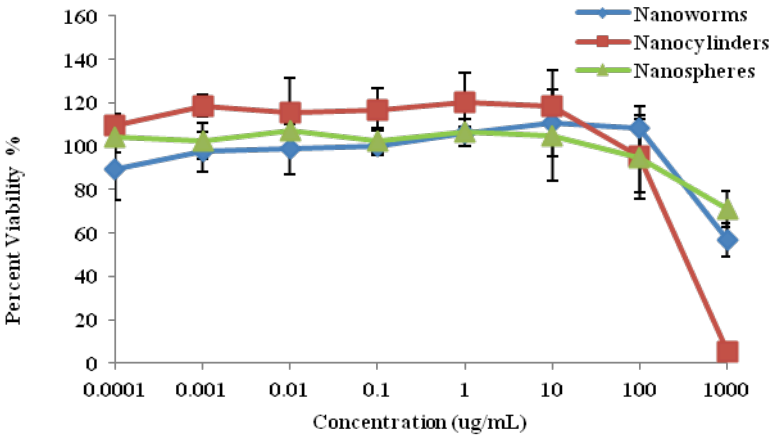

Figure A.2: A549 cellular viability profiles after 72 hour incubation with various concentrations of silica nanoconstructs. The values of 3 different experiments are shown. Proliferative functional alteration was not observed up to approximately 50 ug/mL at which point there was a rapid fall off in proliferation, suggesting a threshold level of activation.

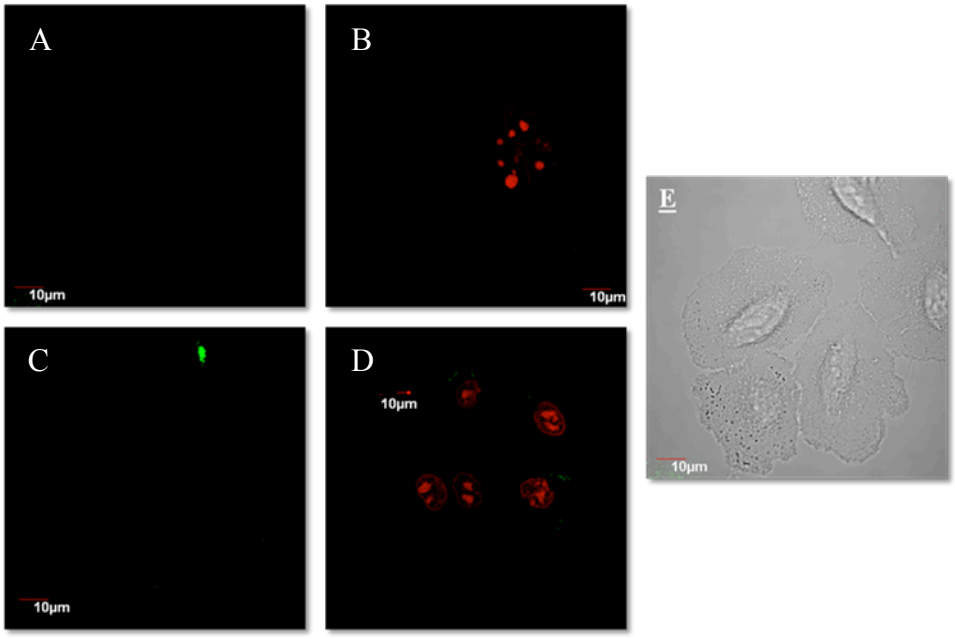

Figure A.3: Mode of cell death induced in A549 cells after 24 hours of incubation with 500 µg/mL of silica nanoparticles. Annexin V (green) staining provides evidence of apoptotic cell death and PI (red) staining provides evidence of necrotic cell death. The combination of the two dyes is usually indicative of late stage apoptosis or necrosis. Representative single plane confocal images of: A) Control; B) Spheres. C) Worms; and D) Cylinders.

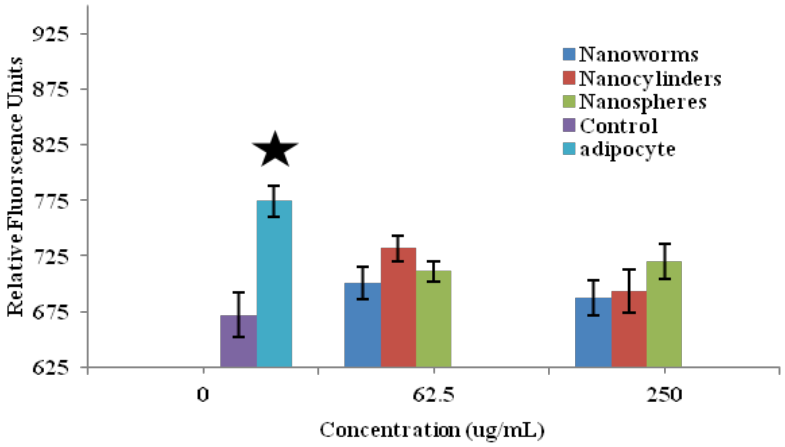

Figure A.4: Relative levels of activated caspase 3 in silica nanoconstruct treated A549 cells. Statistically only adipocyte (positive control) showed a relative change in caspase activation when compared to control. All other treatments provide the same relative fluorescence due to cell treatment and washing. The star indicates a statistically significant increase in caspase activation when compared to control.

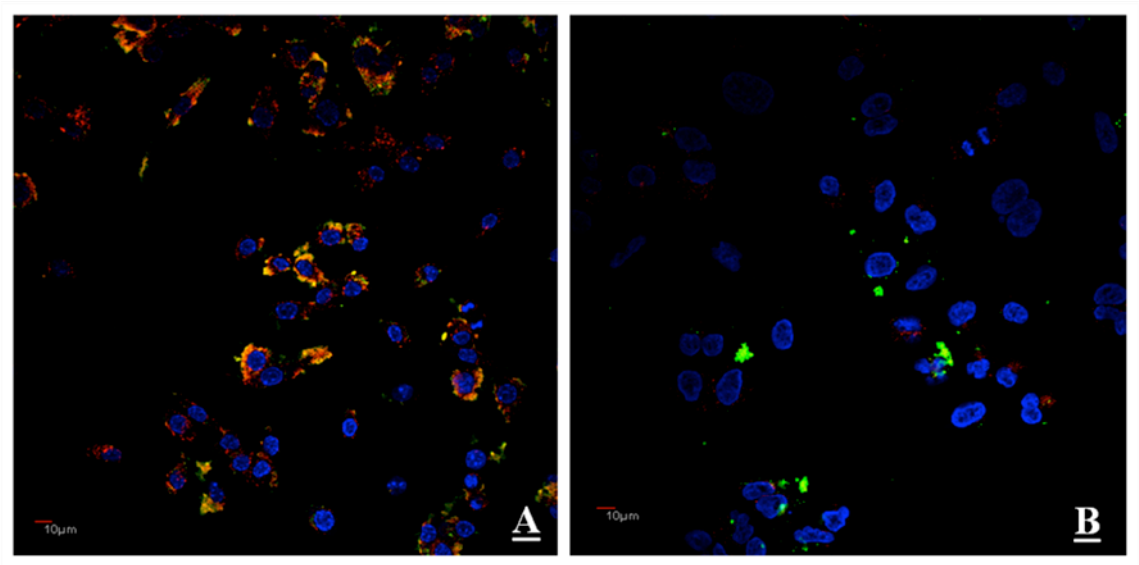

Figure A.5: Assessment of modes of silica nanoparticle uptake by confocal imaging. Modes of nanoparticle uptake were assessed by co-incubating transferrin with each nanoconstruct and analyzing the relative co-localization of the two. Transferrin (red) and 50 μg/mL construct (green) were co-incubated for ~4 hours. Nuclei (blue) of cells were stained with DRAQ5 following incubation. A) Cylinders in RAW 264.7; B) Worms in A549 Cells.

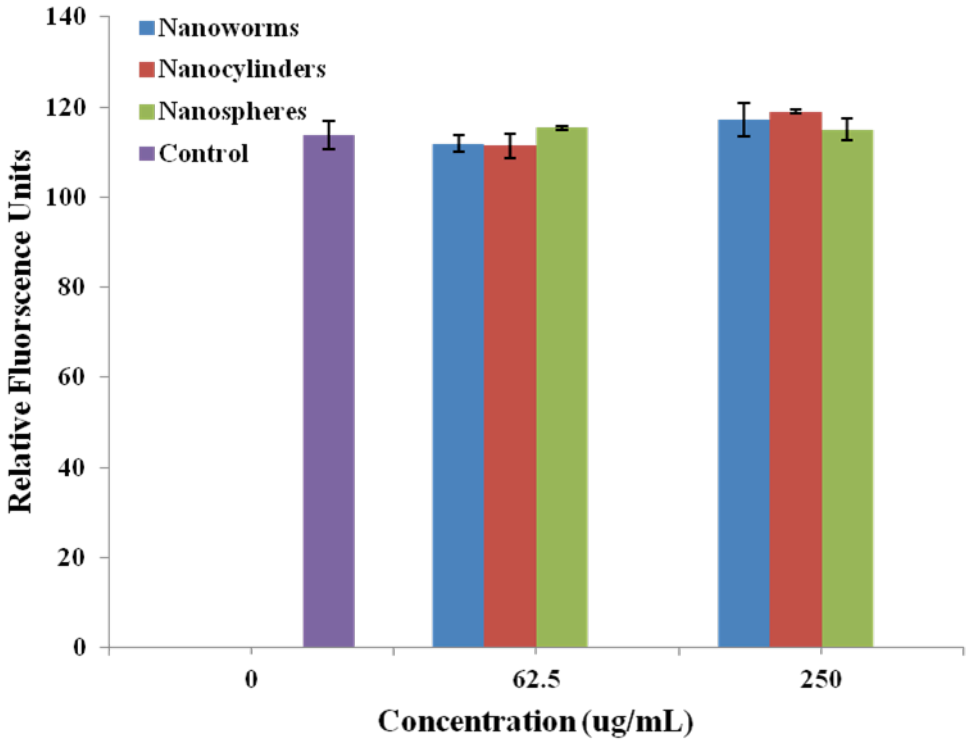

Figure A.6: Phagocytic activity of RAW 264.7 cells in the presence of nanoconstructs

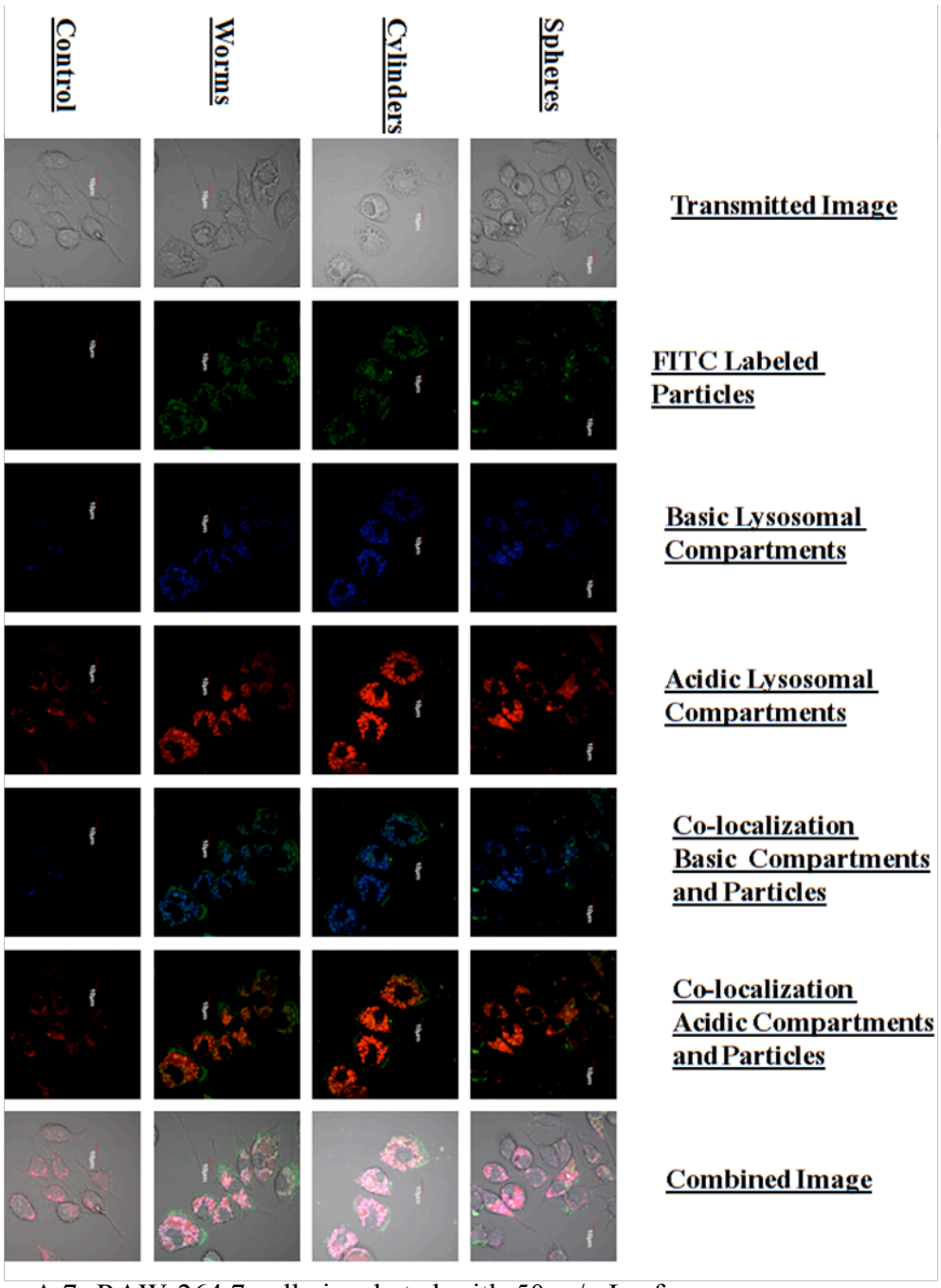

Figure A.7: RAW 264.7 cells incubated with 50μg/mL of worms: green corresponds to FITC labeled particles; blue corresponds to basic lysosomal compartments; red corresponds to acidic lysosomal compartments; orange corresponds to colocalization with acidic compartments and pink corresponds to colocalization with basic compartments.

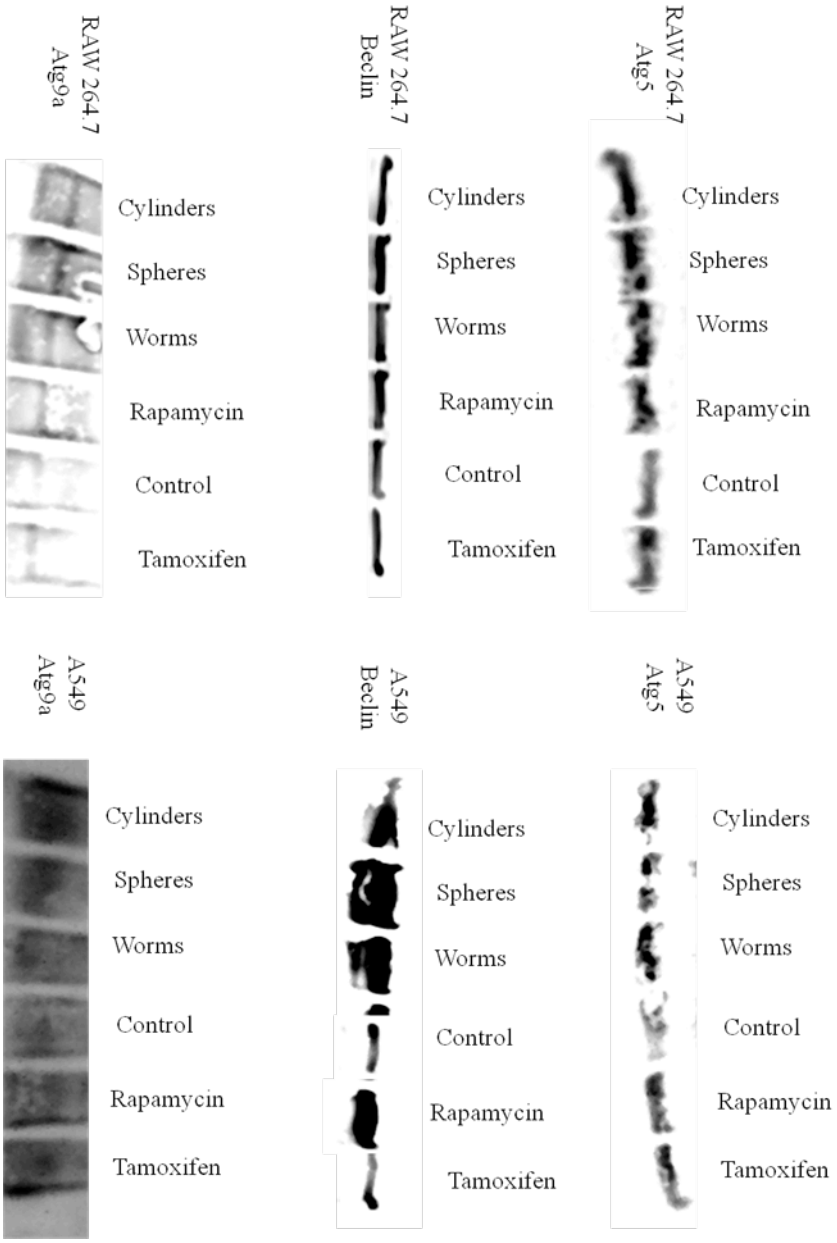

Figure A.8: Western blot images of expressed proteins Atg9a, Beclin and Atg5 in both A549 and RAW 264.7 cell lines. Tamoxifen and Rapamycin were utilized as positive controls, to ensure autophagic expression.

APPENDIX B

SUPPLEMENTAL INFORMATION FOR: NANOPARTICLE GEOMETRY AND SURFACE ORIENTATION INFLUENCE MODE OF CELLULAR UPTAKE

Heather L Herd, Nicole Daum, Arwyn T. Jones,
Hanno Huwer, Hamidreza Ghandehari,
Claus Michael-Lehr

ACS Nano, 2013;7(3):Appendix A(1-15)

Table B.1 Physicochemical characterization of silica nanoparticles

Nanoparticle	Spheres	Cylinders	*Worms*
Size (TEM)	178 ± 27 nm	214 ± 29 nm x 428 ± 66 nm	*232 ± 22 nm x 1348 ± 314 nm*
Dynamic Light Scattering (DLS)	240 ± 20 nm	369 ± 85 nm*	*598.2 ± 119.8 nm**
DLSin Media Containing Serum	355 ± 162 nm**	511± 128 nm **	*583 ± 292 nm***
Fluorescent Units Per Particle	~8 units per particle***	~9 units per particle***	*~11 units per particle****
Zeta Potential	58 mV	79 mV	*87 mV*
Zeta Potential in Media Containing Serum	-8 mV**	-8 mV**	*-8 mV***

**Please note that these particles are not spherical, so the information may not reflect the actual particle configuration, as the DLS theory assumes spherical conformation.*
Serum proteins are also present in significant quantities so results may not reflect the measurements of just the particles or the attachment of the proteins to the surface of the particles. Due to the presence of multiple peaks in the spectra, only the most relevant peak is reported that was not present in just media containing serum.Fluorescent units were determined utilizing a standard fluorescence curve of known FITC concentration. The fluorescence per particle was determined utilizing the surface area of each particle and a density of 2.6 g/mL for silica nanoconstructs.*

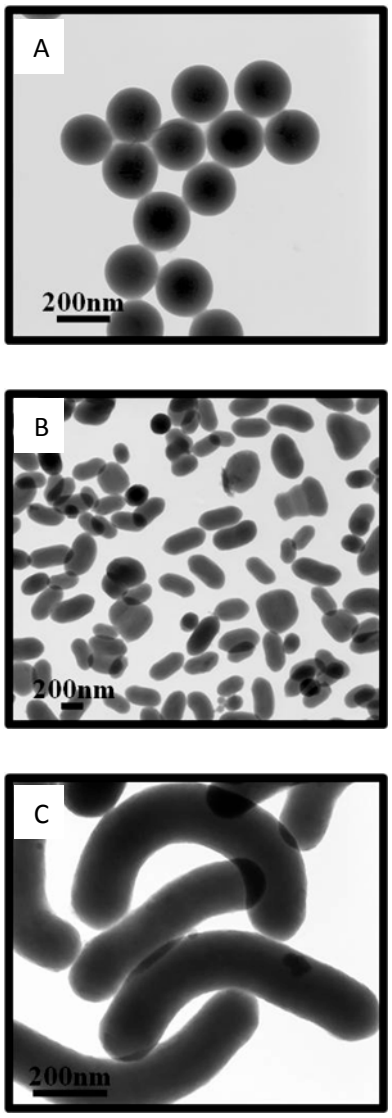

Figure B.1: TEM images of silica nanoparticles used in this study. A: Spheres, B: Rods, C: Worms. Scale bars indicate 200 nm.

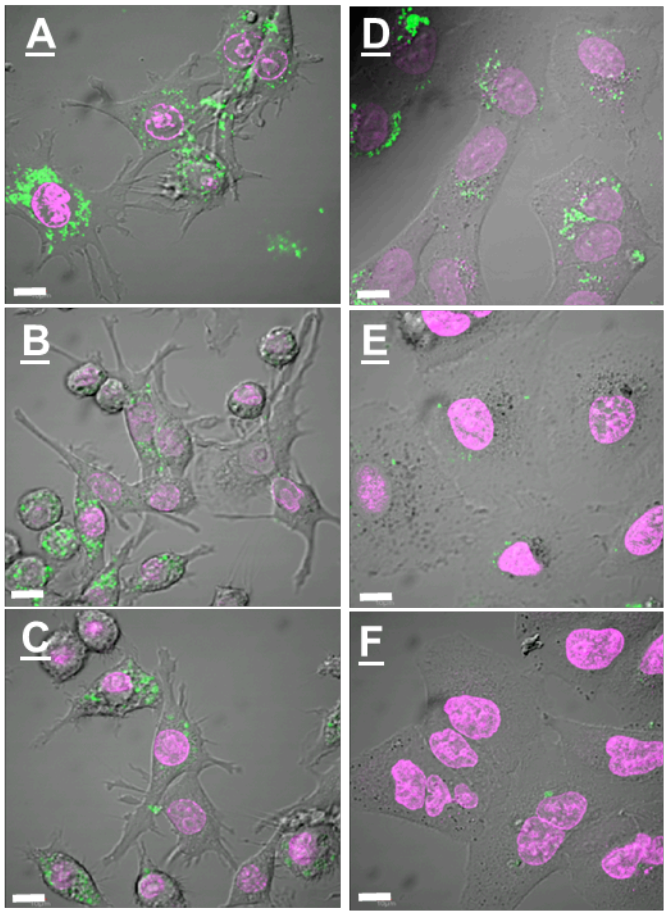

Figure B.2: Confocal images of 50 µg/mL silica nanoconstruct uptake after 24 hours of incubation in RAW264.7 (left) and A549 cells (right). Cell nucleus in pink and particles in green A and D) Worms; B and E) Cylinders; C and F) Spheres. All nanoparticles were observed to be taken up into cells. Scale bar 10 µm.

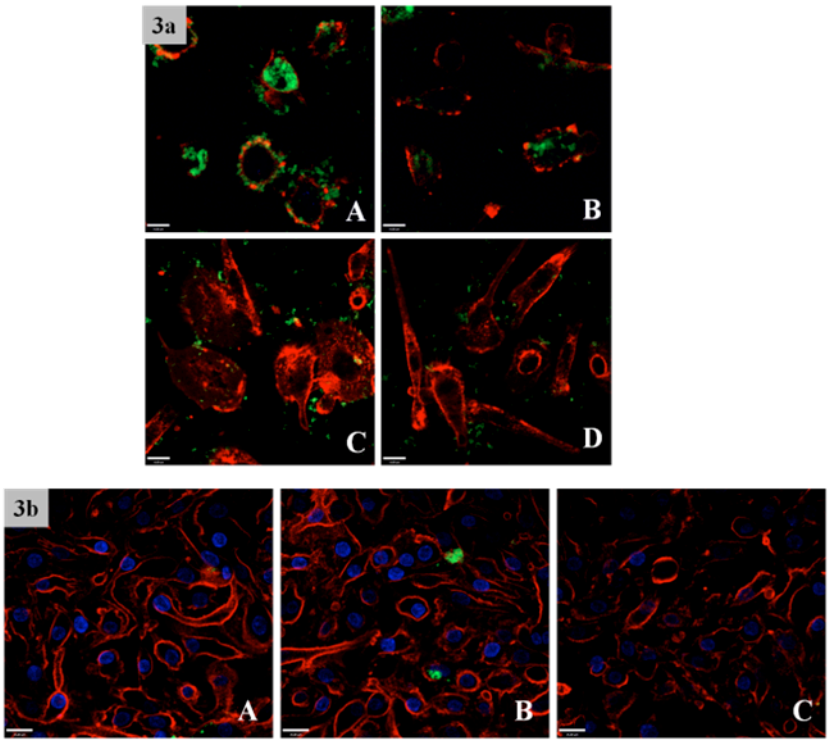

Figure B.3: Confocal image analysis of preliminary uptake of nanoparticles within primary cells. **3a:** Primary macrophage confocal image (membrane stained red) uptake of silica nanoparticles (green). A and B) Alveolar macrophages treated with 75 µg/mL of spherical and worm like nanoparticles, respectively. C and D) Tissue macrophages treated with 75 µg/mL of spherical and worm like nanoparticles, respectively. Alveolar macrophages (A and B), as this figure demonstrates when correlated to our FACS analysis in Figure 4.1, there is a greater degree of nanoparticle uptake when compared to tissue macrophage uptake where much of fluorescence was associated with the cell membrane (C and D). It is also important to note that macrophages treated with spherical nanoparticles (A and D) when compared to worm like nanoparticles (B and D) appear to have a greater degree of nanoparticle uptake (at this time point, 1.5 hours). This suggests a phenotypic and geometric implication. **3b:** Confocal image of uptake of silica nanoparticle constructs in alveolar epithelial cells; limited uptake of silica nanoconstructs was observed in primary epithelial cells similar to what is observed in FACS results presented in Figure 4.1b. Particles (green) at a concentration of 50µg/mL were incubated with primary alveolar epithelial cells for two hours, following incubation to help with cellular visualization of the cell membrane stained with Rhodamine-WGA (red) and nucleus stained with DAPI following cellular fixation; A) Cylinder incubation, B) Spherical incubation, C) Worm incubation. Scale bar = 14.0µm.

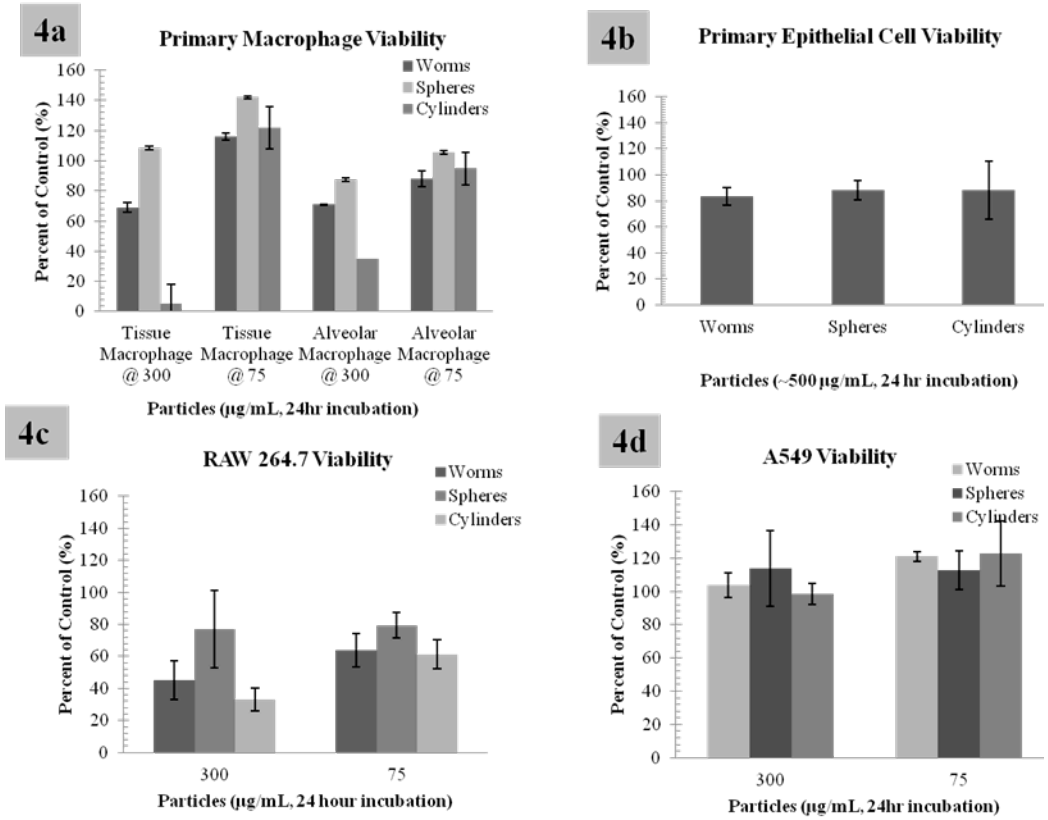

Figure B.4: Vialight assay, assessing the relative ATP level in metabolically active cells. **4a** and **4b**: Vialight assay, assessing the relative ATP level in metabolically active cells. In **4a**, macrophages exhibit a varied response. When exposed to high concentrations of silica nanoparticle constructs they exhibit a degree of toxicity while they appear to tolerate lower concentrations. As shown in **4b**, alveolar epithelial cells show very little decrease in cell viability when exposed to silica nanoparticle constructs **4c**: RAW 264.7 macrophages exhibit a varied response. When exposed to high concentrations of silica nanoparticle constructs they exhibit a degree of toxicity while tolerating lower concentrations. **4d:** A549 epithelial cells show very little decrease in cell viability when exposed to silica nanoparticle constructs. Please note: graphs are represented as percentage of control or the background viability of cells incubated without nanoparticles.

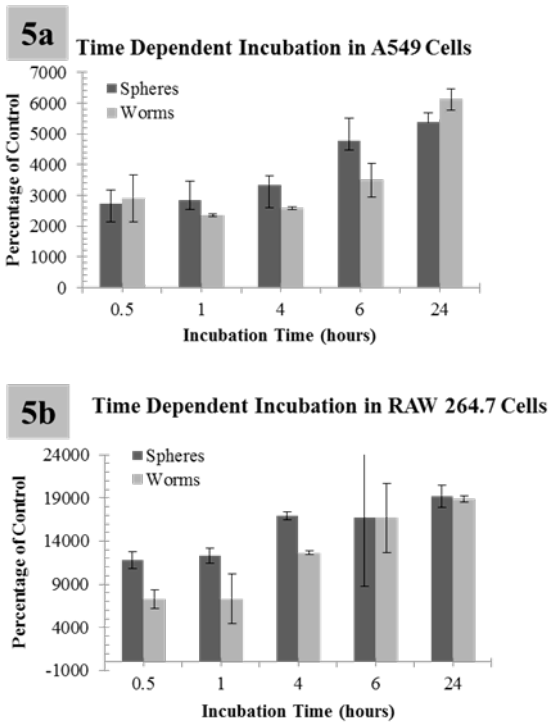

Figure B.5: Time dependent fluorescence uptake of silica nanoparticles. 5a and 5b) All time points tested were of 75 μg/mL in RAW 264.7 cells and A549 cells respectively. A gradual increase in concentration uptake was observed in cells until a concentration threshold was achieved. Above this threshold cells no longer took up nanoparticles. Please note: graphs are represented as percentage of control or the background provided by FACS analysis of cells incubated without nanoparticles. Low levels of autofluorescence were indicated for immortalized lines.

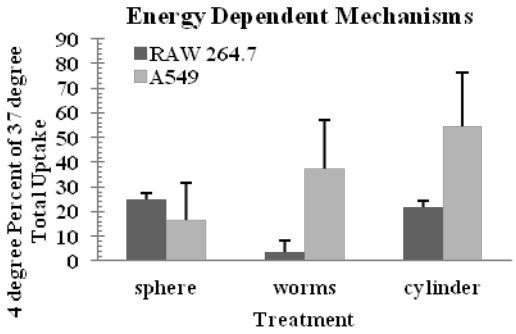

Figure B.6: Uptake of nanoparticles as a function of temperature in model cell lines. The graph provides confirmation of energy dependent mechanisms of uptake. Please note: graph is represented as percentage of uptake at 37 degrees of the respective nanoparticle at 4 degrees. So at 4 degrees RAW 264.7 cells exhibit ~25% of the spherical uptake that they exhibit at 37 degrees.

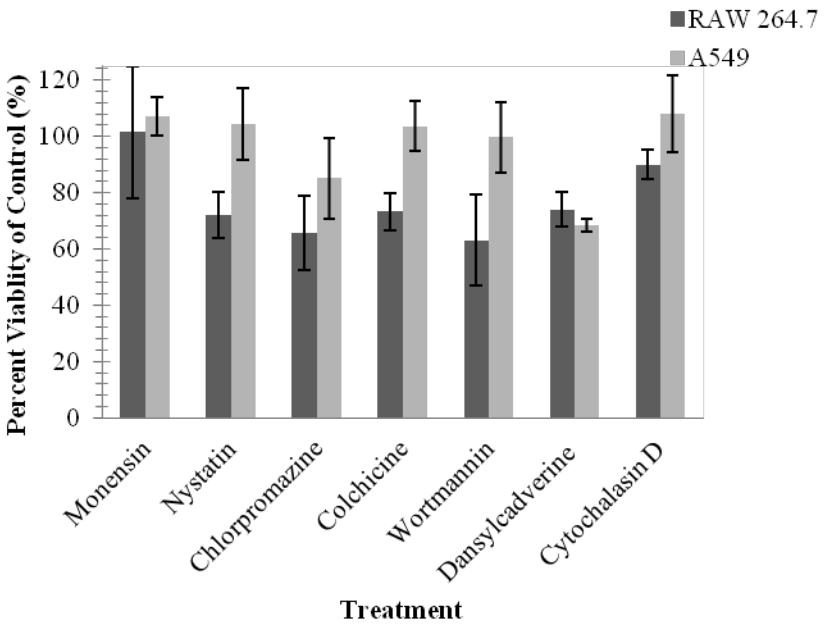

Figure B.7: ATP in metabolically active cells following treatment with uptake inhibitors. Caveolin dependent endocytosis was assessed utilizing Nystatin at a 30 minute pre-incubation at 20 µg/mL. Clathrin dependent endocytosis was assessed utilizing a 30 min pre-incubation with either 100 µmol of Dansylcadaverine or 10 µg/mL of Chlorpromazine. Clathrin and caveolin independent endocytosis were assessed utilizing a 30-minute pretreatment with 30 µg/mL Monensin. Phagocytosis and macropinocytosis were assessed utilizing a 1-hr incubation with 10 µmol or 10 nmol concentrations of Wortmannin or a 30-minute preincubation with 2 µg/mL of Colchicine.

Table B.2
GATHER analysis of upregulated genes of the PI3-kinase pathway

TMΦ Worm	TMΦ Sphere	AMΦ Worm	AMΦ Sphere	GO Analysis	MESH Analysis	KEGG Analysis
	AKT1			Regulation of Cell Growth, Cell Growth, Regulation of Cell Size and Shape, Cellular Morphogenesis, Signal transduction, Cell Communication, Cell Surface Receptor Linked Signal Transduction	Phosphoproteins	Insulin Signaling Pathway, Focal Adhesion, Apoptosis, Toll-like Receptor Signaling Pathway
AKT3	AKT3			Protein Amino Acid Phosphorylation, Phosphorylation, Phosphorus Metabolism, Signal Transduction, Cell Communication		Apoptosis, Toll-like Receptor Signaling Pathway, Insulin Signaling Pathway, Focal Adhesion
	BAD					Apoptosis
	CASP9					Apoptosis
CSNK2A1	CSNK2A1			Protein Amino Acid Phosphorylation, Phosphorylation, Phosphorus Metabolism, Cellular Morphogenesis, Cell Growth and Regulation	Phosphoproteins	

Table B.2 (continued)

TMΦ Worm	TMΦ Sphere	AMΦ Worm	AMΦ Sphere	GO Analysis	MESH Analysis	KEGG Analysis
CTNNB1	CTNNB1			Signal Transduction, Cell Communication, Signal Transduction, Cell Surface Receptor Linked Signal Transduction		Focal Adhesion
	EIF4B					
EIF4EBP1	EIF4EBP1			Signal Transduction	Phosphoproteins	Toll like Receptor Signaling Pathway, Insulin Signaling Pathway
FOXO3	FOXO3					
	JUN					Focal Adhesion, Toll-like Receptor Signaling Pathway
MTOR	MTOR			Protein Amino Acid Phosphorylation, Phosphorylation, Phosphorus Metabolism, Cellular Proliferation	Ribosomal S6 Kinases, Phosphoproteins	

Table B.2 (continued)

TMΦ Worm	TMΦ Sphere	AMΦ Worm	AMΦ Sphere	GO Analysis	MESH Analysis	KEGG Analysis
ITGB1	ITGB1			Signal Transduction, Cell Communication, Cell Surface Receptor Linked Signal Transduction		Focal Adhesion
PABPC1	PABPC1					
	PAK1			Signal Transduction, Cell Communication		Focal Adhesion
	PTEN			Regulation of Body Size, Cell Growth	Phosphoproteins	Focal Adhesion
SHC1	SHC1			Signal Transduction, Protein Kinase Cascade, Regulation for Cell Size and Growth, Cellular Morphogenesis, Cell Proliferation		Insulin Signaling Pathway, Focal Adhesion
			SOS1			

Table B.3
GATHER analysis of downregulated genes of the PI3-kinase pathway

TMΦ Worm	TMΦ Sphere	AMΦ Worm	AMΦ Sphere	GO Analysis	MESH Analysis	KEGG Analysis
B2M	B2M					
		BAD				Insulin Signaling Pathway, Apoptosis
		CDKN1B				
CHUK		CHUK		Protein Amino Acid Phosphorylation, Phosphorylation, Phosphorus Metabolism, Signal Transduction, Cell Communication, Protein Kinase Cascade, NF-kappa B Cascade		Insulin Signaling Pathway, Apoptosis, Toll-like Receptor Signaling Pathway
			ELK1			
FASLG		FASLG		Signal Transduction, Protein Kinase Cascade, NF-kappa B Cascade		Apoptosis

Table B.3 (continued)

TMΦ Worm	TMΦ Sphere	AMΦ Worm	AMΦ Sphere	GO Analysis	MESH Analysis	KEGG Analysis
IGF1				Signal Transduction		Focal Adhesion
		IRS1				Insulin Signaling Pathway,
MAPK3				Protein Amino Acid Phosphorylation, Phosphorylation, Phosphorus Metabolism	Ribosomal Protein S6 Kinases	Insulin Signaling Pathway, Focal Adhesion
MYD88	MYD88			Signal Transduction, Cell Communication, Protein Kinase Cascade, NF-kappa B cascade		Toll-like Receptor Signaling Pathway, Apoptosis
NFKB1	NFKB1		NFKB1	Signal Transduction, Cell Communication, Protein Kinase Cascade, Response to Pathogenic Bacteria		Toll-like Receptor Signaling Pathway, Apoptosis
NFKBIA				Signal Transduction, Cell Communication, NF-kappa B Cascade, Response to Pathogenic Bacteria		Toll-like Receptor Signaling Pathway, Apoptosis

Table B.3 (continued)

TMΦ Worm	TMΦ Sphere	AMΦ Worm	AMΦ Sphere	GO Analysis	MESH Analysis	KEGG Analysis
			PABPC1			
		PDK2				
PIK3CA				Protein Amino Acid Phosphorylation, Phosphorylation, Phosphorus Metabolism, Signal Transduction, Cell Communication		Insulin Signaling Pathway, Toll-like Receptor Signaling Pathway, Focal Adhesion
PIK3CG	PIK3CG			Protein Amino Acid Phosphorylation, Phosphorylation, Phosphorus Metabolism, Signal Transduction, Cell Communication	Ribosomal Protein S6 Kinases, Phosphoproteins	Insulin Signaling Pathway, Apoptosis, Focal Adhesions, Toll-like Receptor Signaling Pathway
PIK3R1		PIK3R1		Signal Transduction, Cell Communication		Insulin Signaling Pathway, Apoptosis, Focal Adhesions, Toll-like Receptor Signaling Pathway

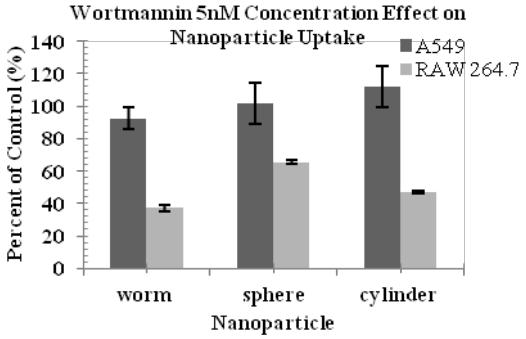

Figure B.8: Quantitative assessment of nanoparticle uptake by flow cytometry. An additional lower concentration of wortmannin was tested to discern between phagocytic and macropinocytic uptake. However, very little differences between the two concentrations were observed. Please also note: graphs are represented as percentage of uptake or the background provided by FACS analysis of cells incubated with the respective nanoparticles without the wortmannin inhibitor.

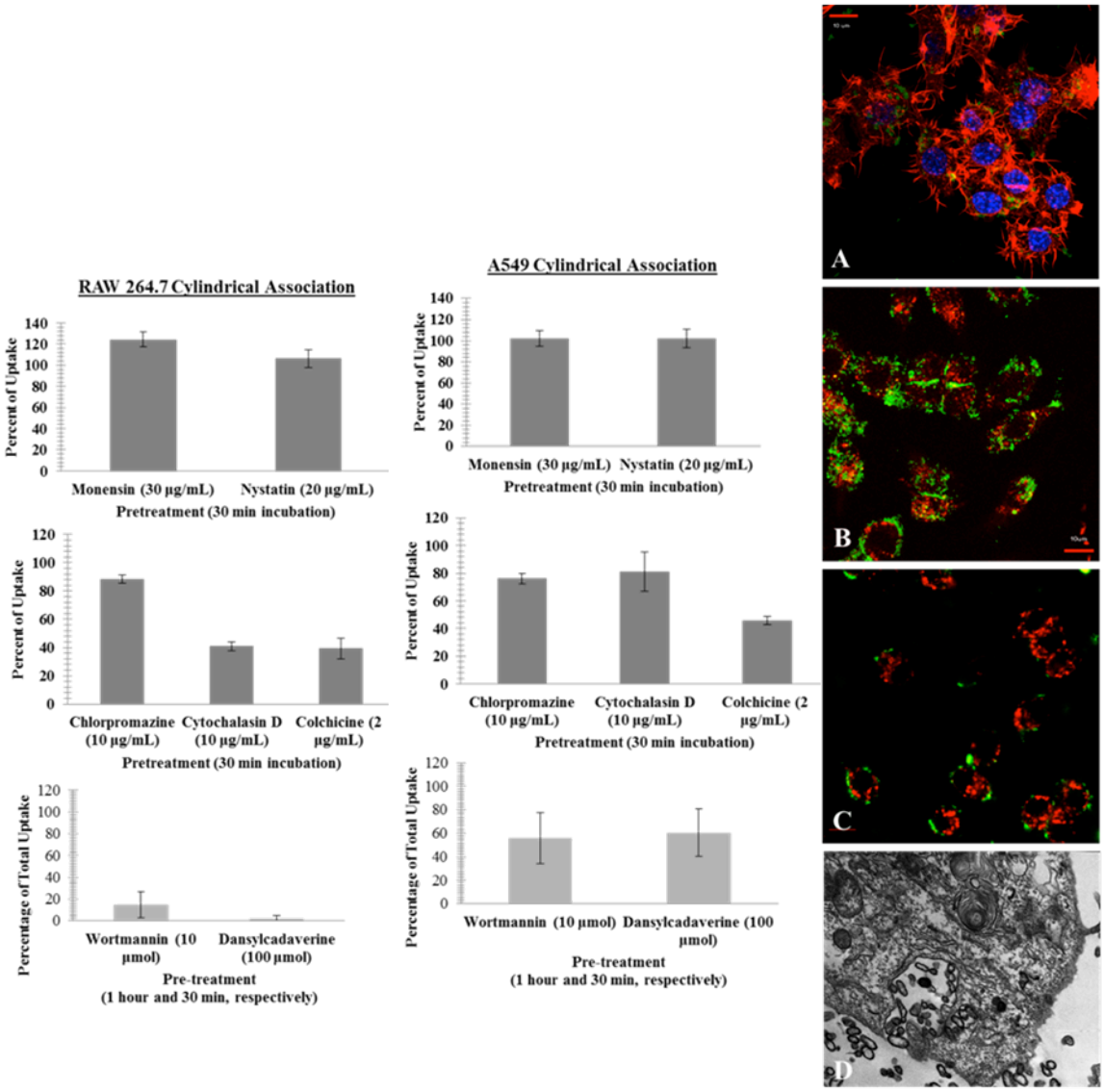

Figure B.9: Uptake and association of cylindrical particles are similar to worm-like particles. A) Actin staining with cylindrical treatment in RAW 264.7 cells, B) Dextran staining with cylindrical treatment in RAW 264.7 cells, C) Transferrin staining with cylindrical treatment RAW 264.7 cells, and D) TEM images of cylindrical treatment RAW 264.7 cells. Note: graphs are represented as percentage of uptake or the background provided by FACS analysis of cells incubated with cylinders without the respective inhibitor.

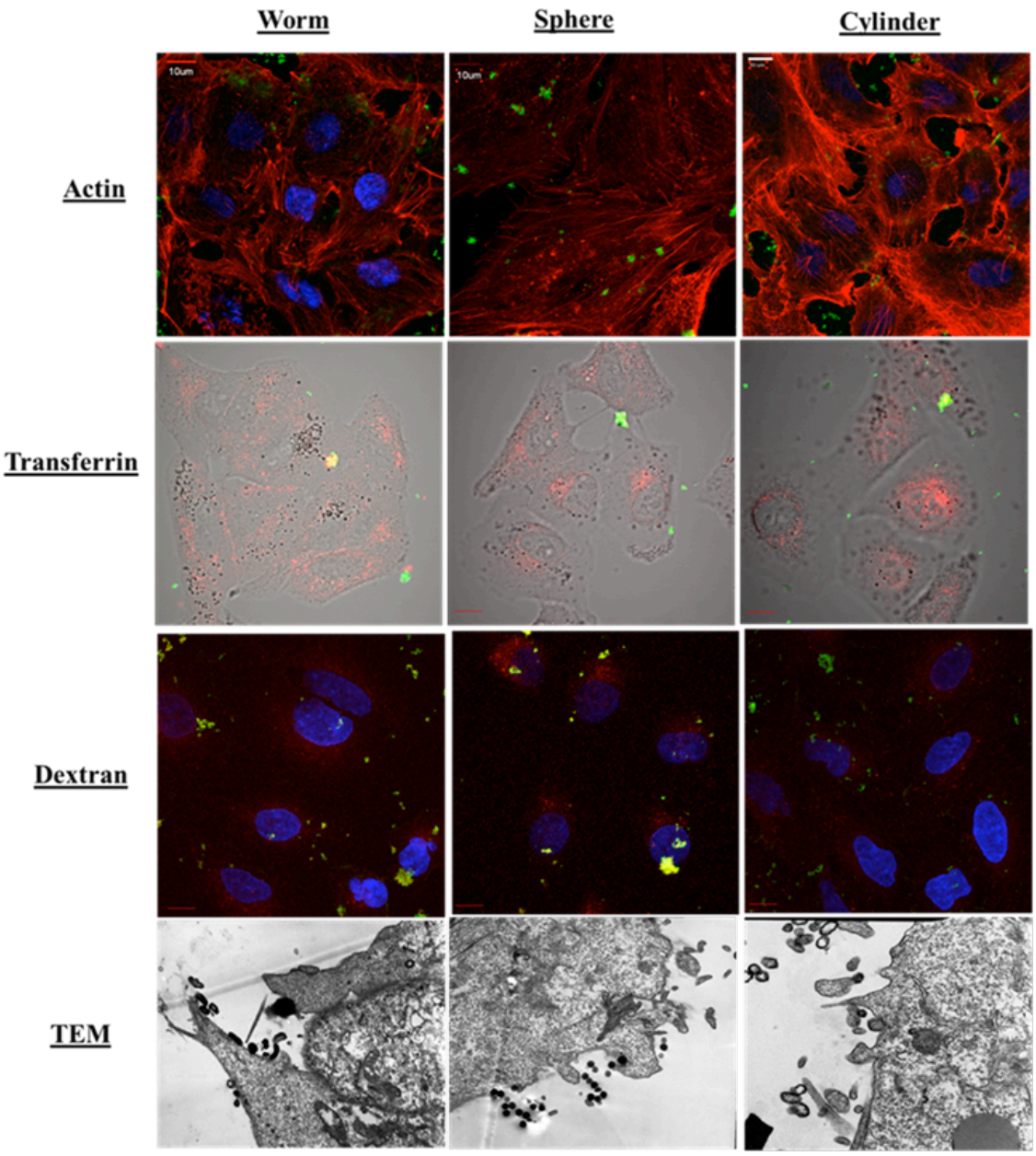

Figure B.10: Microscopy of nanoparticle uptake in A549 cells. A549 data are included to supplement the RAW 264.7 data outlined in the paper. Due to similarities of the images, these were excluded from the text of the paper included as Chapter 4.